SCUOLA DI DOTTORATO
UNIVERSITÀ DEGLI STUDI DI MILANO-BICOCCA

School of Medicine and Surgery

PhD program in Neuroscience - Cycle XXX

Curriculum in Experimental Neuroscience

Antiepileptic Drugs to Treat Cytomegalovirus Infection during Early Brain Development.

Dr. SARA ORNAGHI

Registration number 048763

Supervisor: Prof. Anthony N. van den Pol

Co-Mentor: Prof. Michael J. Paidas

Mentor: Dr. Andrea A. Lissoni

Coordinator: Prof. Guido A. Cavaletti

ACADEMIC YEAR 2016-2017

Abstract

Antiepileptic Drugs to Treat Cytomegalovirus Infection during Early Brain Development.

Cytomegalovirus (CMV) is the most common infectious cause of brain defects and neurological dysfunction in developing human babies. Due to the teratogenicity and toxicity of available CMV antivirals, treatment options during early development are markedly limited. This work reports for the first time that valpromide (VPD) and valnoctamide (VCD), structurally related drugs with anticonvulsant and mood stabilizing properties and no known teratogenic or toxic activity, evoke a substantial and specific inhibition of mouse and human CMV *in vitro*. Also, both compounds safely attenuate mouse CMV in peripheral organs of infected neonatal mice with improved survival, body weight, and developmental maturation. Since VCD shows a superior translational potential into the clinics and CMV-mediated neurological damage represents the most severe complication of viral infection during early development, we further investigated VCD using multiple models of CMV infection in the developing mouse brain. Subcutaneous low-dose VCD effectively suppresses CMV in the brain by both decreasing the level of virus available in the periphery for entry into the brain and by acting directly within the brain to block virus replication and dispersal. VCD during the first 3 weeks of life restored timely acquisition of neurological milestones in neonatal mice and rescued long-term abnormal motor and behavioral outcomes in juvenile animals. CMV-mediated brain defects, including decreased brain size, cerebellar hypoplasia, and neuronal loss, were substantially attenuated by VCD. No adverse side effects on body growth or neurodevelopment of uninfected control mice receiving VCD were detected. Treatment of CMV-infected human fibroblasts and fetal astrocytes with VCD reduced viral infectivity and replication by blocking viral particle attachment to the cell, a mechanism that differs from available anti-CMV drugs. These data suggest that VCD during early development can effectively suppress CMV replication in peripheral organs and in the brain, and safely attenuate virally induced mortality, deficient somatic growth, CNS damage, and adverse neurological outcomes. This work provides a novel potential direction for CMV therapeutics through repurposing of agents already approved for use in neuropsychiatric disorders.

Table of contents

Section Page number

Section Page number

Section Page number

List of abbreviations

CMV: cytomegalovirus

VPD: valpromide

VCD: valnoctamide

hCMV: human cytomegalovirus

HHV-5: human herpes virus-5

ORFs: open reading frames

HSPGs: heparan sulphate proteoglycans

gB: glycoprotein B

NF-kB: nuclear factor kB

IE: immediate early

CNS: central nervous system

NKs: natural killer cells

STD: sexually transmitted disease

SNHL: sensorineural hearing loss

ASD: autism spectrum disorder

EC: endothelial cells

NSCs: neuronal stem cells

NSPCs: neuronal stem progenitor cells

BBB: blood-brain barrier

CSF: cerebrospinal fluid

VZ: ventricular zone

SVZ: subventricular zone

ES: embryonic stem

RhCMV: rhesus macaque CMV

mCMV: murine CMV

E: embryonic day

i.c.: intracranial

i.p.: intraperitoneal

GCV: ganciclovir

valGCV: valganciclovir

HSV: herpes simplex virus

VPD: valpromide

VCD: valnoctamide

VPA: valproate (valproic acid)

HDAC: histone deacetylase

VSV: vesicular stomatitis virus

EBV: Epstein Barr virus

HDF: human dermal fibroblasts

MEM: minimum essential medium

FBS: fetal bovine serum

Pen Strep: penicillin streptomycin

DMEM: Dulbecco's modified Eagle's essential medium

GFP: green fluorescent protein

EF-1: elongation factor 1

CMC: carboxy-methyl-cellulose

HS: heparan sulfate

DMSO: dimethylsulfoxide

MOI: multiplicity of infection

EC_{50}: 50% effective concentration

qRT-PCR: quantitative real-time PCR

CT: comparative threshold

DAPI: 4′-6′-diamidino-2-phenylindole

EthD-1: ethidium homodimer

IACUC: Institutional Animal Care and Use Committee

pfu: plaque-forming units

DOB: day of birth

P: postnatal day

s.c.: subcutaneous

R/O: response or occurrence

T_{LA}: locomotor activity time

PCs: Purkinje cells

ML: molecular layer

IGL: internal granular layer

EGL: external granular layer

GABA: gamma-aminobutyric acid

List of figures

Section **Page number**

Section **Page number**

Acknowledgements

This work represents a collective accomplishment that is shared among many people who are very important to me and who I'd like to thank.

My husband's love, enduring support, and personal philosophy have helped in shaping the person I am now, and for those reasons, this dissertation is his accomplishment as much as it is mine. His intellect and humor never fail to afford me the perspective I need. A thank you is too limited in scope to embody what I owe him.

Everyone I have worked with in the van den Pol's lab deserves my utmost respect. I would particularly like to acknowledge John Davis, who patiently guided me over the last few years in gaining those skills I needed to complete this research project. Yang Yang also provided me with invaluable technical support whenever I so needed, and to her I am indebted.

I deeply thank Lawrence, John, Teresa, Lena, Eduardo, Amedeo, Caterina, and Alberto, for both their invaluable friendship and intellectual support. They all contributed to make my days in the lab and in New Haven both productive and memorable. I especially acknowledge the support of Lawrence, for his encouragement during emotionally hard times and help to overcome scientific and technical hurdles. He has taught me that I should not be afraid to think big and that I can be capable of doing what I set my mind to.

I thank our collaborator, Angelique Bordey, for sharing with us her knowledge and research apparatus for investigating autism-like behavior in our experimental model. I'd also like to thank Zhonghua Tang and Seth Guller, whose input for qPCR experiments has been invaluable.

I am especially indebted to Patrizia Vergani. Her strong faith in me and my capabilities, alongside with her incomparable support, helped me through the most difficult times and allowed me to become the physician scientist I am now.

I reserve my final thanks to Michael Paidas and Anthony van den Pol. Their intelligence and support generated a creative synergy that has been extremely intellectually fulfilling and scientifically productive. I deeply appreciated being treated as an intellectual equal from the very beginning; no suggestion of mine was ever too silly or out of the realm of possibility. I learnt so much from them and cannot thank them enough.

My work was financially supported by grants awarded to Michael Paidas (rEVO Biologics) and to Anthony van den Pol (National Institutes of Health RO1 CA188359, CA175577, CA161048, and NS79274).

Chapter 1

Introduction

1.1 General notions on human CMV.

Human CMV (hCMV) is an ubiquitous virus with worldwide distribution and no seasonal variation (Mocarski et al., 2013). Human CMV infects the majority of the population, spreading efficiently throughout life and all over the world through direct contact with bodily secretions (Sattar N, 1996; Britt, 2011). Sero-epidemiologic studies have shown that the prevalence of antibodies to hCMV is influenced by age, geography, and cultural and socio-economic status. In developing countries, nearly 100% of children are infected by three years of age, whereas in developed countries, as many as 60 to 80% of the population will be infected with hCMV by adulthood (Bate et al., 2010; Cannon et al., 2010; Cannon et al., 2011). U.S. population-based estimates of hCMV prevalence, derived from the National Health and Nutrition Examination Survey, report an overall age-adjusted prevalence of 59%, with about one-half of the U.S. population aged 6 to 49 infected (Staras et al., 2006; Bate et al., 2010). A hCMV prevalence ranging from 60% to 85%, in relation to Italian versus foreign origin, has been reported for Italy (Natali et al., 1997; Barbi et al., 2006).

1.2 Virus structure, replication, and cellular tropism.

Human CMV, or Human Herpesvirus 5 (HHV-5), is the largest member of the herpesvirus family, sub-family β *Herpesviridae*, which also contains HHV-6 and-7 (Kim et al., 1976; Sarov and Friedman, 1976; Stinski, 1976; Whittaker et al., 1996). These viruses share common characteristics, including appearance in electron micrographs, a prolonged replication cycle in cell culture, species specificity, and a tropism for differentiated hematopoietic and epithelial cell types (Mocarski et al., 2007). The virus has a diameter of 200 nm and consists of a 110 nm icosahedral capsid, surrounded by an amorphous tegument and by a lipid bilayer envelope derived from host cell membrane containing viral glycoproteins necessary for viral attachment and entry into cells (Fig. 1.1) (Wright et al., 1964; Smith and de Harven, 1978).

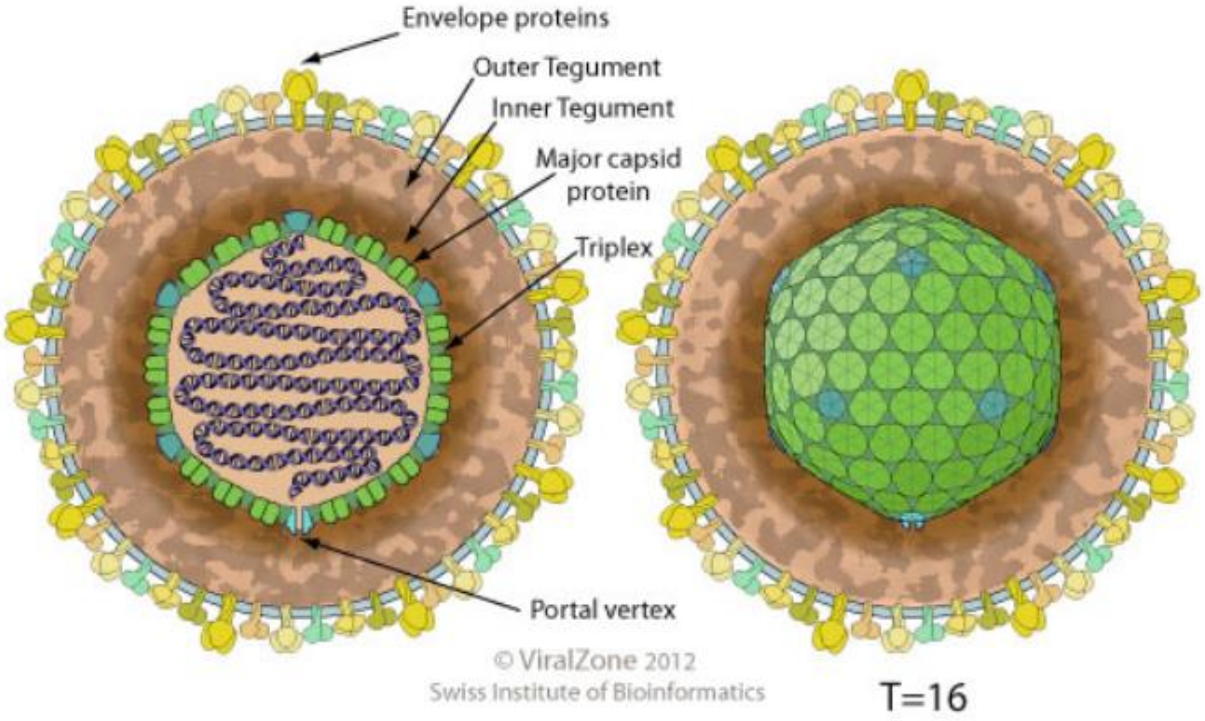

Fig. 1.1 Human CMV virion structure. *Enveloped, spherical to pleomorphic, 200 nm in diameter T=16 icosahedral symmetry. Capsid consists of 162 capsomers and is surrounded by an amorphous tegument. Glycoprotein complexes are embedded in the lipid envelope. Adapted from Viral Zone (Swiss Insititute of Bioinformatics, 2017).*

The genome is a linear double-stranded DNA molecule approximately 230 kilobase pairs in length (Huang et al., 1973; Sarov and Friedman, 1976; Geelen et al., 1978; Lakeman and Osborn, 1979). The hCMV genome has long and short unique sequences which are flanked by homologous repetitive sequences. It consists of 180 to 200 predicted open reading frames (ORFs) which include unique structural and non-structural proteins that are not found in the genome of other herpesvirus (Murphy et al., 2003). From the predicted ORFs, at least 5 distinct capsid proteins, a number of tegument proteins, and over 50 predicted glycoproteins have been identified (Kim et al., 1976; Sarov and Friedman, 1976; Stinski, 1976).

Virus replication begins when hCMV makes contact with the cell surface. Specifically, this interaction can be separated into two phases: (1) attachment of the viral particle to the cell surface heparan sulphate proteoglycans (HSPGs), and (2) fusion of the viral envelope with cellular membranes and penetration into the cytoplasmic space (Mocarski et al., 2007). The initial tethering of hCMV virions to HSPGs, mediated by the viral glycoprotein B (gB), functions to stabilize the virus at the cell surface until

engagement of secondary receptors occurs allowing fusion and penetration (Mocarski et al., 2007; Isaacson and Compton, 2009). Upon attachment, virus can enter the cell directly by fusion with the plasma membrane, as occurs in fibroblasts. Alternatively, the virus is enclosed within a cytoplasmic vacuole followed by uncoating of virus envelope and the trafficking of the nucleocapsid to the nucleus (endocytic route), as occurs in endothelial and epithelial cells (Whittaker et al., 1996). Viral attachment and fusion with the host cell membrane results in a cascade of cellular responses mediated by signaling pathways, with more than 1,400 cellular genes either induced or repressed (Britt, 2011). Included in these early responses are activation of transcription factors such as nuclear factor kB (NF-kB), increases in second messengers such as phosphoinositide-3 kinase activity, increased expression of type I interferons and interferon-stimulated genes, and induction of mechanisms that inhibit cellular innate responses that block virus infection (RNA-activated protein kinase) or lead to apoptosis of the infected cell (DeBiasi et al., 2002; Hildreth et al., 2012; Zhang et al., 2013). Human CMV prepares the host cell for virus replication and inhibits host cellular responses that could attenuate virus infection. Many of the hCMV envelope glycoproteins that are not directly involved in entry or egress have immunomodulatory potential. The earliest phase of the hCMV life cycle has been coined the 'immediate early (IE)' period, characterized by the transcription of immediate-early genes in the absence of *de novo* protein synthesis or replication of viral DNA (Demarchi, 1981; Gibson, 1981; Stinski et al., 1983). IE-1, a transcription factor critical for virus replication is a primary example of an immediate-early gene. The next period of the hCMV life cycle is called the 'early' phase. Immediate-early genes are required for the expression of early genes, which encode for various proteins, such as the viral DNA polymerase and other replicative enzymes as well as some tegument proteins. Genes expressed during the 'early' phase of virus gene transcription typically occurs within 24 hours of infection spanning into the late phase of transcription. This 'late' phase of the hCMV life cycle occurs after viral DNA replication and occurs between 36 to 48 hours post-infection. Late phase proteins are typically structural proteins necessary for encapsidation of the virus genome and for the release of infectious virus progeny. Encapsidation of virus genomes occurs in the nucleus of infected cells (Gibson, 1981). Following release of immature virions from the nucleus, final envelopment of the virus occurs in the cytoplasm. Lastly, mature virions are then released by cell lysis in cells such as fibroblasts or through exocytosis in other cell types (Britt, 2011). Human CMV is the first herpesvirus with evidence of a viral function that facilitates exocytosis of viral particles. Progeny virus is efficiently released from cells, reaching steady state levels where half of the infectivity at very

late times post-infection is found in the culture fluid and half remains cytoplasm-associated (Fig. 1.2) (Mocarski et al., 2013).

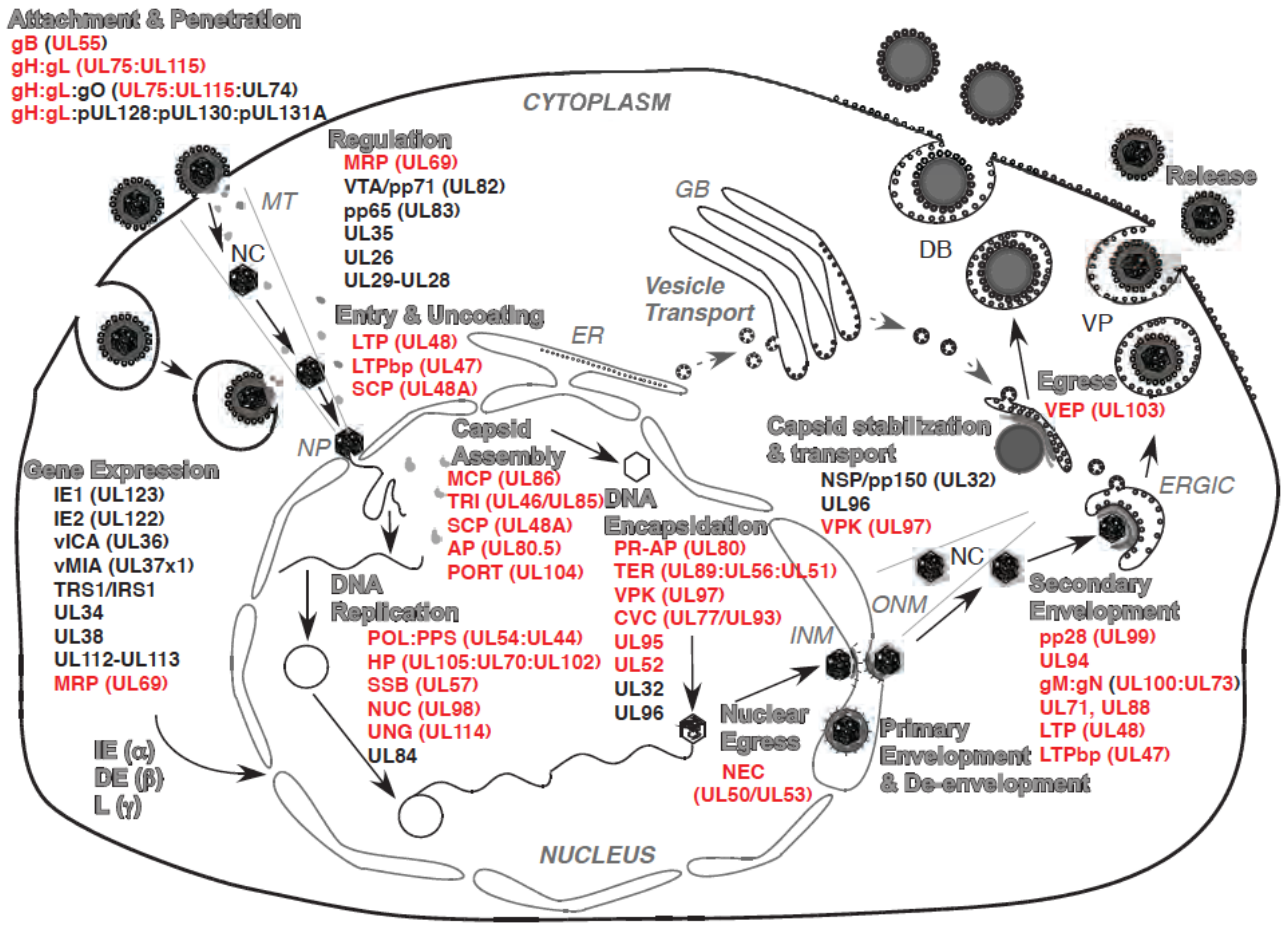

Fig. 1.2 Summary of the human CMV replication pathways. *Major steps in productive replication are indicated in large gray font with outline, black arrows indicate the progression of steps and viral functions. Individual gene products listed under each step are identified by provisional abbreviated names as either herpesvirus core (red text) or beta herpesvirus conserved (black text). Viral attachment and penetration occur either via direct fusion at the cell surface (fibroblasts), dependent on gB, gH:gL and gH:gL:gO, or via endocytosis into other cell types (endothelial and epithelial cells) where the pentameric complex, gH:gL:p128:p130:p131A, also facilitates entry. In addition to the interferon (IFN)-like activation of cells by the process of attachment and penetration, input virion tegument proteins (UL69/MRP, pp71/VTA, pp65, UL35, UL26, and UL29-UL28) regulate cellular pathways. Nucleocapsid (NC)-associated UL47, UL48, and smallest capsid protein (SCP) are predicted to facilitate the final steps in entry and uncoating that deliver input NC via microtubules (MT) to nuclear pore (NP) complexes where the viral genome is released into the nucleus. Transcriptional regulation of viral and host cell gene expression is mediated by IE genes (IE1, IE2) or E genes (UL34, UL35, UL112-UL113, and UL69); cell*

death suppression is mediated by IE gene products vICA and vMIA, and other regulatory processes are facilitated by UL34, UL38, and UL112-UL113 proteins. DNA replication depends on core proteins (POL:PPS, HP, SSB, NUC, and UNG) as well as one beta herpesvirus-specific protein (UL84 gene product) that facilitates initiation of DNA synthesis. Viral DNA is encapsidated by the TER complex (UL89, UL56, UL51). Following primary envelopment at the inner nuclear membrane (INM), and de-envelopment at the outer nuclear membrane (ONM), capsid stabilization is ensured by the function of NSP/pp150 (UL32) and UL96, with nuclear egress and transport facilitated by VPK (UL97). Glycoproteins incorporated into the envelope are synthesized in the endoplasmic reticulum (ER), glycosylated in the Golgi body (GB), and delivered by vesicle transport (dashed gray arrow) to join NC at sites of secondary envelopment on ER Golgi intermediate compartment (ERGIC). Following the acquisition of an envelope, virus particle (VP) as well as capsid-less dense body (DB) egress is facilitated by VEP/UL103 for release into the extracellular space. Adapted from (Mocarski et al., 2013).

The glycoprotein gB is pivotal not only for virus attachment and fusion initiation but also for cell-to-cell spread and cell-cell fusion leading to syncytia, both of which involve membrane fusion (Mocarski et al., 2013). Another envelope glycoprotein complex, gH:gL, controls post-attachment enhancement of fusion, whereas maturation and release of progeny virions seems to be modulated by the envelope glycoprotein complex gM:gN.

Human CMV can be detected in a wide variety of cell types *in vivo* (Sinzger et al., 1993; Li and Kamil, 2015). Studies using tissue from autopsies or biopsies have shown virus in almost every cell type, including epithelial cells, endothelial cells, smooth muscle cells, neuronal cells and supporting cells in the central nervous system (CNS), retinal epithelium, dermal fibroblasts, and cells of the monocyte/macrophage lineage. There seems to be a very limited restriction of the host cellular tropism *in vivo*. However, due to species specificity, completion of hCMV life cycle with viral DNA replication and mature virion release can occur only if the virus infects cells from the same species, namely human (Mocarski et al., 2007). Cells from non-homologous animal species, such as mouse, are non-permissive and allow just the initial steps of viral cycle, including attachment, entry, uncoating, and IE gene expression, to occur.

1.3 Pathogenesis of human CMV infection.

As mentioned above, CMVs are highly species specific and humans are considered the only reservoir for hCMV.

Human CMV infection initiates when exposure for the first time to virus-infected body fluids overcomes innate immune barriers and sustains replication and dissemination (primary infection). These events occur most frequently at mucosal sites. A systemic phase infection takes place where virus can be detected in peripheral blood leukocytes (leukocyte-associated viremia), mostly neutrophils, that are responsible for dissemination to secretory organs, including salivary glands and kidneys. Here, the virus infects ductal epithelial cells and is shed and transmitted to new hosts. Dendritic cells, together with natural killer cells (NKs), produce cytokines that regulate development of adaptive immunity that is crucial for life-long host control of the virus. However, even when active infection is resolved through an effective adaptive cellular immune response, hCMV is never completely cleared and remains latent for the life of the host. A latently infected myeloid cell population remains in the bone marrow precursors of monocytes, macrophages, and dendritic cells (Sattar N, 1996; Bego and St Jeor, 2006; Mocarski et al., 2007). The mechanisms that favor the establishment of latent infections are unknown, and the viral genome in latently infected cells is thought to be maintained in a non-productive state as closed circular viral DNA (episome) and not by integration into the host DNA (Britt, 2011). This source of latently infected cells allows distribution of viral reservoir throughout the body in all tissues and contributes to the risk of transfer of hCMV with organ transplantation (Mocarski et al., 2013).

Although primary infection is eventually controlled, viral shedding in saliva and urine may proceed for months to years, with longer shedding in infected toddlers and children due to a less developed adaptive T-cell response (Waller et al., 2008; Britt, 2011). Persistent shedding in urine contributes to transmission among children as well as from children to adults. Saliva is also an important source in all age groups, whereas cervical or seminal secretions may contribute to transmission patterns in adults (Mercorelli et al., 2011). Cervical secretion and breast milk transmission from mothers to neonates can also occur (Kurath et al., 2010). Coinfection with multiple viral strains, reinfection with additional strains, changes in viral persistence, and reactivation of latent infection all likely contribute to transmission patterns. A high incidence of infection in certain populations and accumulating evidence that hand washing among caregivers prevents acquisition of hCMV from infants provide excellent evidence that this virus reaches a large proportion of the population through a direct route of transmission.

Human CMV is a classic opportunist. Infection with hCMV in immune-competent individuals is usually asymptomatic, with occasional febrile illness and mononucleosis-like symptoms. However, in individuals with suppressed or compromised immune system, including transplant recipients and AIDS patients, disease of diverse severity can be caused by hCMV and the infection can be life-threatening

(Britt, 2011; Mercorelli et al., 2011; Mocarski et al., 2013). Pneumonitis, retinitis, encephalitis, and myocarditis are potential serious complications following hCMV infection in the context of immune deficit. In addition, hCMV is an important pathogen in fetuses and newborns with an immature immune system. It is the leading viral cause of congenital brain defects and sensorineural hearing loss (Gandhi and Khanna, 2004; Mocarski et al., 2007; Cheeran et al., 2009; Tsutsui, 2009); also, hCMV can cause severe, possibly life-threatening disease in preterm infants with low birth weight (Amin et al., 1990; Hamprecht et al., 2001; Takahashi et al., 2007; Fischer et al., 2010; Kurath et al., 2010; Bevot et al., 2012; Okulu et al., 2012; Lanzieri et al., 2013; Brecht et al., 2015).

Adaptive T-cell immunity, in particular, maintains low hCMV levels, but this protection is not absolute, and its modulation by viral functions enables the virus to escape control. Consistent with this view, any compromise to cellular immunity contributes to the importance of this virus as a classic opportunist, whether it is severe, life-threatening disease that follows immunodeficiency, immunotherapy, or immunosuppression, or it is congenital or early neonatal disease where the virus encounters a not fully developed immune system (Mocarski et al., 2013). Notably, increased level of hCMV-specific T cells with successful antiretroviral therapy is the main factor in decreasing hCMV disease in AIDS patients.

1.4 Congenital, intrapartum, and postnatal human CMV infection.

Maternal transmission of hCMV can occur during pregnancy, when infection is associated with placental and fetal infection (congenital disease), as well as at birth via infected cervical secretions (intrapartum infection), or following birth trough breastfeeding (postnatal infection). Intrapartum and postnatal infections are also called perinatal infections (Britt, 2011).

Breastfeeding is the most frequent route of maternal transmission, whereas transplacental transmission is the most medically important in term of possible adverse outcomes in *in utero* infected fetuses and neonates. However, postnatal hCMV infection via breastfeeding can also pose a risk for severe, possibly life-threatening hCMV-mediated disease and long-term mild neurocognitive sequelae if occurring in preterm infants born at birth weight less than 1.5 Kg or gestational age less than 32 weeks (Amin et al., 1990; Hamprecht et al., 2001; Takahashi et al., 2007; Fischer et al., 2010; Kurath et al., 2010; Bevot et al., 2012; Okulu et al., 2012; Lanzieri et al., 2013; Brecht et al., 2015). Exposure to hCMV via breast milk in premature neonates might cause severe infection with multiple organs involvement and development of neutropenia, thrombocytopenia, hepatitis, cholestasis, colitis, pneumonitis, and sepsis-

like symptoms, requiring endovenous administration of antiviral therapy (Amin et al., 1990; Fischer et al., 2010; Okulu et al., 2012).

1.4.1 Congenital human CMV infection.

The level of immunity among women of childbearing age is an important factor in determining the incidence and significance of congenital hCMV infections. Immunity towards hCMV varies widely among different populations. Past reports indicated that seropositivity rates in young women in the United States and Western Europe range from less than 50% to 85%. In contrast, in sub-Saharan Africa, Central and South America, India, and the Far East, the rate of seropositivity is greater than 90% by the end of the second decade of life (Britt, 2011). Figure 1.3 shows data on prevalence of infection in women of childbearing age from Europe, North and South America, Africa, and Asia based on selected studies (Mocarski et al., 2013).

Study location, date	Population	N	Prevalence (%)
Ankara, Turkey	Women 15–49 years	745	99
Cotonou, Benin	Pregnant women	211	97
Seoul, South Korea	Prenatal clinic	575	96
Sendai, Japan	Prenatal clinic	10,218	95
Sao Paulo, Brazil	Pregnant women, middle SES	427	67
	Pregnant women, lower SES	179	84
Northern Italy	Women, pregnant or hospital patients	12,568	77
Helsinki, Finland	Women, prenatal clinics	1,088	71
Birmingham, USA	Prenatal, middle SES	12,140	54
	Prenatal, lower SES	4,078	77
Grenoble, France	Women, prenatal clinic	1,018	52

Fig. 1.3 Prevalence of human CMV infection among women of childbearing age. *Adapted from (Mocarski et al., 2013)*.

The extended, multi-year pattern of shedding in children, resulting from slow development of a virus-specific T-cell response, provides an ample source for transmission, with exposure to children being the most dominant risk for acquisition of infection in women in childbearing age (Waller et al., 2008; Britt,

2011). Figure 1.4 displays rates of hCMV seroconversion observed in various groups, including childcare providers, parents of young children, and patients attending a sexually transmitted disease (STD) clinic, over 1 year period (Mocarski et al., 2013).

Group	Rate
Blood donors	1.57
Hospital employees	
Richmond, VA	2
Birmingham, AL	2.2
Pregnant women	
Middle income	2.5
Low income	6.8
Women in STD clinic	37
Adolescent females	13.8
Parents of CMV shedding child	
0–12 months old	47
≤18 months old	32
19 months –6 years	13
Daycare workers	7.920

Fig. 1.4 Incidence of human CMV seroconversion in various groups. *Rate is percent per year that seroconverted from antibody negative to antibody positive. Adapted from (Mocarski et al., 2013).*

Human CMV intrauterine transmission with placental and fetal infection can occur in both seronegative and seropositive women (Britt, 2011). Congenital infection in women who have already been infected before pregnancy is termed recurrent infection, to acknowledge a likely contribution of reinfection, persistent infection, or reactivation of latent virus in this setting.

Seroconversion rate in immune negative pregnant women is approximately 1 to 7%, with increased risk of acquiring primary hCMV infection if presence of risk factors, such as exposure to toddlers (e.g., child care providers, mothers of children <36 months of age), as previously mentioned (Revello et al., 2015; Britt, 2017). In contrast, the number of immune women susceptible to recurrent infection during pregnancy is unknown, as is the number of reinfections (seroconversion to a new strain of hCMV)/reactivations (Britt, 2017). However, immune pregnant women caring for young children or living in countries with high hCMV seroprevalence are at increased risk for hCMV recurrent infection and vertical transmission. Studies in populations with different seroprevalence have demonstrated a direct correlation between maternal seroprevalence and incidence of congenital hCMV, ranging from 0.3% in populations with 30% seroprevalence to 2% in populations with 98% seroprevalence (Kenneson and Cannon, 2007; Mussi-Pinhata et al., 2009). Whether congenital infection is the consequence of a

reactivation of the latent strain or a reinfection with a new strain in the mother remains undefined. However, studies have argued that maternal infection with a serologically distinct hCMV strain could play a more substantial role in congenital infection than viral reactivation (Boppana et al., 2001; Yamamoto et al., 2010).

Transplacental transmission and subsequent fetal infection is reported in 40% of primary maternal infections. In turn, only 0.2 to 2% of recurrent infections are reported to be complicated by *in utero* infection (Revello and Gerna, 2004; Kenneson and Cannon, 2007; Malm and Engman, 2007; Revello et al., 2014). However, the notion that preexisting natural immunity could reduce the risk of transmission has been recently questioned (Britt, 2017). Assuming several different rates of reinfection/reactivation in immune pregnant women, according to different exposure to risk factors, Britt reports that intrauterine transmission rates might range between 1 and 40%. According to the author, the assumption that all hCMV-immune women have the same risk of recurrent infection and intrauterine transmission has likely led to a substantial overestimate of the effect of preexisting hCMV adaptive immunity on the prevention of intrauterine transmission.

Congenital infection can be differentiated in symptomatic, which occurs in 10-15% of *in utero* infections and it is characterized by clinical and/or laboratory evidence of hCMV disease at birth, and asymptomatic, in the remaining 85-90% (Malm and Engman, 2007; Demmler-Harrison, 2013).
Symptomatic neonates can display deficient growth and low birth weight, jaundice, hepatosplenomegaly, hepatitis, intrahepatic cholestatic disease, ascites, thrombocytopenia with petechiae and purpura, neutropenia, hemolytic anemia, pneumonia, osteitis, cutaneous vasculitis, sensorineural hearing loss (SNHL), and severe CNS damage with microcephaly, intracerebral calcifications, and chorioretinitis. Some newborns may have atypical brain and peripheral involvement, with ventriculomegaly, periventricular leukomalacia, periventricular cystic malformations, polymicrogyria, cerebral thrombosis, and optic atrophy. In 10% of symptomatic newborns, infection is so diffuse and severe, the so called ‘cytomegalic inclusion disease’, to cause multi-organ failure and neonatal death.
As many as 90% of congenitally infected neonates will look completely normal at birth and show no symptoms or signs of hCMV infection. However, 8 to 15 percent of these infants will go on developing unilateral or bilateral deafness or differences in higher-level auditory function, sometimes even years after birth, thus requiring a long follow up to be detected (Bartlett et al., 2017; Boppana and Fowler, 2017; Lanzieri et al., 2017). Retinal lesions and subsequent vision deficits may occur as well. In addition, some studies have suggested that asymptomatically infected children may show mild to moderate

neurocognitive delays and impairment even though conflicting data are available (Connolly et al., 1992; Williamson et al., 1992; Kashden et al., 1998; Coats et al., 2000; Noyola et al., 2000; Bartlett et al., 2017; Boppana and Fowler, 2017; Koyano et al., 2017; Lopez et al., 2017) (Fig. 1.5).

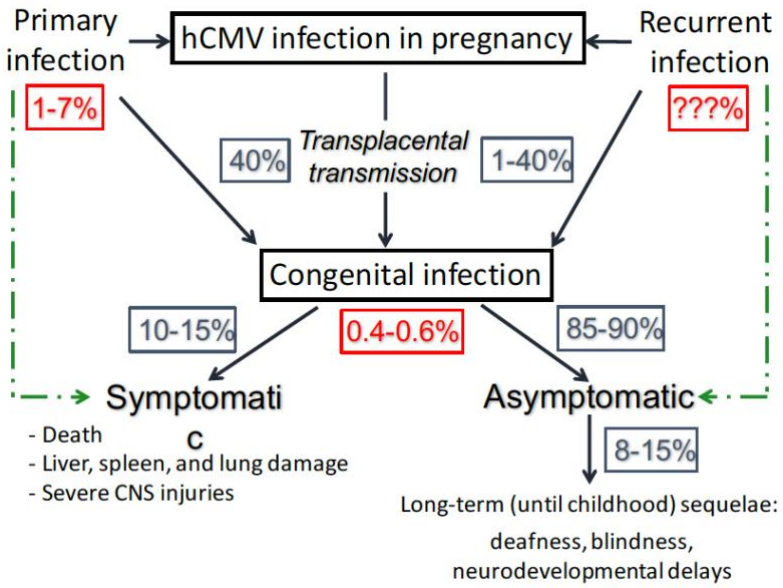

Fig 1.5 Diagram of congenital human CMV disease. *Green dotted lines indicate that symptomatic congenital infection is more common in cases of primary maternal infection whereas asymptomatic congenital infection is more likely in recurrent maternal infections.*

Timing of infection during pregnancy substantially influences the odds of severe fetal damage and adverse sequelae (Picone et al., 2013). Even though the risk of *in utero* transmission increases with gestational age, neurological outcomes are less severe when infection occurs during the third trimester as compared to the first/early second trimester, moment of active neurogenesis (Manicklal et al., 2013). Presence of maternal immunity is also considered pivotal in limiting severity of fetal infection (Revello et al., 2006; Kenneson and Cannon, 2007). However, a number of studies have reported similar percentages of symptomatic infants following either primary (9.8%-30%) or recurrent (11%-28%) maternal infections (Boppana et al., 1999; Ahlfors et al., 2001; Ross et al., 2006; Townsend et al., 2013), thus arguing against the protective role of maternal immunity on severity of congenital disease. Recently, it has been estimated that non-primary maternal infections account for the majority of hCMV-related hearing deficits (de Vries et al., 2013; Townsend et al., 2013).

The birth prevalence of congenital hCMV is 4 to 6/1,000 live births both in the United States and in Italy (Barbi et al., 2006; Boppana et al., 2011; Pinninti et al., 2015). This means that approximately 30,000 children in the United States and 3,000 children in Italy receive a diagnosis of CMV infection every year (Kenneson and Cannon, 2007; James and Kimberlin, 2016), resulting in about 400 deaths, and 8,000 children with life-long neurological disabilities (Cannon, 2009; Boppana et al., 2013). This makes CMV the most common severely disabling intrauterine infectious agent (Kenneson and Cannon, 2007; James and Kimberlin, 2016). More children have disabilities due to congenital CMV than other well-known infections and syndromes, including pediatric HIV/AIDS, Down syndrome, fetal alcohol syndrome, and spina bifida (Cannon and Davis, 2005; Mestas, 2016). Another virus that has recently raised considerable concern, and that can evoke parallel dysfunction in the developing brain, is Zika virus; importantly, in the United States neurological dysfunction due to congenital CMV infections is 100-fold more prevalent than that from Zika virus (Butler, 2016). The disease burden of congenital CMV infection is very high and similar to that for congenital rubella before the introduction of rubella vaccination (Arvin et al., 2004; Ludwig and Hengel, 2009).

1.4.1.1 Damage to the developing brain and neurological outcomes in congenitally infected children.

Among the clinical manifestations associated with congenital hCMV infection, the most devastating are those involving the developing CNS. In fact, CNS damage is considered irreversible whereas other end-organ injuries, including the reticuloendothelial system with cytopenia, hepatosplenomegaly, and jaundice, are transient.

Infection of the developing brain by hCMV can cause a number of brain anomalies that are dependent on the age of the fetus at the time of CNS infection and can be detected by imaging techniques either prenatally or after birth (Perlman and Argyle, 1992; de Vries et al., 2004; Pass et al., 2006; Lipitz et al., 2013; Kimberlin et al., 2015; Oosterom et al., 2015; James and Kimberlin, 2016). Brain abnormalities commonly noted in imaging studies of living fetuses and infants with congenital hCMV infections include periventricular calcifications, ventriculomegaly, loss of white-gray matter demarcation, white matter gliosis, atrophy, loss of normal radial neuronal migration with cortical malformations (most notably polymicrogyria), lissencephaly, porencephaly, schizencephaly, cerebellar hypoplasia, and microcephaly (Bale et al., 1985; Barkovich and Lindan, 1994; Boppana et al., 1997; de Vries et al., 2004) (Fig. 1.6). Although not frequently performed, autopsies have confirmed these imaging abnormalities

and have shown the presence of inflammatory infiltrates throughout the parenchyma of the brain (Gabrielli et al., 2012).

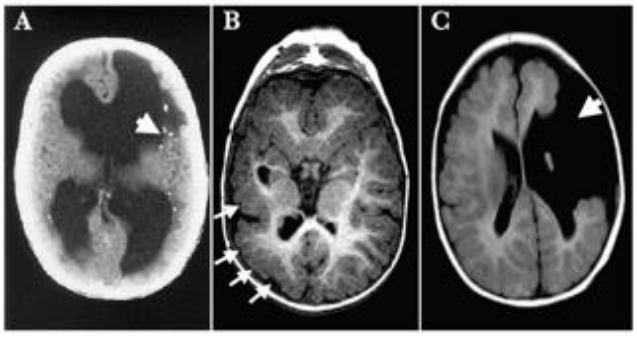

Fig. 1.6 Imaging findings in congenitally human CMV-infected neonates. *Computed tomography (A) and magnetic resonance (B and C) CNS imaging of three infants with severe symptomatic congenital hCMV infection with CNS involvement. The classical pattern of injury is characterized by periventricular calcifications (A, arrow), abnormalities of neuronal migration, such as polymicrogyria (B, arrows) and, in extremely severe cases, profound structural defects such as porencephalic cysts with associated schizencephaly (C, arrow). Adapted from (de Vries et al., 2004).*

Presence of abnormal imaging findings at prenatal and/or early postnatal evaluation of infected fetuses/neonates strictly correlates with development of neurological sequelae, which include cerebral palsy, neurodevelopmental delays, seizures, motor impairment, intellectual disability, visual deficits, and deafness (Boppana et al., 1997; Noyola et al., 2001; Ancora et al., 2007; Oosterom et al., 2015; Leruez-Ville et al., 2016a). Some of these neurological problems may not be evident at birth (e.g., asymptomatic infection) but develop later in life, even several years after birth, in up to 15% of the infected newborns (Dollard et al., 2007; De Kegel et al., 2016).

Cerebral palsy following symptomatic congenital hCMV infection is mostly severe (Noyola et al., 2001), with bilateral spasticity being the most frequent clinical presentation (Dakovic et al., 2014). Approximately 70% of the children with hCMV-related cerebral palsy do not have any ability to walk, as compared to 30% of the cases with non-virus induced cerebral palsy (Himmelmann et al., 2006). Also, association with severe intellectual impairment, lack of speech development, profound hearing and visual deficits, and epilepsy is more frequent, thus indicating a more extensive damage and deficient growth of the brain (Dakovic et al., 2014; Smithers-Sheedy et al., 2014). A strong correlation between cerebral palsy and onset of seizures has been identified, and presence of ventriculomegaly and cortical anomalies

at early postnatal imaging significantly associate with risk of developing epilepsy within the first few years of life (Suzuki et al., 2008). The most common seizure types reported in hCMV-infected children are partial seizure and infantile spasms, often resistant to multiple lines of anticonvulsant treatment.

An increased risk for delayed acquisition of neurological milestones during the first months of life and for late-onset gross motor developmental delay has also been described in cases of symptomatic congenital infection with no evidence of cerebral palsy (Dollard et al., 2007; Kimberlin et al., 2015; De Kegel et al., 2016). Additionally, asymptomatic congenitally infected children have raised odds for motor delay, although mainly related to the development of SNHL and its associated vestibular dysfunctions (Zagolski, 2008; Bernard et al., 2015). Vestibular deficits can have a substantial impact on balance and gross motor performance (De Kegel et al., 2012).

Visual deficits may occur in 10-20% percent of children with symptomatic infection and 1-2% of asymptomatic neonates. Vision abnormalities are related to both peripheral damage, including retinal and eye muscle scars, and central injury at the level of the visual cortex (cortical blindness) (Dollard et al., 2007).

Human CMV is currently the leading cause of non-hereditary SNHL in children, and approximately 25% of all cases of SNHL in children in the United States can be attributed to congenital hCMV infection (Morton and Nance, 2006; Fowler, 2013). The risk of SNHL is higher among children with symptomatic hCMV infections (30 to 65%) than among those with asymptomatic infection (7 to 15%); however, hearing loss represents the most common sequela identified in the latter group (Williamson et al., 1990; Hicks et al., 1993; Bartlett et al., 2017). CMV-related SNHL can be manifested at birth or appear later on, up to 6 years of age (Fowler et al., 1997); it can also be progressive in nature, with deterioration in hearing potentially occurring over the first several years of life. Fifty percent of all children with hCMV-related SNHL will experience progression or further deterioration of their hearing loss over time, in the absence of progression of CNS structural damage, thus suggesting persistence of the virus and/or inflammation in the inner ear and auditory pathways (Dahle et al., 2000; Sugiura et al., 2003; Fowler and Boppana, 2006). This is why CNS involvement in infants with congenital hCMV infection is considered an ongoing condition.

More recently, a link between congenital hCMV infection, both with and without signs of infection at birth and of viral CNS involvement, and autism spectrum disorder (ASD)-like behavioral disturbances in children and adolescents has been proposed (Stubbs et al., 1984; Yamashita et al., 2003; Engman et al., 2015; Sakamoto et al., 2015; Garofoli et al., 2017). In some cases, ASD was reported as

the only long-term neurobehavioral sequela of congenital hCMV infection (Sakamoto et al., 2015; Garofoli et al., 2017; Gentile et al., 2017). These data stress the importance of careful monitoring for early ASD signs, such as delayed speech and social interaction, in all congenitally infected children.

1.4.1.2 Pathogenesis of human CMV-mediated damage to the developing brain.

The precise pathogenesis of hCMV-related injury to the developing fetal CNS is still poorly understood for several reasons, including the lack of a sufficiently large number of cases from autopsy studies (Cheeran et al., 2009). In addition, no well-developed animal models of congenital CMV CNS infection are available (Britt, 2011). Multiple mechanisms have been proposed to play a potential role in hCMV-mediated neuropathogenesis (Cheeran et al., 2007; Cekinovic et al., 2008; Koontz et al., 2008; Mutnal et al., 2011; Burd et al., 2012; Gabrielli et al., 2012). These include the following: 1) hCMV acting as a "teratogen", disrupting normal cellular differentiation and morphogenesis pathways of neuronal progenitors, during critical developmental windows of susceptibility; 2) the potential pathogenic impact of hCMV on the endovascular system, interrupting the blood supply to the developing brain, thus leading to cystic lesion development; 3) the role of the immune responses (i.e., meningoencephalitis with release of inflammatory mediators) in potentiating CNS injury with promotion of aberrant neuronal migration, altered neuronal physiology, and abnormal developmental cues in the developing brain (Zou et al., 1998; Zhu et al., 2002; Koontz et al., 2008); and 4) the detrimental effects of intrauterine hypoxia due to placental hCMV infection and subsequent placental insufficiency (Pereira et al., 2005; Schleiss, 2006b; Adler et al., 2007; Gabrielli et al., 2012).

Most of what we know today about susceptibility of brain cells to hCMV infection has been afforded by experiments performed on cultured human brain cells and from animal models of CMV infection of the brain (Cheeran et al., 2009). In primary human cell culture systems or brain-derived cell lines it has been shown that practically all cell types in the brain have some degree of susceptibility to hCMV infection. Astrocytes, brain microvascular endothelial cells (EC), pericytes, neuronal stem cells (NSCs) and neuronal stem progenitor cells (NSPCs), oligodendrocytes, and microglia/macrophages have a propensity for hCMV infection (Lathey et al., 1990; Poland et al., 1990; Schut et al., 1994; Spiller et al., 1997; Lokensgard et al., 1999; McCarthy et al., 2000; Wilkerson et al., 2015). However, these different cell types vary in their ability to support a complete viral replication cycle. Astrocytes, the major cell type of the brain, support hCMV replication, similarly to EC. Interestingly, hCMV infection of microvascular EC, which form the blood-brain barrier (BBB) together with pericytes and astrocytes, promotes BBB disruption and monocyte migration, which in turn may sustain viral dissemination into

the brain (Bentz et al., 2006; Kawasaki et al., 2017). Infection of astrocytes may also disrupt their normal supportive functions in the brain that are critical for neural circuitry guidance, synaptic integration, and development of the functionally integrated mature neurons (Ma et al., 2005). Further, hCMV infection in NSPCs, the building block of the developing brain, inhibits cell proliferation and alters differentiation profiles, thus supporting a teratogenic role of hCMV during early brain ontogeny (Odeberg et al., 2006; Odeberg et al., 2007; Chavanas, 2016; Rolland et al., 2016; Han et al., 2017; Kawasaki et al., 2017).

According to a recent review on hCMV-mediated developmental anomalies of the CNS using a mouse model of congenital infection, hCMV diffuses throughout the developing brain by hematogenous and cerebrospinal fluid (CSF) spread (Kawasaki et al., 2017). Vessels of the meninges and choroid plexus consist of only endothelial cells; therefore, hCMV particles may easily extravagate outside the vessel into the meninges and lateral ventricle CSF during the first viremic phase. This may explain the meningitis and choroid plexitis frequently observed in human fetal brains with initial hCMV infection. Parenchymal blood vessels consist of EC, pericytes, and astrocyte feet, which collectively form the BBB. Infection of this neurovascular unit with hCMV can lead to BBB disruption, facilitating the spread of hCMV particles into brain parenchyma. Ultimately, meningitis, choroid plexitis, and vasculitis allow diffusion of hCMV into the ventricular zone (VZ) and sub-VZ (SVZ), that contain a dense NSPC population. Here, viral infection inhibits NSPC proliferation and differentiation, resulting in neuronal cell loss. These cellular events may underlie the development of brain malformations observed in severely hCMV-infected fetuses and neonates, such as microcephaly, cortical thinning, and polymicrogyria (Fig. 1.7).

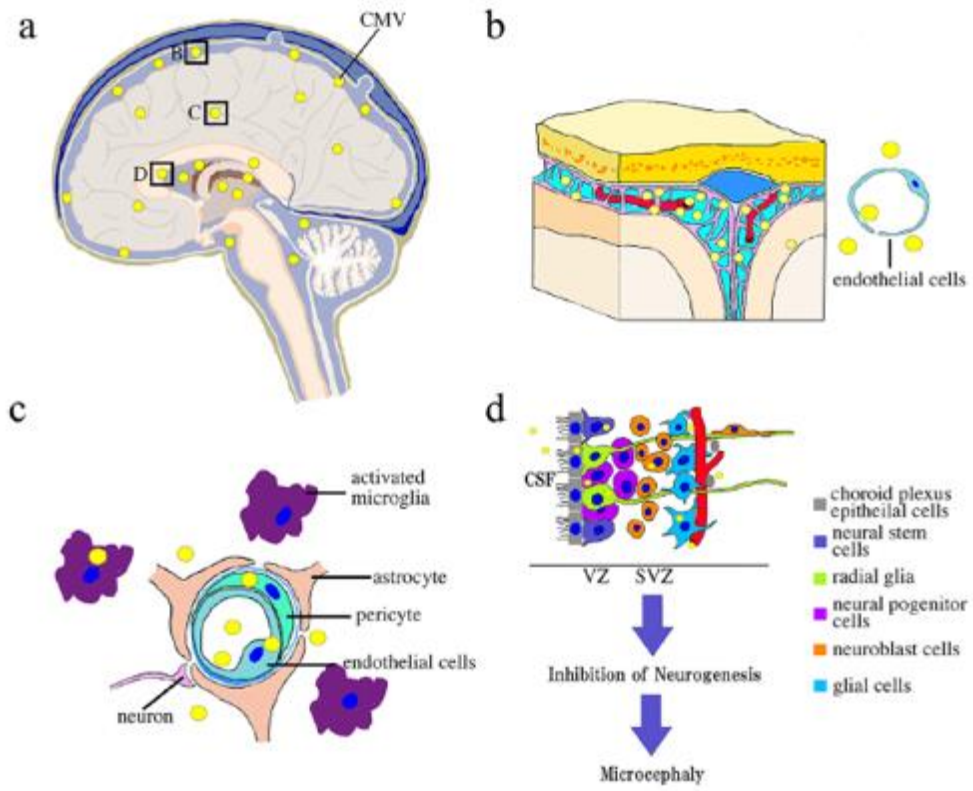

Fig. 1.7 Pathogenesis of congenital human CMV-mediated anomalies of the developing CNS. *a) CMV reaches the developing brain by hematogenous spread or via the CSF. b) Vessels in the meninges and choroid plexus consist of only endothelial cells. Viral particles (yellow circle) extravagate outside the vessel and into CSF. c) Parenchymal blood vessels consist of endothelial cells, pericytes, and astrocyte feet. In severe cases, hCMV infection can infect these cells, disrupting BBB integrity and facilitating viral dissemination into brain parenchyma. d) Both meningitis (b) and vasculitis (c) allow CMV to reach the VZ and SVZ, where NSPCs reside. Infection of these cells inhibits their proliferation and differentiation into neuronal and glial cells, resulting in neuronal cell loss and brain malformations. Adapted from (Kawasaki et al., 2017).*

It has been suggested that NSCs may represent a hCMV reservoir in the developing brain by allowing viral latency, similarly to hematopoietic progenitor cells in the bone marrow (Tsutsui et al., 2005). This could also play a pivotal role in hCMV-mediated abnormal neurontogeny and neuronal functions. Viral reactivation and lytic infection could occur when NSCs are stimulated to differentiate by specific stimuli, thus leading to brain malformations. In addition, persistent infection in glial cells and neurons may influence their functions, resulting in neurological disorders even in the absence of substantial anatomical abnormalities. This hypothesis not only supports the notion that hCMV infection of the fetal CNS is an ongoing process but also helps explaining why SNHL or ASD may be diagnosed

years after birth in congenitally infected children with no anatomical evidence of viral CNS involvement (Fig. 1.8).

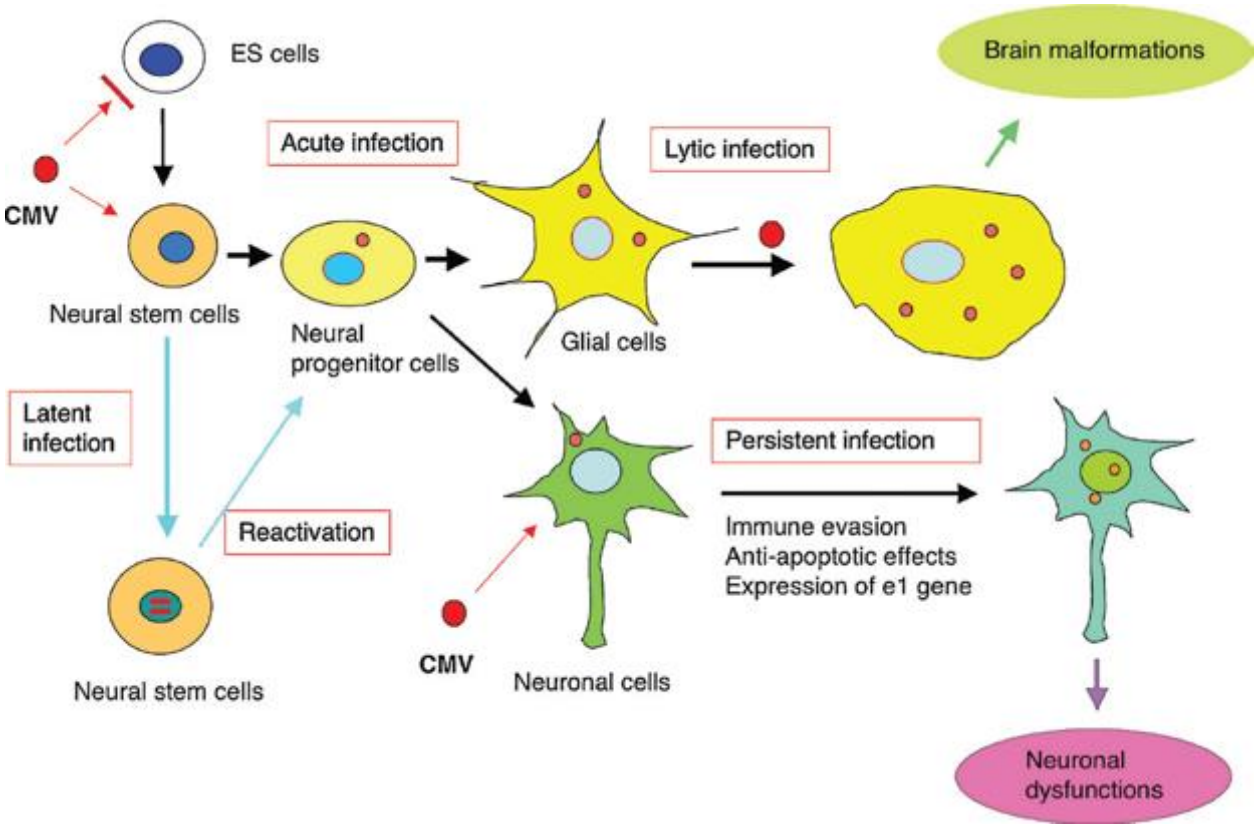

Fig. 1.8 Latency of human CMV in neuronal stem cells and its potential role in virally mediated abnormal neurontogeny. *In the early embryonic stage, embryonic stem (ES) cells are not susceptible to mCMV, whereas NSCs and NPSCs in the embryonic brains are highly susceptible. In acute infection, immature glial cells undergo lytic infection, resulting in brain malformations. Infection of embryonic brains with mCMV may become latent in NSCs. After a long time-period, this latent infection may be reactivated and become lytic, thus further contributing to brain damage. Also, latently infected neuronal or glial cells, derived from differentiation of infected NSCs, may function abnormally, thus leading to development of neurological disorders. Adapted from (Tsutsui et al., 2005).*

It is not completely clear why hCMV infection is particularly damaging to the developing brain in contrast to the adult brain. Findings from experimental models suggest that the developing cells of the CNS, i.e. NSPCs, are particularly susceptible to the lytic and/or apoptotic effects of CMVs (Cheeran et al., 2005; Tsutsui et al., 2005; Luo et al., 2008). The numbers of these cells decrease as the brain develops into adulthood and their spatial distribution becomes more localized to the VZ and cortical marginal areas (Kawasaki et al., 2002). In addition, another key reason for hCMV-mediated detrimental effects in the

developing brain is strictly related to the reduced efficacy of the immature innate and systemic immune response to hCMV in the immature CNS (van den Pol et al., 2002a; Reuter et al., 2004; Barry et al., 2006; van den Pol et al., 2007). In fact, hCMV can generate potentially life-threatening CNS infections also in adults with a compromised immune system, including transplant recipients and AIDS patients (Mercorelli et al., 2011; Mocarski et al., 2013).

1.4.1.3 Use of animal models for studying congenital human CMV pathogenesis and potential therapeutics.

The strict species specificity of CMV precludes experimental infection of animals with hCMV. Therefore, rodent CMVs (mouse, rat, and guinea pig) and rhesus macaque CMV (RhCMV) have been used as model systems to understand hCMV disease pathogenesis and to test the activity of novel vaccines and antiviral agents (Mocarski et al., 2007).

Murine CMV (mCMV) is by far the best and most extensively model system studied (Cheeran et al., 2009; Mussi-Pinhata et al., 2009). Murine CMV infection highly reproduces hCMV infection due to the genomic similarities and matching biological characteristics of these viruses in their natural setting (Rawlinson et al., 1996). Both mCMV and hCMV have large genomes consisting of about 230 kilobase pairs, containing 165-170 predicted ORFs, and with close similarities at the genetic and nucleotide level (Rawlinson et al., 1996). Also, both viruses cause severe infections in the immunocompromised or immunologically immature host, resulting in similar clinical syndromes with involvement of the same target organs (Kern, 1991, 2006). Therefore, the mCMV model represents an excellent tool for testing novel anti-CMV drugs and predicting their efficacy in hCMV-mediated disease since therapies effective against mCMV are highly likely to be similarly effective against hCMV. However, the use of this model for studying congenital hCMV infection has one important limitation, which is the lack of mCMV transplacental transmission due to both murine placenta architecture and immune response to mCMV infection (Cheeran et al., 2009). This has been overcome in the past with direct intra-endometrial, intra-placental, or intra-fetal mCMV inoculation, and peripheral infection of immunodeficient pregnant mice (Baskar et al., 1983; Baskar et al., 1987; Tsutsui, 1995; Kosugi et al., 1998; Li and Tsutsui, 2000; Tsutsui et al., 2005; Woolf et al., 2007; Tsutsui, 2009; Juanjuan et al., 2011; Sakao-Suzuki et al., 2014). In turn, transplacental transmission and fetal infection occurs naturally in other animal models, including rhesus macaque monkeys, guinea pigs, pigs, and rats (Barry et al., 2006; Kern, 2006; Loh et al., 2006; Schleiss, 2006a; Cheeran et al., 2009). Notwithstanding this, the murine model still represents the first choice for

pathogenesis studies and *in vivo* screening of anti-CMV compounds due to the short gestational period, the small size, the high availability of a large number of reagents, including transgenic and knockout animals, and the low cost (Kern, 2006).

Regardless of the mechanisms of transmission into the fetus, the ability of the virus to infect the brain is the single most important contribution to prognosis of hCMV infection in the fetus/neonate (Reuter et al., 2004; Tsutsui et al., 2005). Hence, it is a critically important experimental end-point to keep in perspective in the study of animal models of CMV-associated diseases during early development. When the murine placental and immune system barriers are circumvented by direct viral inoculation into the fetal compartment or by infecting immunodeficient pregnant mice (Baskar et al., 1983; Baskar et al., 1987; Tsutsui, 1995; Li and Tsutsui, 2000; Tsutsui et al., 2005; Woolf et al., 2007; Tsutsui, 2009; Juanjuan et al., 2011; Sakao-Suzuki et al., 2014), the fetal brain becomes susceptible to mCMV infection. The earliest infection can be demonstrated after embryonic day (E) 7.5, with mCMV-positive cells identified predominantly in the VZ and SVZ, the pyramidal layer of the hippocampus, and the cortex. Embryos that survive E12.5 placental infection show intrauterine growth retardation and microencephaly.

Murine CMV infection of the developing CNS has also been studied in neonatal mice since the newborn mouse brain and auditory organs are immature at birth, resembling those of an early second trimester human fetus (Clancy et al., 2001; Branchi et al., 2003; Clancy et al., 2007a; Clancy et al., 2007b; Workman et al., 2013). This a critical period of brain ontogeny where CMV can cause substantive dysfunction (Manicklal et al., 2013). Both intracranial (i.c.) and intraperitoneal (i.p.) mCMV inoculation have been used to establish CNS and cochlea infection in neonatal mice (Shinmura et al., 1997; Kosugi et al., 2000; Kosugi et al., 2002; van den Pol et al., 2002a; Koontz et al., 2008; Kosmac et al., 2013; Wang et al., 2013; Bradford et al., 2015; Ikuta et al., 2015; Li et al., 2015; Li et al., 2016; Almishaal et al., 2017; Carraro et al., 2017). However, the i.p. infection model presents some advantages as compared to the i.c. one, including neuroinvasion following viral hematogenous spread and peripheral control of viral replication by immune response before CNS infection. Both these aspects closely recapitulate events that occur during *in utero* hCMV fetal infection. In addition, the histopathology of the infected neonatal mouse brain resembles that of human infection with widely scattered foci of virus-infected cells associated with infiltrating mononuclear cells throughout the brain. Thus, by more accurately reflecting key aspects of hCMV fetal CNS infection, the i.p. murine model represents a better tool for studying

CMV-mediated neuropathogenesis and novel therapeutics for CMV infection of the developing CNS (Bantug et al., 2008; Koontz et al., 2008; Slavuljica et al., 2014).

1.5 Available anti-hCMV drugs and their mechanisms of action.

Five compounds are currently licensed to treat established hCMV infection in immunocompromised individuals: ganciclovir (GCV) and its oral prodrug valganciclovir (valGCV), foscarnet, cidofovir, and fomivirsen (Fig. 1.9) (Mercorelli et al., 2011).

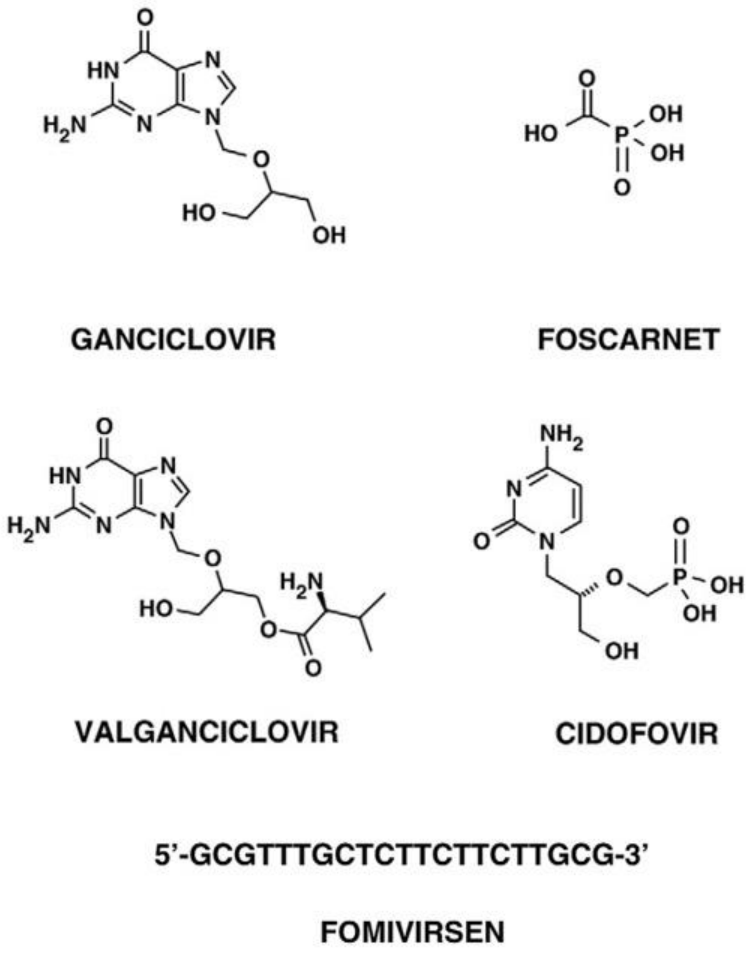

Fig. 1.9 Chemical structure of available drugs for treatment of established hCMV disease. *Adapted from (Mercorelli et al., 2011).*

GCV, an acyclic nucleoside analog of 2′-deoxyguanosine, was the first antiviral agent approved for hCMV infections, and remains the first-line choice for treatment of hCMV-mediated disease (Markham and Faulds, 1994; Razonable and Emery, 2004). In hCMV-infected cells, GCV is phosphorylated to

GCV monophosphate by the viral kinase encoded by the hCMV gene UL97 during infection. Subsequently, cellular kinases catalyze the formation of GCV diphosphate and GCV triphosphate, which is present in 10-fold greater concentration in hCMV-infected cells than uninfected cells. GCV triphosphate is a competitive inhibitor of deoxyguanosine triphosphate incorporation into DNA, thus inhibiting viral DNA polymerase activity in a potent fashion. Additionally, GCV triphosphate can serve as a poor substrate for the growing nucleic acid chain, thus terminating chain elongation and ultimately disrupting viral DNA synthesis (Fig. 1.10) (Matthews and Boehme, 1988; Coen and Richman, 2013; Chen et al., 2014).

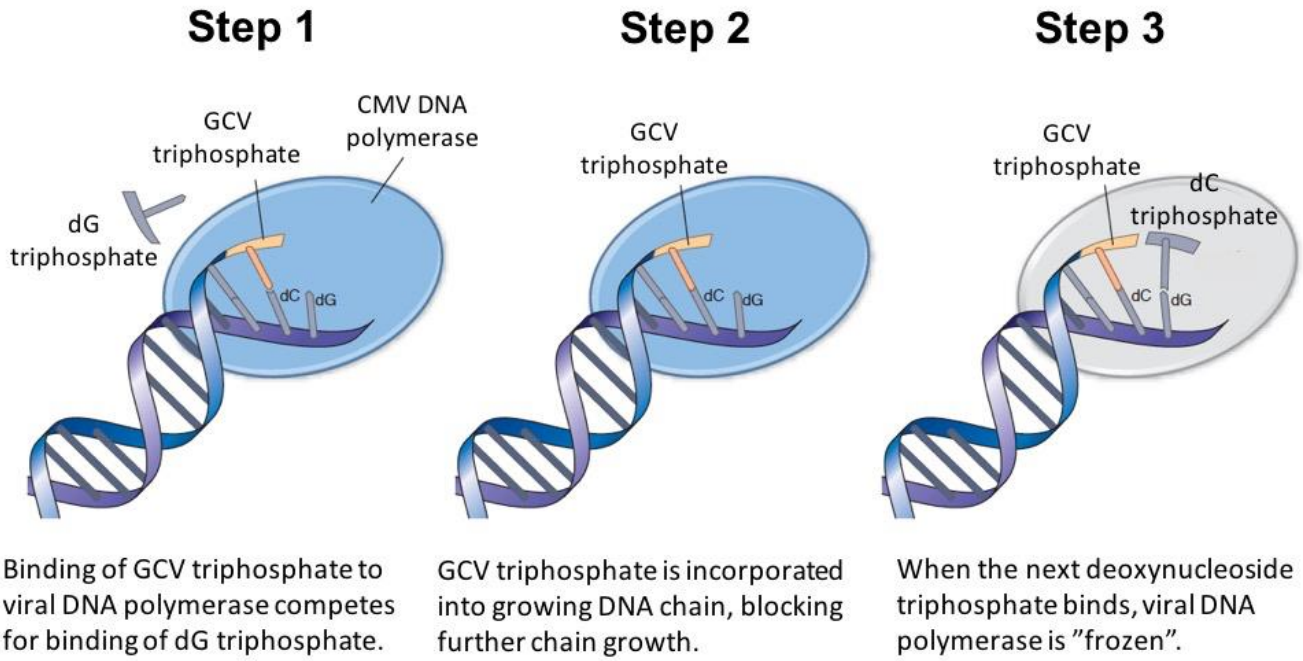

Fig. 1.10 Mechanisms of action of ganciclovir. *Ganciclovir (GCV) triphosphate has a three-step mechanism of inhibition of CMV DNA polymerase in vitro: (1) the drug triphosphate acts as a competitive inhibitor of deoxyguanosine (dG) triphosphate binding; (2) the drug triphosphate can act as a substrate and be incorporated into the growing DNA chain across from deoxycytosine (dC), terminating elongation; and (3) the viral DNA polymerase becomes trapped on the GCV triphosphate-terminated DNA chain when the dC triphosphate binds. Adapted from (Coen and Richman, 2013).*

While GCV requires intravenous administration, valGCV is orally bioavailable. ValGCV is the oral prodrug of GCV and after oral administration is rapidly converted to GCV by intestinal and hepatic esterases, achieving levels similar to intravenous GCV (Genentech USA, 2016).

Cidofovir is another anti-hCMV nucleoside analog which blocks viral DNA replication by inhibiting viral DNA polymerase activity and nucleic acid chain elongation, similarly to GCV and valGCV (Littler et al., 1992). Differently from GCV, cidofovir uses only cellular and not viral kinases for its phosphorylation and subsequent activation. Also, it results in nucleic acid chain termination only if two cidofovir residues are incorporated in a row in the growing DNA. Cidofovir requires intravenous administration and can induce substantial renal toxicity (Coen and Richman, 2013).

Although GCV, valGCV, and cidofovir inhibit the viral DNA polymerase more potently than the cellular DNA polymerases, a drug-mediated action on cellular polymerases occurs (Mar et al., 1985; Matthews and Boehme, 1988). This off-target activity can be particularly dangerous in the context of a developing human genome and cause substantial side-effects, which include bone marrow suppression, long-term gonadal toxicity with impaired fertility, carcinogenicity, and embryo and fetal toxicity and teratogenicity (Faulds and Heel, 1990; Markham and Faulds, 1994; Crumpacker, 1996; Lea and Bryson, 1996; Faqi et al., 1997; Gandhi and Khanna, 2004; Mercorelli et al., 2011; Genentech USA, 2016; Rawlinson et al., 2016).

Efforts have been made to discover less toxic anti-hCMV compounds that might inhibit viral polymerase by different mechanisms. The first of these to be approved for clinical use was foscarnet. Foscarnet is an analog of pyrophosphate, which is a product of polymerization of nucleic acids. Unlike GCV, valGCV, and cidofovir, foscarnet does not require activation by either cell or viral enzymes but rather inhibits hCMV DNA polymerase directly and selectively. Inhibition is not competitive with deoxynucleoside triphosphates. Rather, it appears that foscarnet acts as a product analog, preventing normal pyrophosphate release so the viral DNA polymerase cannot complete the catalytic cycle (Eriksson et al., 1982). Nonetheless, foscarnet displays substantial nephrotoxicity, resulting in electrolyte imbalance and potentially death (Biron, 2006). Therefore, it has been approved only for intravenous treatment of severe hCMV infections that are resistant to front-line anti-hCMV drugs (Coen and Richman, 2013).

Viral mutations in UL97 confers hCMV resistance to GCV and valGCV, but not to cidofovir and foscarnet, whereas viral DNA polymerase mutants are usually resistant to GCV, valGCV, and cidofovir. Also, although foscarnet inhibits DNA polymerase by a mechanism that differs substantially from the nucleoside analogs, many DNA polymerase mutants that are resistant to nucleoside analogs are resistant to foscarnet. Moreover, most foscarnet-resistant mutants are resistant to one or more nucleoside analogs (Gilbert and Boivin, 2005; Coen and Richman, 2013). The appearance of single- and multi-drug-resistant hCMV strains is a substantial issue in immunocompromised patients and a rising concern in neonates

with symptomatic congenital infection requiring prolonged antiviral therapy (Drew, 2000; James and Prichard, 2011; Campanini et al., 2012; Choi et al., 2013; Coen and Richman, 2013).

Fomivirsen is an antisense oligonucleotide that has been developed in the attempt to overcome the therapeutic limitations due to resistant hCMV strain emergence. Fomivirsen can inhibit hCMV replication by its complementarity to the messenger RNA for the major IE protein, an important regulatory protein of hCMV. Thus, fomivirsen acts on a different, earlier step of viral replication cycle as compared to the other available hCMV antivirals (Azad et al., 1993). However, this anti-hCMV drug has been approved only for ophthalmic use in AIDS patients with hCMV-induced retinitis due to evidence of substantial collateral effects associated with systemic drug administration (Mercorelli et al., 2011).

1.5.1 Therapeutic approaches to treat congenital human CMV.

Development of a vaccine focused on protecting newborns from the sequelae of congenital hCMV infection is a major public health priority, as identified by the National Vaccine Program Office and the Institute of Medicine (Institute of Medicine Committee to Study Priorities for Vaccine, 2000; Arvin et al., 2004). Although numerous candidate CMV vaccines are currently under development, an effective vaccine is not available yet (Arvin et al., 2004; Sung and Schleiss, 2010; Griffiths et al., 2013; Schleiss, 2013; James and Kimberlin, 2016; Rawlinson et al., 2016). Thus, anti-hCMV drugs would seem to represent the main therapeutic strategy available for congenital hCMV. However, the use of antivirals licensed for treating hCMV infection in immunocompromised individuals, i.e., GCV, valGCV, cidofovir, foscarnet, and fomivirsen, is substantially limited in hCMV-infected neonates due to acute and long-term toxicity and carcinogenicity. Most important, these drugs cannot be administered to pregnant mothers to prevent transplacental transmission and fetal infection or to treat their infected fetuses owing to drug-related potential for fetal toxicity and teratogenicity (Faulds and Heel, 1990; Markham and Faulds, 1994; Crumpacker, 1996; Lea and Bryson, 1996; Faqi et al., 1997; Gandhi and Khanna, 2004; Mercorelli et al., 2011; Genentech USA, 2016; Rawlinson et al., 2016). The poor oral bioavailability and the limited CNS penetration of the available antivirals, as well as the emergence of drug-resistant CMV strains, also pose a challenge (Mercorelli et al., 2011; Campanini et al., 2012; Choi et al., 2013; Morillo-Gutierrez et al., 2017).

GCV is used as off-label therapy for postnatally infected preterm neonates with life-threatening hCMV-mediated disease (Amin et al., 1990; Fischer et al., 2010; Okulu et al., 2012). Also, GCV and valGCV

are administered off-label in congenitally infected newborns with signs of infection at birth (Kimberlin et al., 2015). However, preventive therapy of asymptomatic congenitally infected neonates to avoid delayed onset of SNHL and/or neurological problems is not recommended due to the drug-related risk of acute and long-term severe toxicity, including neutropenia, gonadal toxicity, and carcinogenicity, even though potentially beneficial (Lackner et al., 2009). Considering that premature infants are at high risk for severe consequences of hCMV-mediated disease and drug-induced toxicity, that up to 15% of not treated asymptomatic congenitally infected neonates will go on to develop permanent neuro-sensorial sequelae, and that postnatal therapy, even though partially effective, is unlikely to revert *in utero* acquired brain damage, novel anti-CMV strategies with safer *in vivo* profiles, alternative mechanisms of action, and improved CNS penetration are urgently needed. The economic burden on the healthcare system in caring for neurodevelopmental disability in early childhood caused by congenital hCMV infection is substantial and represents a compelling argument for developing novel anti-CMV drugs.

In this context, hCMV-specific hyperimmune globulins have been investigated in an Italian multicenter randomized clinical trial (the 'CHIP' study) as potential safe therapeutic approach in pregnant mothers with primary hCMV infection to reduce viral load and prevent transplacental transmission and subsequent fetal infection (Revello et al., 2015). CMV hyperimmune globulins are obtained from donors with high titers of hCMV antibodies, and exert their anti-CMV activity by interacting with viral glycoproteins and therefore neutralizing hCMV infectivity. Unfortunately, the 'CHIP' study failed to show any benefits of this immune-based therapy, partly due to a smaller effect size than the one anticipated (Nigro et al., 2005). A similar trial is currently ongoing in the United States targeting to enroll 800 women, as compared to the 124 patients enrolled in the 'CHIP' trial, in order to possibly overcome an effect size issue and, thus, provide a definite answer on the role of hyperimmune globulins in prevention of congenital hCMV infection (ClinicalTrials.gov Identifier NCT01376778). Results are expected for late 2018. In the meantime, hyperimmune globulin treatment to prevent hCMV transplacental transmission in pregnant mothers with primary hCMV infection is not recommended (James and Kimberlin, 2016; Rawlinson et al., 2016; Leruez-Ville and Ville, 2017), even though sporadically used worldwide (Buxmann et al., 2012; Blazquez-Gamero et al., 2017).

Hyperimmune globulin administration has also been reported as treatment for fetuses with *in utero* signs of hCMV infection, even though no recommendation for their use exists in this situation either (Negishi et al., 1998; Nigro et al., 1999; Nigro et al., 2005; Nigro et al., 2008; Nigro et al., 2012a; Nigro et al., 2012b; Simioni et al., 2013; Nigro et al., 2015; James and Kimberlin, 2016; Rawlinson et al., 2016;

Blazquez-Gamero et al., 2017; De la Calle et al., 2017). Some studies suggest beneficial effects of immune therapy with improvement or complete disappearance of signs of infection during fetal life, including hyperechogenic bowel, intrauterine growth restriction, and ventriculomegaly. Therapy has also been associated with ameliorated/normal outcome at birth and up to 8 years of life (Nigro et al., 2005; Nigro et al., 2008; Nigro et al., 2012a; Nigro et al., 2012b; De la Calle et al., 2017). However, caution should be used in interpreting these results due to significant limitations related to study design.

A recent review focused on administration of endovenous GCV or oral valGCV to pregnant mothers as treatment for fetal hCMV infection (Seidel et al., 2017). A total of four cases are described, showing short-term safety of therapy for both the mother and the fetus and effective control of viral replication. Nonetheless, given that reliable evidence on drug safety and efficacy is still lacking, GCV or valGCV use during pregnancy in the setting of fetal infection is currently not recommended (James and Kimberlin, 2016; Rawlinson et al., 2016).

An antiviral compound, valaciclovir, has also been assessed in pregnant women with hCMV-infected fetuses and signs of mild fetal involvement at the ultrasound imaging in a European multicenter open-label study (Leruez-Ville et al., 2016b). Valaciclovir is a pro-drug of acyclovir and it is commonly used to treat herpes simplex virus (HSV) infections and chicken-pox. Even though valaciclovir is less effective than GCV and valGCV against hCMV *in vitro*, high dosages of this drug have proven efficacious to prevent hCMV infection and disease in high-risk immunocompromised individuals (Tyms et al., 1981; Lowance et al., 1999). This multicenter European study showed that administration of high-doses of valaciclovir to pregnant women reduces hCMV load in fetal blood and increases the proportion of asymptomatic newborns by 40% as compared to a historical cohort. However, the design of the study, i.e., not randomized and one-armed, substantially limits the assessment of the true antiviral effect of valaciclovir, thus preventing implementation of this therapy into clinical practice.

1.5.2. Homologs of valproate as novel potential treatments for congenital human CMV.

In the quest of novel, less toxic anti-CMV agents, we focused our attention on valpromide (VPD) and valnoctamide (VCD), compounds chemically related to valproate (valproic acid, VPA).

VPA is a widely prescribed antiepileptic drug employed for the treatment of multiple psychiatric and neurological diseases, including bipolar disorder, epilepsy, neuropathic pain, and migraine (Perucca, 2002). A free carboxylic group in the chemical structure (Fig. 1.11) and an inhibitory action on histone deacetylase (HDAC) confer teratogenic properties to VPA, which can cause neural tube defects, skeletal

abnormalities, and autism when administered during fetal development (Nau et al., 1991; Radatz et al., 1998; Phiel et al., 2001; Okada et al., 2004; Tung and Winn, 2010; Kataoka et al., 2013; Paradis and Hales, 2013, 2015).

VPD and its constitutional isomer VCD are amide derivatives of VPA (Fig. 1.11) and lack the inhibitory action on HDAC (Haj-Yehia and Bialer, 1990; Shekh-Ahmad et al., 2015). No increased risk of teratogenicity or toxicity has been reported for exposure to either compound in several studies using different treatment schedules in multiple animal models of early development (Nau and Loscher, 1986; Nau and Scott, 1987; Radatz et al., 1998; Okada et al., 2004; Shekh-Ahmad et al., 2014; Mawasi et al., 2015; Wlodarczyk et al., 2015; Bialer et al., 2017). Pregnant mice injected with either VPD or VCD during critical moments of organogenesis experienced rates of fetal loss, neural tube defects, and skeletal and visceral abnormalities similar to vehicle-injected pregnant controls. In turn, injection of VPA or other neuropsychiatric drugs, including risperidone and olanzapine, caused a substantial increase in rates of these adverse events. Further investigation of VCD head-to-head with VPA in rats and rabbits confirmed results obtained in mice, showing absence of VCD-induced teratogenicity. Several previous studies showed that slight changes in the chemical structure of VPA have a great impact on embryotoxic and teratogenic effects without affecting anticonvulsant activity (Hauck and Nau, 1989; Elmazar et al., 1993; Bojic et al., 1996). The amidation of the free carboxylic group of VPA in the molecule of VPD and VCD (Fig. 1.11) has been suggested to underlie the lack of HDAC inhibition and the greatly decreased teratogenicity and toxicity observed with these compounds as compared to VPA.

VPD and VCD have been marketed since the early 1960s as a mood stabilizer and an anxiolytic drug, respectively (Stepansky, 1960; Goldberg, 1961; Harl, 1964; Bialer, 1991). VCD has also been recently tested as a mood stabilizer in patients with acute mania (Bersudsky et al., 2010; Weiser et al., 2017), based on its ability to act on pathogenic mechanisms of bipolar disorder, i.e. increased brain arachidonic acid turnover and intracellular inositol concentrations (Shaltiel et al., 2007; Modi et al., 2014; Modi et al., 2017). Further, both drugs showed better CNS penetration (Blotnik et al., 1996) and a more potent anticonvulsant activity than VPA in multiple animal models of epilepsy (Lindekens et al., 2000; Isoherranen et al., 2003; Mares et al., 2013; Pouliot et al., 2013; Shekh-Ahmad et al., 2014; Shekh-Ahmad et al., 2015; Bialer et al., 2017).

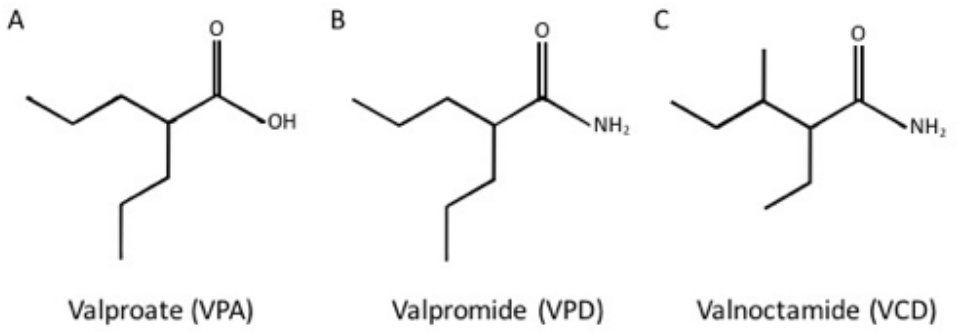

Fig. 1.11 Chemical structure of valproate, valpromide, and valnoctamide. *Adapted from (Haj-Yehia and Bialer, 1990).*

By inhibiting HDAC and thus causing chromatin hyperacetylation and increased cellular gene expression, VPA enhances the infectivity and replication of a large variety of viruses, including HIV (Moog et al., 1996), vesicular stomatitis virus (VSV) (Paglino and van den Pol, 2011), Kaposi's sarcoma-associated herpes virus (Shaw et al., 2000), HSV (Otsuki et al., 2008; Nakashima et al., 2015), HHV-6 (Mardivirin et al., 2009), and, more importantly, hCMV (Kuntz-Simon and Obert, 1995; Michaelis et al., 2004; Michaelis et al., 2005). In turn, both VPA and VPD attenuate reactivation of Epstein Barr virus (EBV), a herpes virus, from latency into the lytic phase of its life cycle (Gorres et al., 2014; Gorres et al., 2016). This antiviral activity is separated from HDAC inhibition, which VPD appears to lack. Treatment of EBV latently infected-cell cultures with either VPA or VPD prevents the expression of viral genes involved in EBV lytic reactivation. Also, VPD decreases the expression levels of cellular immediate-early genes, kinetically upstream of the EBV lytic cycle, when exogenously upregulated. In addition, both VPA and VPD block viral late protein synthesis after viral reactivation has occurred. The antiviral mechanism of VPA and VPD on EBV reactivation has been hypothesized to relate to their chemical structure and anticonvulsant activity (Gorres et al., 2016). VPD has a chemical structure similar not only to VPA but also to VCD (Fig 1.11). Further, VCD, similarly to VPD, has anticonvulsant properties and lacks activity on HDAC. Thus, a potential attenuating/blocking action of VPD and VCD on another herpes virus, hCMV, could be plausible. This constituted our rationale for assessing the potential antiviral activity of VPD and VCD against CMV.

1.6 Aims of the thesis.

The research presented in this thesis attempted to identify a novel and safe therapeutic approach for treating CMV infection during early development.

Congenital CMV infection is the leading viral cause of *in utero* acquired brain damage and neurological deficits in children and a major public health crisis in the developed world (Gandhi and Khanna, 2004; Cheeran et al., 2009; Tsutsui, 2009). However, few strategies are available to treat CMV infection during critical moments of brain ontogeny. Drugs approved for CMV, including GCV and its prodrug valGCV, cidofovir, foscarnet, and fomivirsen, show some efficacy but their use is not recommended during pregnancy due to their potential for fetal toxicity and teratogenicity (Mercorelli et al., 2011; James and Kimberlin, 2016). This causes a significant delay in treatment initiation and, since CMV-mediated CNS damage is irreversible once established, substantially decreases the chances of improving neuropathology and neurological outcomes in infected infants with postnatal therapy. GCV and valGCV are currently administered as off-label treatment in congenitally infected neonates with viral involvement of the CNS (Kimberlin et al., 2003; Kimberlin et al., 2015). However, acute toxicity, namely severe neutropenia, and long-term toxicity, such as fertility impairment and carcinogenicity, limit the use of these drugs only to those newborns with severe signs of infection at birth (Crumpacker, 1996; Gandhi and Khanna, 2004; Mercorelli et al., 2011; Rawlinson et al., 2016). This leaves less severely affected neonates with no treatment and, hence, at high risk for developing late-onset neurological complications (Lackner et al., 2009). The emergence of drug-resistant CMV strains and the limited CNS penetration of available antivirals also pose a challenge in the long-term treatment of congenital CMV (Mercorelli et al., 2011; Campanini et al., 2012; Choi et al., 2013; Morillo-Gutierrez et al., 2017). Thus, it is evident that novel anti-CMV strategies with alternative mechanisms of action, improved CNS targeting, and safer *in vivo* profiles that could be used both during pregnancy and in all infected newborns, are urgently needed. The substantial public health economic burden of congenital CMV-related neurological disability represents a compelling argument for developing alternative anti-CMV drugs.

Previous research investigating VPA and VPD in the context of EBV infection identified a drug-mediated block of viral reactivation from latency. The anti-EBV activity of VPA and VPD appeared to be separated from HDAC inhibition, which VPD lacks, and based on attenuation of both viral and cellular gene expression (Gorres et al., 2014; Gorres et al., 2016). The mechanism by which VPA and VPD suppress EBV reactivation has been postulated to relate to their chemical structure and anticonvulsant activity. Since VPD shares similar chemical structure and anti-seizure action with VCD (Haj-Yehia and Bialer, 1990; Lindekens et al., 2000; Isoherranen et al., 2003; Mares et al., 2013; Pouliot et al., 2013; Shekh-Ahmad et al., 2014; Shekh-Ahmad et al., 2015; Bialer et al., 2017), we hypothesized that both compounds could also act against CMV, a herpes virus as EBV. Of note, differently from VPA, neither

VPD nor VCD inhibits HDAC, thus lacking teratogenicity (Haj-Yehia and Bialer, 1990; Radatz et al., 1998; Okada et al., 2004; Shekh-Ahmad et al., 2014; Mawasi et al., 2015; Shekh-Ahmad et al., 2015; Wlodarczyk et al., 2015; Bialer et al., 2017). Also, both drugs have been clinically used for many years to treat neuropsychiatric disorders and no toxicity-related concerns have been raised (Stepansky, 1960; Goldberg, 1961; Harl, 1964; Bialer, 1991; Bersudsky et al., 2010; Weiser et al., 2017). Importantly, VPD and VCD show better distribution into the brain after peripheral administration than VPA, a fact that may improve targeting of CMV inside the brain (Blotnik et al., 1996).

Investigation of novel therapeutic properties of compounds already approved for treatment of different disorders, i.e. drug repurposing, has been strongly promoted in the last few years (Collins, 2011; Huang et al., 2011; Nosengo, 2016; Sharlow, 2016). This is especially true in those research areas, including congenital CMV, with limited pharmaceutical company investments due to disease (relative) rarity and high costs and failure rates (Scannell et al., 2012). Of note, drug repositioning has recently proven of extremely high value in identifying additional therapeutic applications for already known drugs (Singh et al., 2013; Singh et al., 2016; Xu et al., 2016). Given that VPD and VCD have been already clinically used, they both appear to offer all the promise of drug repurposing, thus further supporting their investigation in the context of congenital CMV infection.

Chapter 2

Materials and Methods

2.1 Cells.

NIH/3T3 (CRL-1658) and Vero (CCL-81) cells were purchased from the American Type Culture Collection (ATCC) (Manassas, VA), normal human dermal fibroblasts (HDF) were obtained from Cambrex (Walkersville, MD), Neuro-2a (CCL-131) were kindly provided by A. Bordey (Yale University, New Haven, CT), U-373 MG cells were a gift from R. Matthews (Syracuse, NY), and primary human fetal brain astrocytes were obtained from Science Cell Research Laboratories.

Vero cells were grown and maintained in Eagle's Minimum Essential Medium (MEM) supplemented with 10% fetal bovine serum (FBS) and 1% penicillin streptomycin (Pen Strep; Invitrogen, Carlsbad, CA). Human fetal astrocytes were grown in poly-L-lysine-coated culture vessels and maintained in Astrocyte Medium (from ScienCell Research Laboratories) supplemented with 2% FBS and 1% Pen Strep. All the other cell lines were maintained in Dulbecco's modified Eagle's essential medium (DMEM) supplemented with 10% FBS and 1% Pen Strep. Primary cultures of mouse glia were established using whole brain tissue harvested from P5 mice and maintained in DMEM (van Den Pol et al., 1999).

All cultures were kept in a humidified atmosphere containing 5% CO_2 at 37°C.

2.2 Viruses.

A brief description of each virus used is given below.

2.2.1 mCMV-GFP.

Recombinant mCMV (MC.55) expressing enhanced green fluorescent protein (GFP) was derived from the K181 strain. The expression cassette containing the GFP gene controlled by the human elongation factor 1 alpha (EF1-alpha) promoter was inserted into the IE gene site (IE-2). NIH/3T3 cells were used for viral propagation and titering by plaque assay (van Den Pol et al., 1999).

2.2.2 hCMV-GFP.

Recombinant hCMV expressing GFP under the control of the EF1-alpha promoter was derived from the Toledo strain. The gene coding for GFP was inserted between US9 and US10 of the hCMV genome, a site that appears to tolerate alterations without affecting viral replication. GFP expression and replication capability were tested on normal human fibroblasts and U-373 human glioblastoma cells (Ma et al., 2005). Human dermal fibroblasts were used for viral propagation and titering by plaque assay.

Recombinant CMVs were generously provided by E. Mocarski (Emory University, Atlanta) and J. Vieira (University of Washington, Seattle).

2.2.3 VSV-GFP.

A recombinant variant of the Indiana serotype of VSV expressing a GFP reporter gene from the first genomic position (VSV-1'GFP) (Ramsburg et al., 2005) was kindly provided by J. K. Rose (Yale University, New Haven, CT). Vero cells were used for viral propagation and titering by plaque assay (van den Pol et al., 2002b).

All the viruses used in the present study express GFP as a reporter and green fluorescence was employed to visualize infected cells and viral plaques. Viral titers were determined by standard plaque assay using 25% carboxy-methyl-cellulose (CMC) overlay for mCMV-GFP and hCMV-GFP (Zurbach et al., 2014) or 0.5% agar overlay for VSV-GFP. Viral stocks were stored in aliquots at -80°C. For each experiment, a new aliquot of virus was thawed and used.

2.3 Chemicals.

VPD (catalog no. V3640), VCD (catalog no. V4765), VPA (catalog no. S0930000), ivermectin (catalog no. I88998), GCV (catalog no. G2536), and heparan sulfate (HS) sodium salt (catalog no. H7640) were purchased from Sigma-Aldrich (St. Louis, MO).

VPA and HS were dissolved in water to give a stock solution of 1 M and 1 mg/mL, respectively. VPD, VCD, ivermectin, and GCV were dissolved in dimethylsulfoxide (DMSO) to yield a stock solution of 1 M (VPD, VCD) and 100 mM (ivermectin, GCV). Ivermectin was used at 1 µM, a concentration recently shown effective against Chikungunya and other alphaviruses (Varghese et al., 2016).

2.4 Quantification of infection.

Effects of the tested compounds on CMV infection were assessed by viral infectivity assay, viral yield reduction assay, and plaque number and size reduction assay.

For the infectivity assay, cells (NIH/3T3, Neuro-2a, mouse glia, Vero, normal human dermal fibroblasts, U-373, and human fetal astrocytes) were seeded at a density of 40,000 cells per well in 48-well plates and incubated overnight before medium (0.2 mL/well) was replaced for pre-treatment with VPA, VPD, VCD, ivermectin, or vehicle at the specified concentrations. After 1 hour or 24 hours of drug exposure, cells were inoculated with virus at different multiplicity of infection (MOI) and incubated at 37°C for 2

h to allow viral adsorption. Following incubation, cultures were washed twice with PBS and overlaid with a viscous solution containing the test compounds/vehicle in cell line-specific medium and CMC or agar. GFP-positive cells were counted at 48 or 72 hours post-infection (hpi).

In the virus yield reduction assay, after viral adsorption, cells were washed twice with PBS and replenished with fresh medium containing the compounds to be tested. At 72 or 96 hpi, medium was collected and titered by plaque assay using NIH/3T3 (mCMV) and HDF (hCMV) monolayers to assess the drug-mediated inhibition of virus replication.

For the plaque number reduction assay, cells pre-treated with drugs or vehicle for 24 h were infected with mCMV-GFP or hCMV-GFP, incubated for 2 h at 37°C to allow viral adsorption, rinsed twice with PBS, and overlaid with a viscous solution containing the tested agents at the specified concentrations in DMEM (75%) and CMC (25%) for 50% effective concentrations (EC_{50}) calculation (Zurbach et al., 2014). Plates were then incubated at 37°C in 5% CO_2 for 4 days (mCMV) and 7 days (hCMV), to allow time for fluorescent plaque development. The mean plaque counts for each drug concentration were expressed as a percentage of the mean plaque count of the control (vehicle). The EC_{50} was then calculated by nonlinear regression from the plots of log drug concentrations against percentage of reduction in plaque number at each antiviral compound concentration.

Plaque size reduction assay was used to assess the effect of the drugs on viral propagation. Briefly, semiconfluent NIH/3T3 and HDF cells in 12-well plates were inoculated using mCMV-GFP and hCMV-GFP (MOI 1), respectively. After 2 h-incubation at 37°C, inoculum was removed and cultures were washed three times with PBS before the addition of CMC overlay containing VPD, VCD, or vehicle at the specified concentrations. Five (mCMV) and 10 (hCMV) days later, the relative size of viral plaques was measured (n=60 plaques/condition), as previously described (Wollmann et al., 2015).

Infected cells were identified as GFP-positive cells using an Olympus IX71 fluorescence microscope (Olympus Optical, Tokyo, Japan) connected to a SPOT RT digital camera (Diagnostic Instruments, Sterling Heights, MI) interfaced with an Apple Macintosh computer. The total number of fluorescent cells per well in each condition was counted by two observers independently. Each condition was tested at least in triplicate, and the whole experiment repeated twice. Camera settings (exposure time and gain) were held constant between images. The contrast and color of collected images were optimized using Adobe Photoshop.

2.5 Assessment of antiviral actions of valpromide and valnoctamide on human CMV.

2.5.1 Time-of-drug addition and CMV promoter (IE1/IE2)-driven reporter plasmid transfection experiments.

To investigate in detail which step of the viral replicative cycle was affected by VPD and VCD, 'time-of-drug addition' experiments were performed, in which human cell cultures were inoculated with hCMV and exposed to the drugs immediately, or 2 h, or 12 h after viral challenge. The effects of the tested agents on hCMV infection were then assessed by a viral yield reduction assay. Briefly, HDF cells were infected with hCMV-GFP (MOI 0.01) (t=0), exposed to the compounds (100 μM) as indicated above, and incubated until the media was collected at 96 hpi. The extent of virus replication was subsequently assessed through titering the media by plaque assay using HDF monolayers. In all conditions, 2 hpi cultures were rinsed twice with PBS to synchronize infection.

To assess the effects of drug on the immediate early phase of viral replication, NIH/3T3 cells exposed to VPD (1 mM) for 24 h, were transfected with a CMV promoter (IE1/IE2)-driven reporter plasmid (pCMV-tdTomato) expressing the red fluorescent protein tdTomato.

2.5.2 Virucidal activity assay.

To test the potential virucidal effect of the compounds, VPD, VCD, or vehicle (100 μM) were added to undiluted aliquots of hCMV-GFP and these virus/compound mixtures were incubated at either 4°C or 37°C for 2 h. After incubation, the samples were diluted with culture medium to reduce the drug concentration to an ineffective dose (10 nM), and hCMV-GFP infectivity was determined by plaque assay on HDF cells. Alternatively, virus and drug mixtures were run through a 0.1 μm filter (Life Sciences) to remove the compounds but not the hCMV (size ~180 nm). Filter membranes were then thoroughly rinsed in culture medium for 2 h at room temperature with periodic shaking to harvest drug-free hCMV before assessing infectivity by plaque assay on HDF monolayers.

2.5.3 Viral entry analysis and quantitative real-time PCR assay.

To evaluate the effects of the drugs on hCMV entry into the cell, i.e. reversible attachment to the cell membrane and subsequent irreversible binding with fusion and adsorption, inoculated cultures were first incubated at 4°C (which allows only virus attachment) and then shifted to 37°C (which allows fusion and subsequent steps of the viral replication cycle) (Mocarski et al., 2007; Chan and Yurochko, 2014).

For assessing the 'attachment' step, pre-chilled HDF cells and human fetal astrocytes at 90% confluency in a 6-well plate were treated with VPD, VCD, vehicle (100 μM), VPA (1 mM, negative control), or HS (0.1 mg/mL, positive control) for 1 h at 4°C and inoculated with pre-cooled hCMV-GFP (MOI 0.1) in the presence of compounds or vehicle for 2 h at 4°C. Cells were then rinsed three times with cold PBS to remove unattached virions and compounds, and harvested by trypsinization for viral DNA quantification using a quantitative real-time PCR (qRT-PCR) assay (HDF cells and human fetal astrocytes) (Chan and Yurochko, 2014), or overlaid with CMC and incubated for 3 days at 37°C for infectivity assessment by GFP-positive cell counting (HDF cells).

To evaluate hCMV internalization into HDF cells and human fetal astrocytes, cultures plated in plain media were inoculated with hCMV-GFP (MOI 0.1) and incubated at 4°C for 2 h. Cells were then washed three times to remove unbound viral particles, exposed to compounds or vehicle at the same concentrations described above, and incubated at 37°C for 2 h (to allow virus internalization) before being overlaid with CMC for infectivity evaluation at 72 hpi (HDF cells) or being harvested by trypsinization for DNA quantification by qRT-PCR (human fetal astrocytes).

DNA was extracted from cells using the QIAamp DNA mini kit (Qiagen), and qRT-PCR was performed using TaqMan assays (Life Technologies) (Gault et al., 2001; Fukui et al., 2008) for hCMV UL132 (Pa03453400_s1) and human albumin (Hs99999922_s1) genes. Ten-fold dilutions of hCMV DNA and cellular DNA from human fibroblasts or human fetal astrocytes were used as quantitative standards. qPCR was carried out with 20-μL reaction mixtures employing the iTaq Universal SYBR Probes Supermix (BioRad) and 100 ng of DNA. Samples from uninfected cells and without a template served as negative controls. Samples from 2 biological replicates were run in duplicate using a Bio-Rad iCycler-IQ instrument (Bio-Rad, Hercules, CA), and results were analyzed with iCycler software. The amount of viral DNA in each sample relative to albumin was calculated using the comparative threshold (CT) cycle method, and hCMV DNA was expressed as the percentage of virus bound (the "attachment" step) or internalized (the "internalization" step) using DMSO-treated samples as 100%.

2.6 Immunocytochemistry.

A mouse monoclonal antibody (a gift of Dr. P. Cresswell, Yale University) against hCMV gB, diluted 1:1000 in PBS with 0.3% Triton X-100, was used to label cells infected with hCMV, as an alternative method to the GFP reporter used for quantification of infection.

A mouse monoclonal antibody against hCMV immediate early (IE)1/2 antigen (1:1000, MAB810, EMD Millipore) was employed to assess drug-mediated effects on IE protein expression.

The secondary antibody was a goat anti-mouse immunoglobulin conjugated with Alexa Fluor 594 (Thermo Fisher Scientific) diluted at 1:500. Cell nuclei were counterstained with DAPI (4′-6′-diamidino-2-phenylindole). Controls included the omission of the primary antibody and the use of non-inoculated cultures where no immunostaining was expected or found.

2.7 Cytotoxicity assay.

An ethidium homodimer assay (EthD-1, Molecular Probes, Eugene, OR) was used to label dead cells. Briefly, NIH/3T3 cells (9 X 10^4 per well) were seeded in a 48-well plate and treated with VPD or vehicle for 24 h before mCMV-GFP inoculation (MOI 0.03). 72 h after viral challenge, cells were washed twice and EthD-1 was added at a final concentration of 4 µM in DMEM. After 20 min of incubation at 37°C, the total number of dead cells per well was counted based on red fluorescence of nuclei. Each condition was tested in quadruplicate, and each experiment was repeated twice. Similarly, the rate of cell death was assessed in uninfected NIH/3T3 and HDF cells exposed to VPD, VCD, vehicle (10 and 1 mM), or plain media for 24 and 72 h before EthD-1 addition.

2.8 Animal infection paradigms, treatment administration, and in vivo testing.

All animal breeding and experiments were performed in accordance with the guidelines of the Yale School of Medicine Institutional Animal Care and Use Committee (IACUC). Research was approved by the IACUC.

Male and female Balb/c strain mice (6-8 weeks of age) from Taconic Biosciences Inc. (Hudson, NY) were maintained on a 12:12 h light cycle under constant temperature (22±2°C) and humidity (55±5%), with access to food and water *ad libitum*. One to two females were cohabited with a male of the same strain for at least 1 week to ensure fertilization. When advanced pregnancy was seen, each pregnant female was caged singularly and checked for delivery twice daily, at 8:30 A.M. and 6:30 P.M. Newborns were inoculated i.p. with 750 plaque-forming units (pfu) of mCMV-GFP in 50 µL of media on the day of birth (DOB), within 14 h of delivery. The DOB was considered to be postnatal day 0 (P0). Control animals received 50 µL of media intraperitoneally. Here we focus on inoculation of newborn mice as a model where brain development in the newborn mouse parallels human brain development during the early second trimester of pregnancy (Clancy et al., 2001; Branchi et al., 2003; Clancy et al., 2007a;

Clancy et al., 2007b; Workman et al., 2013). This is a critical period for human brain development where CMV can cause substantive dysfunction (Manicklal et al., 2013). To avoid any litter-size effect, large litters were culled to a maximum of eight to nine pups (Tanaka, 1998). Infected and control pups were randomly assigned to receive VPD, VCD, or vehicle (DMSO), via subcutaneous (s.c.) injections, once a day, at a dose of 1.4 mg/mL in 20 µL of saline (28 µg/mouse), starting 24 hours after virus inoculation and running from P1 to P21. In some initial experiments, control pups received a similar amount of drug-free saline. Mice were monitored daily for signs of mCMV-induced disease and to determine survival; weaning occurred on P21 and mice of either sex were housed separately until testing was completed, then sacrificed.

In addition to the intraperitoneal route, intracranial injection was performed in a group of newborn mice. Three days after birth, 2 X 10^4 pfu of mCMV-GFP in 1 µL of media was injected into the left cerebral hemisphere of neonatal mice under cryoanesthesia using a 10 µL Hamilton syringe with a 32-gauge needle from a midpoint between the ear and eye. Infected pups were randomly assigned to receive daily doses of VCD or vehicle (DMSO), starting 3 h after virus inoculation until P8. No deaths occurred, and at P9 mice were killed and blood, liver, spleen, and brain were collected, snap frozen, and stored at -80°C until viral titer analysis via qRT-PCR (n=8/experimental group) was performed.

2.8.1 Early somatic and neurobehavioral assessment.

Intraperitoneally infected pups and controls were assessed for early postnatal somatic and neurobehavioral development, as previously described (Fox, 1965; St Omer et al., 1991; Calamandrei et al., 1999; Scattoni et al., 2008). Evaluation was performed without knowledge of the treatment group on every other day from P0 to P22 for somatic parameters and from P2 to P14 for neurobehavioral assessment.

Pups were weighed to the nearest 0.01g and their body and tail lengths were measured. Hair growth, status of eyelid and pinnae detachment, and incisor eruption were also recorded. These somatic variables were rated semi-quantitatively in the following way: 0=no occurrence of the condition, 1=slight/uncertain condition, 2=incomplete condition, and 3=a complete adult-like condition (Scattoni et al., 2008).

Evaluation of neurobehavioral development was performed according to a slightly modified Fox battery (Fox, 1965; St Omer et al., 1991; Calamandrei et al., 1999), in the light phase of the circadian cycle between 9 A.M. and 3 P.M. Each subject was tested at approximately the same time of the day.

Reflexes and responses were scored in the following order: 1) righting reflex, the time used by the pup to turn upright with all four feet when placed on its back; 2) cliff aversion, when placed on the edge of a cliff or table top with the forepaws and face over the edge, the mouse will turn and crawl away from the edge; 3) forelimb grasping reflex, when the forefoot is stroked with a blunt instrument the foot will flex to grasp the instrument; 4) forelimb placing reflex, contact of the dorsum of the foot against the edge of an object will cause the foot to raise and place itself on the surface of the object when the animal is suspended and no other foot is in contact with a solid surface; 5) negative geotaxis, the time used by the pup to turn180° to either side when placed head down on a wire mesh screen (4 X 4 mm) held at a 45° angle; 6) level screen test, pup holds onto a wire-mesh (10 X 10 cm) and is propelled across the mesh horizontally by the tail; 7) screen climbing test, pup climbs up a vertical screen (10 X 10 cm, 90° angle) using both forepaws and hindpaws; maximal response, scored when the subject reaches the top of the vertical screen; and 8) vibrissa placing reflex, when the mouse is suspended by the tail and lowered so that the vibrissae make contact with a solid object, the head is raised and the forelimbs are extended to grasp the object.

Latencies were measured in seconds using a stopwatch for righting reflex and negative geotaxis. The remaining behavioral variables were rated semi-quantitatively, similarly to early postnatal somatic parameters: 0=no response or occurrence of the event (R/O); 1=slight/uncertain R/O; 2=incomplete R/O; and 3=a complete adult-like R/O. All timed responses were limited to a maximum of 60 s; therefore, the absence of a milestone was scored as 0/60 s (semi-quantitative rating/latencies) if the mouse did not exhibit the behavior within 60 s.

This battery of tests provides a detailed assessment of functional and neurobehavioral development throughout the neonatal period since the behaviors measured are each expressed at different stages of development during the first weeks of life. Specific information about vestibular function, motor development and activity, coordination, and muscle strength can be obtained by execution of these tests (St Omer et al., 1991; Schneider and Przewlocki, 2005).

2.8.2 Evaluation of motor coordination and balance in adolescent mice.

Motor performance of infected and control mice, with or without VCD treatment, was assessed at P28-30 by the hindlimb-clasping, vertical pole, and challenging beam traversal tests.

In the hindlimb-clasping test, the mouse is gently lifted by the tail, grasped near its base, and the hindlimb position is observed for 10 s and scored as follows: if the hindlimbs are consistently splayed outward,

away from the abdomen, it is assigned a score of 0; if one hindlimb is retracted toward the abdomen for 50% of the time suspended, it receives a score of 1; if both hindlimbs are partially retracted toward the abdomen for 50% of the time suspended, it receives a score of 2; and if its hindlimbs are entirely retracted and touching the abdomen for 50% of the time suspended, it receives a score of 3 (Tanaka et al., 2004; Guyenet et al., 2010).

The vertical pole test was conducted according to previously established protocols (Ogawa et al., 1985; Soerensen et al., 2008). Briefly, mice were individually placed head downward at the top of a vertical rough-surfaced pole (diameter, 8 mm; height, 55 cm) and allowed to descend in a round of habituation. Then, mice were placed head upward at the top of the pole. The time required for the animal to descend to the floor was recorded as the locomotor activity time (T_{LA}), with a maximum duration of 120 s. If a mouse fell, was unable to turn downward, or was unable to climb down, a default locomotor activity time value was recorded as 120 s. Each mouse was given three trials with a 30-s recovery period between trials.

The challenging beam traversal test was performed as previously described (Fleming et al., 2004; Fleming et al., 2013). The beam consisted of four sections (25 cm each, 1 m total length), each section having a different width. The beam started at a width of 3.5 cm and gradually narrowed to 0.5 cm in the last section. Underhanging ledges (1 cm width) were placed 1 cm below the top surface of the beam to increase the sensitivity of the test and allow detection of subtle motor deficits (Brooks and Dunnett, 2009). Animals were trained to traverse the length of the beam starting at the widest section and ending at the narrow most difficult section. The narrow end of the beam led directly into the home cage of the animal. A bright light illuminated the start of the beam to further encourage the mouse to walk across the beam toward the home cage. Animals received 2 days of training before testing, with five trials for each day. On the day of the test, a mesh grid (1 cm squares) of corresponding width was placed over the beam surface leaving a 1 cm space between the grid and the beam surface. Animals were then videotaped while traversing the grid-surfaced beam for a total of five trials. Videos were viewed and rated in slow motion for hindlimb slips and time to traverse across five trials by an investigator blind to the mouse experimental group. A slip was counted when the mouse was facing and moving forward and a hindlimb slipped through or outside of the grid beyond 0.5 cm below the grid surface (halfway down).

2.8.3 Social behavior and exploratory activity analysis.

Sociability and preference for social novelty were investigated at 5 weeks of age in a three-compartment apparatus (Crawley, 2007; Yang et al., 2011).

Initially, test and control animals were allowed to explore the apparatus freely for a 10-m period (habituation). For the social approach paradigm, an unfamiliar conspecific (same sex, similar age and weight) animal was placed into one of the side compartments and restrained by a small wire object ("social cage"). The compartment on the other side contained an empty wire object ("empty cage"). The test subject was then released into the center compartment and allowed to explore the three-compartment apparatus freely for 10 m. Behavior was videotaped and assessed for the times that the test subject spent in the three compartments and in close proximity to the social and empty cages.

For the social novelty paradigm, another unfamiliar conspecific animal was placed in the previously empty wire object ("novel cage"). The behavior of the test mouse was recorded for 10 m and assessed for the time spent exploring the known and novel conspecifics.

The exploratory activity was assessed in adolescent mice at P30-40 in an adapted small open field, as previously described (Shi et al., 2003; Schneider and Przewlocki, 2005). The apparatus consisted of a plastic rectangular box measuring 20.5 X 17 X 13 cm^3 (length X width X height) with regularly spaced holes in the short (n=2) and long (n=3) walls, and illuminated by ambient fluorescent ceiling lights. The animal was placed in the center of the apparatus and its movements were video recorded over a 3-m period. Exploratory behavior was scored for the number of rearing and nose-poking (nose of an animal put inside the hole) episodes.

2.9 Assessment of murine CMV distribution in the brain and viral-mediated brain abnormalities.

At specific time points after infection, mice were killed by an overdose of anesthetic and transcardially perfused with sterile, cold PBS followed by 4% paraformaldehyde, and brains were harvested and weighed. Brains were then immersed overnight in 4% paraformaldehyde, and cryoprotected in 15% and then 30% sucrose for 24 h before inclusion in Tissue Freezing Medium (General Data). In a few mice, also livers and spleens were collected. Some intraperitoneally infected mice became dehydrated and moribund and showed no sign of recovery; these mice were killed before the predefined killing time points and were recorded as having had a lethal response to the virus.

Fifteen-micrometer-thick sections cut with a Leica cryostat were used for GFP reporter expression assessment and immunofluorescence analysis in the brain. Sections were dried for 4 h at room temperature, rehydrated in 1X PBS, and then used for immunofluorescence assays. Briefly, tissue

sections were incubated overnight at 4°C with monoclonal mouse anti-NeuN antibody (1:500; catalog #MAB377, EMD Millipore; RRID: AB_2298772) for neuronal cells and polyclonal rabbit anti-calbindin D-28K (1:500; catalog #AB1778, EMD Millipore; RRID: AB_2068336) for cerebellar Purkinje cells (PCs). Tissues were washed three times in phosphate buffer plus 0.4% Triton X-100. Secondary antibodies, including goat anti-mouse IgG and donkey anti-rabbit IgG conjugated to Alexa Fluor-594 (1:250; Invitrogen), were applied for 1 h at room temperature and then washed off. Some sections were labeled with DAPI. Vectashield Fluorescent mounting medium (Vector Laboratories) was then used for mounting.

Images were collected by using a fluorescence microscope (model IX 71, Olympus Optical).

Frozen sections were used for morphometric measurements, and cell numbers were quantified after imaging using ImageJ software (https://imagej.nih.gov/ij/; RRID: SCR_003070). The molecular layer (ML) and internal granular layer (IGL) were assessed using images of serial midsagittal cerebellar sections stained with calbindin D-28K and DAPI. Three measurements were taken at each side of the primary fissure in each section, and four sections per animal were evaluated. For the cerebellar area, midsagittal brain sections (three sections/mouse) were stained with blue fluorescent Nissl stain (NeuroTrace, catalog #N21479, Thermo Fisher Scientific), and images were collected using a 2X objective. Cell counts were performed on sections (four sections/mouse) stained with calbindin D-28K, and the number of Purkinje cells was evaluated along 500 µm of the primary fissure (both sides). All measurements and quantifications were performed on at least five animals from three different litters.

2.10 Kinetics of virus spread and replication in vivo.

For detection of infectious viral load in organs, plaque assay analysis and qRT-PCR were performed.

In initial experiments, some of the control and experimental mice were sacrificed on P12, after receiving saline/treatment from P1 to P10. Designated mice were transcardially perfused with PBS to wash out free virus, and tissue samples were collected under sterile conditions from liver, spleen, and lungs, target organs of congenital CMV infection. Tissues were mechanically homogenized in PBS using a microcentrifuge tube tissue grinder. Part of the resulting tissue suspension was plated onto NIH/3T3 monolayers and viral titer was assessed by plaque assay (Brune et al., 2001; Zurbach et al., 2014).

Viral replication in blood, liver, spleen, and brain was also evaluated by means of qRT-PCT. Mice receiving either VCD or vehicle intraperitoneally or intracranially were killed at multiple time points

post-inoculation, and samples were collected under sterile conditions, snap frozen, and stored at -80°C until viral titer analysis via qRT-PCR (n 7-10/experimental group) was performed. Mice used for viral load analysis in liver, spleen, and brain were perfused with sterile cold PBS to remove any virus contained within the blood. Total DNA was isolated using the QIAamp DNA Mini Kit (Qiagen) as per manufacturer instructions. Quantitative PCR was performed using TaqMan assays (Life Technologies) by amplification of a fragment of mCMV IE1 gene exon 4 using the following primers: forward, 5'-GGC TTC ATG ATC CAC CCT GTT A-3'; and reverse, 5'-GCC TTC ATC TGC TGC CAT ACT-3'. The probe (5'-AGC CTT TCC TGG ATG CCA GGT CTC A-3') was labeled with the reporter dye FAM (Kosmac et al., 2013). qRT-PCR was performed using 20 µl reaction mixtures using the iTaq Universal SYBR Probes Supermix (Bio-Rad) and 100 ng of DNA. Samples were run in duplicate using a two-step amplification protocol. Tissue samples from uninfected mice and samples without a template served as negative controls. Viral burden was expressed as the copy number per ml/gram of blood/tissue after comparison with a standard curve generated using serial 10-fold dilutions of mCMV DNA.

2.11 Experimental design and statistical analysis.

Statistical significance in *in vitro* experiments, unless otherwise specified, was determined using one-way Analysis of Variance (ANOVA), followed by Bonferroni's *post hoc* test. Data are presented as percentage of infected or dead cells and viral titers, in drug versus vehicle, as mean±SEM of two independent experiments; each independent experiment consisted of three or four cultures; p-values refer to a comparison of drug to control (vehicle). EC_{50} values were calculated using nonlinear regression curve fit with a variable slope (log[inhibitor] vs response).

Statistical significance for *in vivo* experiments, including motor performance, exploratory behavior, and brain morphometry, was determined by one-way ANOVA or Kruskal-Wallis test followed by Bonferroni's and Dunn's *post hoc* test, respectively. Early somatic and neurobehavioral development, social behavior, and viral load over time were assessed by a mixed-model ANOVA with repeated measures followed by Newman-Keuls test if there was a significant F value. Since no gender-related differences were detected in early neurodevelopment, data from male and female mice were combined. Only male mice were used for examination of motor performance and exploratory and social behavior. Somatic and neurobehavioral assessment was performed blindly with respect to the experimental group.

All analyses were conducted with GraphPad Prism version 6.0 (RRID: SCR_002798), with significance set at $p < 0.05$.

Chapter 3

Results

3.1 Initial in vitro and in vivo screening of valpromide and valnoctamide as potential anti-CMV compounds.

Previous research reported an inhibitory role of VPD on reactivation of the herpes virus EBV from latency, based on attenuation of both viral and cellular gene expression (Gorres et al., 2014; Gorres et al., 2016). Thus, we decided to investigate VPD as a potential antiviral against CMV, another herpes virus (Ornaghi et al., 2016) (see Appendix). Since the anti-EBV action of VPD has been suggested to relate to its chemical structure and anticonvulsant activity (Gorres et al., 2014; Gorres et al., 2016), we also tested VCD (Ornaghi et al., 2016), which shares similar chemical structure and anti-seizure action with VPD (Haj-Yehia and Bialer, 1990; Lindekens et al., 2000; Isoherranen et al., 2003; Mares et al., 2013; Pouliot et al., 2013; Shekh-Ahmad et al., 2014; Shekh-Ahmad et al., 2015; Bialer et al., 2017). Both VPD and VCD appear to lack toxicity and teratogenicity (Stepansky, 1960; Goldberg, 1961; Harl, 1964; Haj-Yehia and Bialer, 1990; Bialer, 1991; Radatz et al., 1998; Okada et al., 2004; Bersudsky et al., 2010; Shekh-Ahmad et al., 2014; Mawasi et al., 2015; Shekh-Ahmad et al., 2015; Wlodarczyk et al., 2015; Bialer et al., 2017; Weiser et al., 2017).

3.1.1 Valpromide inhibits mouse and human CMV in vitro.

We first assessed and compared the effects of VPD and VPA on both mCMV and hCMV in *in vitro* experiments, using several cell types exposed to either drugs or vehicle for 24 h before viral challenge.

In line with previous reports, VPA treatment enhanced infection by and replication of mCMV on mouse fibroblast cells at concentrations of 1 and 10 mM (Fig. 3.1, A-C) (Kuntz-Simon and Obert, 1995; Michaelis et al., 2004; Michaelis et al., 2005). In turn, VPD at the same concentrations showed a robust inhibitory effect (Fig. 3.1, D-F), reducing the number of mCMV-infected fibroblasts as quantified by counting cells expressing the viral GFP reporter gene (Fig. 3.1, D and E). VPD also attenuated mCMV replication as assessed by viral yield assay (Fig. 3.1F). Of note, significant inhibition was identified not only at 10 and 1 mM but also at lower doses of 100 μM, 1 μM, and 100 nM.

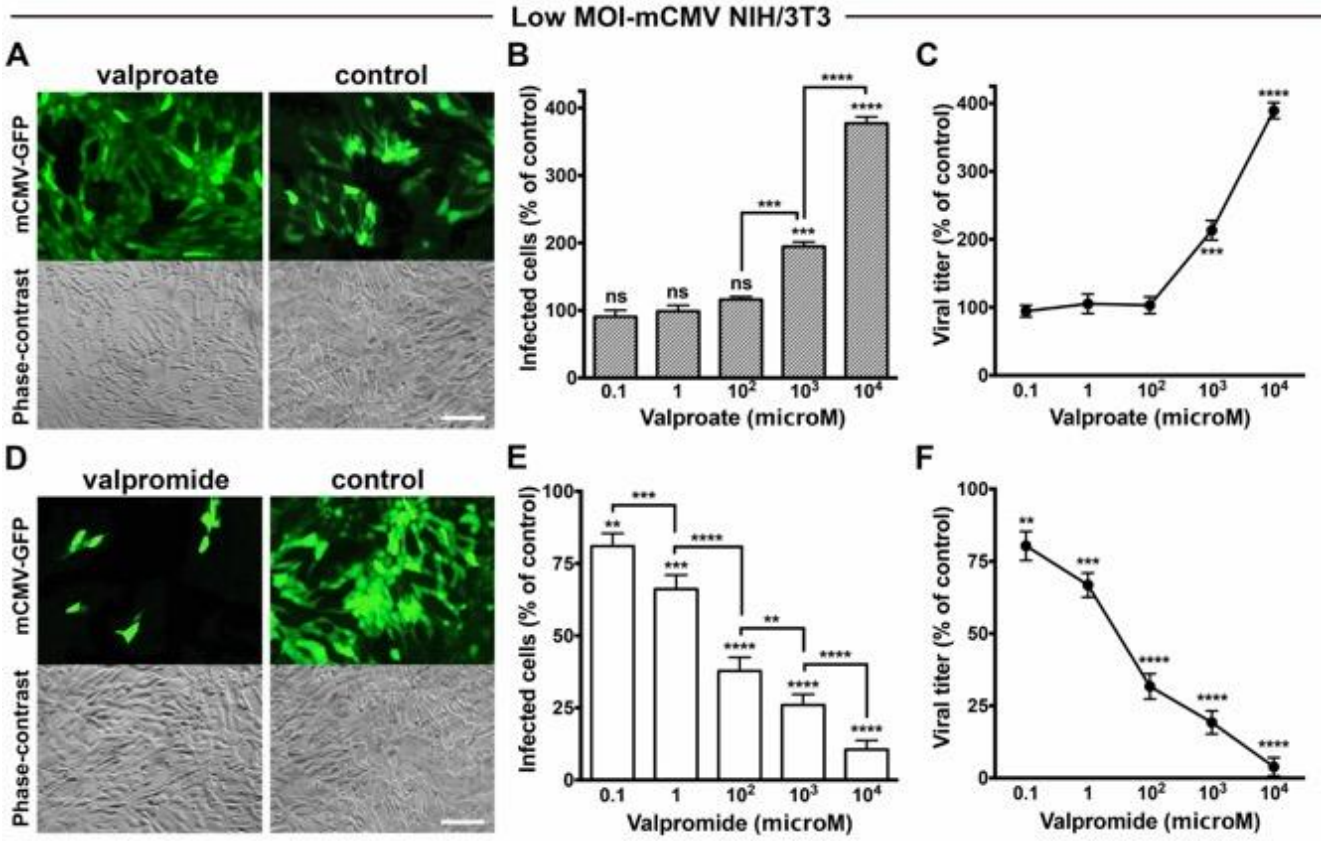

Fig. 3.1 Valproate and valpromide exert opposing effects on low titer-murine CMV. A*. Representative microscopic fields show mCMV-GFP reporter fluorescence and phase contrast of NIH/3T3 cells pre-treated (24 h) with VPA (1 mM) or vehicle (control) prior to inoculation with mCMV using multiplicity of infection (MOI) of 0.03. Photos captured 48 hpi; scale bar 50 µm.* ***B, C.*** *VPA dose-dependent increase in mCMV infection assessed by counting infected GFP-positive cells at 48 hpi (****B****) and viral yield assay at 72 hpi (****C****); other conditions same as* ***A****.* ***D.*** *VPD (1 mM) with other conditions same as* ***A****.* ***E, F.*** *VPD dose-dependent decrease in mCMV infection, as per number of infected cells at 48 hpi (****E****) and viral titer at 72 hpi (****F****); other conditions same as* ***A****. Mean±SEM of 8 cultures (****B, C, E, F****); ns, not significant, **p<0.01, ***p<0.001, ****p<0.0001, as compared to control, ANOVA with Bonferroni's post hoc test.*

Attenuation of mCMV was confirmed at high virus titer and in multiple cell types including NIH/3T3, Neuro-2a, and primary astrocytes from mouse brain (Fig. 3.2, A-D).

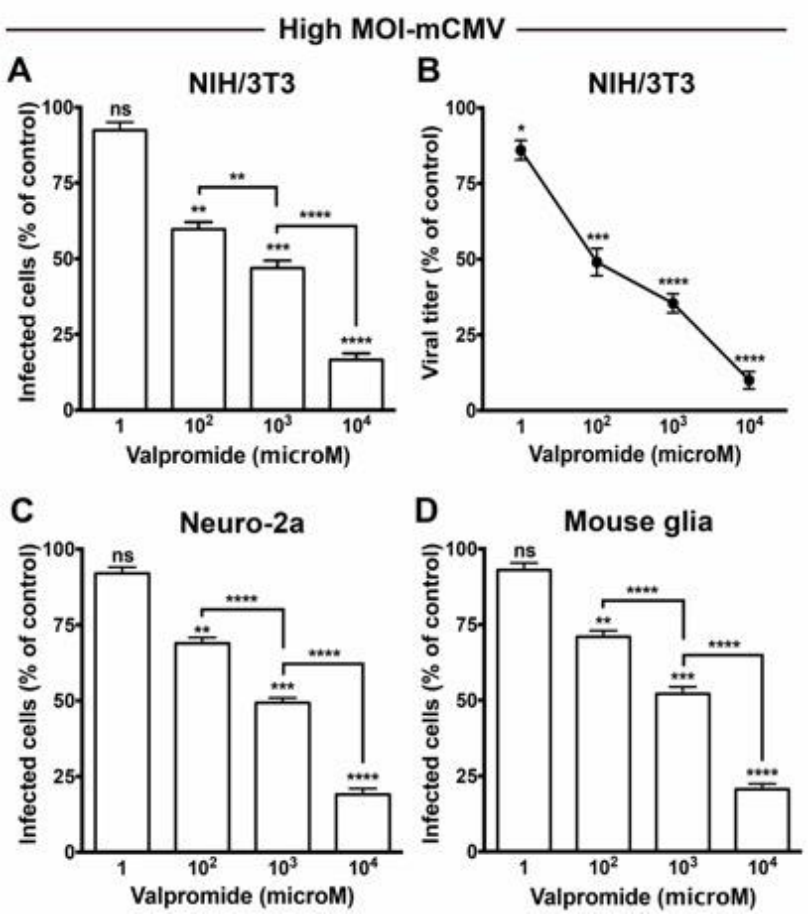

Fig. 3.2 Valpromide reduces infectivity of high titer-murine CMV in multiple cell types. A-D. *VPD dose-dependent decrease in high titer-mCMV (MOI 4) infectivity in NIH/3T3 (**A, B**), immortalized Neuro-2a (**C**), and primary mouse glia (**D**) cells pre-treated with VPD for 24 h. Infectivity assessed by counting GFP-positive cells 24 hpi (**A, C, D**), and by viral yield assay 72 hpi (**B**). Mean±SEM of 6 cultures; ns, not significant, *p<0.05, **p<0.01, ***p<0.001, ****p<0.0001, as compared to control, ANOVA with Bonferroni's post hoc test.*

The anti-mCMV effect observed for VPD could be the result of a drug-mediated cytotoxicity and subsequent reduction of viral survival and replication. Therefore, we tested uninfected NIH/3T3 cells treated for 24 or 72 h with VPD at 1 and 10 mM for cell death. Using an EthD-1 assay to fluorescently label dead cells, we saw no detectable cytotoxicity (Fig. 3.3A), thus suggesting a lack of toxicity of the target cells even at high drug concentrations and with prolonged cell exposure. In turn, VPD-related mCMV inhibition increased cell survival by reducing viral-induced cytotoxicity (Fig. 3.3, B and C).

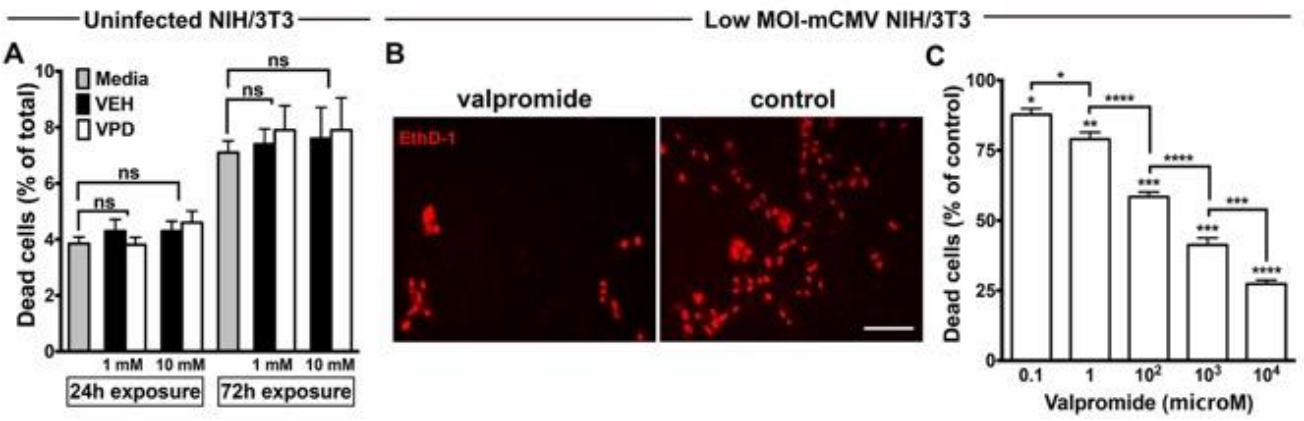

Fig. 3.3 Valpromide is not toxic for uninfected cells and decreases murine CMV-induced cytotoxicity. A. *The potential cytotoxicity of VPD exposure for 24 and 72 h was assessed in uninfected mouse fibroblasts by the red fluorescent EthD-1 assay. The effect of VPD at 1 and 10 mM on NIH/3T3 was compared with vehicle (VEH) at the same concentrations and plain media.* ***B, C.*** *The EthD-1 assay was performed to evaluate VPD protective role on viral-mediated cytotoxicity. Images show red fluorescent photomicrographs of NIH/3T3 cells pre-treated with VPD or vehicle at 10 mM for 24 h prior to viral inoculation (MOI 0.03). 72 hpi, EthD-1 was added to cells. After 20 min, photos were captured (**B**) and red fluorescent-labeled cells were counted (**C**). Scale bar 50 µm. Mean±SEM of 8 cultures (**A, C**); ns, not significant, *p<0.05, **p<0.01, ***p<0.001, ****p<0.0001, as compared to control, ANOVA with Bonferroni's post hoc test.*

To determine if the inhibitory action of VPD would generalize from mCMV to hCMV, we tested VPD against hCMV on human cells. Similar to mCMV, hCMV infection was substantially inhibited by VPD at all the doses tested, independent of virus titer or cell type (Fig. 3.4, A-C). VPD significantly reduced the number of hCMV infected cells and also decreased hCMV replication, even at the low drug concentrations of 100 µM, 1 µM, and 100 nM. We found similar inhibitory actions with both human dermal fibroblasts (Fig. 3.4, A and B) and human glioma cells (Fig. 3.4C).

To corroborate the view that the drug acted on CMV rather than by inhibiting expression of the viral GFP reporter, we used immunocytochemistry to label the hCMV gB (Fig. 3.4D). VPD decreased the number of cells showing hCMV gB immunoreactivity compared to infected cultures not treated with VPD. This result further supports the antiviral effect of VPD on CMV and excludes a potential VPD-mediated inhibitory effect on GFP expression.

The VPD-mediated inhibition of both mouse and human CMV raised the question of whether the antiviral effect of the drug was universal for different types of virus and might act via enhancement of an innate immune block of viral infection in general.

To address this question, we tested VSV, an unrelated single-strand RNA virus sensitive to upregulation of innate immunity. In contrast to mCMV and hCMV, VPD did not inhibit VSV (Fig. 3.4E), suggesting that the observed anti-CMV actions of VPD were not based on a mechanism involving a potentiation of the innate immune response.

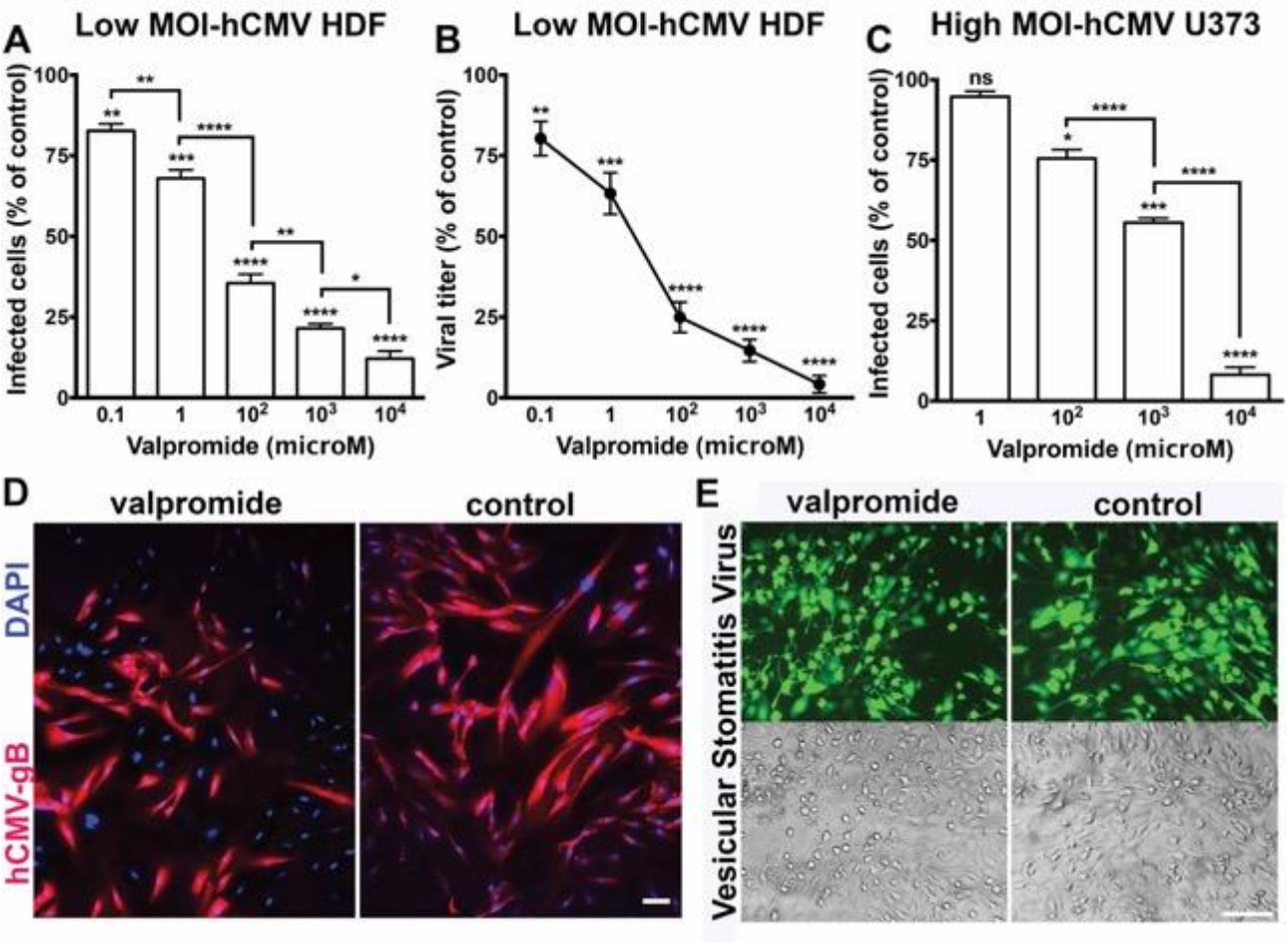

Fig. 3.4 Valpromide inhibits human CMV but has no effect on vesicular stomatitis virus infection. A, B. *Normal human dermal fibroblasts (HDF) were treated with VPD or vehicle at the indicated concentrations for 24 h prior to hCMV-GFP inoculation (MOI 0.01). VPD dose-dependent decrease in hCMV infection assessed by counting infected GFP-positive cells at 72 hpi (**A**) and viral yield assay at 96 hpi (**B**). **C.** Pre-treated human glioma cells infected with hCMV-GFP at high titer (MOI 4). GFP-positive cells counted at 48 hpi. Data presented as mean±SEM of 8 cultures (**A, B**) and 6 cultures (**C**); ns, not significant, *p<0.05, **p<0.01, ***p<0.001, ****p<0.0001, as compared to control, one-way ANOVA (Bonferroni's post hoc test). **D.** Immunostaining for hCMV gB was done to exclude a potential inhibitory effect of VPD on GFP expression. HDF were exposed to VPD or vehicle (1 mM) for 24 h prior to viral challenge (MOI 1). Representative fields with hCMV gB immunoreactivity in red and cell nuclei in blue (DAPI) show VPD-mediated decrease in the relative number of*

infected cells. Scale bar 50 µm. ***E.*** *Images of representative microscopic fields under GFP fluorescence (top) and phase contrast (bottom) of Vero cells pre-treated with VPD or vehicle at 1 mM for 24 h and infected with VSV-GFP (MOI 0.001). No drug-mediated inhibitory effect was identified (101%±5%, compared to control; mean±SEM of 6 cultures). Photos captured at 24 hpi; scale bar 50 µm.*

For control purposes, we also tested ivermectin, a compound with anti-epileptic properties and a strong anti-parasitic activity, which was recently shown to attenuate alphavirus infection (Varghese et al., 2016). Ivermectin had no effect on CMV (99%±9% compared to control), demonstrating that the anti-CMV effect was specific for VPD.

Together these results demonstrate that VPD substantially and selectively inhibits both mouse and human CMV infectivity *in vitro*, and that this antiviral activity is independent of virus titer and cell type.

3.1.2 Valnoctamide, a safer analog of valpromide, blocks mouse and human CMV in cell culture.

Although VPD safety has been demonstrated in animal models of teratogenesis (Radatz et al., 1998; Okada et al., 2004), these findings may not translate to humans where, differently from mice, VPD can be quickly metabolized (>80%) to VPA (Bialer, 1991), which is teratogenic and enhances CMV infection as shown earlier.

VCD is structurally similar to VPD and has shown potent anticonvulsant properties in multiple animal models of epilepsy (Lindekens et al., 2000; Isoherranen et al., 2003; Mares et al., 2013; Pouliot et al., 2013; Shekh-Ahmad et al., 2014; Shekh-Ahmad et al., 2015; Bialer et al., 2017), in part by a mechanism that prolongs miniature inhibitory post-synaptic currents (Spampanato and Dudek, 2014). VCD also lacks the free carboxylic group and HDAC inhibitory activity associated with the embryotoxic and teratogenic effects of VPA (Bialer et al., 1990; Radatz et al., 1998; Shekh-Ahmad et al., 2014; Mawasi et al., 2015; Wlodarczyk et al., 2015; Bialer et al., 2017), and, unlike VPD, shows negligible conversion to its corresponding free acid (valnoctic acid) not only in mice but also in humans (Bialer et al., 1990; Bialer, 1991; Barel et al., 1997; Radatz et al., 1998). Therefore, we tested VCD on mCMV and hCMV *in vitro*.

VCD induced a potent inhibition of mCMV infection independent of virus titer or cell type (Fig. 3.5, A-F), as measured by counting cells expressing the GFP virus reporter or assessing virus replication. Significant anti-CMV activity was still identified in the nanomolar range. Similarly, VCD also blocked infectivity and replication of hCMV at both low and high titer in human fibroblasts (Fig. 3.5, G-I).

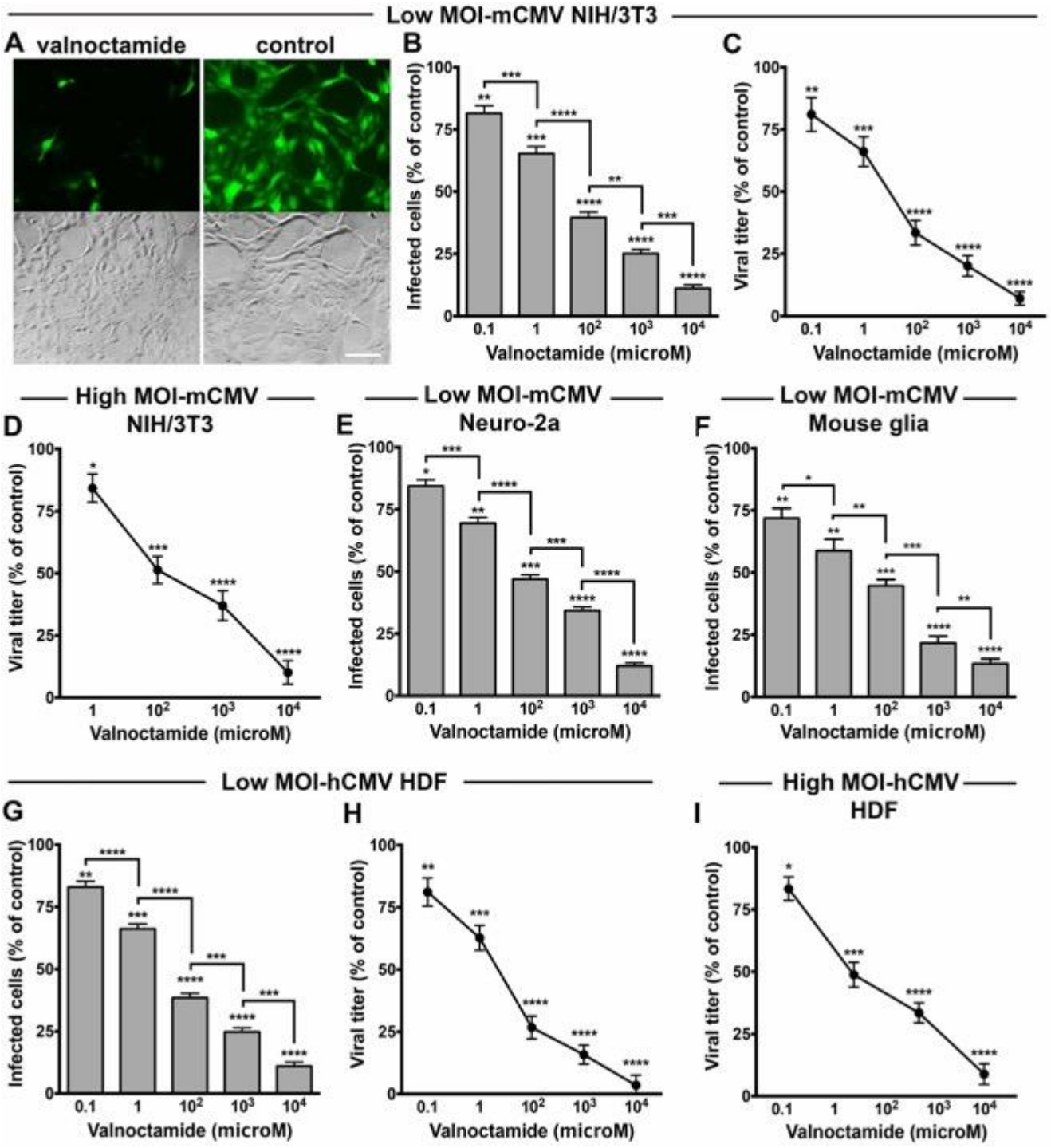

Fig. 3.5 Valnoctamide blocks both murine and human CMV. A. *Microscopic fields show GFP fluorescence (top) and phase contrast (bottom) of NIH/3T3 cells pre-treated (24 h) with VCD (1 mM) or vehicle (control) prior to inoculation with mCMV (MOI 0.03). Photos captured 48 hpi; scale 50 µm.* ***B-F****. VCD-mediated dose-dependent decrease in mCMV infection at low MOI (0.03) (**B, C, E, F**) and high MOI (4) (**D**) in NIH/3T3 (**B-D**), Neuro-2a (**E**), and mouse glia (**F**) cells pre-treated for 24 h, as assessed by counting infected GFP-positive cells at 48 hpi*

*(**B, E, F**) and viral yield assay at 72 hpi (**C, D**). **G-I.** VCD-mediated decrease in hCMV infection at low MOI (0.01) (**G, H**) and high MOI (1) (**I**) in human dermal fibroblasts, evaluated by GFP-positive cell counting at 72 hpi (**G**) and viral yield assay at 96 hpi (**H, I**). Mean±SEM of 8 (**B, C, E-H**) and 6 (**D, I**) cultures; *p<0.05, **p<0.01, ***p<0.001, ****p<0.0001, as compared to control, one-way ANOVA (Bonferroni's post hoc test).*

3.1.3 Dose-response analysis comparison among valpromide, valnoctamide, ganciclovir, and heparan sulfate.

GCV and HS are well-known inhibitors of CMV infection. GCV targets viral DNA polymerase and is approved as first-line CMV treatment in humans (Mercorelli et al., 2011). HS acts as a soluble mimic of HSPGs, cell surface anionic polysaccharides used by CMV for attachment to the cell membrane (Compton et al., 1993). HS is not approved as anti-CMV drug due to its strong anticoagulant activity *in vivo*, an undesired side-effect.

Since our *in vitro* experiments demonstrated a substantial inhibition of CMV infectivity and replication by both VPD and VCD, we compared the antiviral potency of VPD and VCD with that of GCV and HS.

A dose-escalation analysis by means of plaque reduction assay was performed in HDF cells infected with hCMV (MOI 0.01). Fibroblasts treated with VPD or VCD displayed a substantial dose-dependent inhibition of hCMV infectivity with an EC_{50} concentration of 2.9±1.3 μM and 3.5±1.1 μM, respectively (Fig. 3.6, A and B). No cytotoxic effects were identified in uninfected HDF cells exposed to VPD or VCD at 10 mM for 72 hours as compared to vehicle and plain media (Fig. 3.6C), thus defining an excellent selectivity index (SI), i.e. the ratio of cytotoxic concentration $(CC)_{50}$ to EC_{50}, for both compounds against hCMV.

Similarly, hCMV infectivity was inhibited by both GCV and HS in a dose-dependent manner with EC_{50} of 1.1±0.3 μM for GCV (Fig. 3.6D) and 51.4±8.2 μg/mL (~80 μM) for HS (Fig. 3.6E).

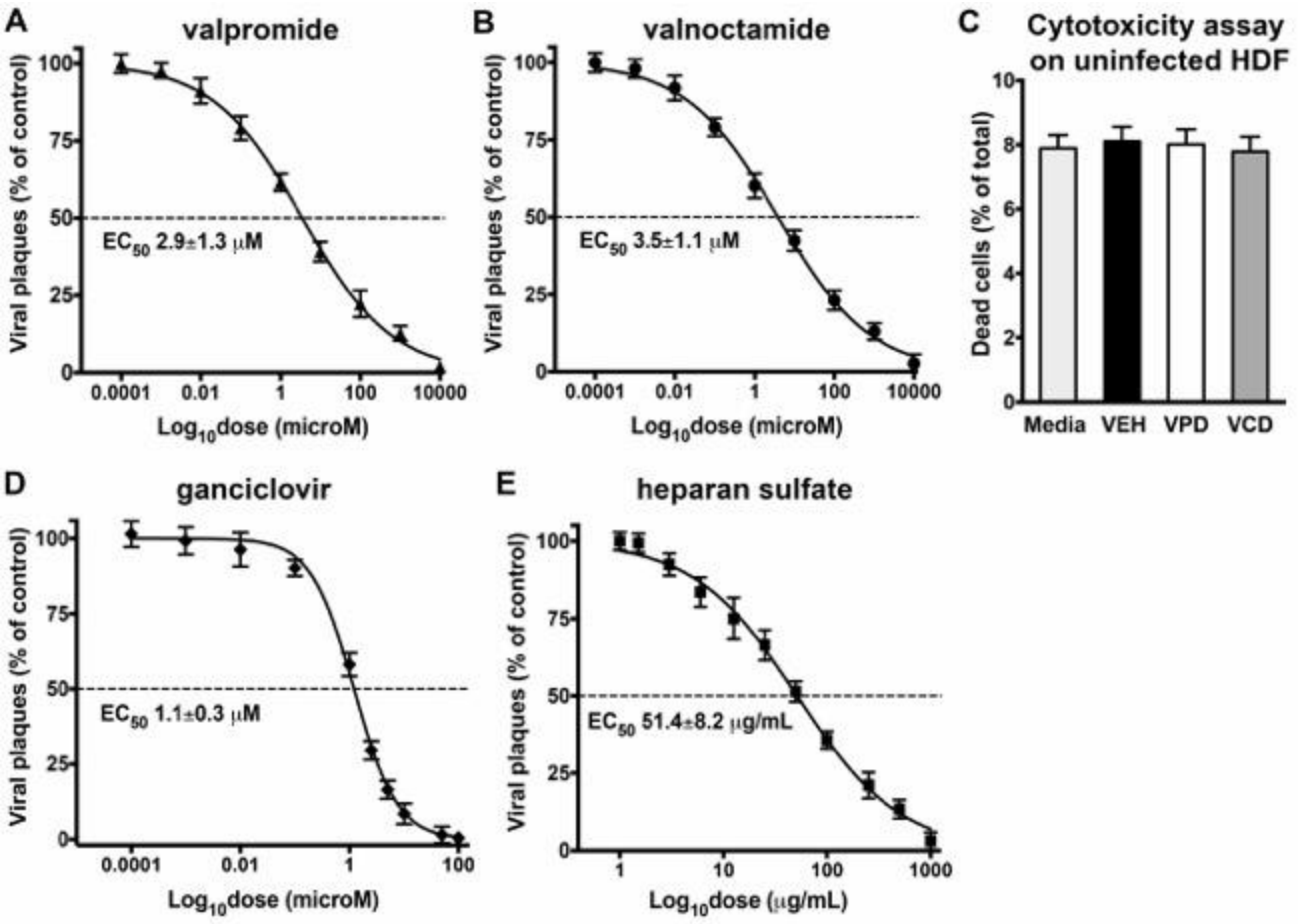

Fig. 3.6 Valpromide and valnoctamide safely suppress hCMV infectivity with potency similar to ganciclovir. A, B. *HDF cells pre-treated with VPD (**A**) or VCD (**B**) for 24 h and infected with hCMV-GFP (MOI 0.01) were incubated for 7 days before viral fluorescent plaques counting. The mean plaque count for each drug concentration was expressed as a percentage of the control (vehicle) and plotted as a function of the drug dose in logarithmic scale. The concentration producing 50% reduction in plaque formation (EC_{50}) is shown. Mean±SEM of 2 independent experiments.* ***C.*** *The potential cytotoxicity of 10 mM-VPD and VCD exposure for 72 h was assessed in uninfected HDF cells by the EthD-1 assay and compared with vehicle (VEH) at the same concentration and plain media. Mean±SEM of 6 cultures; one-way ANOVA (Bonferroni's post hoc test).* ***D, E.*** *Dose-response analysis by plaque reduction assay in HDF cells pre-treated with known anti-CMV agents, GCV (**D**) and HS (**E**); other conditions same as **A, B**.*

3.1.4 Valpromide and valnoctamide substantially attenuate CMV-related disease in vivo.

Human CMV infection during early development can cause serious and potentially fatal disease in fetuses and neonates (Mocarski et al., 2013), in whom therapeutic options are severely limited by the

teratogenicity and toxicity of available antivirals (Mercorelli et al., 2011; James and Kimberlin, 2016; Rawlinson et al., 2016).

Both VPD and VCD showed substantial block of CMV infection *in vitro*. Also, no toxic effects have been reported for either compound in multiple animal models of early development and treated human subjects (Stepansky, 1960; Goldberg, 1961; Harl, 1964; Haj-Yehia and Bialer, 1990; Bialer, 1991; Radatz et al., 1998; Okada et al., 2004; Bersudsky et al., 2010; Shekh-Ahmad et al., 2014; Mawasi et al., 2015; Shekh-Ahmad et al., 2015; Wlodarczyk et al., 2015; Bialer et al., 2017; Weiser et al., 2017). Therefore, we tested VPD and VCD anti-CMV efficacy in an *in vivo* model of severe perinatal mCMV infection (Slavuljica et al., 2014).

First, we confirmed drug safety with daily administration of both agents in control, uninfected neonatal mice. No adverse effects on postnatal body growth were detected (Fig. 3.7A). Inasmuch as the drugs appeared safe in developing mice, we next assessed VPD and VCD administration in newborn animals infected with mCMV intraperitoneally on the day of birth (Fig. 3.7B).

VPD and VCD treatment throughout the neonatal period induced substantial improvement in infected newborns health, with a three-fold decrease in death rate in adult mice (Fig. 3.7C). Survival of mCMV-infected, untreated animals was 23%, compared to 72% for VPD- or VCD-treated mice.

Additional benefits of drug treatment were also identified. VPD and VCD administration ameliorated the mCMV-induced detrimental effects on body growth as assessed by body weight, body length, and tail length (Fig. 3.7, D-G); infected mice weighed nearly 50% less than control mice at P20 ($p<0.001$), whereas VPD- or VCD-treated infected pups showed a body weight reduction of only 18% (Fig. 3.7E). Thus, both VPD and VCD attenuated the deficient body growth induced by perinatal mCMV infection.

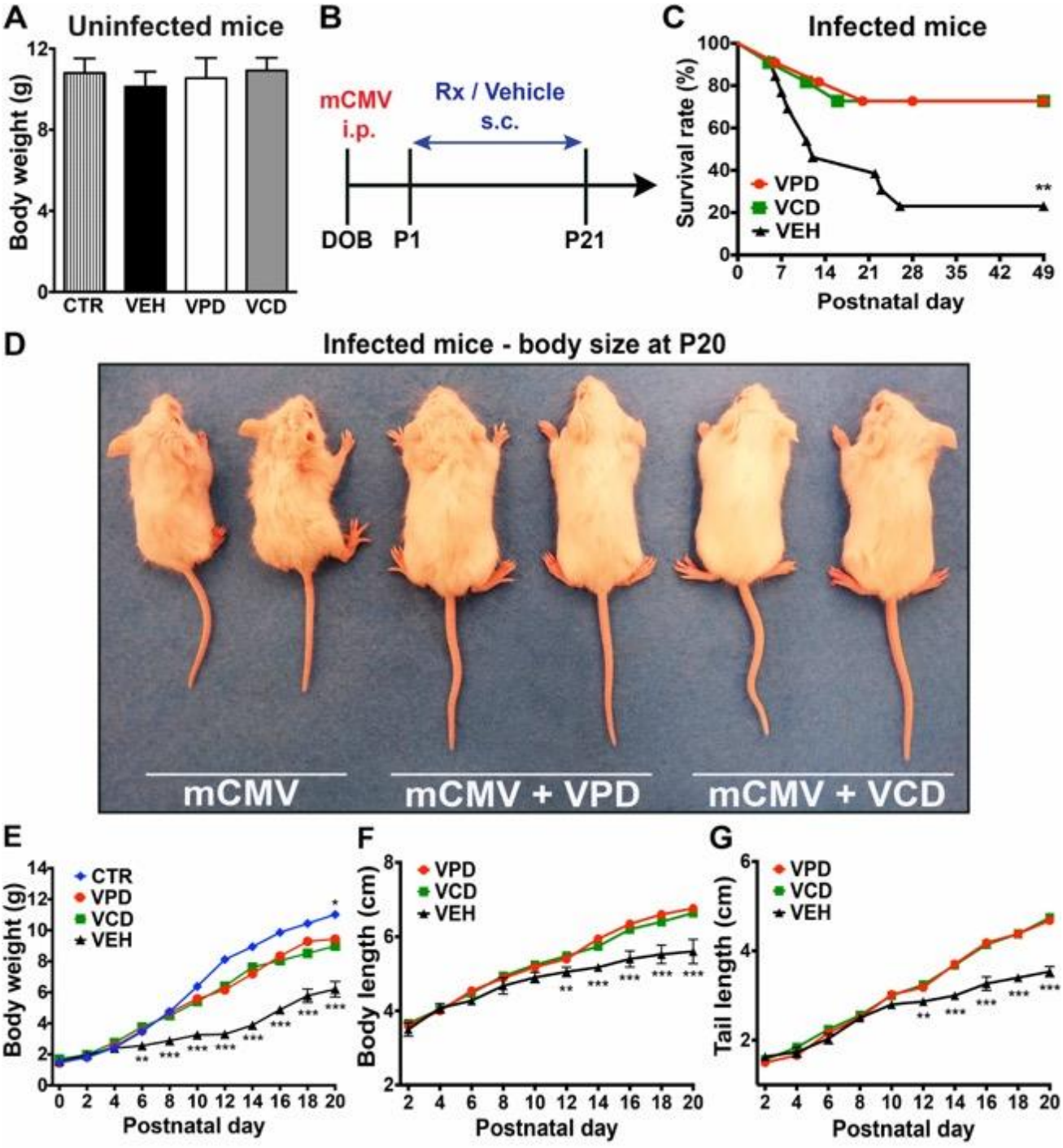

Fig. 3.7 Valpromide and valnoctamide safely improve survival and postnatal body growth of infected newborns. ***A.*** *Uninfected pups received 20 µL of saline (CTR), vehicle (VEH), VPD, or VCD (1.4 mg/mL), once a day, subcutaneously, from P1 to P21, when the body weight was assessed. Mean±SEM, one-way ANOVA with Bonferroni's post hoc test; N=8 mice/experimental group.* ***B.*** *Timeline of the experimental paradigm employed, with mCMV infection of newborn mice and subsequent compound administration throughout the neonatal period.* ***C.*** *Survival in 7 week-old mCMV-infected mice receiving VPD, VCD, or VEH assessed by Log-rank (Mantel-Cox)*

test; N=11–13 mice/group. ***D-G.*** *Drug-induced improvement in postnatal body growth. Photo shows enhanced body size of VPD- (middle) and VCD-treated (right) mice compared to vehicle (left) (**D**). Graphs show postnatal body weight (**E**), body length (**F**), and tail length (**G**) increase from DOB to P20. CTR, control uninfected mice receiving saline; VPD, VCD, and VEH, mCMV-infected newborns treated with the indicated compounds. Mean±SEM; error bars shown only for VEH group for clarity; N=6–9 mice/group; mixed-model ANOVA (Newman Keuls test) for VPD and VCD versus CTR (above CTR line, **E**) and for VPD and VCD versus VEH (below VEH line, **E-G**); *p<0.05, **p<0.01, ***p<0.001.*

Both drugs markedly improved other parameters of somatic development, including eyelid opening, pinnae detachment, fur maturation, and incisor eruption (Fig. 3.8, A-F).

Of note, VPD and VCD generated a significant (p<0.01) improvement in mCMV-infected neonate health as early as 5 days after treatment initiation.

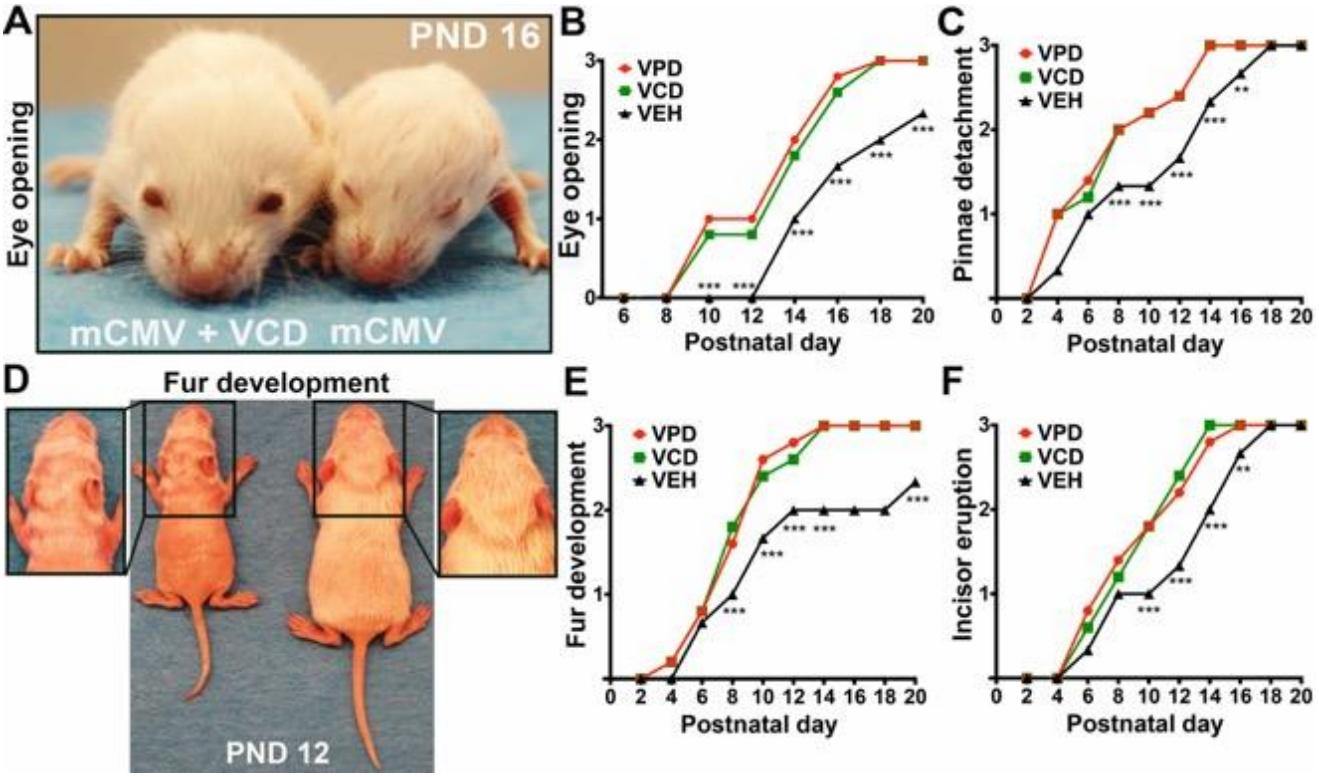

Fig. 3.8 Daily valpromide and valnoctamide administration ameliorates postnatal somatic development. A-F. *Graphs show progressive improvement of multiple parameters of postnatal growth. Mean±SEM; error bars not shown for clarity. N=6–9 mice/group; mixed-model ANOVA (Newman Keuls test) for VPD and VCD versus VEH; **p<0.01, ***p<0.001. Photos show the differential status of eye opening in P16 mice (**A**) and the delayed*

*development of fur in an infected/untreated pup (left) compared to an infected newborn treated with VCD (right) at day 12 after birth (**D**); marked difference in growth is also evident.*

The amelioration of postnatal growth and long-term survival in infected mice receiving VPD or VCD might be the result of a drug-mediated antiviral activity in target peripheral organs of infection, including liver, spleen, and lungs. To investigate whether the observed beneficial effects were related to the ability of VPD and VCD to decrease mCMV levels *in vivo*, we analyzed these organs from infected mice at 12 dpi by viral plaque assay (Fig. 3.9, A-D). Viral titers were decreased by greater than 2 logs in all tested tissues of drug-treated infected newborns, thus suggesting that the VPD- and VCD-mediated inhibitory effects on CMV infection observed *in vitro* also occur *in vivo* and associate with a substantial improvement in mCMV-infected animal outcome.

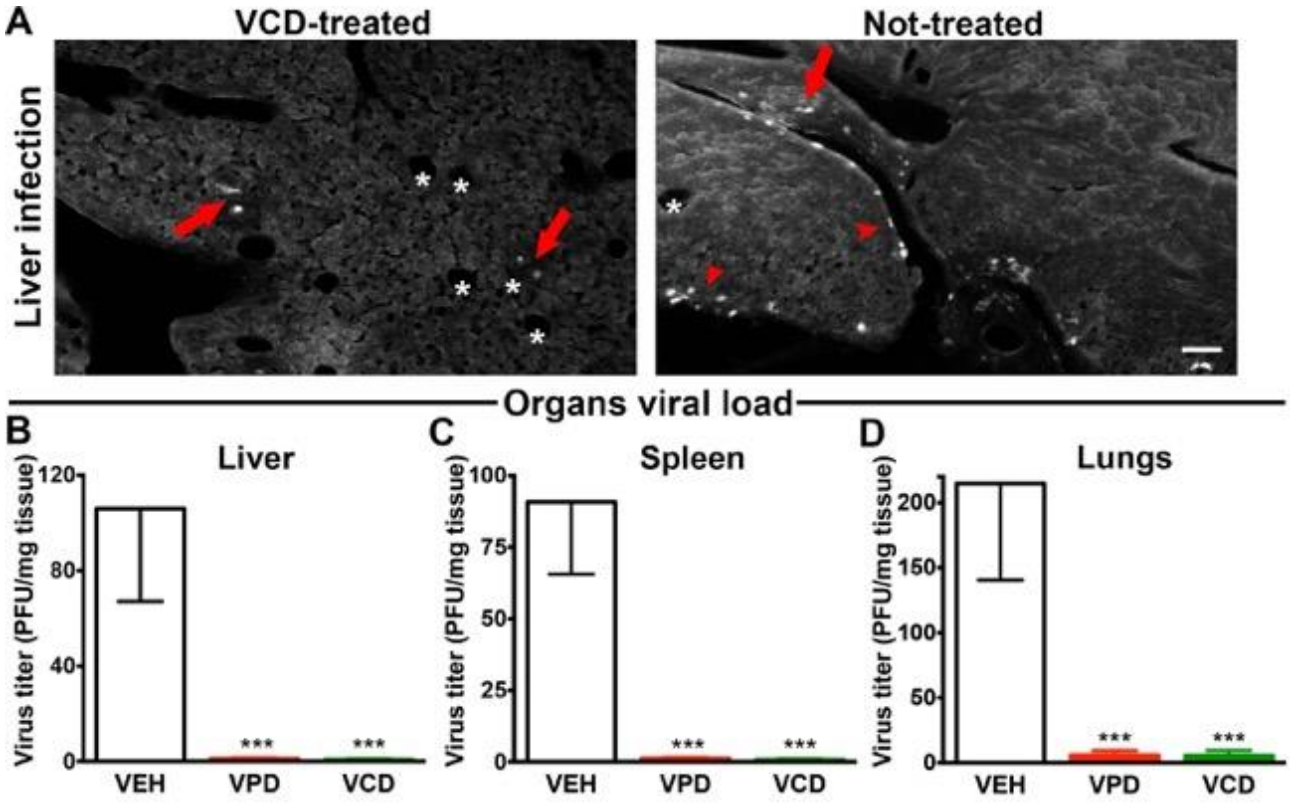

Fig. 3.9 Valpromide and valnoctamide substantially decrease murine CMV load in target organs. A. *A small number of cells show mCMV infection in the liver of P12 mice infected on DOB and treated daily with VCD until P10 (left); in contrast, a higher number was commonly found in the liver of pups receiving vehicle (right). GFP-positive cells are localized both in the parenchyma (arrows) and in the sub-peritoneal area (arrowheads). Asterisks indicate lobule central veins. Scale 100 µm.* ***B-D.*** *Infected newborns treated with VPD, VCD, or VEH*

*from P1-10 were euthanized at P12, and tissue samples from liver, spleen, and lungs were collected for measurement of viral titer by plaque assay. Bar graphs show titers as PFU/mg of tissue; mean±SEM; N=6 mice/group; ***p<0.001, one-way ANOVA, Bonferroni's post hoc test.*

3.1.5 Valpromide and valnoctamide suppress human CMV by inhibiting virus attachment to the cell.

Despite being used for decades to treat neurological dysfunctions, the mechanism(s) of action of VPD and VCD in the brain remain unclear (Monti et al., 2009; Spampanato and Dudek, 2014; Bialer et al., 2017). VPA-mediated inhibition of HDAC enhances infection by hCMV (Kuntz-Simon and Obert, 1995; Michaelis et al., 2004; Michaelis et al., 2005). Both VPD and VCD lack this epigenetic activity (Okada et al., 2004; Fujiki et al., 2013).

To gain insight into the underlying mechanisms of VPD and VCD inhibition of CMV, we tested the drugs by addition at different time-points during the course of hCMV infection (Fig. 3.10A). The drug concentration employed for testing was 100 µM, which is below the therapeutic range for safely treating mood disorders and epilepsy in humans (Pisani et al., 1986; Brodie and Dichter, 1996; Barel et al., 1997; Witvrouw et al., 1997; Bersudsky et al., 2010; Matalon et al., 2011; Shekh-Ahmad et al., 2014; Spampanato and Dudek, 2014; Bialer et al., 2017; Weiser et al., 2017). When the compounds were present from the time of viral challenge through 96 hpi, viral yield decreased approximately 60%. A similar inhibition of hCMV replication was also observed with 2 h drug exposure at the time of viral challenge, followed by drug wash out (44.8±2.5% for VPD and 42.9%±3.2% for VCD, compared to vehicle-treated cultures). However, no reduction in viral yield was identified when the compounds were added 2-12 h after virus inoculation (Fig. 3.10A). These results indicate that the block of hCMV mediated by VPD and VCD is exerted early in the infection process, within the first 2 h of the replication cycle.
We therefore tested the possibility that these agents directly inactivate virions by pre-incubating the compounds with an undiluted stock of hCMV prior to cell inoculation. When the inhibitors were subsequently diluted below an effective concentration prior to culture inoculation, i.e. 10 nM, no direct inactivation of free virions was observed, as determined by the absence of a drug-mediated inhibitory effect (Fig. 3.10B). Similar results were obtained when the pre-incubation mix was run through a 100 nm-pore size filter to remove the compounds but not the virus, prior to analysis of virus infectivity at physiological and cold temperatures (percentages show hCMV viral titers in drug-treated samples as compared to vehicle: 37°C, 98.5%±8% for VPD, 99.3%±5% for VCD; 4°C, 100.6%±5% for VPD, 98.3%±8% for VCD).

The IE1/2 hCMV promoter is active in the first few hours of hCMV infection, inducing IE protein expression which in turn promotes viral replication (Mocarski et al., 2013). We investigated whether the drugs interfere with the activity of this promoter by testing a plasmid with hCMV IE1/2 driving tdTomato expression. No decrease in the number of red cells was identified in the presence of VPD compared to control (96%±4%) after plasmid transfection, suggesting VPD does not inhibit the activity of the hCMV IE1/2 promoter. In addition, we assessed IE1/2 antigen expression in hCMV infected cells exposed to the compounds either simultaneously or 2 h after viral challenge (Fig. 3.10C). Substantial IE1/2 was detected in fibroblasts that received drugs after 2 hpi, similarly to vehicle-treated cultures. In contrast, cells treated with the compounds at the time of hCMV inoculation showed markedly decreased IE1/2 expression, thus suggesting that hCMV inhibition by VPD and VCD occurs prior to the IE stages of the viral replication cycle.

We next examined hCMV entry into the cell, which precedes IE protein expression and can be separated into two phases: (1) attachment of the viral particle to the cell surface and (2) fusion of the viral envelope with cellular membranes and penetration into the cytoplasmic space (Compton et al., 1993; Mocarski et al., 2013). Investigation of these phases was performed by a 2 h incubation at 4°C, a temperature that allows attachment but not fusion, followed by a temperature shift to 37°C, which allows fusion and internalization (Chan and Yurochko, 2014), and subsequent infectivity assessment by GFP-positive cell counting. Analysis showed substantial VPD- and VCD-mediated interference with hCMV attachment to the cell (Fig. 3.10D). These results were confirmed by qRT-PCR with quantification of the relative amount of hCMV DNA in infected human fibroblasts exposed to the compounds at 4°C (Fig. 3.10E). In these assays, heparan sulfate was employed as a positive control given its ability to block hCMV attachment *in vitro* by mimicking HSPGs (Compton et al., 1993).

Current approved anti-CMV compounds target viral DNA synthesis (GCV, cidofovir, foscarnet) or the hCMV major IE gene locus (fomivirsen). Since our data indicate that VPD and VCD may block a different, earlier step of hCMV infection, similar to HS, we postulated that a combined administration of GCV with VCD or HS might induce a stronger viral inhibition than single drug therapy or VCD/HS association (Fig. 3.10F). When cells were exposed to GCV+VCD or GCV+HS, the decrease in hCMV plaques nearly doubled compared to single drug treatment, i.e. GCV alone, VCD alone, or HS alone. In contrast, combination of VCD+HS only slightly increased the viral inhibition obtained with VCD alone or HS alone, supporting the hypothesis that VPD, VCD, and HS may act on the same step of hCMV infection.

Prolonged cell exposure to VPD and VCD followed by drug wash out immediately before hCMV inoculation resulted in no attenuation of infection (Fig. 3.10G), consistent with the view that the drugs did not exert persistent effects on antiviral cellular targets, such as enhancement of innate immunity. These data also suggest that the anti-CMV actions of VPD and VCD are not the result of an irreversible association of the compounds with cell surface proteins.

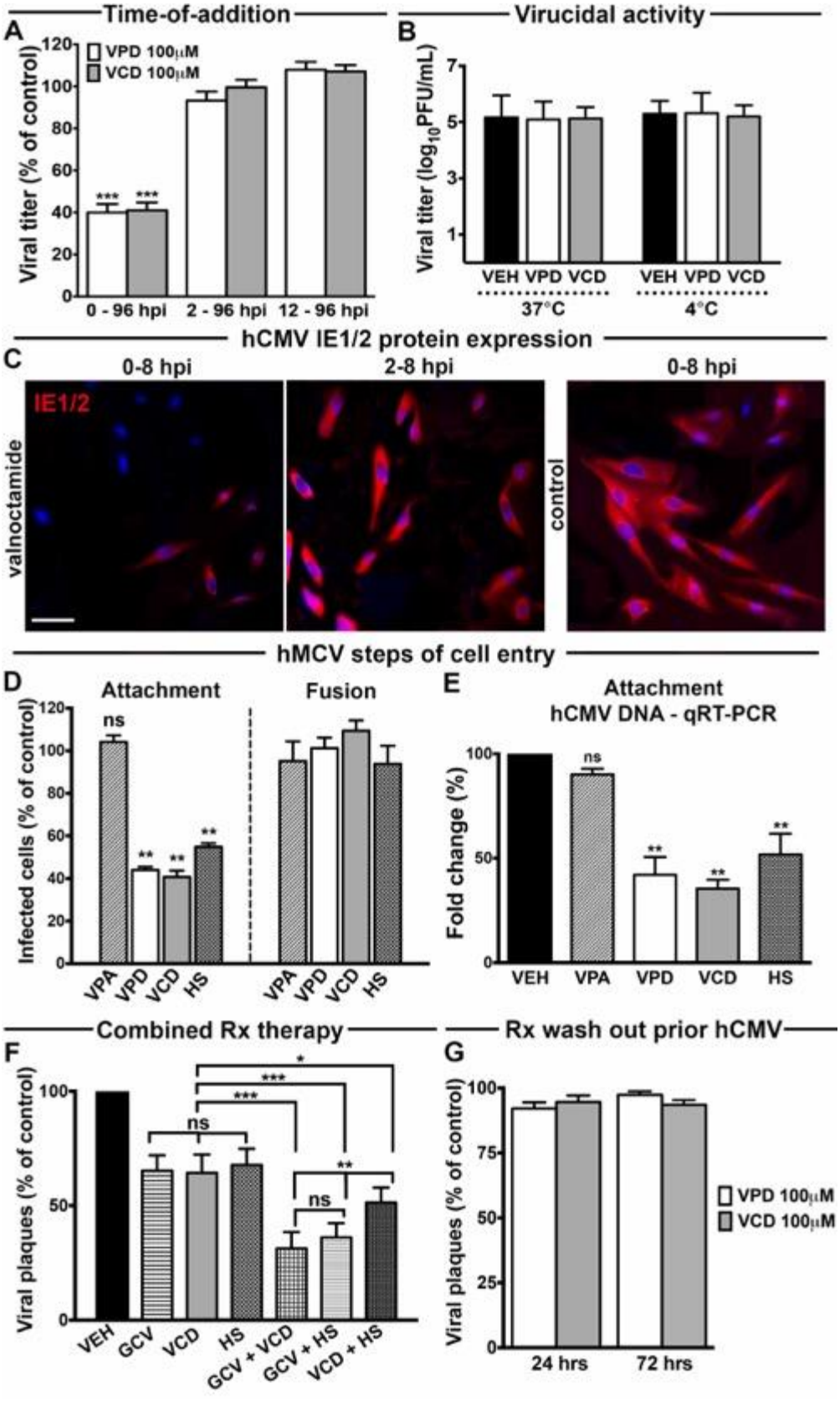
Time-of-addition
A
VPD 100μM
VCD 100μM
Viral titer (% of control)
0 - 96 hpi
2 - 96 hpi
12 - 96 hpi
Virucidal activity
B
Viral titer (log10PFU/mL)
VEH VPD VCD
37°C
VEH VPD VCD
4°C
hCMV IE1/2 protein expression
C
0-8 hpi
2-8 hpi
0-8 hpi
IE1/2
valnoctamide
control
hMCV steps of cell entry
D
Attachment
Fusion
Infected cells (% of control)
ns
VPA VPD VCD HS
VPA VPD VCD HS
E
Attachment
hCMV DNA - qRT-PCR
Fold change (%)
VEH VPA VPD VCD HS
Combined Rx therapy
F
Viral plaques (% of control)
VEH GCV VCD HS GCV + VCD GCV + HS VCD + HS
Rx wash out prior hCMV
G
Viral plaques (% of control)
24 hrs
72 hrs
VPD 100μM
VCD 100μM

Fig. 3.10 Valpromide and valnoctamide inhibit human CMV attachment to cell. A. *HDF cells infected with hCMV-GFP (MOI 0.01) (t=0) were exposed to VPD, VCD, or vehicle (100 μM) simultaneously, or 2 or 12 h after virus inoculation until media collection at 96 hpi. Viral replication assessed by titer determination using a plaque assay on HDF monolayers.* ***B.*** *A drug (100 μM)/undiluted hCMV mixture was incubated for 2 h at 37°C or 4°C. Before cell inoculation, the solution was diluted to 10 nM (ineffective drug concentration).* ***C.*** *Human fibroblasts infected with hCMV (MOI 0.01) and treated with the compounds (100 μM) starting from viral challenge (t=0) or 2 hpi, were fixed and permeabilized at 8 hpi for immunofluorescence with anti-IE1/2 monoclonal antibody and DAPI nuclear staining. Scale bar 100 μm.* ***D, E.*** *Attachment and fusion assays were performed as described in Materials and Methods. GFP-positive cells were counted at 72 hpi (**D**). Results presented as the fold change ($2^{-\Delta\Delta CT}$) of hCMV DNA in each experimental condition relative to vehicle (mean±SEM of 2 biological replicates) (**E**).* ***F.*** *Plaque reduction assay on HDF cells exposed to vehicle, GCV (100 nM), VCD (100 μM), HS (25 μg/mL - approximately 40 μM), or a combination of these compounds as indicated for 24 h before hCMV inoculation (MOI 0.01). Fluorescent plaques counted at 7 dpi. The mean plaque counts for each drug were expressed as a percentage of the control (vehicle) mean plaque count, defined as 100% (vehicle bar shown on the left for clarity); p<0.001 for VEH vs GCV, VCD, and HS. Rx, drug.* ***G.*** *After 24 h- or 72 h-VPD, VCD, or vehicle pre-treatment (100 μM), cultures were rinsed three times and given drug-free media prior to hCMV inoculation (MOI 0.01). Plaques counted at 7 dpi. Bars: mean±SEM of 5 (**F, G**), 8 (**A, B**), and 12 cultures (**D**); ns, not significant, *p<0.05, **p<0.01, ***p<0.001, one-way ANOVA with Bonferroni's post hoc test.*

3.1.6 Valpromide and valnoctamide decrease spread of murine and human CMV infection.

Inhibition of CMV attachment to the target cell may play a role not only in the initiation of infection but also on subsequent virus spread.

Murine and human fibroblast cells were exposed to the drugs after mCMV and hCMV inoculation and adsorption, respectively, and assessed for viral plaque size at 5 (mCMV) and 10 (hCMV) dpi. Both VPD and VCD effectively decreased spread of the CMV infection as shown by the reduced plaque size in CMV-infected, drug-treated monolayers compared with the plaque size from vehicle-treated cultures (Fig. 3.11, A-C).

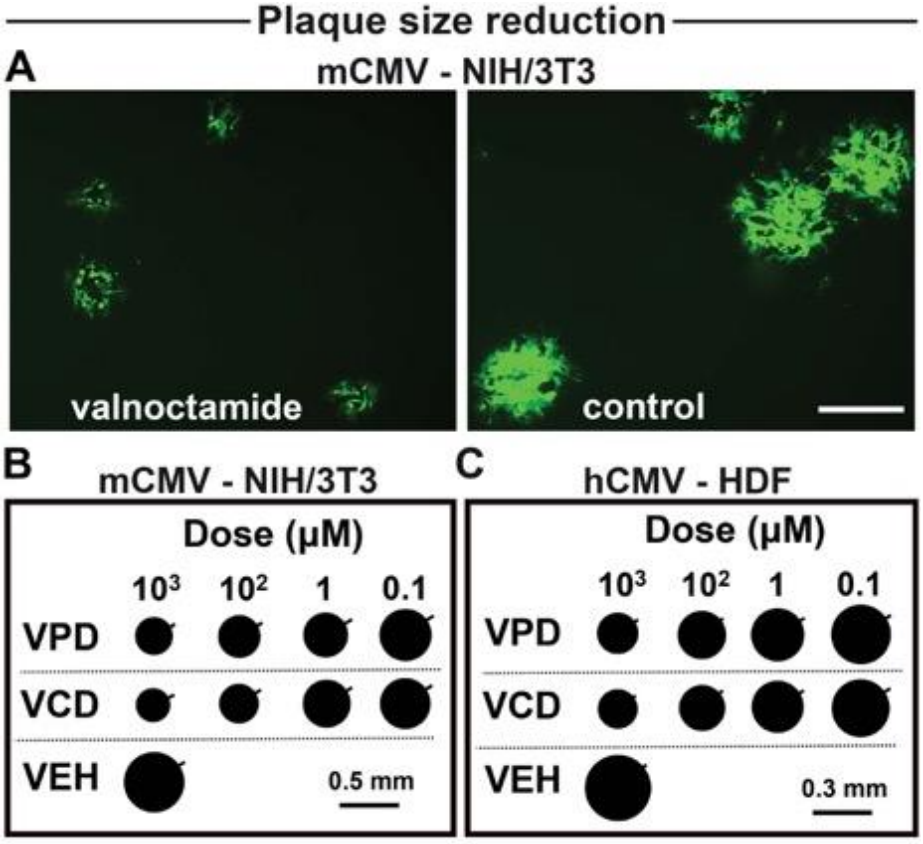

Fig. 3.11 Valpromide and valnoctamide effectively decrease spread of CMV infection. A-C. *Plaque size assay of NIH/3T3 cells (**A, B**) and human fibroblasts (**C**) infected with mCMV-GFP and hCMV-GFP (MOI 1) and treated with VPD, VCD, or vehicle. Viral plaque size measured 5 (mCMV) and 10 (hCMV) dpi. Representative plaques in 100 μM VCD (left) or vehicle (right); scale 300 μm (**A**). Mean diameter of 60 random plaques; SEM, bar on upper right side (**B, C**); $p<0.05$ in 0.1 μM, $p<0.01$ in 1 μM, $p<0.001$ in 100 μM and 1 mM, versus vehicle.*

3.2 Investigation of valnoctamide activity against CMV in the developing brain and of drug-mediated benefits on neurodevelopment and behavior.

We demonstrated that VPD and VCD exert a substantial and specific inhibition of mouse and human CMV *in vitro*. Also, by means of a mouse model of severe perinatal mCMV infection, we showed potent antiviral activity of both drugs on mCMV replication in peripheral target organs of infection, including the liver, the spleen, and the lungs, with improved health outcomes of infected mice. Both VPD and VCD lack teratogenic effects (Haj-Yehia and Bialer, 1990; Radatz et al., 1998; Okada et al., 2004; Shekh-Ahmad et al., 2014; Mawasi et al., 2015; Shekh-Ahmad et al., 2015; Wlodarczyk et al., 2015; Bialer et al., 2017), have been used in clinics for many years with no evidence of safety concerns (Stepansky, 1960; Goldberg, 1961; Harl, 1964; Bialer, 1991; Bersudsky et al., 2010; Weiser et al., 2017),

and show optimal CNS distribution after peripheral administration (Blotnik et al., 1996). However, VCD has better translational potential than VPD. VCD has been shown to act as a drug on its own, with only negligible conversion to its corresponding free acid (valnoctic acid), in mice, rats, dogs, and humans (Haj-Yehia and Bialer, 1988; Bialer et al., 1990; Bialer, 1991; Blotnik et al., 1996; Barel et al., 1997; Radatz et al., 1998). In turn, VPD, while displaying only minimal conversion to VPA in mice (Radatz et al., 1998), is largely metabolized (>80%) to VPA in humans (Bialer et al., 1990; Bialer, 1991; Barel et al., 1997). VPA is teratogenic and enhances hCMV infection (Nau et al., 1991; Kuntz-Simon and Obert, 1995; Radatz et al., 1998; Phiel et al., 2001; Michaelis et al., 2004; Okada et al., 2004; Michaelis et al., 2005; Tung and Winn, 2010; Kataoka et al., 2013; Paradis and Hales, 2013, 2015). Therefore, we decided to proceed with further investigation of VCD only.

Human CMV infection of the developing brain can cause brain damage and life-long neurological problems with substantial impact on everyday life, including cerebral palsy, motor impairment, and intellectual disability (Gandhi and Khanna, 2004; Cheeran et al., 2009; Tsutsui, 2009; Mocarski et al., 2013). Considering this and that VCD can cross the BBB and act inside the brain, we asked whether low-dose VCD given subcutaneously to mCMV-infected neonatal mice could safely suppress mCMV inside the developing brain and exert beneficial effects on neurodevelopment and behavior (Ornaghi et al., 2017) (see Appendix). Of note, brain development in the newborn mouse parallels human brain development during the early second trimester of pregnancy (Clancy et al., 2001; Branchi et al., 2003; Clancy et al., 2007a; Clancy et al., 2007b; Workman et al., 2013), a critical period of neurontogeny where CMV can cause substantive dysfunction (Manicklal et al., 2013).

3.2.1 Peripheral inoculation of murine CMV causes widespread infection of the developing mouse brain.

First, we characterized the kinetics of mCMV replication and dissemination after intraperitoneal inoculation of the virus in newborn mice on the DOB (P0). Forty-eight hours after intraperitoneal injection, mCMV was found in the blood and at lower levels in the spleen and liver of infected mice, with only a small amount detected in the brain (Fig. 3.12A). Analysis of viral kinetics in these four organs over the course of 50 days revealed that mCMV, after entering the bloodstream, quickly gained access to peripheral target organs (i.e., the liver and spleen) and began replicating to yield high viral titers by 4 dpi (Fig. 3.12, B-D). In turn, similar viral titers were measured in the brain only after 8 dpi (Fig. 3.12E). After entering the brain, the virus could effectively replicate *in situ*, as suggested by the measurement of

mCMV loads similar to those found in the liver and spleen at the viral peak between P8 and P12 (Fig. 3.12, C-E).

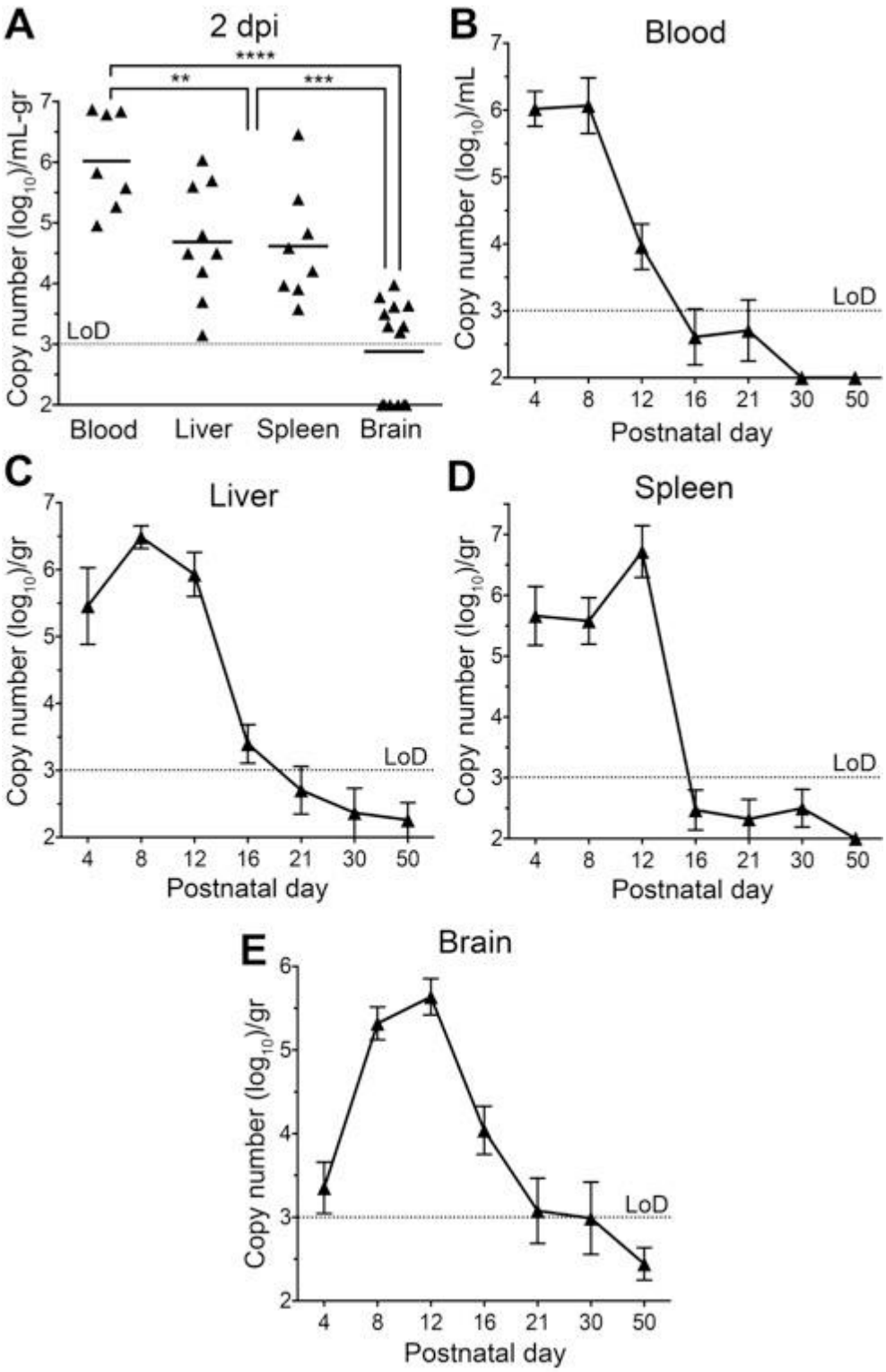

Fig. 3.12 Kinetics of murine CMV replication after intraperitoneal inoculation on day of birth. *Newborn mice were infected on the DOB (day 0) with 750 pfu of mCMV. Viral load in whole blood, liver, spleen, and brain was evaluated by qRT-PCR at the indicated time points and expressed as log_{10} genome copies per mL/gram of harvested blood/tissue. In **A**, each symbol represents an individual mouse, and horizontal bars show mean values of the groups; in **B-E**, data are presented as the mean±SEM with 7-10 mice/time point. Viral titers below the limit of detection (LoD, dotted line) were plotted as 2 log_{10} genome copies. In **A**, **p<0.01, ***p<0.001, ****p<0.0001; one-way ANOVA with Bonferroni's post hoc test.*

Upon histological examination, after peripheral inoculation, mCMV-GFP infection of the developing mouse brain appeared widespread and scattered in nature. Isolated infected cells and infectious foci containing up to 20-25 cells could be found in multiple distant areas within the same brain. The pattern of infection also appeared heterogeneous, with different brains displaying infection in different regions. These observations are consistent with a hematogenous spread of mCMV from the periphery into the developing brain of neonatal mice. Infected cells were identified in the olfactory bulb and nuclei, the cortex, corpus callosum, hippocampus, basal nuclei, choroid plexus, midbrain, superior and inferior colliculi, sylvian aqueduct, pons, medulla, cerebellum, and meninges (Fig. 3.13, A-I). No mCMV was detected in the spinal cord. Infection of the choroid plexus in the lateral ventricles was frequently associated with evidence of infected cells in the brain parenchyma in close proximity to the ventricle (Fig. 3.13, E and F), a site of NPSC localization (Semple et al., 2013).

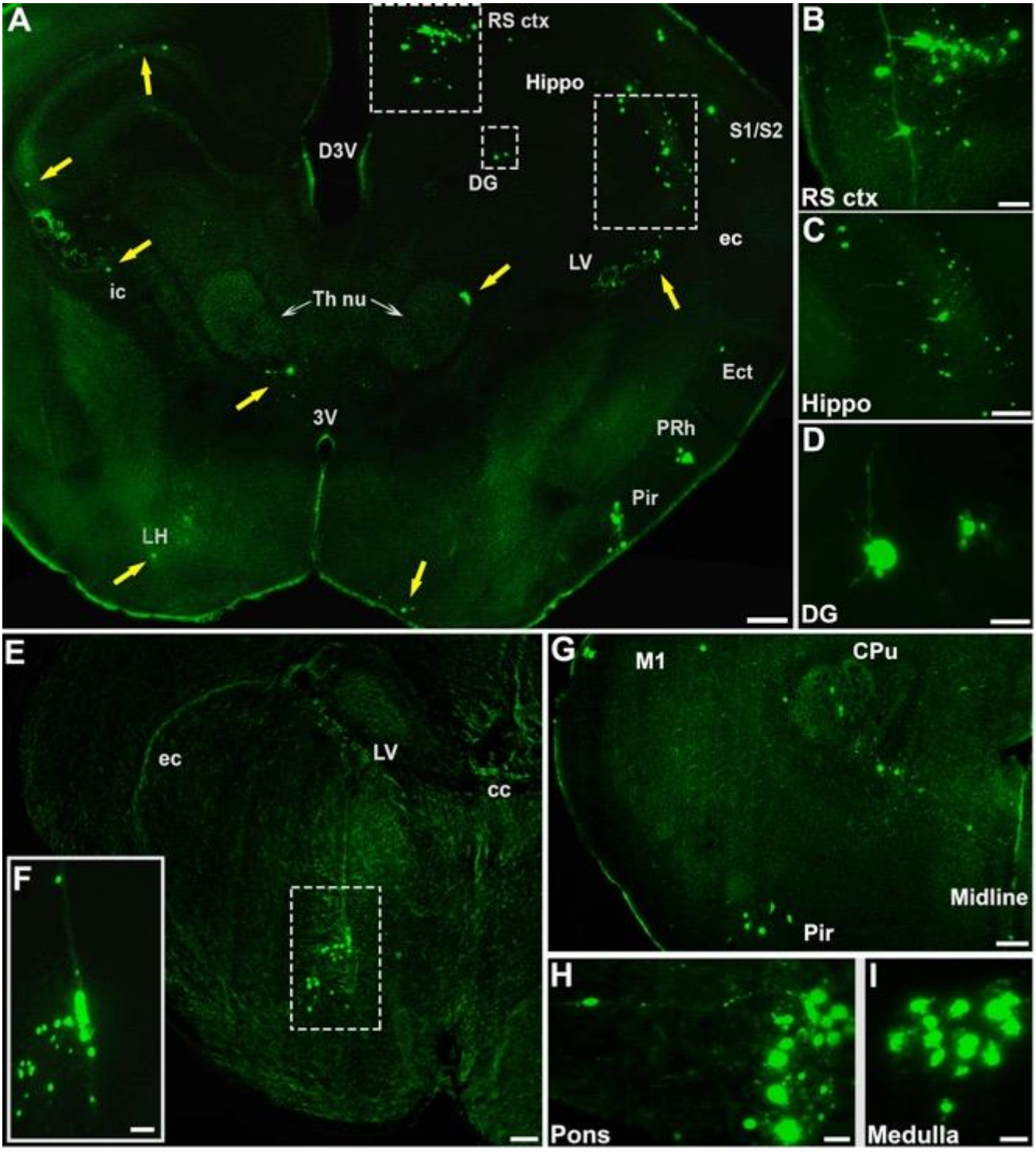

Fig. 3.13 Scattered widespread distribution of murine CMV-GFP in brains after infection of newborn mice. A-I. *Detection of virus-infected cells by means of mCMV-GFP reporter expression in representative coronal sections of P8 and P12 mouse brains (n=5). Single infected cells or small foci of infection (yellow arrows) can be identified in the retrosplenial cortex (RS ctx), primary and secondary somatosensory cortex (S1/S2), ectorhinal cortex (Ect), perirhinal cortex (Prh), piriform cortex (Pir), hippocampus (hippo) and dentate gyrus (DG), lateral ventricle (LV),*

*external and internal capsule of the corpus callosum (ec and ic, respectively), lateral hypothalamic area (LH), and thalamic nuclei (Th Nu) of a P12 mouse brain (**A**). D3V, dorsal third ventricle. Magnifications of the boxed areas in A (**B-D**). Infection of the lateral ventricle and diffusion to the adjacent brain parenchyma in a P8 brain (**E**). Magnification of the boxed area in E (**F**). cc, corpus callosum. Photomicrograph of a P12 brain showing infection in the motor (M1) and piriform cortex, and in the striatum [caudate–putamen (CPu)] (**G**). Large foci of mCMV-infected cells in the pons and the medulla of a P8 animal (**H, I**). Scale bars: 50 µm (**H**); 100 µm (**A, D, E, G, I**); 200 µm (**C, F**); 400 µm (**B**).*

Infection of certain brain areas, such as the thalamus and the hypothalamus, was observed less frequently compared with other regions, including the cerebellum, hippocampus, and cortex. The cerebellum was the only site consistently displaying viral infection in all the brains examined (n=20), with robust GFP labeling in both Purkinje cells and granule neurons (Fig. 3.14, A and B). Viral GFP was also identified in neurons of the hippocampus and in the cerebral cortex (Fig. 3.14, C-G). In cortical pyramidal cells, GFP was seen in both the apical dendrite extending toward the cortical surface and in basal dendrites ramifying closer to the cell body. Some infected neurons in the cortex displayed signs of degeneration, characterized by abnormal swelling along the dendrites (Fig. 3.14F).

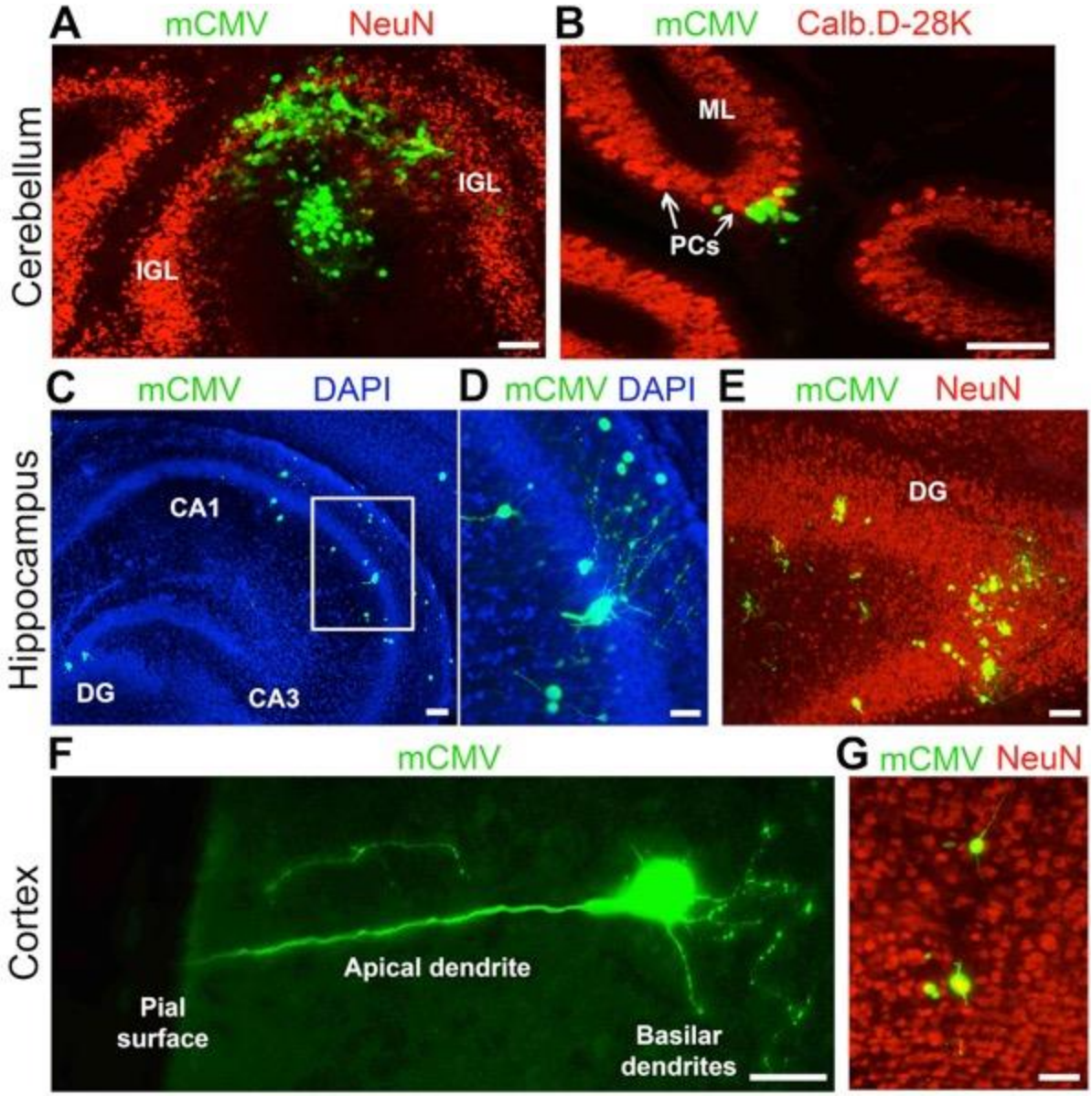

Fig. 3.14 Murine CMV infection of neuronal cells in the cerebellum, hippocampus, and cortex of the developing mouse brain. A, B. *Photomicrographs show GFP labeling of different cerebellar cell types, including neurons in the internal granular layer (**A**) and Purkinje cells (**B**), as assessed by NeuN and calbindin D-28K staining at 8 dpi (n=2 brains).* ***C-E.*** *Photographs display infection of different areas of the hippocampus (**C**), a magnification of the viral involvement of pyramidal cells in CA1 field (boxed area; **D**), and infected neurons in the dentate gyrus (DG) (**E**) (n=2 brains).* ***F.*** *Robust GFP expression in a pyramidal neuron of the motor cortex (n=1 brain); note the beaded aspect of the basilar dendrites, sign of neuronal pathology.* ***G.*** *Photomicrograph of neuronal infection in the visual cortex (n=1 brain). Scale bars: 100 µm (**A-E, G**); 50 µm (**F**).*

Together, these results indicate that intraperitoneally administered mCMV, after replicating in peripheral target organs, enters the developing brain of neonatal mice via the bloodstream or immune cells in the blood, producing a scattered and widespread infection with a highly heterogeneous pattern of propagation. Nonetheless, mCMV appears to display a particular preference for the cerebellum as an infectious site.

3.2.2 Subcutaneous valnoctamide blocks murine CMV replication within the brain.

Mice were infected intraperitoneally on the day of birth, and we compared the brains of infected mice treated subcutaneously with VCD with non-treated mCMV-infected mice. Viral load in the brain was quantified at multiple time points after mCMV inoculation. Cerebrum (cortex, hippocampus, thalamus, hypothalamus, and striatum) and cerebellum were assessed separately to determine whether the viral preference for the cerebellar region, as observed in the brain section analysis, was also accompanied by higher levels of virus replication. VCD decreased the amount of virus detected in both the cerebrum and cerebellum substantially, with an ~100- to 1000-fold decrease at all time points tested (Fig. 3.15, A and B). The anti-CMV effect displayed a rapid onset, suppressing the viral load after only 1 and 3 days of treatment in the cerebellum and the cerebrum, respectively. In untreated mCMV-infected mice, higher viral titers were identified in cerebellar samples compared with cerebrum at the beginning of infection (P4: $t=3.704$, $p=0.004$, paired Student's t test), suggesting that the cerebellum may represent a preferential site for initial mCMV targeting in the brain. These data indicate that VCD can attenuate mCMV infection detected in the brain.

The observed antiviral effect of VCD in the CNS could be the consequence of a drug-mediated decrease in viral replication in the periphery. Along this line, we corroborated that VCD also attenuated mCMV in the blood, liver, and spleen, starting quickly after therapy initiation and continuing to the end of the experiment (Fig. 3.15, C-E). This reduction of mCMV outside the brain would benefit the brain by reducing the amount of virus that ultimately can enter the CNS.

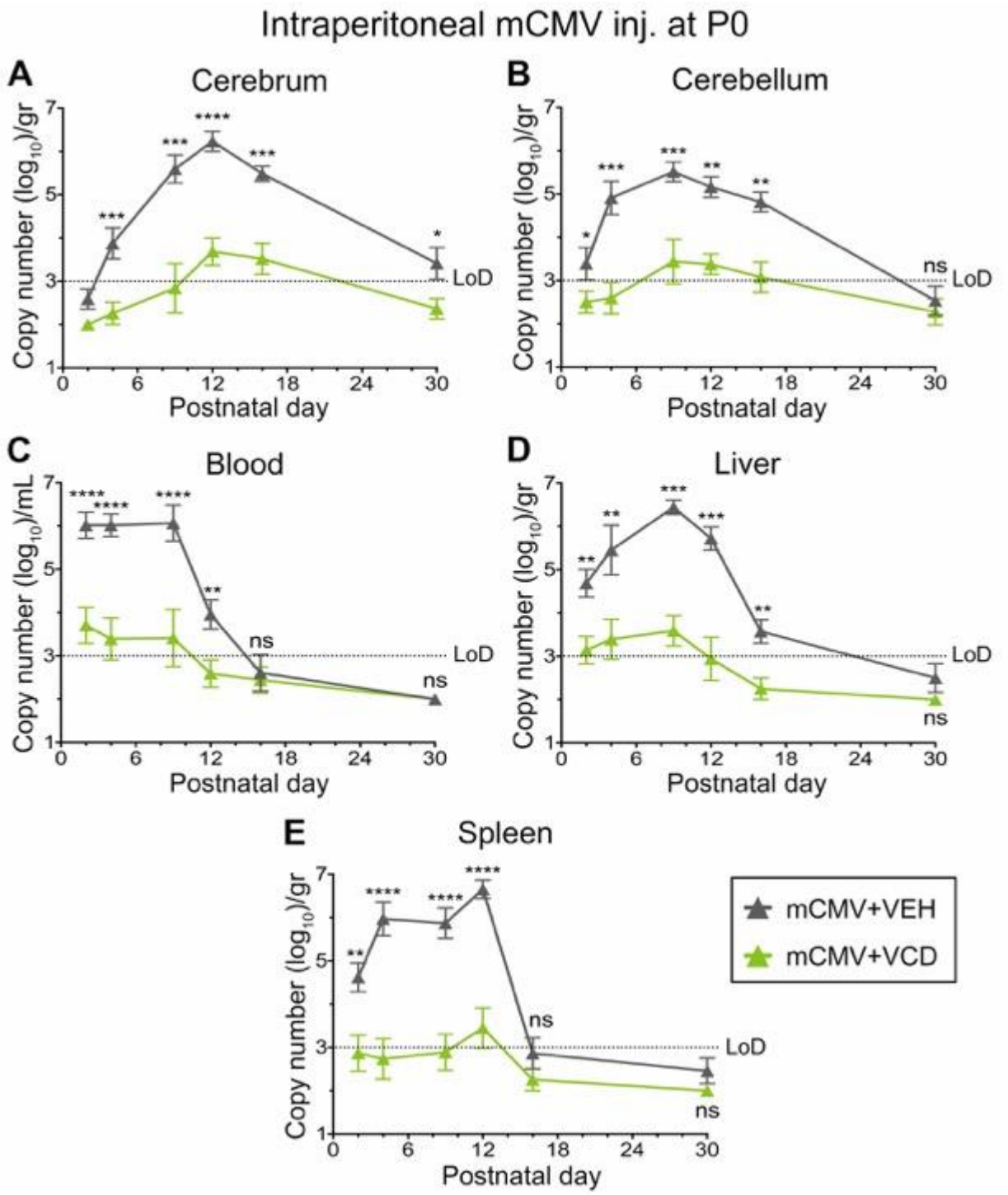

Fig. 3.15 Valnoctamide suppresses murine CMV load in the brain of mice infected intraperitoneally on the day of birth. *Newborn mice were infected at P0 with 750 pfu of mCMV intraperitoneally and were randomized to receive either vehicle (mCMV+VEH) or VCD (mCMV+VCD) subcutaneously from P1 until P21.* ***A-E.*** *Viral load was quantified in the cerebrum (**A**), cerebellum (**B**), whole blood (**C**), liver (**D**), and spleen (**E**) by qRT-PCR at the specified time points and were expressed as log_{10} genome copies per gram/mL harvested tissue/blood. Data are*

*presented as the mean±SEM; n=7-10 mice/time point. Viral titers below the limit of detection (LoD, dotted line) were plotted as 2 log_{10} genome copies. ns, not significant. *p<0.05, **p<0.01, ***p<0.001, ****p<0.0001; two-way ANOVA with postnatal day as repeated measures.*

To investigate whether VCD can act directly in the brain to decrease mCMV, we infected pups on P3 by direct intracranial virus inoculation. Analysis of mCMV load in the blood, liver, and spleen of untreated infected mice at P9 showed no viral spread outside the CNS (Fig. 3.16A). Viral titers in the brain were substantially lower by 100-fold in mCMV-infected animals receiving VCD treatment compared with untreated mCMV-infected mice (Fig. 3.16B). These results indicate that subcutaneously administered low-dose VCD can enter the brain at sufficient concentrations to effectively suppress mCMV replication *in situ*.

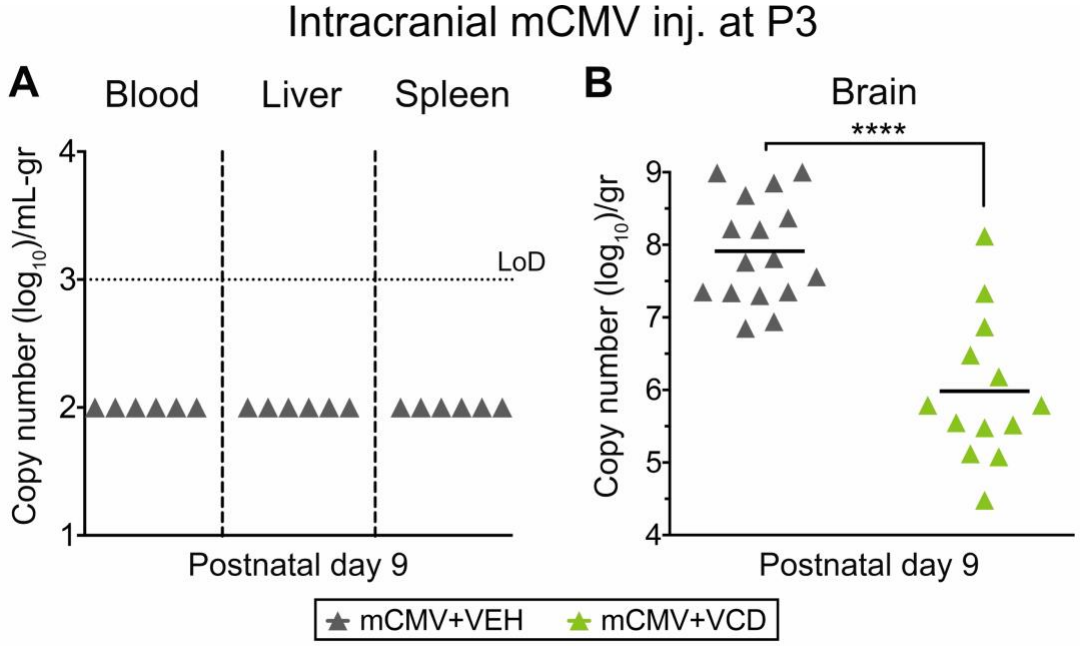

Fig. 3.16 Subcutaneously injected valnoctamide enters the brain and suppresses murine CMV replication within the brain. A, B. *Quantification of mCMV load in the blood, liver, spleen (**A**), and brain (**B**) of mice intracranially infected with 2 X10^4 pfu of mCMV on day 3 after birth. The amount of virus in tested samples was calculated by qRT-PCR in P9 mice receiving either vehicle (mCMV+VEH) or VCD (mCMV+VCD) subcutaneously from P3 through P8 and expressed as genome copies per mL/gram of harvested blood/tissue. Each symbol represents an individual mouse, and horizontal bars show mean values of the groups. Viral titers below the limit of detection (LoD, dotted line) were plotted as 2 log_{10} genome copies. ****p<0.0001, Mann-Whitney U test (**B**).*

3.2.3 Reversal of early neurological dysfunction in murine CMV-infected neonatal mice.

Human infants with CMV infection during early development can display substantial delays in the acquisition of neurological milestones during the first months of life (Dollard et al., 2007; Kimberlin et al., 2015). Since VCD showed a robust antiviral activity in the CNS of infected mice with a rapid attenuation of viral replication, we investigated whether this would translate into a positive therapeutic effect on the early neurological outcomes of neonatal mice.

Neurobehavioral assessments were performed using a battery of tests to examine body righting and tactile reflexes, motor coordination, and muscular strength. These tests provide a detailed examination of neurontogeny throughout the neonatal period since the behaviors measured are each expressed at different periods during the first 3 weeks of postnatal life (Fox, 1965; Scattoni et al., 2008).

Here and in a number of experiments below, we compared neurological function in the following four groups of mice: non-infected controls; VCD-treated non-infected controls; mCMV-infected mice; and mCMV-infected mice treated with VCD. VCD was administered in a single daily subcutaneous dose.

Murine CMV infection on the day of birth induced abnormal acquisition of all the neurological milestones assessed, with infected mice showing a delay of 6-10 days in the demonstration of responses similar to the uninfected controls (Fig. 3.17, A-H). In turn, infected VCD-treated neonatal pups displayed a timely acquisition of neurological milestones in all the behaviors measured. No differences were identified in the early neurontogeny of uninfected mice receiving VCD or vehicle. Together, these data indicate that VCD treatment during early development can safely improve the short-term neurodevelopmental outcomes observed in infected neonatal mice.

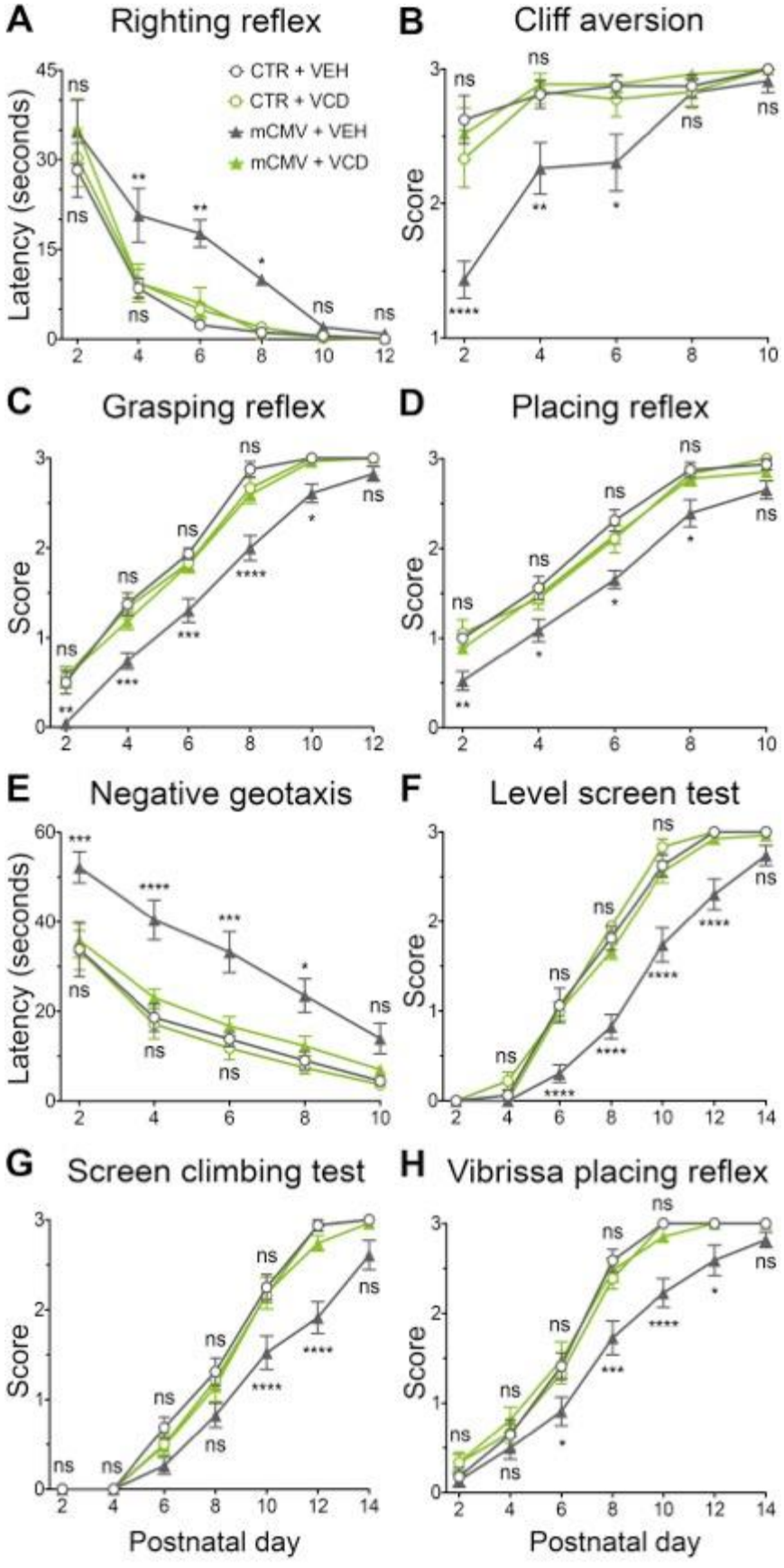
A
Righting reflex
Latency (seconds)
CTR + VEH
CTR + VCD
mCMV + VEH
mCMV + VCD
B
Cliff aversion
Score
C
Grasping reflex
Score
D
Placing reflex
Score
E
Negative geotaxis
Latency (seconds)
F
Level screen test
Score
G
Screen climbing test
Score
Postnatal day
H
Vibrissa placing reflex
Score
Postnatal day

Fig. 3.17 Delayed acquisition of neurological milestones induced by murine CMV infection is completely rescued by valnoctamide therapy. A-H. *Graphs show neurodevelopmental delays in mCMV-infected not treated pups (solid gray triangles) as assessed by the righting reflex (**A**), the cliff aversion (**B**), the forelimb grasping and placing reflex (**C, D**), the negative geotaxis (**E**), the level screen test (**F**), the screen climbing test (**G**), and the vibrissa placing reflex (**H**) (for a detailed description, see Materials and Methods). VCD-treated mCMV-infected animals (solid green triangles) showed neurological responses similar to uninfected controls receiving either vehicle (VEH; empty gray circles) or VCD (empty green circles). Values are reported as the mean±SEM, n=20-24 mice (9-12 males)/experimental group. ns, not significant. *p<0.05, **p<0.01, ***p<0.001, ****p<0.0001; two-way ANOVA with postnatal day as repeated measures. Significance is shown next to the infected, untreated mice (mCMV+VEH) line for comparison with uninfected controls (CTR+VEH and CTR+VCD) and next to control lines for comparison with infected, VCD-treated pups (mCMV+VCD).*

3.2.4 Amelioration of long-term neurobehavioral outcomes in infected juvenile mice.

CMV-infected infants with evidence of neurological delays during the neonatal period are at increased risk of developing long-term permanent neurological and behavioral sequelae, which manifest with a delayed onset after the first years of life (James and Kimberlin, 2016). Abnormal motor function is a commonly observed long-term neurological complication (Turner et al., 2014). More recently, a link between ASD-like behavioral disturbances in children and adolescents and hCMV infection during early development has been proposed (Sakamoto et al., 2015; Garofoli et al., 2017). Given the substantial improvement induced by VCD in the early neurontogeny of mCMV-infected neonatal mice, we examined whether these beneficial effects could also ameliorate late-onset neurobehavioral abnormalities, including motor performance and social and exploratory behavior.

3.2.4.1 Motor performance.

As indicated above, the cerebellum appears to be a preferential site for mCMV targeting in the mouse brain. We investigated cerebellar-mediated motor functions in infected and control juvenile mice using a hindlimb-clasping test, a vertical pole test, and a challenging beam traversal test (Brooks and Dunnett, 2009; Guyenet et al., 2010; Fleming et al., 2013).

The hindlimb clasping test is a marker of cerebellar pathology commonly used for severity scoring in mouse models of cerebellar degeneration (Guyenet et al., 2010). The majority of the mCMV-infected mice (9 of 13 mice) displayed an abnormal response to the clasping test, with both hindlimbs partially or entirely retracted to the abdomen when the mice were suspended by their tail for 10 seconds

(Fig. 3.18, A and B). VCD administration completely reversed this altered behavior, restoring a response similar to the uninfected counterparts.

By placing a mouse head upward on a vertical wooden pole, the vertical pole test allows for the examination of the ability of the animal to turn through 180° and successfully climb down the pole (Brooks and Dunnett, 2009). Infected, untreated juvenile mice required a longer period to complete the task compared with both uninfected controls and mCMV-infected VCD-treated animals (Fig. 3.18C). Three of 20 infected mice (15%) without treatment failed the test (e.g., showed an inability to turn the head downward or falling) in all of the three trials given, whereas no VCD-treated infected mice or uninfected controls failed in performing the task ($p=0.03$, χ^2 test).

In addition, we evaluated fine motor coordination and balance by the challenging beam traversal test, which assesses the ability of a mouse to maintain balance while traversing a narrow, 1 m-long beam to reach a safe platform (Carter et al., 2001; Brooks and Dunnett, 2009; Luong et al., 2011; Fleming et al., 2013). Murine CMV infection during early development increased the time needed by the mice to cross the beam and also the frequency of slipping (Fig. 3.18, D and E). VCD treatment significantly improved the coordination and balance of mCMV-infected mice, reducing both the beam traversal time and the number of slips recorded.

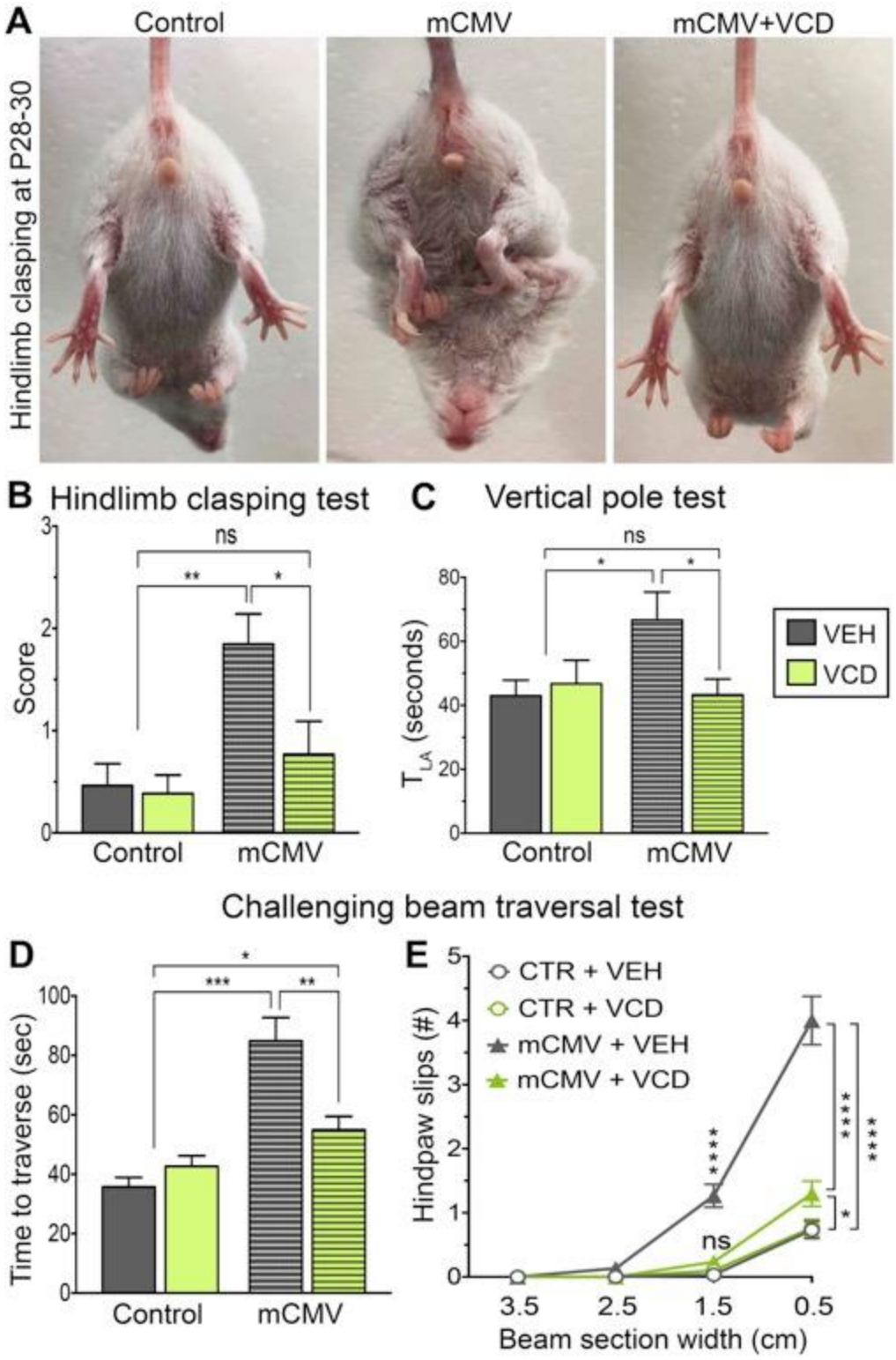

Fig. 3.18 Impaired cerebellar-mediated motor functions in murine CMV-infected mice are ameliorated by valnoctamide treatment. A. *Photographs display stereotypical clasping response with hindlimbs retracted to the abdomen in an infected mouse (mCMV, middle), and a normal response with splayed out hindlimbs in an*

uninfected control (left) and in an infected, VCD-treated animal (mCMV+VCD, right). ***B.*** *Scoring of clasping response according to hindlimb position.* ***C.*** *Increased T_{LA} in mCMV-infected, untreated mice in the vertical pole test, compared with VCD-treated infected animals and uninfected controls.* ***D, E.*** *Investigation of fine motor coordination and balance by challenging beam traversal test. Infected mice need more time to traverse the beam (**D**) and slip more (**E**) than the control mice. Both aspects are improved by VCD administration. Values are reported as the mean±SEM; n=10-13 mice/group. ns, not significant, *p<0.05, **p<0.01, ***p<0.001, ****p<0.0001; Kruskal-Wallis test with Dunn's post hoc test in **B-D**, and two-way ANOVA with repeated measures and Bonferroni's post hoc comparison in **E**.*

3.2.4.2 Social and exploratory behavior.

ASD is characterized by pervasive impairments in social interactions coupled with restricted and repetitive behaviors and decreased exploratory activity (American Psychiatric Association, 2013). To investigate whether adolescent mice with perinatal mCMV infection would display social and exploratory behavioral disturbances, we assessed social interaction and novel environment exploration by means of the three-chamber test and an adapted small open field test.

Infected untreated mice showed normal sociability when exposed to a first stranger mouse, preferring the conspecific over the empty cage (novel object) (Fig. 3.19A). However, a lack of preference for social novelty was found when a second stranger mouse was introduced in the apparatus, with infected untreated mice spending an equal amount of time in investigating the known and the novel animal (Fig. 3.19B). VCD therapy restored social novelty responses similar to levels shown in uninfected controls, with increased time devoted to examining the second stranger mouse. Of note, locomotor activity within the three-chambered social interaction apparatus was comparable among the four experimental groups, as defined by the number of entries in side chambers during habituation, social approach, and social novelty paradigms ($p>0.05$, two-way ANOVA, Bonferroni's *post hoc* analysis).

Exploratory activity was assessed by quantifying the number of rearings and nose pokings of mice exposed to a novel environment over a 3 min-test session (Fig. 3.19, C and D). A substantial reduction in both rearing and hole-poking events was identified in mCMV-infected untreated mice compared with control animals. Normal levels of exploratory activity were restored in infected mice receiving VCD treatment.

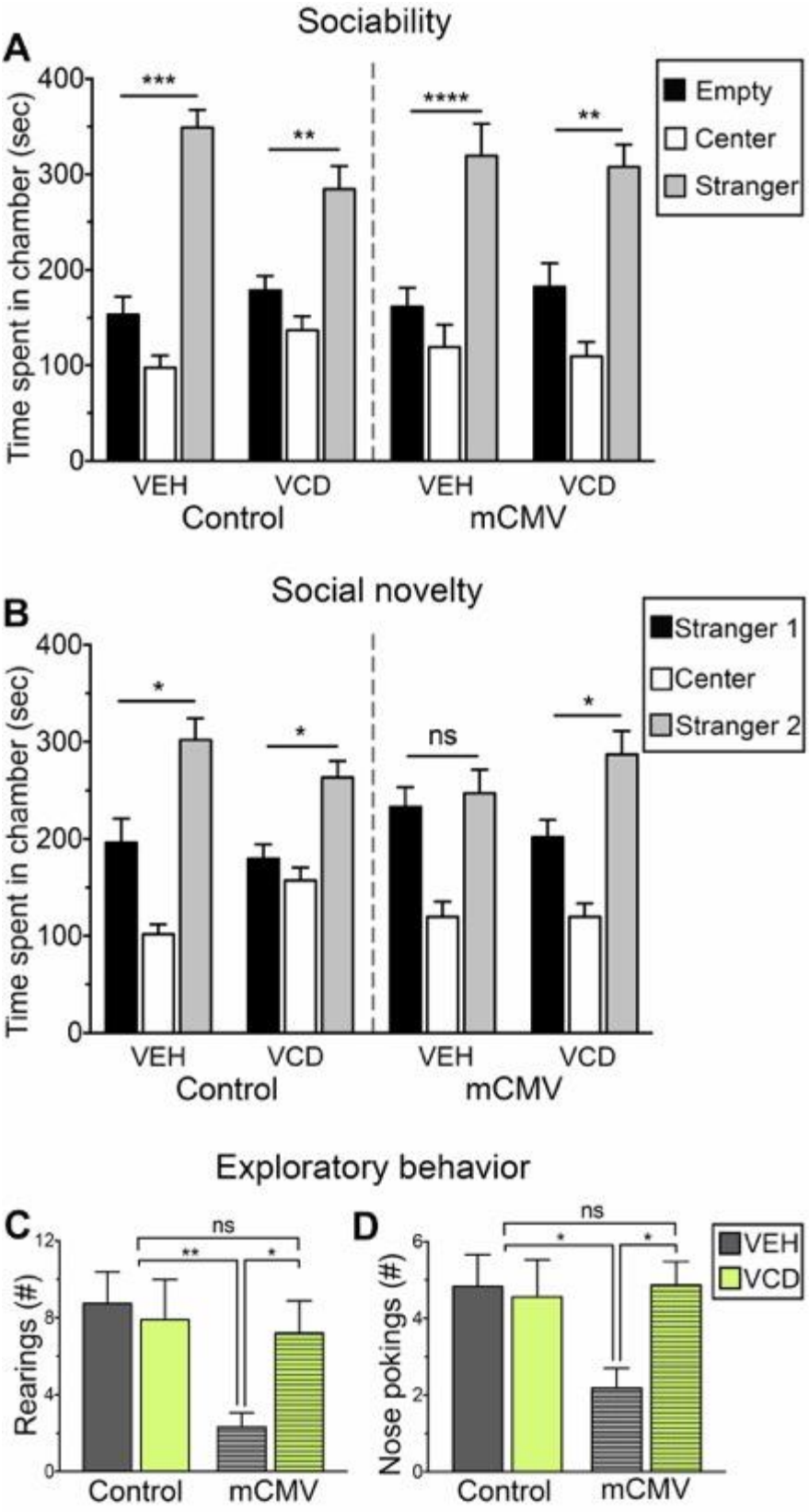
Sociability
A
Time spent in chamber (sec)
400
300
200
100
0
***
**
****
**
Empty
Center
Stranger
VEH
VCD
VEH
VCD
Control
mCMV
Social novelty
B
Time spent in chamber (sec)
400
300
200
100
0
*
*
ns
*
Stranger 1
Center
Stranger 2
VEH
VCD
VEH
VCD
Control
mCMV
Exploratory behavior
C
Rearings (#)
12
8
4
0
ns
**
*
Control
mCMV
D
Nose pokings (#)
6
4
2
0
ns
*
*
VEH
VCD
Control
mCMV

Fig. 3.19 Murine CMV infection during early development causes disturbances in social behavior and exploratory activity in adolescent mice. A, B. *Sociability (**A**) and preference for social novelty (**B**) assessment in infected and control mice, with or without VCD treatment, by means of the three-chamber test. Infected mice display regular sociability compared with control mice but lack preference for a novel mouse over a known mouse. This lack of preference for social novelty is restored by VCD administration.* ***C, D.*** *Exploratory activity was assessed by quantification of rearing (**C**) and nose-poking (**D**) events in a novel environment. The altered exploratory behavior with decreased number of events identified in mCMV-infected animals is rescued by VCD. Values are reported as the mean±SEM; n=10-13 mice/group for social behavior, n=18-22 mice/group for exploratory activity. ns, not significant. *p<0.05, **p<0.01, ***p<0.001, ****p<0.0001; two-way ANOVA with repeated measures and Bonferroni's post hoc comparison in **A, B**; Kruskal-Wallis with Dunn's post hoc test in **C, D**.*

3.2.5 Valnoctamide attenuates murine CMV-induced brain defects in early development.

Early-onset neurodevelopmental delays and long-term permanent neurobehavioral disabilities are commonly observed in hCMV-infected babies with evidence of virally induced brain abnormalities, including decreased brain size and cerebellar hypoplasia (de Vries et al., 2004; Gandhi and Khanna, 2004; Cheeran et al., 2009; Oosterom et al., 2015; James and Kimberlin, 2016). Since VCD showed a potent and fast-acting anti-CMV activity in the brains of infected mice and appeared beneficial to both short- and long-term neurobehavioral outcomes, we investigated whether drug treatment during early development could also exert therapeutic actions on mCMV-induced brain defects.

Brain size was analyzed in 1 month-old-mice by assessing the brain-to-body weight ratio (Fig. 3.20, A and B). This measurement allows a more objective evaluation of the postnatal brain growth, compared with absolute brain weight, when somatic growth restriction is present. Subcutaneous VCD rescued the deficient brain growth induced by mCMV, restoring brain-to-body weight ratio values similar to those in uninfected control mice.

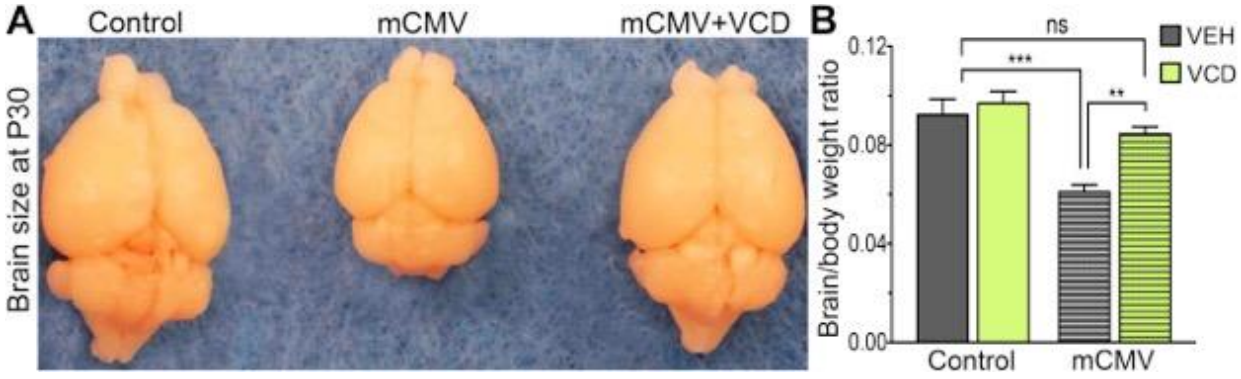

Fig. 3.20 Valnoctamide reverses deficient brain growth induced by murine CMV infection. ***A.*** *Photograph shows decreased brain size in an infected, untreated mouse (i.e., mCMV; middle) compared with an uninfected control (left). VCD treatment restores normal brain growth (mCMV+VCD, right).* ***B.*** *Quantification of VCD-mediated benefits on postnatal brain growth by calculation of brain-to-body weight ratio. Values are reported as the mean±SEM; n=10 mice/group (3 litters). ns, not significant. **p<0.01, ***p<0.001; one-way ANOVA with Bonferroni's post hoc test (**B**).*

Hypoplasia of the cerebellum is a common radiological finding in CMV-infected human babies (de Vries et al., 2004; Oosterom et al., 2015). A temporary delay in early postnatal cerebellar development was reported in newborn mice injected intraperitoneally with low titers of mCMV (Koontz et al., 2008). In our infected mice, we identified the cerebellum as a preferential site for viral localization in the brain. We examined cerebellar anatomy and histology in control and infected mice with or without VCD therapy. Murine CMV infection of the developing brain resulted in the disruption of cerebellar development, with a 60% decrease in the total area of this region compared with uninfected controls ($F=8.56$, $p<0.001$ ANOVA; Fig. 3.21, A and B). Infected mice displayed a substantial loss of PCs and a thinner ML, which contains PC dendritic trees, parallel fibers of the granule cells, Bergmann glia radial processes, and basket and stellate cells (Fig. 3.21, C-E). Reduced thickness of the cerebellar IGL was also found (Fig. 3.21F). PCs were not only decreased in number but also misplaced (Fig. 3.21G). In addition, the external granular layer (EGL), normally undetectable after P21 in rodent brains (Ferguson, 1996), could still be identified in mCMV-infected untreated mice at P30, whereas no EGL was visible in controls (Fig. 3.21H). Alignment of PCs and maturation of their dendritic trees, as well as granule cell precursor proliferation and inward migration from the EGL to the IGL, occur during the first 3 postnatal weeks of life in rodents (Inouye and Murakami, 1980; Ferguson, 1996). VCD treatment rescued the altered cerebellar development of infected animals, restoring normal cortical layer thickness and

representation and markedly increasing PC number (Fig. 3.21, C-H). These drug-mediated positive effects ultimately resulted in normalization of cerebellar size (Fig. 3.21, A and B).

No adverse side effects on either brain growth or morphometric parameters were detected in uninfected controls receiving VCD compared with their vehicle-treated counterparts.

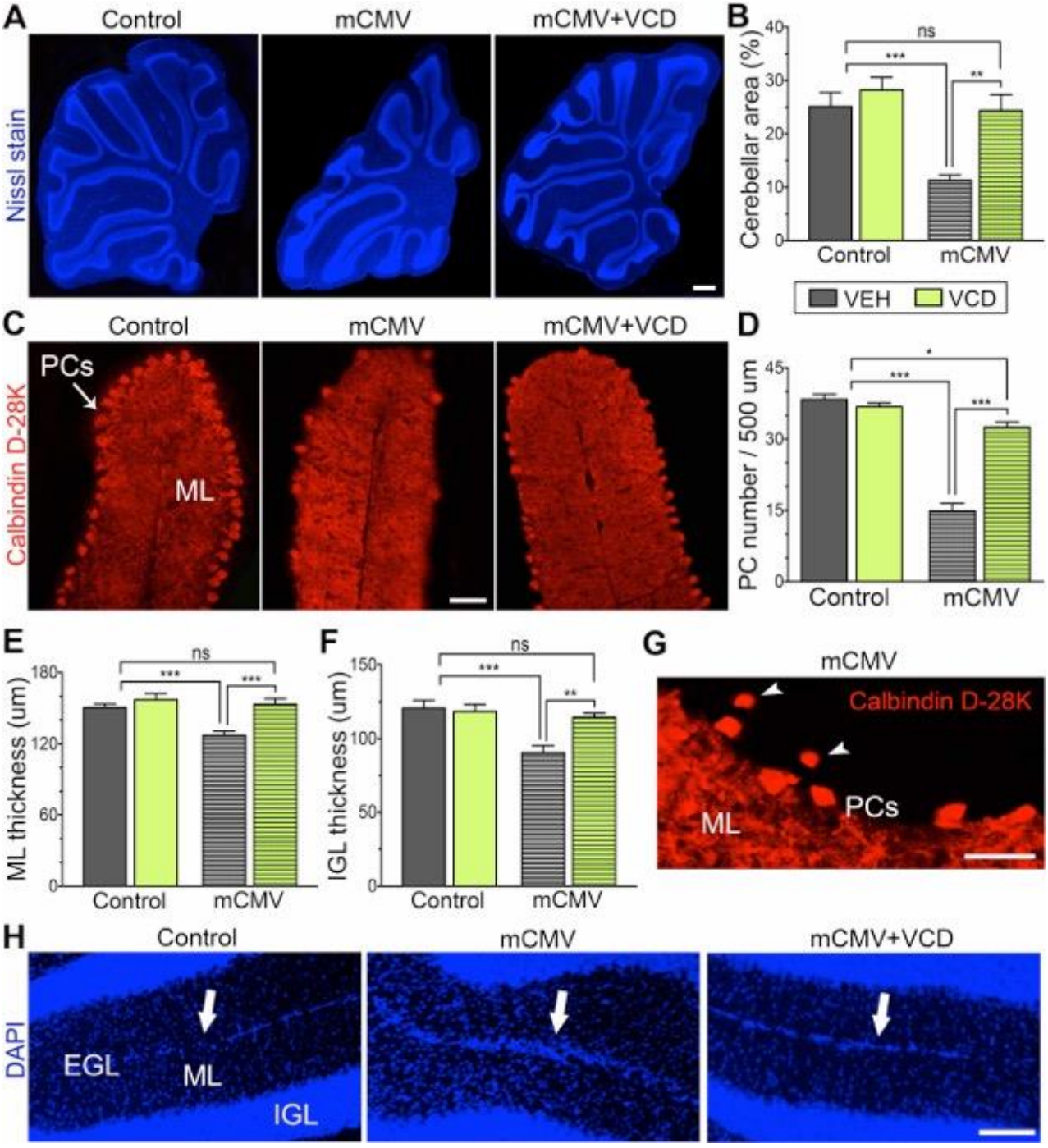

Fig. 3.21 Valnoctamide substantially ameliorates cerebellar development in murine CMV-infected mice. A. *Photomicrograph of representative fluorescent Nissl-stained cerebellar areas in control (left) and infected mice with (right, mCMV+VCD) or without (middle, mCMV) VCD. Note the delayed foliation in infected, untreated cerebellum, rescued by VCD. Scale bar, 200 µm.* ***B.*** *Graph depicts cerebellar area, expressed as a percentage of total brain area (three sagittal sections/animal, five animals/group).* ***C.*** *Photomicrograph showing cerebellar PCs and ML by means of calbindin D-28K staining. Infected, untreated cerebellum (middle) displays loss of PCs and thinner ML compared with uninfected control (left); VCD improves both parameters (right). Scale bar, 200 µm.* ***D-F.*** *Quantification of PC number (**D**), and ML (**E**) and IGL thickness (**F**) along 500 µm of the primary fissure (both sides; three sagittal sections/mouse, five mice/group).* ***G.*** *Fluorescent micrograph of heterotopic PCs (arrowheads) identified in an infected untreated cerebellum. Scale bar, 100 µm.* ***H.*** *Photomicrograph displays pathological persistence of EGL in mCMV-infected, untreated cerebellum at P30 (middle); no EGL could be identified at the same time point in uninfected control (left) and infected, VCD-treated cerebellum (right). Scale bar, 200 µm. Values are reported as the mean±SEM. ns, not significant. *p<0.05, **p<0.01, ***p<0.001; one-way ANOVA with Bonferroni's post hoc test.*

3.2.6 Block of human CMV infection in human fetal brain cells.

Mouse and human forms of CMV share a close similarity in their viral genomes, but each retains species specificity (Rawlinson et al., 1996; Mocarski et al., 2013). In the experiments above, we used mCMV in mice. Here, to corroborate that the results we found above in our *in vivo* model with mCMV generalize to hCMV, we examined the actions of VCD on hCMV-infected human fetal astrocytes, a common cellular target that can play an important role in virus dispersal in the brain (Lokensgard et al., 1999; van Den Pol et al., 1999). VCD substantially decreased hCMV infectivity of human fetal astrocytes as assessed by quantification of cells expressing the hCMV-GFP-reporter (Fig. 3.22A). Viral replication was also diminished in the presence of the drug, with a reduction in viral titer by 100-fold ($4.92 \times 10^5 \pm 5.84 \times 10^4$ pfu/ml in vehicle-treated cultures vs $6.31 \times 10^3 \pm 3.06 \times 10^3$ pfu/ml in VCD-treated cultures; $p<0.0001$, Mann-Whitney U test; Fig. 3.22B).

In our initial *in vitro* experiments, we observed that VPD and VCD appear to act at an early stage of hCMV infection in human dermal fibroblasts. To determine whether VCD could exert a similar early block of hCMV replication cycle also in human fetal astrocytes, we used a series of experiments assessing virus attachment to the cellular surface and penetration into the cytoplasmic space as described above. Briefly, this was accomplished by shifting the incubation temperature from 4°C, which allows virus attachment but not fusion and internalization, to 37°C, which allows virus fusion and internalization

(Chan and Yurochko, 2014). Viral genome quantification by qRT-PCR showed that VCD appeared to block hCMV attachment to fetal astrocytes (Fig. 3.22C). In the presence of VCD, the amount of virus bound to the cell surface was decreased by 60% compared with control cultures not treated with VCD (p=0.0007, unpaired Student's t test). VCD did not appear to block hCMV fusion/internalization in the astrocytes. This also corroborates that the mechanism of VCD block of hCMV occurs at an early stage of infection and appears unrelated to the genomic mechanisms of other approved anti-CMV compounds.

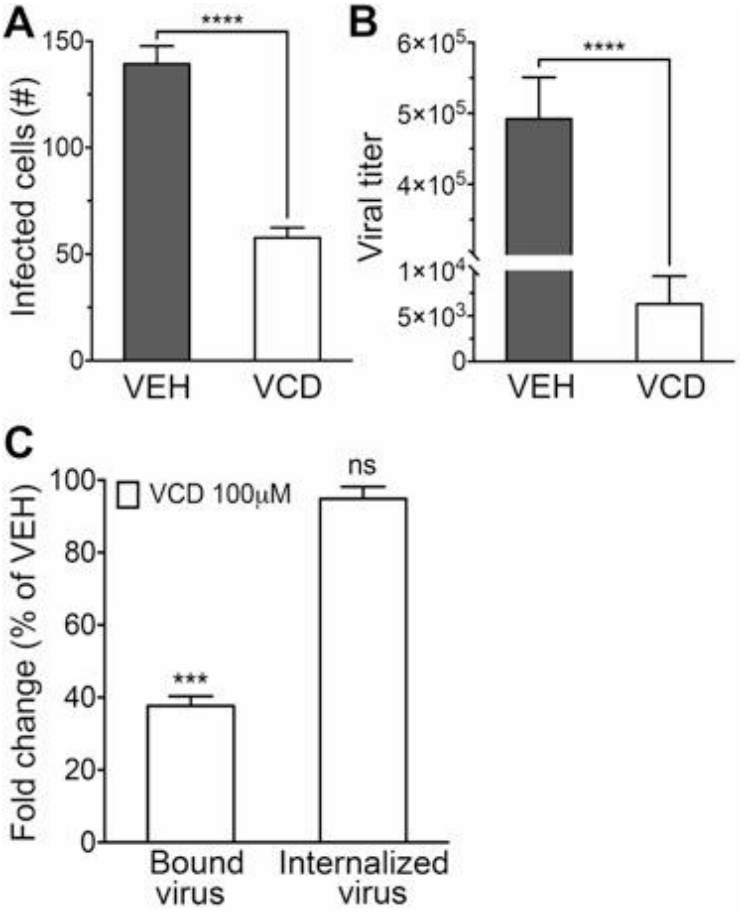

Fig. 3.22 Valnoctamide suppresses human CMV infectivity and replication in human fetal astrocytes by blocking virus attachment to the cell. A, B. *Human fetal astrocyte cells were pretreated (for 1 h) with VCD (100 µM) or vehicle (VEH) before inoculation with hCMV using an MOI of 0.1. VCD treatment decreased hCMV infectivity and replication as assessed by GFP-positive cell counting (**A**) and viral yield assay (**B**) at 48 hpi. **C.** Virus-inoculated human fetal astrocytes were exposed to VCD or vehicle (100 µM) for 1 h at either 4°C or 37°C to assess hCMV attachment to ("bound virus") and internalization into ("internalized virus") the cell. Viral DNA was quantified by qRT-PCR and results expressed as the percentage of control (vehicle-treated cultures considered as 100%). Graphs represent the average of three separate experiments each performed in triplicate;*

*error bars correspond to SE. ns, not significant. ***p<0.001, ****p<0.0001, unpaired Student's t test in **A, C**; Mann-Whitney U test in **B**; in **C**, significance refers to the comparison between VCD and vehicle-treated cultures in each assay.*

Chapter 4

Discussion and Conclusions.

4.1 Discussion.

Our work shows that VPD and VCD, two orally available drugs used for many years in clinics to treat neuropsychiatric disorders, evoke a substantial and specific inhibition of both mouse and human CMV. The anti-CMV activity of these compounds has never been described.

The VPD- and VCD-mediated antiviral effect is substantiated by multiple converging lines of *in vitro* evidence, including: 1) reduction in infected cell number, as determined with GFP reporter expression, immunocytochemistry against hCMV gB, and qPCR; 2) reduction in virally induced cell death quantified with ethidium homodimer; 3) reduction in virus plaque number and size; and 4) reduction in viral replication and virion release. Neither VPD nor VCD displayed detectable cytotoxicity even at highest concentrations tested.

Importantly, both compounds also block CMV infection *in vivo*, leading to increased survival, improved body weight, ameliorated postnatal somatic development, and decreased viral load in peripheral target organs of infected neonatal mice receiving treatment subcutaneously. Also, low-dose VCD administered outside the brain during early development effectively suppresses CMV inside the brain of infected animals via two different sites of action. One is that VCD reduces peripheral levels of CMV, thereby decreasing the amount of virus available for entry into the brain. A second is that VCD acts directly within the brain to block existing brain CMV infection. Of note, the antiviral action of VCD begins shortly after drug administration and effectively attenuates CMV levels throughout the brain during the critical period of postnatal brain development. This decrease in viral load is accompanied by a concomitant restoration of normal early neurological outcomes in infected neonatal mice treated with VCD. Late-onset neurobehavioral dysfunction, including motor impairment and social and exploratory behavior disturbances, as well as virally induced deficient brain growth and disrupted cerebellar development, are substantially attenuated in CMV-infected adolescent mice which received VCD during the neonatal period, suggesting long-lasting beneficial effects of drug administration.

An important underlying rationale of our study is that the newborn mouse brain is substantially less developed than the newborn human brain. Based on the timing of the brain growth spurt, initial neurogenesis, cerebellar foliation and maturation, establishment and refinement of connections, myelination, and gliogenesis, the mouse CNS at birth is proposed to parallel the early second-trimester human fetal CNS (Clancy et al., 2001; Branchi et al., 2003; Clancy et al., 2007a; Clancy et al., 2007b;

Workman et al., 2013). This is a critical period for human brain development and for CMV infection (Manicklal et al., 2013). By infecting mouse pups on the day of birth, this animal model provides an informative means to study the effects of CMV on the developing brain. Infected newborn mice display similar brain pathology and neurological symptoms to that reported in congenitally infected human infants, including microcephaly, cerebellar hypoplasia, neuronal loss, neurodevelopmental delays, motor impairments, and behavioral disturbances (Perlman and Argyle, 1992; de Vries et al., 2004; Pass et al., 2006; Lipitz et al., 2013; Kimberlin et al., 2015; De Kegel et al., 2016; James and Kimberlin, 2016). These data support the validity of this *in vivo* model for investigating CMV infection and novel anti-CMV treatments during early brain development. Further confirmation of viability of this experimental model for assessing virally induced neurological complications during early neurontogeny also derives from our recent study on the effects of Zika virus in the developing brain (van den Pol et al., 2017) (see Appendix).

Despite being partially effective, currently available CMV antiviral agents, including GCV and its prodrug valGCV, cidofovir, foscarnet, and fomivirsen, display both toxic and teratogenic actions (Mercorelli et al., 2011; James and Kimberlin, 2016). For this reason, they are not approved or recommended for the treatment of pregnant women and their infected fetuses, thus depriving those who may need it the most or at best delaying treatment and hindering potential prevention or amelioration of CMV-induced brain defects during *in utero* development (Kimberlin et al., 2015). GCV and valGCV are currently administered as off-label treatment in postnatally infected premature infants with life-threatening CMV-mediated disease (Amin et al., 1990; Fischer et al., 2010; Okulu et al., 2012) and in congenitally infected neonates with viral involvement of the CNS (Kimberlin et al., 2003; Kimberlin et al., 2015). However, acute and long-term toxicity, namely neutropenia, gonadal toxicity, and carcinogenicity, limit the use of these drugs only to those newborns with severe signs of infection (Crumpacker, 1996; Gandhi and Khanna, 2004; Mercorelli et al., 2011; Rawlinson et al., 2016), leaving less severely affected neonates with no treatment and, hence, at risk for developing late-onset neurological complications (Lackner et al., 2009). The toxicity associated with anti-CMV drug administration also represents a substantial issue in immunocompromised patients, who are at high risk for developing severe, possibly life-threatening CMV-mediated disease (Britt, 2011; Mercorelli et al., 2011; Mocarski et al., 2013). Therefore, it is evident that development of anti-CMV compounds with safer *in vivo* profiles that can be used not only during pregnancy but also in all infected neonates and in cases of compromised systemic immunity would be of substantive benefit. The high burden of CMV-

related morbidity during early development and in conditions of reduced immunity strongly supports research efforts towards identification of novel anti-CMV therapies (Cannon and Davis, 2005; Kenneson and Cannon, 2007; Cannon, 2009; Boppana et al., 2013; James and Kimberlin, 2016; McIntosh et al., 2016; Mestas, 2016).

VPD and VCD have been marketed since the early 1960s and no safety concerns have been raised (Stepansky, 1960; Goldberg, 1961; Harl, 1964; Bialer, 1991; Bersudsky et al., 2010; Weiser et al., 2017). Further confirmation of safety profile has derived from preclinical investigations of drug-related anti-convulsant activity in several experimental models of epilepsy (Porter et al., 1984; Lindekens et al., 2000; Isoherranen et al., 2003; Mares et al., 2013; Shekh-Ahmad et al., 2013; Shekh-Ahmad et al., 2014; Shekh-Ahmad et al., 2015; Bialer et al., 2017). In addition, neither compound showed increased teratogenic or toxic potential compared to vehicle in multiple studies using different animal models of early development (Nau and Loscher, 1986; Nau and Scott, 1987; Radatz et al., 1998; Okada et al., 2004; Shekh-Ahmad et al., 2014; Mawasi et al., 2015; Wlodarczyk et al., 2015; Bialer et al., 2017). Importantly, we detected no adverse collateral effects on postnatal body growth and neurodevelopmental and behavioral outcomes of uninfected control mice receiving VPD or VCD throughout the neonatal period. However, VCD has better translational potential than VPD. VCD acts as a drug on its own in mice, rats, dogs, and humans (Haj-Yehia and Bialer, 1988; Bialer et al., 1990; Bialer, 1991; Blotnik et al., 1996; Barel et al., 1997; Radatz et al., 1998). In turn, VPD, while showing negligible conversion to VPA in mice (Radatz et al., 1998), is largely metabolized (>80%) to VPA in humans (Bialer et al., 1990; Bialer, 1991; Barel et al., 1997). As mentioned above, VPA is toxic, teratogenic, and can enhance virus infections (Nau et al., 1991; Kuntz-Simon and Obert, 1995; Moog et al., 1996; Radatz et al., 1998; Shaw et al., 2000; Phiel et al., 2001; Michaelis et al., 2004; Okada et al., 2004; Michaelis et al., 2005; Otsuki et al., 2008; Mardivirin et al., 2009; Tung and Winn, 2010; Paglino and van den Pol, 2011; Kataoka et al., 2013; Paradis and Hales, 2013; Nakashima et al., 2015; Paradis and Hales, 2015). Therefore, VCD represents the best candidate for further investigation in both pre-clinical and clinical settings of CMV-mediated disease during early development and in conditions of compromised systemic immunity.

Alongside with toxicity and teratogenicity, currently approved anti-CMV drugs display additional drawbacks, including a shared mechanism of action based on block of viral DNA replication and limited CNS penetration (Mercorelli et al., 2011; Campanini et al., 2012; Choi et al., 2013; Morillo-Gutierrez et al., 2017). Given the increasing emergence of drug-resistant CMV strains and the substantial

burden of congenital CMV-induced brain damage and neurological disability, these therapeutic limitations pose further challenges in the treatment of CMV infection.

VCD, as well as VPD, appears to act on an early stage of CMV infection by interfering with viral attachment to cell surface HSPGs, as we demonstrated both in human fibroblasts and human fetal astrocytes. This is a different mechanism of action as compared to the available CMV antivirals. Also, it differs from the antiviral mechanism suggested to underlie VPD-mediated inhibition of herpes virus EBV reactivation, based on VPD-induced suppression of viral and cellular gene expression (Gorres et al., 2014; Gorres et al., 2016). The drug-mediated block of CMV attachment may be due to a reversible interaction with either HSPGs or free virions or may require the simultaneous presence of both the virus and the cell. The alternative mechanism of action of VCD against CMV suggests the potential of this compound to act as a valid therapeutic option in case of resistant viral isolates, a substantial concern in immunocompromised patients and an increasing issue in congenitally infected infants undergoing prolonged antiviral therapy (Mercorelli et al., 2011; Campanini et al., 2012; Choi et al., 2013; Morillo-Gutierrez et al., 2017). Also, the different mechanism of anti-CMV activity of VCD supports the use of this drug in combination treatment with already approved anti-CMV compounds to decrease the emergence of resistant viral mutants and enhance efficacy of antiviral therapy (Drew, 2000; James and Prichard, 2011; Campanini et al., 2012; Choi et al., 2013; Coen and Richman, 2013). Here we show that VCD used together with GCV generates an additive effect in blocking CMV. Targeting of CMV attachment by VCD may also associate with additional therapeutic benefits, including the lack of need to enter the cell to exert its antiviral actions and the inhibition of the synthesis of viral proteins, which can both be cytotoxic (Mercorelli et al., 2011). We did not identify any VCD-induced cytotoxicity even at highest drug concentrations tested. Moreover, block of virus attachment might better prevent CMV transmission via bodily fluids, such as urine, saliva, breast milk, and genital secretions, containing cell-free virus at high titers (Britt, 2008). This is of particular importance for both pregnant or breast-feeding mothers and immunocompromised individuals.

Preclinical investigation of pharmacokinetic properties of VCD head-to-head with VPA showed improved CNS distribution of VCD after peripheral administration (Blotnik et al., 1996). By using intracranial inoculation of CMV in mouse pups, we demonstrated that low-dose VCD administered subcutaneously can cross the BBB, enter the brain, and effectively block viral replication and dispersal within the brain, with improved short- and long-term neurological outcomes of infected mice. This enhanced CNS targeting of VCD, as compared to the available CMV antivirals, is of utmost value since

CMV-mediated brain dysfunctions are the most severe complications following infection during early development.

Dose-response relationship analyses revealed that GCV, currently the first-line therapy for CMV, is a more potent compound than VCD *in vitro*. Thus, a less effective anti-CMV activity of VCD compared to GCV might be expected *in vivo*. Nonetheless, we found substantial CMV inhibition in both peripheral organs and brain of infected mice with subcutaneous drug delivery. The dose of VCD we use here, with a 6 g-developing mouse body weight, is 5 mg/kg, corresponding to 1/199.8 fraction of the VCD-LD_{50} value (Wlodarczyk et al., 2015). This amount is similar to or less than the dose of existing compounds used to treat CMV in clinical settings. For instance, assuming a 60 kg-body weight, GCV can be used from 5 up to 20 mg/kg/day, corresponding to 1/400 to 1/100 fraction of the GCV-LD_{50} value (Wishart et al., 2006), in patients with serious infections (Kotton et al., 2013; Choopong et al., 2016; Genentech USA, 2016). Furthermore, the 5 mg/kg dose of VCD for treating CMV infection is lower than the dose used to safely attenuate seizures and neuropathic pain in neonatal and adult rodent experiments (Winkler et al., 2005; Kaufmann et al., 2010; Mares et al., 2013; Shekh-Ahmad et al., 2014), and is less than the 20 mg/kg dose that has been used in humans to treat psychiatric dysfunction with no evidence of safety concerns (Stepansky, 1960; Goldberg, 1961; Harl, 1964; Bersudsky et al., 2010; Weiser et al., 2017). Together, these findings suggest that VCD may be able to attenuate CMV in the human brain at doses that should be both effective and tolerable. The reduction of CMV infection of human fetal astrocytes by VCD further supports the hypothesis that VCD should be effective against CMV in the human brain.

Epilepsy is among the most severe neurological complications that can develop in neonates with symptomatic congenital CMV infection (Suzuki et al., 2008; Smithers-Sheedy et al., 2017). VPA is the first-line therapy for pediatric epilepsy (Guerrini, 2006); however, VPA at therapeutic doses for anticonvulsant purposes can be toxic to the liver (Guerrini, 2006; Monti et al., 2009) and enhance CMV infectivity and replication (Pisani et al., 1986; Kuntz-Simon and Obert, 1995; Michaelis et al., 2004; Michaelis et al., 2005). VCD has proven to be as a less toxic and more potent anti-seizure agent than VPA in multiple animal models of epilepsy (Barel et al., 1997; Radatz et al., 1998; Kaufmann et al., 2010; White et al., 2012; Mares et al., 2013; Shekh-Ahmad et al., 2013; Shekh-Ahmad et al., 2014; Wlodarczyk et al., 2015), partly by acting on gamma-aminobutyric acid A ($GABA_A$) receptors with prolongation of miniature inhibitory post-synaptic currents (Spampanato and Dudek, 2014). Here we demonstrate that VCD administered subcutaneously enters the brain and effectively blocks CMV infection *in situ*. This CNS-targeted antiviral activity of VCD occurs at doses lower than the doses found

to be effective in suppressing seizures in epileptic adult and, more importantly, neonatal rodents (Kaufmann et al., 2010; Mares et al., 2013; Shekh-Ahmad et al., 2014). These results indicate that VCD might be able to safely and effectively act as both an anti-CMV drug and an antiepileptic agent in congenitally CMV-infected neonates experiencing seizures.

Congenital CMV infection, both with and without brain abnormalities and sensorial deficits, has been suggested as a potential etiological factor of ASD (Stubbs et al., 1984; Yamashita et al., 2003; Engman et al., 2015; Sakamoto et al., 2015; Garofoli et al., 2017). A five percent prevalence of CMV DNA has been reported in cord blood-derived dried spots from ASD children as compared to a 0.2% prevalence identified in the general population (Gentile et al., 2017). Notably, this five percent prevalence of congenital CMV among ASD individuals is similar to the prevalence of other disorders already known to be associated with ASD, such as Fragile X syndrome and tuberous sclerosis (Eriksson et al., 2013). Virally induced immune activation and subsequent brain inflammation during critical moments of neurontogeny, as well as brain deficits, including cerebellar hypoplasia and PC dysfunction and loss, might play a role in congenital CMV-associated ASD development (Shi et al., 2003; Shi et al., 2009; Fatemi et al., 2012; Tsai et al., 2012; Basson and Wingate, 2013; Hampson and Blatt, 2015; Mazarati et al., 2017). Abnormal GABA signaling in selective neuronal circuits with delayed excitatory-to-inhibitory switch, as a possible consequence of viral challenge mediated-immune activation (Corradini et al., 2017), may lead to excitatory/inhibitory imbalance in the developing brain and ASD-like behavioral disturbances (Sgado et al., 2011; Cellot and Cherubini, 2014; Jung et al., 2017). Additionally, PCs are the sole output of the cerebellar cortex and missing/dysfunctional PCs could translate to decreased GABA inhibition to excitatory cells in the deep cerebellar nuclei and subsequent increased excitatory input to the thalamus and cerebral cortex, likely contributing to ASD phenotype (Hampson and Blatt, 2015). Widespread foci of virus infected cells surrounded by mononuclear cells, increased expression of proinflammatory cytokines and interferon-stimulated genes, and substantial microgliosis have been described in the brain of neonatal mice infected i.p. with low titer-CMV (Koontz et al., 2008; Kosmac et al., 2013; Seleme et al., 2017). In addition, CMV i.p. infection during early mouse development and virally induced mouse brain inflammation associated with abnormal expression of developmentally regulated genes in the cerebellum, including $GABA_A$ receptor, and delayed cerebellar foliation and maturation. Here we show that CMV inoculated i.p. in newborn mice on the day of birth consistently targets the cerebellum as preferential site for initial viral localization in the brain, with evidence of robust viral GFP labeling in both PCs and granule neurons. Infected adolescent animals

display disrupted cerebellar ontogeny with decreased cerebellar area, PC loss and misplacement, and reduced ML and IGL thickness, alongside with ASD-like behavioral abnormalities, including lack of preference for social novelty and impaired novel environment exploration. VCD treatment throughout the neonatal period effectively control CMV replication in the developing brain, rescues cerebellar deficits, and restores behavioral responses similar to the uninfected controls. These results corroborate the utility of our *in vivo* model for investigating CMV-mediated neurobehavioral anomalies and novel anti-CMV therapeutics, and may provide initial evidence for a potential role of CMV infection during early development in ASD. Importantly, VCD action on $GABA_A$ receptors (Spampanato and Dudek, 2014) may play an additional beneficial role on CMV-related ASD-like behavioral phenotype by balancing excitatory/inhibitory signaling within the developing brain (Cellot and Cherubini, 2014; Hampson and Blatt, 2015). If the pathogenic role of congenital CMV in ASD should be confirmed in future studies, this would represent a potential treatable cause of ASD. Also, this would support the inclusion of dried blood spot-CMV DNA detection in the diagnostic work-up for ASD cases, as recently proposed (Engman et al., 2015).

4.2 Concluding remarks and future perspectives.

We examined two drugs, VPD and VCD, which display unexpected anti-CMV properties. Both compounds are amide derivatives of VPA but lack the inhibitory action on HDAC which underlies VPA-mediated detrimental effects on early fetal development. In humans, VPD can be metabolized to the toxic, teratogenic, and CMV-enhancing VPA. Therefore, VPD would not be an ideal anti-CMV drug candidate in the clinic, particularly in the treatment of pregnant mothers and their fetuses. In contrast, VCD has minimal conversion to its corresponding free acid and no conversion to VPA in humans, thus representing the compound of choice for further investigation in both pre-clinical and clinical settings of CMV-mediated disease. However, the evidence of a potent anti-CMV activity for both VPD and VCD, which are related compounds, suggests that other structurally related molecules may also possess antiviral potential. Also, because VPD and VCD have similar antiepileptic actions and sedative properties in psychiatric patients, this raises the possibility that the neurotropic and antiviral mechanisms of action may not be unrelated.

Our study shows that subcutaneous low-dose VCD effectively and safely attenuates CMV replication in the developing mouse, with increased survival and improved postnatal growth and somatic development. Also, VCD treatment rescues infected animals from virally induced brain defects and

adverse short- and long-term neurological outcomes. Here we focused on newborn mice; further studies focusing on VCD anti-CMV efficacy in *in utero* fetal development and on the inhibition of transplacental transmission leading to fetal infection will be beneficial.

Our results also show that VCD suppresses CMV replication in human fetal brain cells and human fibroblasts by blocking viral attachment to the cell surface, a different mechanism of action compared to the available CMV antivirals. This suggests the potential of VCD as a therapeutic option in congenitally infected neonates requiring prolonged antiviral therapy and in immunocompromised adults, for whom the emergence of drug-resistant CMV strains has become a challenge. Combination therapies, which can include two or more antiviral compounds, may help in controlling this problem, but are limited by drug-related toxicity and CMV cross-resistance to currently approved antiviral agents. By displaying a good safety profile and a novel mechanism of anti-CMV activity, VCD may represent a valid therapeutic choice for effective and safe combination treatments potentially meriting clinical testing in infected infants and immunocompromised individuals.

Human CMV has been detected in a substantial number of brain tumors and has been postulated to play a role in the initiation or progression of malignant gliomas (Cobbs et al., 2007; Odeberg et al., 2007; Knight et al., 2013), although the possibility remains that CMV has a greater affinity for existing glial-type cancer cells than for normal brain cells (van Den Pol et al., 1999) rather than a causative role in oncogenesis. Although further substantiation is merited (Lau et al., 2005), if CMV does play a role in the enhancement of human brain tumor growth, the use of VCD to attenuate CNS CMV may prove beneficial in attenuating tumor progression.

In conclusion, considering that VCD has already been used clinically for many years with no safety concerns, has proven to be safe in multiple models of early development, has optimal CNS targeting, and displays a novel mechanism of anti-CMV action, it may merit further clinical testing for possible therapeutic utility in the treatment of CMV infection during early human development and in conditions of reduced systemic immunity. The fact that VCD is already approved for the treatment of neuropsychiatric disorders in adult individuals should greatly reduce the typically long period required to bring a new antiviral drug into use. Results from clinical testing in immunocompromised adults with CMV-mediated disease could help in paving the way for clinical studies during *in utero* and early postnatal human development.

References

Adler SP, Nigro G, Pereira L (2007) Recent advances in the prevention and treatment of congenital cytomegalovirus infections. Semin Perinatol 31:10-18.

Ahlfors K, Ivarsson SA, Harris S (2001) Secondary maternal cytomegalovirus infection--A significant cause of congenital disease. Pediatrics 107:1227-1228.

Almishaal AA, Mathur PD, Hillas E, Chen L, Zhang A, Yang J, Wang Y, Yokoyama WM, Firpo MA, Park AH (2017) Natural killer cells attenuate cytomegalovirus-induced hearing loss in mice. PLoS Pathog 13:e1006599.

American Psychiatric Association (2013) Diagnostic and statistical manual of mental disorders (DSM-5®): American Psychiatric Pub.

Amin H, Jadavji T, Sauve R, Gill J (1990) Use of ganciclovir in the treatment of acquired cytomegalovirus disease in a preterm infant. Can J Infect Dis 1:28-30.

Ancora G, Lanari M, Lazzarotto T, Venturi V, Tridapalli E, Sandri F, Menarini M, Ferretti E, Faldella G (2007) Cranial ultrasound scanning and prediction of outcome in newborns with congenital cytomegalovirus infection. J Pediatr 150:157-161.

Arvin AM, Fast P, Myers M, Plotkin S, Rabinovich R (2004) Vaccine development to prevent cytomegalovirus disease: report from the National Vaccine Advisory Committee. Clin Infect Dis 39:233-239.

Azad RF, Driver VB, Tanaka K, Crooke RM, Anderson KP (1993) Antiviral activity of a phosphorothioate oligonucleotide complementary to RNA of the human cytomegalovirus major immediate-early region. Antimicrob Agents Chemother 37:1945-1954.

Bale JF, Jr., Bray PF, Bell WE (1985) Neuroradiographic abnormalities in congenital cytomegalovirus infection. Pediatr Neurol 1:42-47.

Bantug GR, Cekinovic D, Bradford R, Koontz T, Jonjic S, Britt WJ (2008) CD8+ T lymphocytes control murine cytomegalovirus replication in the central nervous system of newborn animals. J Immunol 181:2111-2123.

Barbi M, Binda S, Caroppo S, Calvario A, Germinario C, Bozzi A, Tanzi ML, Veronesi L, Mura I, Piana A, Solinas G, Pugni L, Bevilaqua G, Mosca F (2006) Multicity Italian study of congenital cytomegalovirus infection. Pediatr Infect Dis J 25:156-159.

Barel S, Yagen B, Schurig V, Soback S, Pisani F, Perucca E, Bialer M (1997) Stereoselective pharmacokinetic analysis of valnoctamide in healthy subjects and in patients with epilepsy. Clin Pharmacol Ther 61:442-449.

Barkovich AJ, Lindan CE (1994) Congenital cytomegalovirus infection of the brain: imaging analysis and embryologic considerations. AJNR Am J Neuroradiol 15:703-715.

Barry PA, Lockridge KM, Salamat S, Tinling SP, Yue Y, Zhou SS, Gospe SM, Jr., Britt WJ, Tarantal AF (2006) Nonhuman primate models of intrauterine cytomegalovirus infection. Ilar j 47:49-64.

Bartlett AW, McMullan B, Rawlinson WD, Palasanthiran P (2017) Hearing and neurodevelopmental outcomes for children with asymptomatic congenital cytomegalovirus infection: A systematic review. Rev Med Virol.

Baskar JF, Stanat SC, Sulik KK, Huang ES (1983) Murine cytomegalovirus-induced congenital defects and fetal maldevelopment. J Infect Dis 148:836-843.

Baskar JF, Peacock J, Sulik KK, Huang ES (1987) Early-stage developmental abnormalities induced by murine cytomegalovirus. J Infect Dis 155:661-666.
Basson MA, Wingate RJ (2013) Congenital hypoplasia of the cerebellum: developmental causes and behavioral consequences. Front Neuroanat 7:29.
Bate SL, Dollard SC, Cannon MJ (2010) Cytomegalovirus seroprevalence in the United States: the national health and nutrition examination surveys, 1988-2004. Clin Infect Dis 50:1439-1447.
Bego MG, St Jeor S (2006) Human cytomegalovirus infection of cells of hematopoietic origin: HCMV-induced immunosuppression, immune evasion, and latency. Exp Hematol 34:555-570.
Bentz GL, Jarquin-Pardo M, Chan G, Smith MS, Sinzger C, Yurochko AD (2006) Human cytomegalovirus (HCMV) infection of endothelial cells promotes naive monocyte extravasation and transfer of productive virus to enhance hematogenous dissemination of HCMV. J Virol 80:11539-11555.
Bernard S, Wiener-Vacher S, Van Den Abbeele T, Teissier N (2015) Vestibular Disorders in Children With Congenital Cytomegalovirus Infection. Pediatrics 136:e887-895.
Bersudsky Y, Applebaum J, Gaiduk Y, Sharony L, Mishory A, Podberezsky A, Agam G, Belmaker RH (2010) Valnoctamide as a valproate substitute with low teratogenic potential in mania: a double-blind, controlled, add-on clinical trial. Bipolar Disord 12:376-382.
Bevot A, Hamprecht K, Krageloh-Mann I, Brosch S, Goelz R, Vollmer B (2012) Long-term outcome in preterm children with human cytomegalovirus infection transmitted via breast milk. Acta Paediatr 101:e167-172.
Bialer M (1991) Clinical pharmacology of valpromide. Clin Pharmacokinet 20:114-122.
Bialer M, Haj-Yehia A, Barzaghi N, Pisani F, Perucca E (1990) Pharmacokinetics of a valpromide isomer, valnoctamide, in healthy subjects. Eur J Clin Pharmacol 38:289-291.
Bialer M, Johannessen SI, Levy RH, Perucca E, Tomson T, White HS (2017) Progress report on new antiepileptic drugs: A summary of the Thirteenth Eilat Conference on New Antiepileptic Drugs and Devices (EILAT XIII). Epilepsia 58:181-221.
Biron KK (2006) Antiviral drugs for cytomegalovirus diseases. Antiviral Res 71:154-163.
Blazquez-Gamero D, Galindo Izquierdo A, Del Rosal T, Baquero-Artigao F, Izquierdo Mendez N, Soriano-Ramos M, Rojo Conejo P, Gonzalez-Tome MI, Garcia-Burguillo A, Perez Perez N, Sanchez V, Ramos-Amador JT, De la Calle M (2017) Prevention and treatment of fetal cytomegalovirus infection with cytomegalovirus hyperimmune globulin: a multicenter study in Madrid. J Matern Fetal Neonatal Med:1-211.
Blotnik S, Bergman F, Bialer M (1996) Disposition of valpromide, valproic acid, and valnoctamide in the brain, liver, plasma, and urine of rats. Drug Metab Dispos 24:560-564.
Bojic U, Elmazar MM, Hauck RS, Nau H (1996) Further branching of valproate-related carboxylic acids reduces the teratogenic activity, but not the anticonvulsant effect. Chem Res Toxicol 9:866-870.
Boppana SB, Fowler KB (2017) Insight Into Long-term Neurodevelopmental Outcomes in Asymptomatic Congenital CMV Infection. Pediatrics.
Boppana SB, Ross SA, Fowler KB (2013) Congenital cytomegalovirus infection: clinical outcome. Clin Infect Dis 57 Suppl 4:S178-181.
Boppana SB, Fowler KB, Britt WJ, Stagno S, Pass RF (1999) Symptomatic congenital cytomegalovirus infection in infants born to mothers with preexisting immunity to cytomegalovirus. Pediatrics 104:55-60.

Boppana SB, Rivera LB, Fowler KB, Mach M, Britt WJ (2001) Intrauterine transmission of cytomegalovirus to infants of women with preconceptional immunity. N Engl J Med 344:1366-1371.

Boppana SB, Fowler KB, Vaid Y, Hedlund G, Stagno S, Britt WJ, Pass RF (1997) Neuroradiographic findings in the newborn period and long-term outcome in children with symptomatic congenital cytomegalovirus infection. Pediatrics 99:409-414.

Boppana SB, Ross SA, Shimamura M, Palmer AL, Ahmed A, Michaels MG, Sanchez PJ, Bernstein DI, Tolan RW, Jr., Novak Z, Chowdhury N, Britt WJ, Fowler KB (2011) Saliva polymerase-chain-reaction assay for cytomegalovirus screening in newborns. N Engl J Med 364:2111-2118.

Bradford RD, Yoo YG, Golemac M, Pugel EP, Jonjic S, Britt WJ (2015) Murine CMV-induced hearing loss is associated with inner ear inflammation and loss of spiral ganglia neurons. PLoS Pathog 11:e1004774.

Branchi I, Bichler Z, Berger-Sweeney J, Ricceri L (2003) Animal models of mental retardation: from gene to cognitive function. Neurosci Biobehav Rev 27:141-153.

Brecht KF, Goelz R, Bevot A, Krageloh-Mann I, Wilke M, Lidzba K (2015) Postnatal human cytomegalovirus infection in preterm infants has long-term neuropsychological sequelae. J Pediatr 166:834-839.e831.

Britt W (2008) Manifestations of human cytomegalovirus infection: proposed mechanisms of acute and chronic disease. Curr Top Microbiol Immunol 325:417-470.

Britt W (2011) Cytomegalovirus, in Infectious Diseases of Fetus and Newborn; chapter 23, pages 706-755: W.B. Saunders Company, Philadelphia, PA, United States.

Britt WJ (2017) Congenital Human Cytomegalovirus Infection and the Enigma of Maternal Immunity. J Virol 91.

Brodie MJ, Dichter MA (1996) Antiepileptic drugs. N Engl J Med 334:168-175.

Brooks SP, Dunnett SB (2009) Tests to assess motor phenotype in mice: a user's guide. Nat Rev Neurosci 10:519-529.

Brune W, Hengel H, Koszinowski UH (2001) A mouse model for cytomegalovirus infection. Curr Protoc Immunol Chapter 19:Unit 19.17.

Burd I, Balakrishnan B, Kannan S (2012) Models of fetal brain injury, intrauterine inflammation, and preterm birth. Am J Reprod Immunol 67:287-294.

Butler D (2016) Zika raises profile of more common birth-defect virus. Nature 535:17.

Buxmann H, Stackelberg OM, Schlosser RL, Enders G, Gonser M, Meyer-Wittkopf M, Hamprecht K, Enders M (2012) Use of cytomegalovirus hyperimmunoglobulin for prevention of congenital cytomegalovirus disease: a retrospective analysis. J Perinat Med 40:439-446.

Calamandrei G, Venerosi A, Branchi I, Chiarotti F, Verdina A, Bucci F, Alleva E (1999) Effects of prenatal AZT on mouse neurobehavioral development and passive avoidance learning. Neurotoxicol Teratol 21:29-40.

Campanini G, Zavattoni M, Cristina E, Gazzolo D, Stronati M, Baldanti F (2012) Multiple ganciclovir-resistant strains in a newborn with symptomatic congenital human cytomegalovirus infection. J Clin Virol 54:86-88.

Cannon MJ (2009) Congenital cytomegalovirus (CMV) epidemiology and awareness. J Clin Virol 46 Suppl 4:S6-10.

Cannon MJ, Davis KF (2005) Washing our hands of the congenital cytomegalovirus disease epidemic. BMC Public Health 5:70.

Cannon MJ, Schmid DS, Hyde TB (2010) Review of cytomegalovirus seroprevalence and demographic characteristics associated with infection. Rev Med Virol 20:202-213.
Cannon MJ, Hyde TB, Schmid DS (2011) Review of cytomegalovirus shedding in bodily fluids and relevance to congenital cytomegalovirus infection. Rev Med Virol 21:240-255.
Carraro M, Almishaal A, Hillas E, Firpo M, Park A, Harrison RV (2017) Cytomegalovirus (CMV) Infection Causes Degeneration of Cochlear Vasculature and Hearing Loss in a Mouse Model. J Assoc Res Otolaryngol 18:263-273.
Carter RJ, Morton J, Dunnett SB (2001) Motor coordination and balance in rodents. Curr Protoc Neurosci Chapter 8:Unit 8.12.
Cekinovic D, Golemac M, Pugel EP, Tomac J, Cicin-Sain L, Slavuljica I, Bradford R, Misch S, Winkler TH, Mach M, Britt WJ, Jonjic S (2008) Passive immunization reduces murine cytomegalovirus-induced brain pathology in newborn mice. J Virol 82:12172-12180.
Cellot G, Cherubini E (2014) GABAergic signaling as therapeutic target for autism spectrum disorders. Front Pediatr 2:70.
Chan GC, Yurochko AD (2014) Analysis of cytomegalovirus binding/entry-mediated events. Methods Mol Biol 1119:113-121.
Chavanas S (2016) Peroxisome proliferator-activated receptor gamma (PPARgamma) activation: A key determinant of neuropathogeny during congenital infection by cytomegalovirus. Neurogenesis (Austin) 3:e1231654.
Cheeran MC, Lokensgard JR, Schleiss MR (2009) Neuropathogenesis of congenital cytomegalovirus infection: disease mechanisms and prospects for intervention. Clin Microbiol Rev 22:99-126, Table of Contents.
Cheeran MC, Hu S, Palmquist JM, Bakken T, Gekker G, Lokensgard JR (2007) Dysregulated interferon-gamma responses during lethal cytomegalovirus brain infection of IL-10-deficient mice. Virus Res 130:96-102.
Cheeran MC, Hu S, Ni HT, Sheng W, Palmquist JM, Peterson PK, Lokensgard JR (2005) Neural precursor cell susceptibility to human cytomegalovirus diverges along glial or neuronal differentiation pathways. J Neurosci Res 82:839-850.
Chen H, Beardsley GP, Coen DM (2014) Mechanism of ganciclovir-induced chain termination revealed by resistant viral polymerase mutants with reduced exonuclease activity. Proc Natl Acad Sci U S A 111:17462-17467.
Choi KY, Sharon B, Balfour HH, Jr., Belani K, Pozos TC, Schleiss MR (2013) Emergence of antiviral resistance during oral valganciclovir treatment of an infant with congenital cytomegalovirus (CMV) infection. J Clin Virol 57:356-360.
Choopong P, Vivittaworn K, Konlakij D, Thoongsuwan S, Pituksung A, Tesavibul N (2016) Treatment outcomes of reduced-dose intravitreal ganciclovir for cytomegalovirus retinitis. BMC Infect Dis 16:164.
Clancy B, Darlington RB, Finlay BL (2001) Translating developmental time across mammalian species. Neuroscience 105:7-17.
Clancy B, Finlay BL, Darlington RB, Anand KJ (2007a) Extrapolating brain development from experimental species to humans. Neurotoxicology 28:931-937.
Clancy B, Kersh B, Hyde J, Darlington RB, Anand KJ, Finlay BL (2007b) Web-based method for translating neurodevelopment from laboratory species to humans. Neuroinformatics 5:79-94.

Coats DK, Demmler GJ, Paysse EA, Du LT, Libby C (2000) Ophthalmologic findings in children with congenital cytomegalovirus infection. J aapos 4:110-116.
Cobbs CS, Soroceanu L, Denham S, Zhang W, Britt WJ, Pieper R, Kraus MH (2007) Human cytomegalovirus induces cellular tyrosine kinase signaling and promotes glioma cell invasiveness. J Neurooncol 85:271-280.
Coen DM, Richman DD (2013) Antiviral Agents, in Fields Virology; chapter 13, pages: 338-373: Wolters Kluwer Health, Lippincott Williams & Wilkins, Philadelphia, PA, United States.
Collins FS (2011) Reengineering translational science: the time is right. Sci Transl Med 3:90cm17.
Compton T, Nowlin DM, Cooper NR (1993) Initiation of human cytomegalovirus infection requires initial interaction with cell surface heparan sulfate. Virology 193:834-841.
Connolly PK, Jerger S, Williamson WD, Smith RJ, Demmler G (1992) Evaluation of higher-level auditory function in children with asymptomatic congenital cytomegalovirus infection. Am J Otol 13:185-193.
Corradini I, Focchi E, Rasile M, Morini R, Desiato G, Tomasoni R, Lizier M, Ghirardini E, Fesce R, Morone D, Barajon I, Antonucci F, Pozzi D, Matteoli M (2017) Maternal Immune Activation Delays Excitatory-to-Inhibitory Gamma-Aminobutyric Acid Switch in Offspring. Biol Psychiatry.
Crawley JN (2007) Mouse behavioral assays relevant to the symptoms of autism. Brain Pathol 17:448-459.
Crumpacker CS (1996) Ganciclovir. N Engl J Med 335:721-729.
Dahle AJ, Fowler KB, Wright JD, Boppana SB, Britt WJ, Pass RF (2000) Longitudinal investigation of hearing disorders in children with congenital cytomegalovirus. J Am Acad Audiol 11:283-290.
Dakovic I, da Graca Andrada M, Folha T, Neubauer D, Hollody K, Honold M, Horber V, Duranovic V, Bosnjak VM (2014) Clinical features of cerebral palsy in children with symptomatic congenital cytomegalovirus infection. Eur J Paediatr Neurol 18:618-623.
De Kegel A, Maes L, Baetens T, Dhooge I, Van Waelvelde H (2012) The influence of a vestibular dysfunction on the motor development of hearing-impaired children. Laryngoscope 122:2837-2843.
De Kegel A, Maes L, Dhooge I, van Hoecke H, De Leenheer E, Van Waelvelde H (2016) Early motor development of children with a congenital cytomegalovirus infection. Res Dev Disabil 48:253-261.
De la Calle M, Baquero F, Rodriguez R, Gonzalez M, Fernandez A, Omenaca F, Bartha JL (2017) Successful treatment of intrauterine cytomegalovirus infection with an intraventricular cyst in a dichorionic diamniotic twin gestation using cytomegalovirus immunoglobulin. J Matern Fetal Neonatal Med:1-4.
de Vries JJ, Vesseur A, Rotteveel LJ, Korver AM, Rusman LG, Wessels E, Kroes AC, Mylanus EA, Oudesluys-Murphy AM, Frijns JH, Vossen AC (2013) Cytomegalovirus DNA detection in dried blood spots and perilymphatic fluids from pediatric and adult cochlear implant recipients with prelingual deafness. J Clin Virol 56:113-117.
de Vries LS, Gunardi H, Barth PG, Bok LA, Verboon-Maciolek MA, Groenendaal F (2004) The spectrum of cranial ultrasound and magnetic resonance imaging abnormalities in congenital cytomegalovirus infection. Neuropediatrics 35:113-119.
DeBiasi RL, Kleinschmidt-DeMasters BK, Richardson-Burns S, Tyler KL (2002) Central nervous system apoptosis in human herpes simplex virus and cytomegalovirus encephalitis. J Infect Dis 186:1547-1557.

Demarchi JM (1981) Human cytomegalovirus DNA: restriction enzyme cleavage maps and map locations for immediate-early, early, and late RNAs. Virology 114:23-38.
Demmler-Harrison GJ (2013) Cytomegalovirus, in Feigin and Cherry's Textbook of Pediatric Infectious Diseases; chapter 158, pages: 1968-1991: W.B. Saunders Company, Philadelphia, PA, United States.
Dollard SC, Grosse SD, Ross DS (2007) New estimates of the prevalence of neurological and sensory sequelae and mortality associated with congenital cytomegalovirus infection. Rev Med Virol 17:355-363.
Drew WL (2000) Ganciclovir resistance: a matter of time and titre. Lancet 356:609-610.
Elmazar MM, Hauck RS, Nau H (1993) Anticonvulsant and neurotoxic activities of twelve analogues of valproic acid. J Pharm Sci 82:1255-1258.
Engman ML, Sundin M, Miniscalco C, Westerlund J, Lewensohn-Fuchs I, Gillberg C, Fernell E (2015) Prenatal acquired cytomegalovirus infection should be considered in children with autism. Acta Paediatr 104:792-795.
Eriksson B, Oberg B, Wahren B (1982) Pyrophosphate analogues as inhibitors of DNA polymerases of cytomegalovirus, herpes simplex virus and cellular origin. Biochim Biophys Acta 696:115-123.
Eriksson MA, Westerlund J, Hedvall A, Amark P, Gillberg C, Fernell E (2013) Medical conditions affect the outcome of early intervention in preschool children with autism spectrum disorders. Eur Child Adolesc Psychiatry 22:23-33.
Faqi AS, Klug A, Merker HJ, Chahoud I (1997) Ganciclovir induces reproductive hazards in male rats after short-term exposure. Hum Exp Toxicol 16:505-511.
Fatemi SH et al. (2012) Consensus paper: pathological role of the cerebellum in autism. Cerebellum 11:777-807.
Faulds D, Heel RC (1990) Ganciclovir. A review of its antiviral activity, pharmacokinetic properties and therapeutic efficacy in cytomegalovirus infections. Drugs 39:597-638.
Ferguson SA (1996) Neuroanatomical and functional alterations resulting from early postnatal cerebellar insults in rodents. Pharmacol Biochem Behav 55:663-671.
Fischer C, Meylan P, Bickle Graz M, Gudinchet F, Vaudaux B, Berger C, Roth-Kleiner M (2010) Severe postnatally acquired cytomegalovirus infection presenting with colitis, pneumonitis and sepsis-like syndrome in an extremely low birthweight infant. Neonatology 97:339-345.
Fleming SM, Ekhator OR, Ghisays V (2013) Assessment of sensorimotor function in mouse models of Parkinson's disease. J Vis Exp.
Fleming SM, Salcedo J, Fernagut PO, Rockenstein E, Masliah E, Levine MS, Chesselet MF (2004) Early and progressive sensorimotor anomalies in mice overexpressing wild-type human alpha-synuclein. J Neurosci 24:9434-9440.
Fowler KB (2013) Congenital cytomegalovirus infection: audiologic outcome. Clin Infect Dis 57 Suppl 4:S182-184.
Fowler KB, Boppana SB (2006) Congenital cytomegalovirus (CMV) infection and hearing deficit. J Clin Virol 35:226-231.
Fowler KB, McCollister FP, Dahle AJ, Boppana S, Britt WJ, Pass RF (1997) Progressive and fluctuating sensorineural hearing loss in children with asymptomatic congenital cytomegalovirus infection. J Pediatr 130:624-630.
Fox WM (1965) Reflex-ontogeny and behavioural development of the mouse. Anim Behav 13:234-241.

Fujiki R, Sato A, Fujitani M, Yamashita T (2013) A proapoptotic effect of valproic acid on progenitors of embryonic stem cell-derived glutamatergic neurons. Cell Death Dis 4:e677.
Fukui Y, Shindoh K, Yamamoto Y, Koyano S, Kosugi I, Yamaguchi T, Kurane I, Inoue N (2008) Establishment of a cell-based assay for screening of compounds inhibiting very early events in the cytomegalovirus replication cycle and characterization of a compound identified using the assay. Antimicrob Agents Chemother 52:2420-2427.
Gabrielli L, Bonasoni MP, Santini D, Piccirilli G, Chiereghin A, Petrisli E, Dolcetti R, Guerra B, Piccioli M, Lanari M, Landini MP, Lazzarotto T (2012) Congenital cytomegalovirus infection: patterns of fetal brain damage. Clin Microbiol Infect 18:E419-427.
Gandhi MK, Khanna R (2004) Human cytomegalovirus: clinical aspects, immune regulation, and emerging treatments. Lancet Infect Dis 4:725-738.
Garofoli F, Lombardi G, Orcesi S, Pisoni C, Mazzucchelli I, Angelini M, Balottin U, Stronati M (2017) An Italian Prospective Experience on the Association Between Congenital Cytomegalovirus Infection and Autistic Spectrum Disorder. J Autism Dev Disord.
Gault E, Michel Y, Dehee A, Belabani C, Nicolas JC, Garbarg-Chenon A (2001) Quantification of human cytomegalovirus DNA by real-time PCR. J Clin Microbiol 39:772-775.
Geelen JL, Walig C, Wertheim P, van der Noordaa J (1978) Human cytomegalovirus DNA. I. Molecular weight and infectivity. J Virol 26:813-816.
Genentech USA (2016) Cytovene (ganciclovir sodium), prescribing information.
Gentile I, Zappulo E, Riccio MP, Binda S, Bubba L, Pellegrinelli L, Scognamiglio D, Operto F, Margari L, Borgia G, Bravaccio C (2017) Prevalence of Congenital Cytomegalovirus Infection Assessed Through Viral Genome Detection in Dried Blood Spots in Children with Autism Spectrum Disorders. In Vivo 31:467-473.
Gibson W (1981) Immediate-early proteins of human cytomegalovirus strains AD 169, Davis, and Towne differ in electrophoretic mobility. Virology 112:350-354.
Gilbert C, Boivin G (2005) Human cytomegalovirus resistance to antiviral drugs. Antimicrob Agents Chemother 49:873-883.
Goldberg M (1961) Effects of a new tranquilizer, valmethamide, in psychiatric outpatient care. Dis Nerv Syst 22:346-348.
Gorres KL, Daigle D, Mohanram S, Miller G (2014) Activation and repression of Epstein-Barr Virus and Kaposi's sarcoma-associated herpesvirus lytic cycles by short- and medium-chain fatty acids. J Virol 88:8028-8044.
Gorres KL, Daigle D, Mohanram S, McInerney GE, Lyons DE, Miller G (2016) Valpromide Inhibits Lytic Cycle Reactivation of Epstein-Barr Virus. MBio 7.
Griffiths P, Plotkin S, Mocarski E, Pass R, Schleiss M, Krause P, Bialek S (2013) Desirability and feasibility of a vaccine against cytomegalovirus. Vaccine 31 Suppl 2:B197-203.
Guerrini R (2006) Valproate as a mainstay of therapy for pediatric epilepsy. Paediatr Drugs 8:113-129.
Guyenet SJ, Furrer SA, Damian VM, Baughan TD, La Spada AR, Garden GA (2010) A simple composite phenotype scoring system for evaluating mouse models of cerebellar ataxia. J Vis Exp.
Haj-Yehia A, Bialer M (1988) Pharmacokinetics of a valpromide isomer, valnoctamide, in dogs. J Pharm Sci 77:831-834.
Haj-Yehia A, Bialer M (1990) Structure-pharmacokinetic relationships in a series of short fatty acid amides that possess anticonvulsant activity. J Pharm Sci 79:719-724.

Hamprecht K, Maschmann J, Vochem M, Dietz K, Speer CP, Jahn G (2001) Epidemiology of transmission of cytomegalovirus from mother to preterm infant by breastfeeding. Lancet 357:513-518.
Hampson DR, Blatt GJ (2015) Autism spectrum disorders and neuropathology of the cerebellum. Front Neurosci 9:420.
Han D, Byun SH, Kim J, Kwon M, Pleasure SJ, Ahn JH, Yoon K (2017) Human Cytomegalovirus IE2 Protein Disturbs Brain Development by the Dysregulation of Neural Stem Cell Maintenance and the Polarization of Migrating Neurons. J Virol 91.
Harl FM (1964) [CLINICAL STUDY OF VALNOCTAMIDE ON 70 NEUROPSYCHIATRIC CLINIC PATIENTS UNDERGOING AMBULATORY TREATMENT]. Presse Med 72:753-754.
Hauck RS, Nau H (1989) Asymmetric synthesis and enantioselective teratogenicity of 2-n-propyl-4-pentenoic acid (4-en-VPA), an active metabolite of the anticonvulsant drug, valproic acid. Toxicol Lett 49:41-48.
Hicks T, Fowler K, Richardson M, Dahle A, Adams L, Pass R (1993) Congenital cytomegalovirus infection and neonatal auditory screening. J Pediatr 123:779-782.
Hildreth RL, Bullough MD, Zhang A, Chen HL, Schwartz PH, Panchision DM, Colberg-Poley AM (2012) Viral mitochondria-localized inhibitor of apoptosis (UL37 exon 1 protein) does not protect human neural precursor cells from human cytomegalovirus-induced cell death. J Gen Virol 93:2436-2446.
Himmelmann K, Beckung E, Hagberg G, Uvebrant P (2006) Gross and fine motor function and accompanying impairments in cerebral palsy. Dev Med Child Neurol 48:417-423.
Huang ES, Chen ST, Pagano JS (1973) Human cytomegalovirus. I. Purification and characterization of viral DNA. J Virol 12:1473-1481.
Huang R, Southall N, Wang Y, Yasgar A, Shinn P, Jadhav A, Nguyen DT, Austin CP (2011) The NCGC pharmaceutical collection: a comprehensive resource of clinically approved drugs enabling repurposing and chemical genomics. Sci Transl Med 3:80ps16.
Ikuta K, Ogawa H, Hashimoto H, Okano W, Tani A, Sato E, Kosugi I, Kobayashi T, Omori K, Suzutani T (2015) Restricted infection of murine cytomegalovirus (MCMV) in neonatal mice with MCMV-induced sensorineural hearing loss. J Clin Virol 69:138-145.
Inouye M, Murakami U (1980) Temporal and spatial patterns of Purkinje cell formation in the mouse cerebellum. J Comp Neurol 194:499-503.
Institute of Medicine Committee to Study Priorities for Vaccine D (2000) The National Academies Collection: Reports funded by National Institutes of Health. In: Vaccines for the 21st Century: A Tool for Decisionmaking (Stratton KR, Durch JS, Lawrence RS, eds). Washington (DC): National Academies Press (US)

Isaacson MK, Compton T (2009) Human cytomegalovirus glycoprotein B is required for virus entry and cell-to-cell spread but not for virion attachment, assembly, or egress. J Virol 83:3891-3903.
Isoherranen N, White HS, Klein BD, Roeder M, Woodhead JH, Schurig V, Yagen B, Bialer M (2003) Pharmacokinetic-pharmacodynamic relationships of (2S,3S)-valnoctamide and its stereoisomer (2R,3S)-valnoctamide in rodent models of epilepsy. Pharm Res 20:1293-1301.
James SH, Prichard MN (2011) The genetic basis of human cytomegalovirus resistance and current trends in antiviral resistance analysis. Infect Disord Drug Targets 11:504-513.

James SH, Kimberlin DW (2016) Advances in the prevention and treatment of congenital cytomegalovirus infection. Curr Opin Pediatr 28:81-85.
Juanjuan C, Yan F, Li C, Haizhi L, Ling W, Xinrong W, Juan X, Tao L, Zongzhi Y, Suhua C (2011) Murine model for congenital CMV infection and hearing impairment. Virol J 8:70.
Jung E-M, Moffat JJ, Liu J, Dravid SM, Gurumurthy CB, Kim W-Y (2017) Arid1b haploinsufficiency disrupts cortical interneuron development and mouse behavior. Nature Neuroscience:1.
Kashden J, Frison S, Fowler K, Pass RF, Boll TJ (1998) Intellectual assessment of children with asymptomatic congenital cytomegalovirus infection. J Dev Behav Pediatr 19:254-259.
Kataoka S, Takuma K, Hara Y, Maeda Y, Ago Y, Matsuda T (2013) Autism-like behaviours with transient histone hyperacetylation in mice treated prenatally with valproic acid. Int J Neuropsychopharmacol 16:91-103.
Kaufmann D, Yagen B, Minert A, Wlodarczyk B, Finnell RH, Schurig V, Devor M, Bialer M (2010) Evaluation of the antiallodynic, teratogenic and pharmacokinetic profile of stereoisomers of valnoctamide, an amide derivative of a chiral isomer of valproic acid. Neuropharmacology 58:1228-1236.
Kawasaki H, Kosugi I, Arai Y, Tsutsui Y (2002) The amount of immature glial cells in organotypic brain slices determines the susceptibility to murine cytomegalovirus infection. Lab Invest 82:1347-1358.
Kawasaki H, Kosugi I, Meguro S, Iwashita T (2017) Pathogenesis of developmental anomalies of the central nervous system induced by congenital cytomegalovirus infection. Pathol Int 67:72-82.
Kenneson A, Cannon MJ (2007) Review and meta-analysis of the epidemiology of congenital cytomegalovirus (CMV) infection. Rev Med Virol 17:253-276.
Kern ER (1991) Value of animal models to evaluate agents with potential activity against human cytomegalovirus. Transplant Proc 23:152-155, discussion 155.
Kern ER (2006) Pivotal role of animal models in the development of new therapies for cytomegalovirus infections. Antiviral Res 71:164-171.
Kim KS, Sapienza VJ, Carp RI, Moon HM (1976) Analysis of structural polypeptides of purified human cytomegalovirus. J Virol 20:604-611.
Kimberlin DW, Lin CY, Sanchez PJ, Demmler GJ, Dankner W, Shelton M, Jacobs RF, Vaudry W, Pass RF, Kiell JM, Soong SJ, Whitley RJ (2003) Effect of ganciclovir therapy on hearing in symptomatic congenital cytomegalovirus disease involving the central nervous system: a randomized, controlled trial. J Pediatr 143:16-25.
Kimberlin DW et al. (2015) Valganciclovir for symptomatic congenital cytomegalovirus disease. N Engl J Med 372:933-943.
Knight A, Arnouk H, Britt W, Gillespie GY, Cloud GA, Harkins L, Su Y, Lowdell MW, Lamb LS (2013) CMV-independent lysis of glioblastoma by ex vivo expanded/activated Vdelta1+ gammadelta T cells. PLoS One 8:e68729.
Koontz T, Bralic M, Tomac J, Pernjak-Pugel E, Bantug G, Jonjic S, Britt WJ (2008) Altered development of the brain after focal herpesvirus infection of the central nervous system. J Exp Med 205:423-435.
Kosmac K, Bantug GR, Pugel EP, Cekinovic D, Jonjic S, Britt WJ (2013) Glucocorticoid treatment of MCMV infected newborn mice attenuates CNS inflammation and limits deficits in cerebellar development. PLoS Pathog 9:e1003200.

Kosugi I, Kawasaki H, Arai Y, Tsutsui Y (2002) Innate immune responses to cytomegalovirus infection in the developing mouse brain and their evasion by virus-infected neurons. Am J Pathol 161:919-928.

Kosugi I, Shinmura Y, Li RY, Aiba-Masago S, Baba S, Miura K, Tsutsui Y (1998) Murine cytomegalovirus induces apoptosis in non-infected cells of the developing mouse brain and blocks apoptosis in primary neuronal culture. Acta Neuropathol 96:239-247.

Kosugi I, Shinmura Y, Kawasaki H, Arai Y, Li RY, Baba S, Tsutsui Y (2000) Cytomegalovirus infection of the central nervous system stem cells from mouse embryo: a model for developmental brain disorders induced by cytomegalovirus. Lab Invest 80:1373-1383.

Kotton CN, Kumar D, Caliendo AM, Asberg A, Chou S, Danziger-Isakov L, Humar A (2013) Updated international consensus guidelines on the management of cytomegalovirus in solid-organ transplantation. Transplantation 96:333-360.

Koyano S, Morioka I, Oka A, Moriuchi H, Asano K, Ito Y, Yoshikawa T, Yamada H, Suzutani T, Inoue N (2017) More than two years follow-up of infants with congenital cytomegalovirus infection in Japan. Pediatr Int.

Kuntz-Simon G, Obert G (1995) Sodium valproate, an anticonvulsant drug, stimulates human cytomegalovirus replication. J Gen Virol 76 (Pt 6):1409-1415.

Kurath S, Halwachs-Baumann G, Muller W, Resch B (2010) Transmission of cytomegalovirus via breast milk to the prematurely born infant: a systematic review. Clin Microbiol Infect 16:1172-1178.

Lackner A, Acham A, Alborno T, Moser M, Engele H, Raggam RB, Halwachs-Baumann G, Kapitan M, Walch C (2009) Effect on hearing of ganciclovir therapy for asymptomatic congenital cytomegalovirus infection: four to 10 year follow up. J Laryngol Otol 123:391-396.

Lakeman AD, Osborn JE (1979) Size of infectious DNA from human and murine cytomegaloviruses. J Virol 30:414-416.

Lanzieri TM, Dollard SC, Josephson CD, Schmid DS, Bialek SR (2013) Breast milk-acquired cytomegalovirus infection and disease in VLBW and premature infants. Pediatrics 131:e1937-1945.

Lanzieri TM, Chung W, Flores M, Blum P, Caviness AC, Bialek SR, Grosse SD, Miller JA, Demmler-Harrison G (2017) Hearing Loss in Children With Asymptomatic Congenital Cytomegalovirus Infection. Pediatrics 139.

Lathey JL, Wiley CA, Verity MA, Nelson JA (1990) Cultured human brain capillary endothelial cells are permissive for infection by human cytomegalovirus. Virology 176:266-273.

Lau SK, Chen YY, Chen WG, Diamond DJ, Mamelak AN, Zaia JA, Weiss LM (2005) Lack of association of cytomegalovirus with human brain tumors. Mod Pathol 18:838-843.

Lea AP, Bryson HM (1996) Cidofovir. Drugs 52:225-230; discussion 231.

Leruez-Ville M, Ville Y (2017) Fetal cytomegalovirus infection. Best Pract Res Clin Obstet Gynaecol 38:97-107.

Leruez-Ville M, Stirnemann J, Sellier Y, Guilleminot T, Dejean A, Magny JF, Couderc S, Jacquemard F, Ville Y (2016a) Feasibility of predicting the outcome of fetal infection with cytomegalovirus at the time of prenatal diagnosis. Am J Obstet Gynecol 215:342.e341-349.

Leruez-Ville M, Ghout I, Bussieres L, Stirnemann J, Magny JF, Couderc S, Salomon LJ, Guilleminot T, Aegerter P, Benoist G, Winer N, Picone O, Jacquemard F, Ville Y (2016b) In utero treatment of congenital cytomegalovirus infection with valacyclovir in a multicenter, open-label, phase II study. Am J Obstet Gynecol 215:462.e461-462.e410.

Li G, Kamil JP (2015) Viral Regulation of Cell Tropism in Human Cytomegalovirus. J Virol 90:626-629.
Li RY, Tsutsui Y (2000) Growth retardation and microcephaly induced in mice by placental infection with murine cytomegalovirus. Teratology 62:79-85.
Li X, Shi X, Wang C, Niu H, Zeng L, Qiao Y (2016) Cochlear Spiral Ganglion Neuron Apoptosis in Neonatal Mice with Murine Cytomegalovirus-Induced Sensorineural Hearing Loss. J Am Acad Audiol 27:345-353.
Li X, Shi X, Wang C, Niu H, Zeng L, Qiao Y, Xu K (2015) Pathological changes of the inner ear cochlea in different time windows of murine cytomegalovirus-induced hearing loss in a mouse model. Acta Otolaryngol 135:536-541.
Lindekens H, Smolders I, Khan GM, Bialer M, Ebinger G, Michotte Y (2000) In vivo study of the effect of valpromide and valnoctamide in the pilocarpine rat model of focal epilepsy. Pharm Res 17:1408-1413.
Lipitz S, Yinon Y, Malinger G, Yagel S, Levit L, Hoffman C, Rantzer R, Weisz B (2013) Risk of cytomegalovirus-associated sequelae in relation to time of infection and findings on prenatal imaging. Ultrasound Obstet Gynecol 41:508-514.
Littler E, Stuart AD, Chee MS (1992) Human cytomegalovirus UL97 open reading frame encodes a protein that phosphorylates the antiviral nucleoside analogue ganciclovir. Nature 358:160-162.
Loh HS, Mohd-Lila MA, Abdul-Rahman SO, Kiew LJ (2006) Pathogenesis and vertical transmission of a transplacental rat cytomegalovirus. Virol J 3:42.
Lokensgard JR, Cheeran MC, Gekker G, Hu S, Chao CC, Peterson PK (1999) Human cytomegalovirus replication and modulation of apoptosis in astrocytes. J Hum Virol 2:91-101.
Lopez AS, Lanzieri TM, Claussen AH, Vinson SS, Turcich MR, Iovino IR, Voigt RG, Caviness AC, Miller JA, Williamson WD, Hales CM, Bialek SR, Demmler-Harrison G (2017) Intelligence and Academic Achievement With Asymptomatic Congenital Cytomegalovirus Infection. Pediatrics 140.
Lowance D, Neumayer HH, Legendre CM, Squifflet JP, Kovarik J, Brennan PJ, Norman D, Mendez R, Keating MR, Coggon GL, Crisp A, Lee IC (1999) Valacyclovir for the prevention of cytomegalovirus disease after renal transplantation. International Valacyclovir Cytomegalovirus Prophylaxis Transplantation Study Group. N Engl J Med 340:1462-1470.
Ludwig A, Hengel H (2009) Epidemiological impact and disease burden of congenital cytomegalovirus infection in Europe. Euro Surveill 14:26-32.
Luo MH, Schwartz PH, Fortunato EA (2008) Neonatal neural progenitor cells and their neuronal and glial cell derivatives are fully permissive for human cytomegalovirus infection. J Virol 82:9994-10007.
Luong TN, Carlisle HJ, Southwell A, Patterson PH (2011) Assessment of motor balance and coordination in mice using the balance beam. J Vis Exp.
Ma DK, Ming GL, Song H (2005) Glial influences on neural stem cell development: cellular niches for adult neurogenesis. Curr Opin Neurobiol 15:514-520.
Malm G, Engman ML (2007) Congenital cytomegalovirus infections. Semin Fetal Neonatal Med 12:154-159.
Manicklal S, Emery VC, Lazzarotto T, Boppana SB, Gupta RK (2013) The "silent" global burden of congenital cytomegalovirus. Clin Microbiol Rev 26:86-102.
Mar EC, Chiou JF, Cheng YC, Huang ES (1985) Inhibition of cellular DNA polymerase alpha and human cytomegalovirus-induced DNA polymerase by the triphosphates of 9-(2-

hydroxyethoxymethyl)guanine and 9-(1,3-dihydroxy-2-propoxymethyl)guanine. J Virol 53:776-780.
Mardivirin L, Descamps V, Lacroix A, Delebassee S, Ranger-Rogez S (2009) Early effects of drugs responsible for DRESS on HHV-6 replication in vitro. J Clin Virol 46:300-302.
Mares P, Kubova H, Hen N, Yagen B, Bialer M (2013) Derivatives of valproic acid are active against pentetrazol-induced seizures in immature rats. Epilepsy Res 106:64-73.
Markham A, Faulds D (1994) Ganciclovir. An update of its therapeutic use in cytomegalovirus infection. Drugs 48:455-484.
Matalon S, Rasmussen TA, Dinarello CA (2011) Histone deacetylase inhibitors for purging HIV-1 from the latent reservoir. Mol Med 17:466-472.
Matthews T, Boehme R (1988) Antiviral activity and mechanism of action of ganciclovir. Rev Infect Dis 10 Suppl 3:S490-494.
Mawasi H, Shekh-Ahmad T, Finnell RH, Wlodarczyk BJ, Bialer M (2015) Pharmacodynamic and pharmacokinetic analysis of CNS-active constitutional isomers of valnoctamide and sec-butylpropylacetamide--Amide derivatives of valproic acid. Epilepsy Behav 46:72-78.
Mazarati AM, Lewis ML, Pittman QJ (2017) Neurobehavioral comorbidities of epilepsy: Role of inflammation. Epilepsia 58 Suppl 3:48-56.
McCarthy M, Auger D, Whittemore SR (2000) Human cytomegalovirus causes productive infection and neuronal injury in differentiating fetal human central nervous system neuroepithelial precursor cells. J Hum Virol 3:215-228.
McIntosh M, Hauschild B, Miller V (2016) Human cytomegalovirus and transplantation: drug development and regulatory issues. J Virus Erad 2:143-148.
Mercorelli B, Lembo D, Palu G, Loregian A (2011) Early inhibitors of human cytomegalovirus: state-of-art and therapeutic perspectives. Pharmacol Ther 131:309-329.
Mestas E (2016) Congenital Cytomegalovirus. Adv Neonatal Care 16:60-65.
Michaelis M, Kohler N, Reinisch A, Eikel D, Gravemann U, Doerr HW, Nau H, Cinatl J, Jr. (2004) Increased human cytomegalovirus replication in fibroblasts after treatment with therapeutical plasma concentrations of valproic acid. Biochem Pharmacol 68:531-538.
Michaelis M, Suhan T, Reinisch A, Reisenauer A, Fleckenstein C, Eikel D, Gumbel H, Doerr HW, Nau H, Cinatl J, Jr. (2005) Increased replication of human cytomegalovirus in retinal pigment epithelial cells by valproic acid depends on histone deacetylase inhibition. Invest Ophthalmol Vis Sci 46:3451-3457.
Mocarski, Shenk T, Pass RF (2007) Cytomegaloviruses. In: Fields Virology (Fields BN, Knipe DM, Howley PM, eds), pp 2702-2751. Philadelphia, PA: Lippincott, Williams & Wilkins.
Mocarski ES, Shenk T, Griffiths PD, Pass RF (2013) Cytomegaloviruses, in Fields Virology; chapter 62, pages: 1960-2014, 6th Edition: Wolters Kluwer Health, Lippincott Williams & Wilkins, Philadelphia, PA, United States.
Modi HR, Basselin M, Rapoport SI (2014) Valnoctamide, a non-teratogenic amide derivative of valproic acid, inhibits arachidonic acid activation in vitro by recombinant acyl-CoA synthetase-4. Bipolar Disord 16:875-880.
Modi HR, Ma K, Chang L, Chen M, Rapoport SI (2017) Valnoctamide, which reduces rat brain arachidonic acid turnover, is a potential non-teratogenic valproate substitute to treat bipolar disorder. Psychiatry Res 254:279-283.

Monti B, Polazzi E, Contestabile A (2009) Biochemical, molecular and epigenetic mechanisms of valproic acid neuroprotection. Curr Mol Pharmacol 2:95-109.
Moog C, Kuntz-Simon G, Caussin-Schwemling C, Obert G (1996) Sodium valproate, an anticonvulsant drug, stimulates human immunodeficiency virus type 1 replication independently of glutathione levels. J Gen Virol 77 (Pt 9):1993-1999.
Morillo-Gutierrez B, Waugh S, Pickering A, Flood T, Emonts M (2017) Emerging (val)ganciclovir resistance during treatment of congenital CMV infection: a case report and review of the literature. BMC Pediatr 17:181.
Morton CC, Nance WE (2006) Newborn hearing screening--a silent revolution. N Engl J Med 354:2151-2164.
Murphy E, Rigoutsos I, Shibuya T, Shenk TE (2003) Reevaluation of human cytomegalovirus coding potential. Proc Natl Acad Sci U S A 100:13585-13590.
Mussi-Pinhata MM, Yamamoto AY, Moura Brito RM, de Lima Isaac M, de Carvalho e Oliveira PF, Boppana S, Britt WJ (2009) Birth prevalence and natural history of congenital cytomegalovirus infection in a highly seroimmune population. Clin Infect Dis 49:522-528.
Mutnal MB, Cheeran MC, Hu S, Lokensgard JR (2011) Murine cytomegalovirus infection of neural stem cells alters neurogenesis in the developing brain. PLoS One 6:e16211.
Nakashima H, Kaufmann JK, Wang PY, Nguyen T, Speranza MC, Kasai K, Okemoto K, Otsuki A, Nakano I, Fernandez S, Goins WF, Grandi P, Glorioso JC, Lawler S, Cripe TP, Chiocca EA (2015) Histone deacetylase 6 inhibition enhances oncolytic viral replication in glioma. J Clin Invest 125:4269-4280.
Natali A, Valcavi P, Medici MC, Dieci E, Montali S, Chezzi C (1997) Cytomegalovirus infection in an Italian population: antibody prevalence, virus excretion and maternal transmission. New Microbiol 20:123-133.
Nau H, Loscher W (1986) Pharmacologic evaluation of various metabolites and analogs of valproic acid: teratogenic potencies in mice. Fundam Appl Toxicol 6:669-676.
Nau H, Scott WJ (1987) Teratogenicity of valproic acid and related substances in the mouse: drug accumulation and pHi in the embryo during organogenesis and structure-activity considerations. Arch Toxicol Suppl 11:128-139.
Nau H, Hauck RS, Ehlers K (1991) Valproic acid-induced neural tube defects in mouse and human: aspects of chirality, alternative drug development, pharmacokinetics and possible mechanisms. Pharmacol Toxicol 69:310-321.
Negishi H, Yamada H, Hirayama E, Okuyama K, Sagawa T, Matsumoto Y, Fujimoto S (1998) Intraperitoneal administration of cytomegalovirus hyperimmunoglobulin to the cytomegalovirus-infected fetus. J Perinatol 18:466-469.
Nigro G, Adler SP, La Torre R, Best AM (2005) Passive immunization during pregnancy for congenital cytomegalovirus infection. N Engl J Med 353:1350-1362.
Nigro G, La Torre R, Anceschi MM, Mazzocco M, Cosmi EV (1999) Hyperimmunoglobulin therapy for a twin fetus with cytomegalovirus infection and growth restriction. Am J Obstet Gynecol 180:1222-1226.
Nigro G, Capretti I, Manganello AM, Best AM, Adler SP (2015) Primary maternal cytomegalovirus infections during pregnancy: association of CMV hyperimmune globulin with gestational age at birth and birth weight. J Matern Fetal Neonatal Med 28:168-171.

Nigro G, La Torre R, Pentimalli H, Taverna P, Lituania M, de Tejada BM, Adler SP (2008) Regression of fetal cerebral abnormalities by primary cytomegalovirus infection following hyperimmunoglobulin therapy. Prenat Diagn 28:512-517.

Nigro G, Adler SP, Gatta E, Mascaretti G, Megaloikonomou A, La Torre R, Necozione S (2012a) Fetal hyperechogenic bowel may indicate congenital cytomegalovirus disease responsive to immunoglobulin therapy. J Matern Fetal Neonatal Med 25:2202-2205.

Nigro G, Adler SP, Parruti G, Anceschi MM, Coclite E, Pezone I, Di Renzo GC (2012b) Immunoglobulin therapy of fetal cytomegalovirus infection occurring in the first half of pregnancy--a case-control study of the outcome in children. J Infect Dis 205:215-227.

Nosengo N (2016) Can you teach old drugs new tricks? Nature 534:314-316.

Noyola DE, Demmler GJ, Williamson WD, Griesser C, Sellers S, Llorente A, Littman T, Williams S, Jarrett L, Yow MD (2000) Cytomegalovirus urinary excretion and long term outcome in children with congenital cytomegalovirus infection. Congenital CMV Longitudinal Study Group. Pediatr Infect Dis J 19:505-510.

Noyola DE, Demmler GJ, Nelson CT, Griesser C, Williamson WD, Atkins JT, Rozelle J, Turcich M, Llorente AM, Sellers-Vinson S, Reynolds A, Bale JF, Jr., Gerson P, Yow MD (2001) Early predictors of neurodevelopmental outcome in symptomatic congenital cytomegalovirus infection. J Pediatr 138:325-331.

Odeberg J, Wolmer N, Falci S, Westgren M, Seiger A, Soderberg-Naucler C (2006) Human cytomegalovirus inhibits neuronal differentiation and induces apoptosis in human neural precursor cells. J Virol 80:8929-8939.

Odeberg J, Wolmer N, Falci S, Westgren M, Sundtrom E, Seiger A, Soderberg-Naucler C (2007) Late human cytomegalovirus (HCMV) proteins inhibit differentiation of human neural precursor cells into astrocytes. J Neurosci Res 85:583-593.

Ogawa N, Hirose Y, Ohara S, Ono T, Watanabe Y (1985) A simple quantitative bradykinesia test in MPTP-treated mice. Res Commun Chem Pathol Pharmacol 50:435-441.

Okada A, Kurihara H, Aoki Y, Bialer M, Fujiwara M (2004) Amidic modification of valproic acid reduces skeletal teratogenicity in mice. Birth Defects Res B Dev Reprod Toxicol 71:47-53.

Okulu E, Akin IM, Atasay B, Ciftci E, Arsan S, Turmen T (2012) Severe postnatal cytomegalovirus infection with multisystem involvement in an extremely low birth weight infant. J Perinatol 32:72-74.

Oosterom N, Nijman J, Gunkel J, Wolfs TF, Groenendaal F, Verboon-Maciolek MA, de Vries LS (2015) Neuro-imaging findings in infants with congenital cytomegalovirus infection: relation to trimester of infection. Neonatology 107:289-296.

Ornaghi S, Davis JN, Gorres KL, Miller G, Paidas MJ, van den Pol AN (2016) Mood stabilizers inhibit cytomegalovirus infection. Virology 499:121-135.

Ornaghi S, Hsieh LS, Bordey A, Vergani P, Paidas MJ, van den Pol AN (2017) Valnoctamide Inhibits Cytomegalovirus Infection in Developing Brain and Attenuates Neurobehavioral Dysfunctions and Brain Abnormalities. J Neurosci 37:6877-6893.

Otsuki A, Patel A, Kasai K, Suzuki M, Kurozumi K, Chiocca EA, Saeki Y (2008) Histone deacetylase inhibitors augment antitumor efficacy of herpes-based oncolytic viruses. Mol Ther 16:1546-1555.

Paglino JC, van den Pol AN (2011) Vesicular stomatitis virus has extensive oncolytic activity against human sarcomas: rare resistance is overcome by blocking interferon pathways. J Virol 85:9346-9358.
Paradis FH, Hales BF (2013) Exposure to valproic acid inhibits chondrogenesis and osteogenesis in mid-organogenesis mouse limbs. Toxicol Sci 131:234-241.
Paradis FH, Hales BF (2015) Valproic Acid Induces the Hyperacetylation of P53, Expression of P53 Target Genes, and Markers of the Intrinsic Apoptotic Pathway in Midorganogenesis Murine Limbs. Birth Defects Res B Dev Reprod Toxicol 104:177-183.
Pass RF, Fowler KB, Boppana SB, Britt WJ, Stagno S (2006) Congenital cytomegalovirus infection following first trimester maternal infection: symptoms at birth and outcome. J Clin Virol 35:216-220.
Pereira L, Maidji E, McDonagh S, Tabata T (2005) Insights into viral transmission at the uterine-placental interface. Trends Microbiol 13:164-174.
Perlman JM, Argyle C (1992) Lethal cytomegalovirus infection in preterm infants: clinical, radiological, and neuropathological findings. Ann Neurol 31:64-68.
Perucca E (2002) Pharmacological and therapeutic properties of valproate: a summary after 35 years of clinical experience. CNS Drugs 16:695-714.
Phiel CJ, Zhang F, Huang EY, Guenther MG, Lazar MA, Klein PS (2001) Histone deacetylase is a direct target of valproic acid, a potent anticonvulsant, mood stabilizer, and teratogen. J Biol Chem 276:36734-36741.
Picone O, Vauloup-Fellous C, Cordier AG, Guitton S, Senat MV, Fuchs F, Ayoubi JM, Grangeot Keros L, Benachi A (2013) A series of 238 cytomegalovirus primary infections during pregnancy: description and outcome. Prenat Diagn 33:751-758.
Pinninti SG, Ross SA, Shimamura M, Novak Z, Palmer AL, Ahmed A, Tolan RW, Jr., Bernstein DI, Michaels MG, Sanchez PJ, Fowler KB, Boppana SB (2015) Comparison of saliva PCR assay versus rapid culture for detection of congenital cytomegalovirus infection. Pediatr Infect Dis J 34:536-537.
Pisani F, Fazio A, Oteri G, Ruello C, Gitto C, Russo F, Perucca E (1986) Sodium valproate and valpromide: differential interactions with carbamazepine in epileptic patients. Epilepsia 27:548-552.
Poland SD, Costello P, Dekaban GA, Rice GP (1990) Cytomegalovirus in the brain: in vitro infection of human brain-derived cells. J Infect Dis 162:1252-1262.
Porter RJ, Cereghino JJ, Gladding GD, Hessie BJ, Kupferberg HJ, Scoville B, White BG (1984) Antiepileptic Drug Development Program. Cleve Clin Q 51:293-305.
Pouliot W, Bialer M, Hen N, Shekh-Ahmad T, Kaufmann D, Yagen B, Ricks K, Roach B, Nelson C, Dudek FE (2013) A comparative electrographic analysis of the effect of sec-butyl-propylacetamide on pharmacoresistant status epilepticus. Neuroscience 231:145-156.
Radatz M, Ehlers K, Yagen B, Bialer M, Nau H (1998) Valnoctamide, valpromide and valnoctic acid are much less teratogenic in mice than valproic acid. Epilepsy Res 30:41-48.
Ramsburg E, Publicover J, Buonocore L, Poholek A, Robek M, Palin A, Rose JK (2005) A vesicular stomatitis virus recombinant expressing granulocyte-macrophage colony-stimulating factor induces enhanced T-cell responses and is highly attenuated for replication in animals. J Virol 79:15043-15053.

Rawlinson WD, Farrell HE, Barrell BG (1996) Analysis of the complete DNA sequence of murine cytomegalovirus. J Virol 70:8833-8849.
Rawlinson WD, Hamilton ST, van Zuylen WJ (2016) Update on treatment of cytomegalovirus infection in pregnancy and of the newborn with congenital cytomegalovirus. Curr Opin Infect Dis 29:615-624.
Razonable RR, Emery VC (2004) Management of CMV infection and disease in transplant patients. 27-29 February 2004. Herpes 11:77-86.
Reuter JD, Gomez DL, Wilson JH, Van Den Pol AN (2004) Systemic immune deficiency necessary for cytomegalovirus invasion of the mature brain. J Virol 78:1473-1487.
Revello MG, Gerna G (2004) Pathogenesis and prenatal diagnosis of human cytomegalovirus infection. J Clin Virol 29:71-83.
Revello MG, Zavattoni M, Furione M, Fabbri E, Gerna G (2006) Preconceptional primary human cytomegalovirus infection and risk of congenital infection. J Infect Dis 193:783-787.
Revello MG, Furione M, Rognoni V, Arossa A, Gerna G (2014) Cytomegalovirus DNAemia in pregnant women. J Clin Virol 61:590-592.
Revello MG, Tibaldi C, Masuelli G, Frisina V, Sacchi A, Furione M, Arossa A, Spinillo A, Klersy C, Ceccarelli M, Gerna G, Todros T (2015) Prevention of Primary Cytomegalovirus Infection in Pregnancy. EBioMedicine 2:1205-1210.
Rolland M, Li X, Sellier Y, Martin H, Perez-Berezo T, Rauwel B, Benchoua A, Bessieres B, Aziza J, Cenac N, Luo M, Casper C, Peschanski M, Gonzalez-Dunia D, Leruez-Ville M, Davrinche C, Chavanas S (2016) PPARgamma Is Activated during Congenital Cytomegalovirus Infection and Inhibits Neuronogenesis from Human Neural Stem Cells. PLoS Pathog 12:e1005547.
Ross SA, Fowler KB, Ashrith G, Stagno S, Britt WJ, Pass RF, Boppana SB (2006) Hearing loss in children with congenital cytomegalovirus infection born to mothers with preexisting immunity. J Pediatr 148:332-336.
Sakamoto A, Moriuchi H, Matsuzaki J, Motoyama K, Moriuchi M (2015) Retrospective diagnosis of congenital cytomegalovirus infection in children with autism spectrum disorder but no other major neurologic deficit. Brain Dev 37:200-205.
Sakao-Suzuki M, Kawasaki H, Akamatsu T, Meguro S, Miyajima H, Iwashita T, Tsutsui Y, Inoue N, Kosugi I (2014) Aberrant fetal macrophage/microglial reactions to cytomegalovirus infection. Ann Clin Transl Neurol 1:570-588.
Sarov I, Friedman A (1976) Electron microscopy of human cytomegalovirus DNA. Arch Virol 50:343-347.
Sattar N GA, Packard Cj,Greer IA (1996) - Potential pathogenic roles of aberrant lipoprotein and fatty acid metabolism in pre-eclampsia. Br J Obstet Gynaecol 103:614-620.
Scannell JW, Blanckley A, Boldon H, Warrington B (2012) Diagnosing the decline in pharmaceutical R&D efficiency. Nat Rev Drug Discov 11:191-200.
Scattoni ML, Gandhy SU, Ricceri L, Crawley JN (2008) Unusual repertoire of vocalizations in the BTBR T+tf/J mouse model of autism. PLoS One 3:e3067.
Schleiss MR (2006a) Nonprimate models of congenital cytomegalovirus (CMV) infection: gaining insight into pathogenesis and prevention of disease in newborns. Ilar j 47:65-72.
Schleiss MR (2006b) The role of the placenta in the pathogenesis of congenital cytomegalovirus infection: is the benefit of cytomegalovirus immune globulin for the newborn mediated through improved placental health and function? Clin Infect Dis 43:1001-1003.

Schleiss MR (2013) Developing a Vaccine against Congenital Cytomegalovirus (CMV) Infection: What Have We Learned from Animal Models? Where Should We Go Next? Future Virol 8:1161-1182.
Schneider T, Przewlocki R (2005) Behavioral alterations in rats prenatally exposed to valproic acid: animal model of autism. Neuropsychopharmacology 30:80-89.
Schut RL, Gekker G, Hu S, Chao CC, Pomeroy C, Jordan MC, Peterson PK (1994) Cytomegalovirus replication in murine microglial cell cultures: suppression of permissive infection by interferon-gamma. J Infect Dis 169:1092-1096.
Seidel V, Feiterna-Sperling C, Siedentopf JP, Hofmann J, Henrich W, Buhrer C, Weizsacker K (2017) Intrauterine therapy of cytomegalovirus infection with valganciclovir: review of the literature. Med Microbiol Immunol.
Seleme MC, Kosmac K, Jonjic S, Britt WJ (2017) Tumor Necrosis Factor Alpha-Induced Recruitment of Inflammatory Mononuclear Cells Leads to Inflammation and Altered Brain Development in Murine Cytomegalovirus-Infected Newborn Mice. J Virol 91.
Semple BD, Blomgren K, Gimlin K, Ferriero DM, Noble-Haeusslein LJ (2013) Brain development in rodents and humans: Identifying benchmarks of maturation and vulnerability to injury across species. Prog Neurobiol 106-107:1-16.
Sgado P, Dunleavy M, Genovesi S, Provenzano G, Bozzi Y (2011) The role of GABAergic system in neurodevelopmental disorders: a focus on autism and epilepsy. Int J Physiol Pathophysiol Pharmacol 3:223-235.
Shaltiel G, Mark S, Kofman O, Belmaker RH, Agam G (2007) Effect of valproate derivatives on human brain myo-inositol-1-phosphate (MIP) synthase activity and amphetamine-induced rearing. Pharmacol Rep 59:402-407.
Sharlow ER (2016) Revisiting Repurposing. Assay Drug Dev Technol 14:554-556.
Shaw RN, Arbiser JL, Offermann MK (2000) Valproic acid induces human herpesvirus 8 lytic gene expression in BCBL-1 cells. Aids 14:899-902.
Shekh-Ahmad T, Hen N, McDonough JH, Yagen B, Bialer M (2013) Valnoctamide and sec-butyl-propylacetamide (SPD) for acute seizures and status epilepticus. Epilepsia 54 Suppl 6:99-102.
Shekh-Ahmad T, Mawasi H, McDonough JH, Yagen B, Bialer M (2015) The potential of sec-butylpropylacetamide (SPD) and valnoctamide and their individual stereoisomers in status epilepticus. Epilepsy Behav 49:298-302.
Shekh-Ahmad T, Hen N, Yagen B, McDonough JH, Finnell RH, Wlodarczyk BJ, Bialer M (2014) Stereoselective anticonvulsant and pharmacokinetic analysis of valnoctamide, a CNS-active derivative of valproic acid with low teratogenic potential. Epilepsia 55:353-361.
Shi L, Fatemi SH, Sidwell RW, Patterson PH (2003) Maternal influenza infection causes marked behavioral and pharmacological changes in the offspring. J Neurosci 23:297-302.
Shi L, Smith SE, Malkova N, Tse D, Su Y, Patterson PH (2009) Activation of the maternal immune system alters cerebellar development in the offspring. Brain Behav Immun 23:116-123.
Shinmura Y, Kosugi I, Aiba-Masago S, Baba S, Yong LR, Tsutsui Y (1997) Disordered migration and loss of virus-infected neuronal cells in developing mouse brains infected with murine cytomegalovirus. Acta Neuropathol 93:551-557.
Simioni C, Sanchez Oliveira Rde C, Moscovi T, A DAD, Cordioli E, Santos E (2013) Twin pregnancy and congenital cytomegalovirus: case report and review. J Matern Fetal Neonatal Med 26:622-624.

Singh N, Halliday AC, Thomas JM, Kuznetsova OV, Baldwin R, Woon EC, Aley PK, Antoniadou I, Sharp T, Vasudevan SR, Churchill GC (2013) A safe lithium mimetic for bipolar disorder. Nat Commun 4:1332.

Singh N, Sharpley AL, Emir UE, Masaki C, Herzallah MM, Gluck MA, Sharp T, Harmer CJ, Vasudevan SR, Cowen PJ, Churchill GC (2016) Effect of the Putative Lithium Mimetic Ebselen on Brain Myo-Inositol, Sleep, and Emotional Processing in Humans. Neuropsychopharmacology 41:1768-1778.

Sinzger C, Plachter B, Stenglein S, Jahn G (1993) Immunohistochemical detection of viral antigens in smooth muscle, stromal, and epithelial cells from acute human cytomegalovirus gastritis. J Infect Dis 167:1427-1432.

Slavuljica I, Kvestak D, Csaba Huszthy P, Kosmac K, Britt WJ, Jonjic S (2014) Immunobiology of congenital cytomegalovirus infection of the central nervous system-the murine cytomegalovirus model. Cell Mol Immunol.

Smith JD, de Harven E (1978) Herpes simplex virus and human cytomegalovirus replication in WI-38 cells. III. Cytochemical localization of lysosomal enzymes in infected cells. J Virol 26:102-109.

Smithers-Sheedy H, Raynes-Greenow C, Badawi N, McIntyre S, Jones CA (2014) Congenital cytomegalovirus is associated with severe forms of cerebral palsy and female sex in a retrospective population-based study. Dev Med Child Neurol 56:846-852.

Smithers-Sheedy H, Raynes-Greenow C, Badawi N, Fernandez MA, Kesson A, McIntyre S, Leung KC, Jones CA (2017) Congenital Cytomegalovirus among Children with Cerebral Palsy. J Pediatr 181:267-271.e261.

Soerensen J, Jakupoglu C, Beck H, Forster H, Schmidt J, Schmahl W, Schweizer U, Conrad M, Brielmeier M (2008) The role of thioredoxin reductases in brain development. PLoS One 3:e1813.

Spampanato J, Dudek FE (2014) Valnoctamide enhances phasic inhibition: a potential target mechanism for the treatment of benzodiazepine-refractory status epilepticus. Epilepsia 55:e94-98.

Spiller OB, Borysiewicz LK, Morgan BP (1997) Development of a model for cytomegalovirus infection of oligodendrocytes. J Gen Virol 78 (Pt 12):3349-3356.

St Omer VE, Ali SF, Holson RR, Duhart HM, Scalzo FM, Slikker W, Jr. (1991) Behavioral and neurochemical effects of prenatal methylenedioxymethamphetamine (MDMA) exposure in rats. Neurotoxicol Teratol 13:13-20.

Staras SA, Dollard SC, Radford KW, Flanders WD, Pass RF, Cannon MJ (2006) Seroprevalence of cytomegalovirus infection in the United States, 1988-1994. Clin Infect Dis 43:1143-1151.

Stepansky W (1960) A clinical study in the use of valmethamide, an anxiety-reducing drug. Curr Ther Res Clin Exp 2:144-147.

Stinski MF (1976) Human cytomegalovirus: glycoproteins associated with virions and dense bodies. J Virol 19:594-609.

Stinski MF, Thomsen DR, Stenberg RM, Goldstein LC (1983) Organization and expression of the immediate early genes of human cytomegalovirus. J Virol 46:1-14.

Stubbs EG, Ash E, Williams CP (1984) Autism and congenital cytomegalovirus. J Autism Dev Disord 14:183-189.

Sugiura S, Yoshikawa T, Nishiyama Y, Morishita Y, Sato E, Hattori T, Nakashima T (2003) Detection of human cytomegalovirus DNA in perilymph of patients with sensorineural hearing loss using real-time PCR. J Med Virol 69:72-75.

Sung H, Schleiss MR (2010) Update on the current status of cytomegalovirus vaccines. Expert Rev Vaccines 9:1303-1314.

Suzuki Y, Toribe Y, Mogami Y, Yanagihara K, Nishikawa M (2008) Epilepsy in patients with congenital cytomegalovirus infection. Brain Dev 30:420-424.

Swiss Insititute of Bioinformatics (2017) Cytomegalovirus. In www.expasy.org/viralzone, accessed in September 2017. In.

Takahashi R, Tagawa M, Sanjo M, Chiba H, Ito T, Yamada M, Nakae S, Suzuki A, Nishimura H, Naganuma M, Tominaga N, Moriuchi M, Moriuchi H (2007) Severe postnatal cytomegalovirus infection in a very premature infant. Neonatology 92:236-239.

Tanaka M, Machida Y, Niu S, Ikeda T, Jana NR, Doi H, Kurosawa M, Nekooki M, Nukina N (2004) Trehalose alleviates polyglutamine-mediated pathology in a mouse model of Huntington disease. Nat Med 10:148-154.

Tanaka T (1998) Effects of litter size on behavioral development in mice. Reprod Toxicol 12:613-617.

Townsend CL, Forsgren M, Ahlfors K, Ivarsson SA, Tookey PA, Peckham CS (2013) Long-term outcomes of congenital cytomegalovirus infection in Sweden and the United Kingdom. Clin Infect Dis 56:1232-1239.

Tsai PT, Hull C, Chu Y, Greene-Colozzi E, Sadowski AR, Leech JM, Steinberg J, Crawley JN, Regehr WG, Sahin M (2012) Autistic-like behaviour and cerebellar dysfunction in Purkinje cell Tsc1 mutant mice. Nature 488:647-651.

Tsutsui Y (1995) Developmental disorders of the mouse brain induced by murine cytomegalovirus: animal models for congenital cytomegalovirus infection. Pathol Int 45:91-102.

Tsutsui Y (2009) Effects of cytomegalovirus infection on embryogenesis and brain development. Congenit Anom (Kyoto) 49:47-55.

Tsutsui Y, Kosugi I, Kawasaki H (2005) Neuropathogenesis in cytomegalovirus infection: indication of the mechanisms using mouse models. Rev Med Virol 15:327-345.

Tung EW, Winn LM (2010) Epigenetic modifications in valproic acid-induced teratogenesis. Toxicol Appl Pharmacol 248:201-209.

Turner KM, Lee HC, Boppana SB, Carlo WA, Randolph DA (2014) Incidence and impact of CMV infection in very low birth weight infants. Pediatrics 133:e609-615.

Tyms AS, Scamans EM, Naim HM (1981) The in vitro activity of acyclovir and related compounds against cytomegalovirus infections. J Antimicrob Chemother 8:65-72.

van den Pol AN, Reuter JD, Santarelli JG (2002a) Enhanced cytomegalovirus infection of developing brain independent of the adaptive immune system. J Virol 76:8842-8854.

van den Pol AN, Dalton KP, Rose JK (2002b) Relative neurotropism of a recombinant rhabdovirus expressing a green fluorescent envelope glycoprotein. J Virol 76:1309-1327.

van Den Pol AN, Mocarski E, Saederup N, Vieira J, Meier TJ (1999) Cytomegalovirus cell tropism, replication, and gene transfer in brain. J Neurosci 19:10948-10965.

van den Pol AN, Mao G, Yang Y, Ornaghi S, Davis JN (2017) Zika Virus Targeting in the Developing Brain. J Neurosci 37:2161-2175.

van den Pol AN, Robek MD, Ghosh PK, Ozduman K, Bandi P, Whim MD, Wollmann G (2007) Cytomegalovirus induces interferon-stimulated gene expression and is attenuated by interferon in the developing brain. J Virol 81:332-348.
Varghese FS, Kaukinen P, Glasker S, Bespalov M, Hanski L, Wennerberg K, Kummerer BM, Ahola T (2016) Discovery of berberine, abamectin and ivermectin as antivirals against chikungunya and other alphaviruses. Antiviral Res 126:117-124.
Waller EC, Day E, Sissons JG, Wills MR (2008) Dynamics of T cell memory in human cytomegalovirus infection. Med Microbiol Immunol 197:83-96.
Wang Y, Patel R, Ren C, Taggart MG, Firpo MA, Schleiss MR, Park AH (2013) A comparison of different murine models for cytomegalovirus-induced sensorineural hearing loss. Laryngoscope 123:2801-2806.
Weiser M, Levi L, Levine SZ, Bialer M, Shekh-Ahmad T, Matei V, Tiugan A, Cirjaliu D, Sava C, Sinita E, Zamora D, Davis JM (2017) A randomized, double-blind, placebo- and risperidone-controlled study on valnoctamide for acute mania. Bipolar Disord 19:285-294.
White HS, Alex AB, Pollock A, Hen N, Shekh-Ahmad T, Wilcox KS, McDonough JH, Stables JP, Kaufmann D, Yagen B, Bialer M (2012) A new derivative of valproic acid amide possesses a broad-spectrum antiseizure profile and unique activity against status epilepticus and organophosphate neuronal damage. Epilepsia 53:134-146.
Whittaker G, Bui M, Helenius A (1996) The role of nuclear import and export in influenza virus infection. Trends Cell Biol 6:67-71.
Wilkerson I, Laban J, Mitchell JM, Sheibani N, Alcendor DJ (2015) Retinal pericytes and cytomegalovirus infectivity: implications for HCMV-induced retinopathy and congenital ocular disease. J Neuroinflammation 12:2.
Williamson WD, Demmler GJ, Percy AK, Catlin FI (1992) Progressive hearing loss in infants with asymptomatic congenital cytomegalovirus infection. Pediatrics 90:862-866.
Williamson WD, Percy AK, Yow MD, Gerson P, Catlin FI, Koppelman ML, Thurber S (1990) Asymptomatic congenital cytomegalovirus infection. Audiologic, neuroradiologic, and neurodevelopmental abnormalities during the first year. Am J Dis Child 144:1365-1368.
Winkler I, Blotnik S, Shimshoni J, Yagen B, Devor M, Bialer M (2005) Efficacy of antiepileptic isomers of valproic acid and valpromide in a rat model of neuropathic pain. Br J Pharmacol 146:198-208.
Wishart DS, Knox C, Guo AC, Shrivastava S, Hassanali M, Stothard P, Chang Z, Woolsey J (2006) DrugBank: a comprehensive resource for in silico drug discovery and exploration. Nucleic Acids Res 34:D668-672.
Witvrouw M, Schmit JC, Van Remoortel B, Daelemans D, Este JA, Vandamme AM, Desmyter J, De Clercq E (1997) Cell type-dependent effect of sodium valproate on human immunodeficiency virus type 1 replication in vitro. AIDS Res Hum Retroviruses 13:187-192.
Wlodarczyk BJ, Ogle K, Lin LY, Bialer M, Finnell RH (2015) Comparative teratogenicity analysis of valnoctamide, risperidone, and olanzapine in mice. Bipolar Disord 17:615-625.
Wollmann G, Drokhlyansky E, Davis JN, Cepko C, van den Pol AN (2015) Lassa-vesicular stomatitis chimeric virus safely destroys brain tumors. J Virol 89:6711-6724.
Woolf NK, Jaquish DV, Koehrn FJ (2007) Transplacental murine cytomegalovirus infection in the brain of SCID mice. Virol J 4:26.
Workman AD, Charvet CJ, Clancy B, Darlington RB, Finlay BL (2013) Modeling transformations of neurodevelopmental sequences across mammalian species. J Neurosci 33:7368-7383.

Wright HT, Jr., Goodheart CR, Lielausis A (1964) HUMAN CYTOMEGALOVIRUS. MORPHOLOGY BY NEGATIVE STAINING. Virology 23:419-424.
Xu M et al. (2016) Identification of small-molecule inhibitors of Zika virus infection and induced neural cell death via a drug repurposing screen. Nat Med 22:1101-1107.
Yamamoto AY, Mussi-Pinhata MM, Boppana SB, Novak Z, Wagatsuma VM, Oliveira Pde F, Duarte G, Britt WJ (2010) Human cytomegalovirus reinfection is associated with intrauterine transmission in a highly cytomegalovirus-immune maternal population. Am J Obstet Gynecol 202:297.e291-298.
Yamashita Y, Fujimoto C, Nakajima E, Isagai T, Matsuishi T (2003) Possible association between congenital cytomegalovirus infection and autistic disorder. J Autism Dev Disord 33:455-459.
Yang M, Silverman JL, Crawley JN (2011) Automated three-chambered social approach task for mice. Curr Protoc Neurosci Chapter 8:Unit 8.26.
Zagolski O (2008) Vestibular-evoked myogenic potentials and caloric stimulation in infants with congenital cytomegalovirus infection. J Laryngol Otol 122:574-579.
Zhang A, Hildreth RL, Colberg-Poley AM (2013) Human cytomegalovirus inhibits apoptosis by proteasome-mediated degradation of Bax at endoplasmic reticulum-mitochondrion contacts. J Virol 87:5657-5668.
Zhu Y, Yu T, Zhang XC, Nagasawa T, Wu JY, Rao Y (2002) Role of the chemokine SDF-1 as the meningeal attractant for embryonic cerebellar neurons. Nat Neurosci 5:719-720.
Zou YR, Kottmann AH, Kuroda M, Taniuchi I, Littman DR (1998) Function of the chemokine receptor CXCR4 in haematopoiesis and in cerebellar development. Nature 393:595-599.
Zurbach KA, Moghbeli T, Snyder CM (2014) Resolving the titer of murine cytomegalovirus by plaque assay using the M2-10B4 cell line and a low viscosity overlay. Virol J 11:71.

Appendix

Virology 499 (2016) 121–135

Contents lists available at ScienceDirect

Virology

journal homepage: www.elsevier.com/locate/yviro

Mood stabilizers inhibit cytomegalovirus infection

Sara Ornaghi [a,b,c,d], John N. Davis [a], Kelly L. Gorres [e,1], George Miller [e], Michael J. Paidas [b], Anthony N. van den Pol [a,*]

[a] Department of Neurosurgery, Yale University School of Medicine, 333 Cedar Street, 06510 New Haven, CT, USA
[b] Department of Obstetrics, Gynecology, and Reproductive Sciences, Yale University School of Medicine, Yale Women and Children's Center for Blood Disorders and Preeclampsia Advancement, 333 Cedar Street, 06510 New Haven, CT, USA
[c] School of Medicine and Surgery, Ph.D. Program in Neuroscience, University of Milan-Bicocca, via Cadore 48, 20900 Monza, Italy
[d] Department of Obstetrics and Gynecology, Foundation MBBM, University of Milan-Bicocca, via Pergolesi 33, 20900 Monza, Italy
[e] Department of Pediatrics, Yale University School of Medicine, 333 Cedar Street, 06510 New Haven, CT, USA

ARTICLE INFO

Article history:
Received 29 June 2016
Returned to author for revisions
14 August 2016
Accepted 12 September 2016

Keywords:
Cytomegalovirus
Mood stabilizers
Perinatal infection
Development

ABSTRACT

Cytomegalovirus (CMV) infection can generate debilitating disease in immunocompromised individuals and neonates. It is also the most common infectious cause of congenital birth defects in infected fetuses. Available anti-CMV drugs are partially effective but are limited by some toxicity, potential viral resistance, and are not recommended for fetal exposure. Valproate, valpromide, and valnoctamide have been used for many years to treat epilepsy and mood disorders. We report for the first time that, in contrast to the virus-enhancing actions of valproate, structurally related valpromide and valnoctamide evoke a substantial and specific inhibition of mouse and human CMV in vitro. In vivo, both drugs safely attenuate mouse CMV, improving survival, body weight, and developmental maturation of infected newborns. The compounds appear to act by a novel mechanism that interferes with CMV attachment to the cell. Our work provides a novel potential direction for CMV therapeutics through repositioning of agents already approved for use in psychiatric disorders.

1. Introduction

Human cytomegalovirus (hCMV) is a common and potentially life-threatening infectious complication in susceptible individuals with immature or compromised immune systems, including neonates, AIDS patients, and transplant recipients. CMV is also the leading viral cause of congenital brain defects, including microcephaly (Cheeran et al., 2009; Gandhi and Khanna, 2004; Mocarski et al., 2007; Tsutsui, 2009). No vaccine is available to prevent CMV infection. Acute and long-term toxicity, carcinogenicity, poor oral bioavailability, and drug resistance significantly limit the use of the current antivirals ganciclovir (GCV), valganciclovir, foscarnet, cidofovir, and fomivirsen (Mercorelli et al., 2011); there are no recommended treatments for pregnant mothers and infected fetuses due to the potential teratogenic actions of these compounds (Gandhi and Khanna, 2004). Thus, development of less toxic agents with activity against resistant CMV isolates is needed.

Valproate (VPA) is a widely prescribed anti-epileptic drug employed for the treatment of multiple psychiatric and neurological diseases including bipolar disorder, epilepsy, neuropathic pain, and migraine (Perucca, 2002). VPA is the first-line therapy for pediatric epilepsy (Guerrini, 2006). Significant side effects of VPA administration include liver toxicity and teratogenesis (Guerrini, 2006; Monti et al., 2009). A free carboxylic group in the chemical structure and an inhibitory action on histone deacetylase (HDAC) underlie the detrimental effects exerted by VPA on fetal development and can lead to neural tube defects, skeletal abnormalities, and autism (Nau et al., 1991; Radatz et al., 1998; Okada et al., 2004; Phiel et al., 2001; Tung and Winn, 2010; Paradis and Hales, 2013; Kataoka et al., 2013).

Valpromide (VPD), a more effective and less toxic anti-epileptic homolog of VPA, has been used as mood stabilizer in bipolar disorder for over 25 years (Bialer, 1991). In contrast to VPA, VPD lacks the free carboxylic group and the HDAC inhibitory activity and therefore the related teratogenic risk, as demonstrated in a number of animal models (Radatz et al., 1998; Okada et al., 2004).

Although both VPA and VPD attenuate reactivation from latency of Epstein Barr virus (Gorres et al., 2016), VPA enhances the infectivity and replication of a large variety of other viruses including HIV (Moog et al., 1996), vesicular stomatitis virus (VSV) (Paglino and van den Pol, 2011), Kaposi's sarcoma-associated herpes virus (Shaw et al., 2000), herpes simplex viruses (Nakashima et al., 2015; Otsuki et al., 2008), human herpes virus 6

* Corresponding author.
E-mail address: anthony.vandenpol@yale.edu (A.N. van den Pol).
[1] Present address: Department of Chemistry and Biochemistry, University of Wisconsin-La Crosse, La Crosse, WI, USA.

http://dx.doi.org/10.1016/j.virol.2016.09.012
0042-6822/

(Mardivirin et al., 2009), and hCMV (Kuntz-Simon and Obert, 1995; Michaelis et al., 2004, 2005) through a mechanism involving HDAC inhibition. These virus-enhancing effects are exerted at doses therapeutic for anti-epileptic and mood stabilizing purposes (Brodie and Dichter, 1996; Pisani et al., 1986; Matalon et al., 2011), thus raising concerns over the use of VPA in congenitally CMV-infected neonates experiencing seizures and in AIDS patients with CMV- and HIV-mediated neurological disorders (Jennings and Romanelli, 2000). Given the absence of HDAC inhibition, we hypothesized that VPD might show a reduced enhancement of CMV infection compared with VPA.

2. Materials and methods

2.1. Cells

NIH/3T3 (CRL-1658) and Vero (CCL-81) cells were purchased from the American Type Culture Collection (ATCC) (Manassas, VA), normal human dermal fibroblasts (HDF) were obtained from Cambrex (Walkersville, MD), Neuro-2a (CCL-131) were kindly provided by A. Bordey (Yale University, New Haven, CT), and U-373 MG cells were a gift from R. Matthews (Syracuse, NY). Vero cells were grown and maintained in Eagle's Minimum Essential Medium (MEM) supplemented with 10% fetal bovine serum (FBS) and 1% pen/strep (Invitrogen, Carlsbad, CA). All the other cell lines were maintained in Dulbecco's modified Eagle's essential medium (DMEM) supplemented with 10% FBS and 1% pen/strep. Primary cultures of mouse glia were established using whole brain tissue harvested from P5 mice and maintained in DMEM (van den Pol et al., 1999). All cultures were kept in a humified atmosphere containing 5% CO_2 at 37 °C.

2.2. Viruses

A brief description of each virus used is given below.

2.2.1. mCMV-GFP

Recombinant murine CMV (mCMV, MC.55) expressing enhanced green fluorescent protein (EGFP) was derived from the K181 strain. The expression cassette containing the EGFP gene controlled by the human elongation factor 1 alpha (EF1-alpha) promoter was inserted into the immediate early gene (IE-2) site. NIH/3T3 cells were used for viral propagation and titering by plaque assay (van den Pol et al., 1999).

2.2.2. hCMV-GFP

Recombinant hCMV expressing EGFP under the control of the EF1-alpha promoter was derived from the Toledo strain. The gene coding for EGFP was inserted between US9 and US10 of the hCMV genome, a site that appears to tolerate alterations without affecting viral replication. EGFP expression and replication capability were tested on normal human fibroblasts and U-373 human glioblastoma cells (Vieira et al., 1998; Jarvis et al., 1999). Human dermal fibroblasts were used for viral propagation and titering by plaque assay.

Recombinant CMVs were generously provided by E. Mocarski (Emory University, Atlanta) and J. Vieira (University of Washington, Seattle).

2.2.3. VSV-GFP

A recombinant variant of the Indiana serotype of VSV expressing a GFP reporter gene from the first genomic position (VSV-1'GFP) (Ramsburg et al., 2005) was kindly provided by J. K. Rose (Yale University, New Haven, CT). Vero cells were used for viral propagation and titering by plaque assay (van den Pol et al., 2002).

All the viruses used in the present study express EGFP as a reporter and green fluorescence was employed to visualize infected cells and viral plaques. Viral titers were determined by standard plaque assay using 25% carboxy-methyl-cellulose (CMC) overlay for mCMV-GFP and hCMV-GFP (Zurbach et al., 2014) or 0.5% agar overlay for VSV-GFP. Viral stocks were stored in aliquots at −80 °C. For each experiment, a new aliquot of virus was thawed and used.

2.3. Chemicals

Valpromide (catalog no. V3640), valnoctamide (catalog no. V4765), valproate (catalog no. S0930000), ivermectin (catalog no. I88998), ganciclovir (catalog no. G2536), and heparan sulfate sodium salt (catalog no. H7640) were purchased from Sigma-Aldrich (St. Louis, MO). Valproate and heparan sulfate were dissolved in water to give a stock solution of 1 M and 1 mg/mL, respectively. Valpromide, valnoctamide, ivermectin, and ganciclovir were dissolved in dimethylsulfoxide (DMSO) to yield a stock solution of 1 M (valpromide, valnoctamide) and 100 mM (ivermectin, ganciclovir). Ivermectin was used at 1 μM, a concentration recently shown effective against Chikungunya and other alphaviruses (Varghese et al., 2016).

2.4. Quantification of infection

Effects of the tested compounds on CMV infection were assessed by counting the number of infected GFP-positive cells and viral plaques, and measuring plaque size.

Cells (NIH/3T3, Neuro-2a, mouse glia, Vero, normal human dermal fibroblasts, and U-373) were seeded at a density of 40,000 cells per well in 48-well plates and incubated overnight before medium (0.2 mL per well) was replaced for pre-treatment with VPA, VPD, VCD, ivermectin, or vehicle at the specified concentrations. After 24 h of drug exposure, cells were inoculated with virus and incubated at 37 °C for 2 h. Following incubation, cultures were washed twice with PBS and replenished with fresh media containing the test compounds. GFP-positive cells were counted at 48 (mCMV) and 72 (hCMV) hours post-infection (hpi). In addition, media was collected at 72 (mCMV) or 96 (hCMV) hpi and titered by plaque assay using NIH/3T3 (mCMV) and HDF (hCMV) monolayers to assess the drug-mediated inhibition of virus replication (virus yield reduction assay).

For the plaque reduction assay, cells pre-treated with drugs or vehicle for 24 h were infected with mCMV-GFP or hCMV-GFP, incubated for 2 h at 37 °C to allow viral adsorption, rinsed twice with PBS, and overlaid with a viscous solution containing the tested agents at the specified concentrations in DMEM (75%) and CMC (25%) for 50% effective concentrations (EC_{50}) calculation (Zurbach et al., 2014). Plates were then incubated at 37 °C in 5% CO_2 for 4 days (mCMV) and 7 days (hCMV), to allow time for fluorescent plaque development. The mean plaque counts for each drug concentration were expressed as a percentage of the mean plaque count of the control (vehicle). The EC_{50} was then calculated by nonlinear regression from the plots of log drug concentrations against percentage of reduction in plaque number at each antiviral compound concentration.

To assess which step of the viral replicative cycle was affected by VPD and VCD, 'time-of-drug addition' experiments were performed, in which cultures were inoculated with virus (t=0) and exposed to the drugs simultaneously, or 2 h or 12 h after viral challenge. The effects of the tested agents on CMV infection were then assessed by a viral yield reduction assay. Briefly, HDF cells were infected with hCMV-GFP (multiplicity of infection, MOI 0.01)

(t=0), exposed to the compounds (100 μM) as indicated above, and incubated until the media was collected at 96 hpi. The extent of virus replication was subsequently assessed through titering the media by plaque assay using HDF monolayers. In all conditions, 2 hpi cultures were rinsed twice with PBS to synchronize infection.

Infected cells were identified as GFP-positive cells using an Olympus IX71 fluorescence microscope (Olympus Optical, Tokyo, Japan) connected to a SPOT RT digital camera (Diagnostic Instruments, Sterling Heights, MI) interfaced with an Apple Macintosh computer. The total number of fluorescent cells per well in each condition was counted by two observers independently.

Each condition was tested at least in triplicate, and the whole experiment repeated twice. Camera settings (exposure time and gain) were kept consistent between images. The contrast and color of collected images were optimized using Adobe Photoshop.

To investigate the effects on the immediate early phase of viral replication, NIH/3T3 cells exposed to VPD (1 mM) for 24 h, were transfected with a CMV promoter (IE1/IE2)-driven reporter plasmid (pCMV-tdTomato) expressing the red fluorescent protein tdTomato.

2.5. Virucidal activity assay

To assess the potential virucidal effect of the compounds, VPD, VCD, or vehicle (100 μm) were added to undiluted aliquots of hCMV-GFP and these virus/compound mixtures were incubated at either 4 °C or 37 °C for 2 h. After incubation, the samples were diluted with culture medium to reduce the drug concentration to an ineffective dose (10 nM in the antiviral assay), and hCMV-GFP infectivity was determined by plaque assay on HDF cells. Alternatively, virus and drug mixtures were run through a 0.1 μm filter (Life Sciences) to remove the compounds but not the hCMV (size ~180 nm). Filter membranes were subsequently thoroughly rinsed in culture medium for 2 h at room temperature with periodic shaking to harvest drug-free hCMV before assessing infectivity by plaque assay on HDF monolayers.

2.6. Viral entry analysis

To evaluate the effects of the drugs on viral entry into the cell, i.e. reversible attachment of hCMV to the cell membrane and subsequent irreversible binding with fusion and adsorption, inoculated cultures were first incubated at 4 °C (which allows only virus attachment) and then shifted to 37 °C (which allows fusion and subsequent steps of the viral replication cycle) (Mocarski et al., 2007; Chan and Yurochko, 2014). For assessing the 'attachment' step, pre-chilled HDF cells at 90% confluency in a 6-well plate were treated with VPD, VCD, vehicle (100 μM), VPA (1 mM, negative control), or heparan sulfate (0.1 mg/mL, positive control) for 30 min at 4 °C and inoculated with pre-cooled hCMV-GFP (MOI 0.1) in the presence of compounds or vehicle for 2 h at 4 °C. Fibroblasts were then rinsed three times with cold PBS to remove unattached virions and compounds, and harvested by trypsinization for DNA extraction in the quantitative PCR assay (Chan and Yurochko, 2014) or overlaid with CMC and incubated for 3 days at 37 °C for infectivity assessment by GFP-positive cell counting. To evaluate the 'fusion' step of the hCMV entry, cultures plated in plain media were inoculated with hCMV-GFP (MOI 0.1) and incubated at 4 °C for 2 h. Cells were then washed three times, exposed to compounds or vehicle at the same concentrations described above, and incubated at 37 °C for 2 h before being overlaid with CMC for infectivity evaluation at 72 hpi.

2.7. Quantitative real-time PCR assay

DNA samples were prepared from the hCMV-infected cells in the viral entry experiment using a commercial kit (QIAamp DNA mini kit; Qiagen). Quantitative real time PCR (qPCR) assays for hCMV UL132 (Pa03453400_s1) and human albumin (Hs99999922_s1) genes were performed using TaqMan gene expression assays (Life Technologies) (Gault et al., 2001; Fukui et al., 2008). Ten-fold dilutions of hCMV DNA and cellular DNA from human fibroblasts were used as quantitative standards. qPCR was carried out with 20-μL reaction mixtures employing the iTaq Universal SYBR Probes Supermix (BioRad) and 100 ng of DNA. Samples from uninfected cells and without template served as negative controls. Samples from 2 biological replicates were run in duplicate using a Bio-Rad iCycler-IQ instrument (Bio-Rad, Hercules, CA), and results were analyzed with iCycler software. For the relative quantification of hCMV DNA expression, the comparative threshold cycle (C_T) method was employed and results presented as mean ± SEM of the fold change ($2^{-\Delta\Delta CT}$) relative to the control (vehicle).

2.8. Immunocytochemistry

A mouse monoclonal antibody (a gift of Dr. P. Cresswell, Yale University) against hCMV glycoprotein B (gB), diluted 1:1000 in PBS with 0.3% Triton X-100, was used to label cells infected with hCMV, as an alternative method to the GFP reporter used for quantification of infection. A mouse monoclonal antibody against hCMV immediate early (IE)1/2 antigen (1:1000, MAB810, EMD Millipore) was employed to assess drug-mediated effects on IE protein expression. The secondary antibody was a goat anti-mouse immunoglobulin conjugated with Alexa Fluor 594 (Thermo Fisher Scientific) diluted at 1:500. Cell nuclei were counterstained with DAPI (4′-6′-diamidino-2-phenylindole). Controls included the omission of the primary antibody and the use of non-inoculated cultures where no immunostaining was expected or found.

2.9. Cytotoxicity assay

An ethidium homodimer assay (EthD-1, Molecular Probes, Eugene, OR) was used to label dead cells. Briefly, NIH/3T3 cells (9×10^4 per well) were seeded in a 48-well plate and treated with VPD, VCD, or vehicle for 24 h before mCMV-GFP inoculation (MOI 0.03). 72 h after viral challenge, cells were washed twice and EthD-1 was added at a final concentration of 4 μM in DMEM. After 20 min of incubation at 37 °C, the total number of dead cells per well was counted based on red fluorescence of nuclei. Each condition was tested in quadruplicate, and each experiment was repeated twice. Similarly, the rate of cell death was assessed in uninfected NIH/3T3 and HDF cells exposed to VPD, VCD, vehicle (10 and 1 mM) or plain media for 24 and 72 h before EthD-1 addition.

2.10. Plaque size assay

Plaque size was used to assess the effect of the drugs on viral propagation. Briefly, semiconfluent NIH/3T3 and HDF cells in 12-well plates were inoculated using mCMV-GFP and hCMV-GFP (MOI 1), respectively. After 2 h-incubation at 37 °C to allow viral adsorption, inoculum was removed and cultures were washed three times with PBS before the addition of CMC overlay containing VPD, VCD, or vehicle at the specified concentrations. Five (mCMV) and 10 (hCMV) days later, the relative size of viral plaques was measured (n=60 plaques/condition), as previously described (Wollmann et al., 2015). Each condition was tested at least in triplicate, and the experiment repeated twice. All measurements were performed at the same time using similar camera settings (exposure time and gain).

2.11. Animal procedures

Male and female Balb/c strain mice (6–8 weeks of age) from Taconic Biosciences Inc. (Hudson, NY) were maintained on a 12:12 h light cycle under constant temperature (22 ± 2 °C) and humidity (55 ± 5%), with access to food and water ad libitum. One to two females were cohabited with a male of the same strain for at least 1 week to ensure fertilization. When advanced pregnancy was seen, each pregnant female was caged singularly and checked for delivery twice daily, at 8:30 a.m. and 6:30 p.m. Newborns were inoculated intraperitoneally (i.p.) with 750 plaque-forming units (PFU) of mCMV-GFP in 50 μL of media on the day of birth (DOB), within 14 h of delivery. The DOB was considered postnatal day (PND) 0. Control animals received 50 μL of media i.p.. Infected pups were randomly assigned to receive VPD, VCD, or vehicle (DMSO), via subcutaneous (s.c.) injections, once a day, at a dose of 1.4 mg/mL in 20 μL of saline (~30 μg), starting after virus inoculation from PND 1 to PND 21. Control pups received a similar amount of drug-free saline. Mice were monitored daily for survival until PND 49. Additionally, on each day from PND 0-22, without knowledge of the treatment group, pups were weighed to the nearest 0.01*g* and their body and tail lengths were measured. Hair growth, status of eyelid and pinnae detachment, and incisor eruption, as compared to adult mice, were also recorded, as previously described (Scattoni et al., 2008). Briefly, these somatic variables were rated semi-quantitatively in the following way: 0 = no occurrence of the condition, 1 = slight/uncertain condition, 2 = incomplete condition, and 3 = a complete adult-like condition. For detection of infectious viral load in organs, some of the control and experimental mice were sacrificed on PND 12, after receiving saline/treatment from PND 1 to PND 10. Designated mice were transcardially perfused with PBS to wash out free virus, and tissue samples were collected under sterile conditions from liver, spleen, and lungs, three organs markedly involved in severe perinatal infection in humans. Tissues were mechanically homogenized in PBS using a microcentrifuge tube tissue grinder. Part of the resulting tissue suspension was plated onto NIH/3T3 monolayers and viral titer was assessed by plaque assay (Zurbach et al., 2014; Brune et al., 2001). All animal breeding and experiments were performed in accordance with the guidelines of the Yale School of Medicine Institutional Animal Care and Use Committee (IACUC). Research was approved by the IACUC.

2.12. Statistical analysis

Statistical significance in in vitro experiments was determined using one-way Analysis of Variance (ANOVA), followed by post-hoc analysis (Bonferroni's test). Data are presented as percentage of infected or dead cells and viral titers, in drug versus vehicle, as mean ± SEM of two independent experiments; each independent experiment consisted of three or four cultures; p-values refer to a comparison of drug to control (vehicle). Fifty percent effective concentration (EC_{50}) values were calculated using nonlinear regression curve fit with a variable slope (log[inhibitor] vs response). For markers of somatic development, a mixed-model ANOVA with PND as the Repeated Measures factor was used, followed by Newman Keuls test only if a significant F-value was determined. Analysis was performed with GraphPad Prism 6.0 and SPSS Statistics 21, with significance set at $p < 0.05$. Survival studies and assessment of somatic development parameters were performed blindly with respect to the experimental group.

3. Results

3.1. Valpromide inhibits mouse and human CMV in vitro

We performed experiments with several cell types treated with VPA, VPD, or vehicle for 24 h before viral challenge. VPA (Fig. 1A) increased infection by and replication of mCMV on mouse cells at concentrations of 1 and 10 mM, as previously reported (Fig. 1B–D) (Kuntz-Simon and Obert, 1995; Michaelis et al., 2004, 2005). Remarkably, VPD (Fig. 1E) at the same concentrations showed a robust inhibitory effect (Fig. 1F–H), reducing the number of mCMV-infected cells, as quantified by counting cells expressing the viral GFP reporter gene (Fig. 1F and G). VCD also attenuated mCMV replication, assessed by a viral yield assay (Fig. 1H). Significant inhibition was also identified at lower doses of 100 μM, 1 μM, and 100 nM. Attenuation of mCMV was confirmed at high virus titer and in multiple cell types including NIH/3T3, Neuro-2a and primary astrocytes from mouse brain (Fig. 1I–L). Using an EthD-1 assay to fluorescently label dead cells, VPD at 1 and 10 mM showed no detectable cytotoxicity in uninfected NIH/3T3 cells treated for 24 or 72 h (Fig. 1M), thus suggesting a lack of toxicity of the target cells even at high drug concentrations and with prolonged cell exposure. In turn, VPD-related CMV inhibition increased cell survival by reducing viral-mediated cytotoxicity (Fig. 1N and O).

To determine if the inhibitory action of VPD would generalize from mCMV to hCMV, we tested VPD against hCMV on human cells. Similar to mCMV, hCMV infection was enhanced by VPA and substantially inhibited by VPD at 1 and 10 mM, independent of virus titer or cell type (Fig. 2A–D). VPD significantly reduced the number of hCMV infected cells and also reduced hCMV replication even at the lower drug concentrations of 100 μM, 1 μM, and 100 nM. We found similar inhibitory actions with both human dermal fibroblasts (Fig. 2B and C) and human glioma cells (Fig. 2D). To corroborate the view that the drug acted on CMV rather than by inhibiting expression of the viral GFP reporter, we used immunocytochemistry to label the hCMV glycoprotein B (gB) (Fig. 2E). VPD decreased the number of cells showing hCMV gB immunoreactivity compared to infected cultures not treated with VPD, further corroborating the antiviral effect of VPD on CMV and excluding a potential VPD-mediated inhibitory effect on GFP expression.

Fibroblasts treated with VPD displayed a substantial dose-dependent inhibition of mCMV and hCMV infectivity in the plaque reduction assay with EC_{50} concentrations of 6.8 ± 2.8 μM and 2.9 ± 1.3 μM (Fig. 2F), respectively. The absence of cytotoxic effects at the high dose of 10 mM gives VPD an excellent selectivity index (SI), i.e. the ratio of cytotoxic concentration $(CC)_{50}$ to EC_{50}, for both viruses. An effective antiviral activity was still evident in the nanomolar range, i.e. 100 nM (mCMV: 79% ± 3% infected cells in VPD-treated cultures as compared to vehicle-treated controls, $p = 0.01$; hCMV: 77% ± 2% infected cells in VPD-treated cultures as compared to controls, $p = 0.004$).

The VPD-mediated inhibition of both mouse and human CMV raised the question of whether the antiviral effect of the drug was universal for different types of virus and might act via enhancement of an innate immune block of viral infection in general. To address this question, we tested VSV, an unrelated single-strand RNA virus sensitive to upregulation of innate immunity. In contrast to mCMV and hCMV, VPD did not inhibit VSV (Fig. 2G), suggesting that VPD antiviral actions were not based on a mechanism involving an enhancement of the innate immune response.

We also tested ivermectin, a compound with anti-epileptic properties and a strong anti-parasitic activity which was recently shown to attenuate alphavirus infection (Varghese et al., 2016). Ivermectin had no effect on CMV (99% ± 9% compared to control), demonstrating that the anti-CMV effect was specific for VPD.

Together these results demonstrate that VPD substantially and

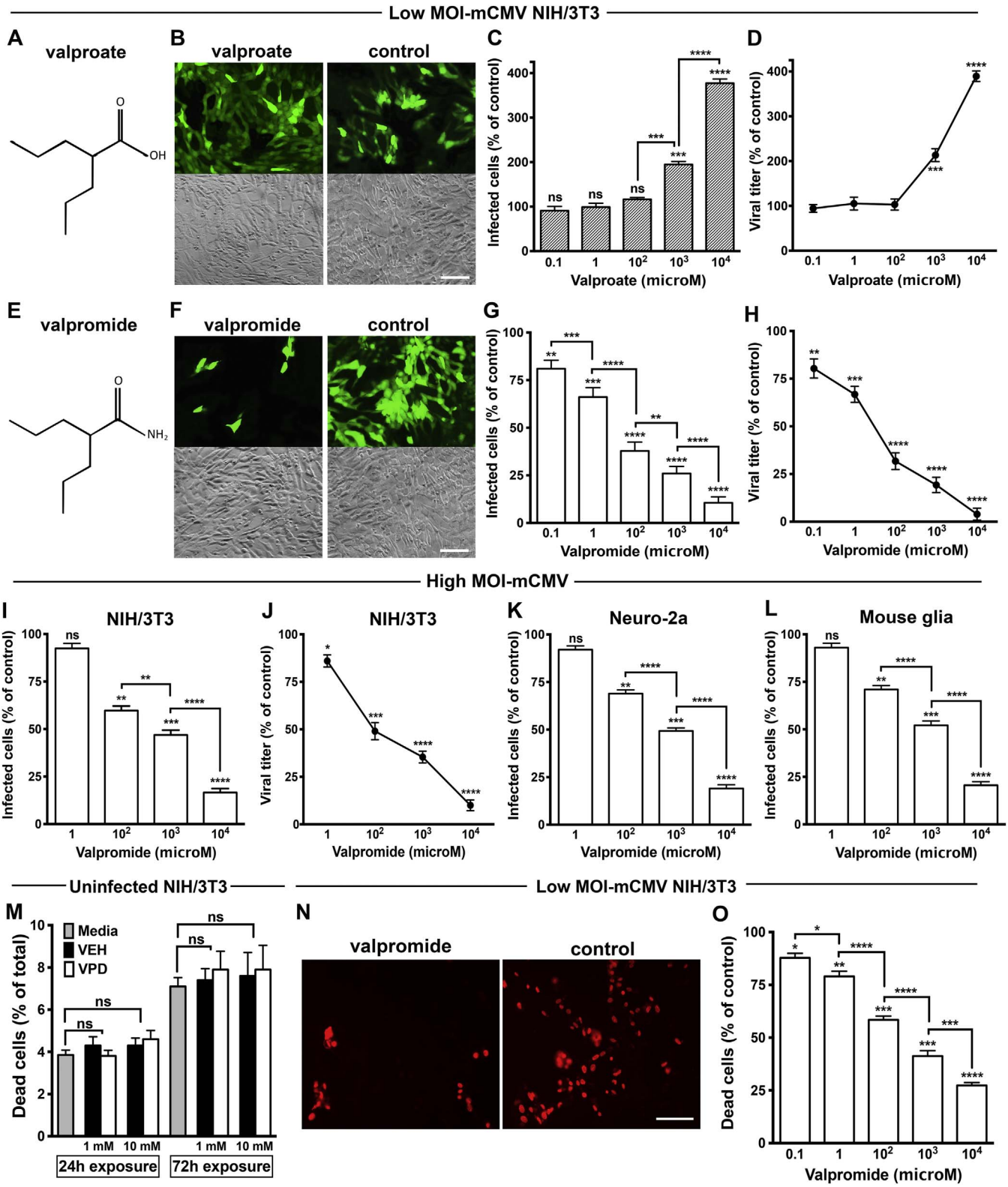

Fig. 1. Valproate and valpromide exert opposing effects on mouse CMV. (A) Chemical structure of valproate. (B) Representative microscopic fields show mCMV-GFP reporter fluorescence (top) and phase contrast (bottom) of NIH/3T3 cells pre-treated (24 h) with VPA (1 mM) or vehicle (control) prior to inoculation with mCMV using multiplicity of infection (MOI) of 0.03. Photos captured 48 hpi; scale bar 50 μm. (C and D) VPA dose-dependent increase in mCMV infection assessed by counting infected GFP-positive cells at 48 hpi (C) and viral yield assay at 72 hpi (D); other conditions same as B. (E) Chemical structure of valpromide. (F) VPD (1 mM) with other conditions same as B. (G and H) VPD dose-dependent decrease in mCMV infection, as per number of infected cells at 48 hpi (G) and viral titer at 72 hpi (H); other conditions same as B. (I–L) VPD dose-dependent decrease in mCMV-infectivity in NIH/3T3 (I and J), immortalized Neuro-2a (K) and primary mouse glia (L) cells (MOI 4) pre-treated with VPD for 24 h. Infectivity assessed by counting GFP-positive cells 24 hpi (I, K, and L) and by viral yield assay 72 hpi (J). (M) The potential cytotoxicity of VPD exposure for 24 and 72 h was assessed in uninfected mouse fibroblasts by the red fluorescent EthD-1 assay. The effect of VPD at 1 and 10 mM on NIH/3T3 was compared with vehicle (VEH) at the same concentrations and plain media. (N and O) The EthD-1 assay was performed to evaluate VPD protective role on viral-mediated cytotoxicity. Images show red fluorescent photomicrographs of NIH/3T3 cells pre-treated with VPD or vehicle at 10 mM for 24 h prior to viral inoculation (MOI of 0.03). 72 hpi, EthD-1 was added to cells. After 20 min, photos were captured (N) and red fluorescent-labeled cells were counted (O). Scale bar 50 μm. Mean ± SEM of 8 (C, D, G, H, M, and O) and 6 (I–L) cultures; ns, not significant, $^{*}p < 0.05$, $^{**}p < 0.01$, $^{***}p < 0.001$, $^{****}p < 0.0001$, as compared to control, ANOVA with Bonferroni's post-hoc test.

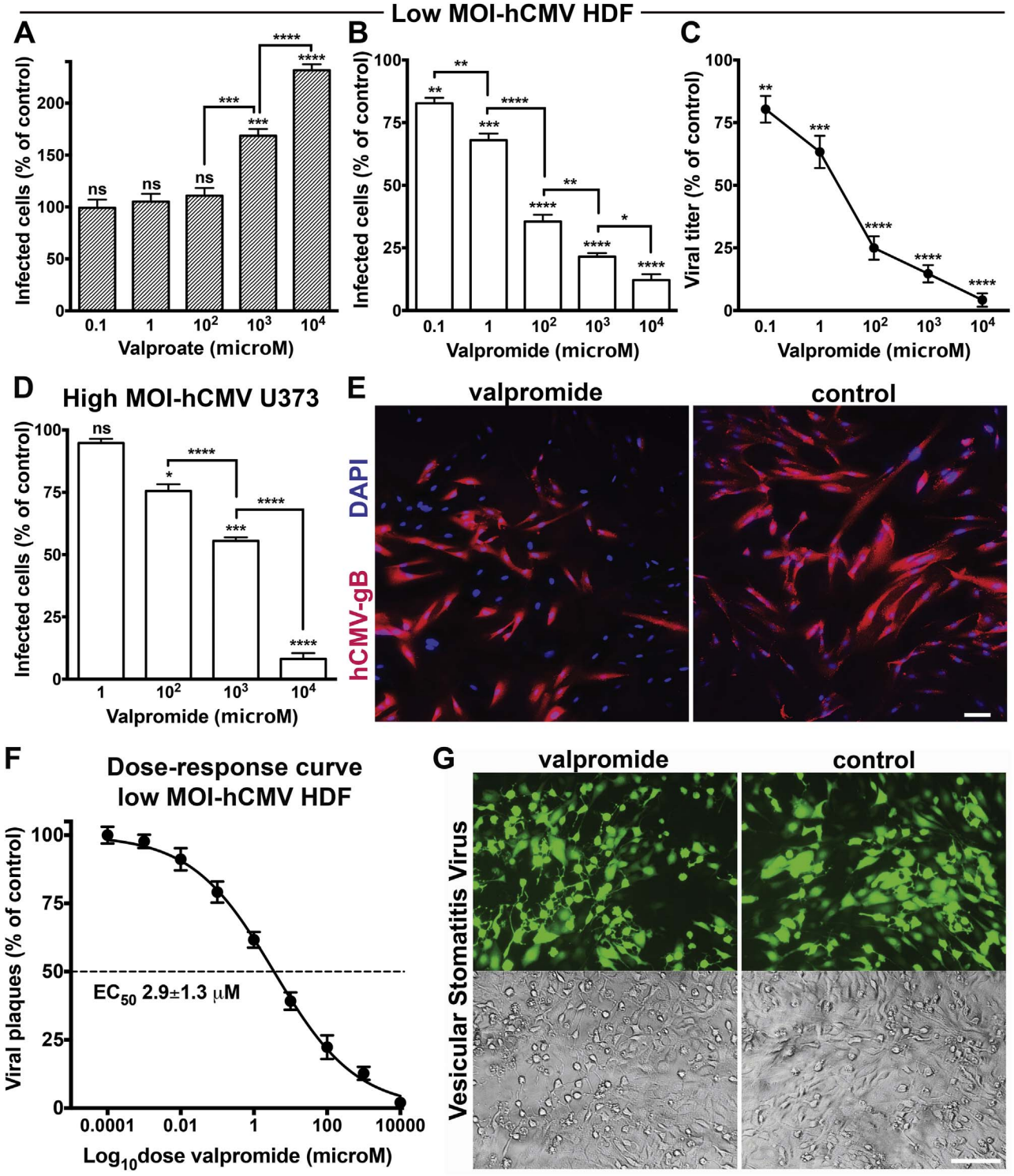

Fig. 2. Valpromide inhibits human CMV but has no effect on vesicular stomatitis virus infection. (A) Normal human dermal fibroblasts (HDF) were treated with VPA or vehicle at the indicated concentrations for 24 h prior to hCMV-GFP inoculation (MOI 0.01). Results collected at 72 hpi. (B and C) VPD dose-dependent decrease in hCMV infection assessed by counting infected GFP-positive cells at 72 hpi (B) and viral yield assay at 96 hpi (C); other conditions same as A. (D) Pre-treated human glioma cells infected with hCMV-GFP at high titer (MOI 4). GFP-positive cells counted at 48 hpi. Data presented as mean ± SEM of 8 cultures (A–C) and 6 cultures (D); ns, not significant, $^{*}p < 0.05$, $^{**}p < 0.01$, $^{***}p < 0.001$, $^{****}p < 0.0001$, one-way ANOVA (Bonferroni's post-hoc test). (E) Immunostaining for hCMV gB was done to exclude a potential inhibitory effect of VPD on GFP expression. HDF were exposed to VPD or vehicle (1 mM) for 24 h prior to viral challenge (MOI 1). Representative fields with hCMV gB immunoreactivity in red and cell nuclei in blue (DAPI) show VPD-mediated decrease in the relative number of infected cells. Scale bar 50 μm. (F) HDF cells pre-treated with VPD for 24 h and infected with hCMV-GFP (MOI 0.01) were incubated for 7 days before viral fluorescent plaques counting. The mean plaque count for each drug concentration was expressed as a percentage of the control (vehicle) and plotted as a function of the drug dose in logarithmic scale. The concentration producing 50% reduction in plaque formation (EC_{50}) is shown. Mean ± SEM of 2 independent experiments. (G) Images of representative microscopic fields under GFP fluorescence (top) and phase contrast (bottom) of Vero cells pre-treated with VPD or vehicle at 1 mM for 24 h and infected with VSV-GFP (MOI 0.001). No drug-mediated inhibitory effect was identified (101% ± 5%, compared to control; mean ± SEM of 6 cultures). Photos captured at 24 hpi; scale bar 50 μm.

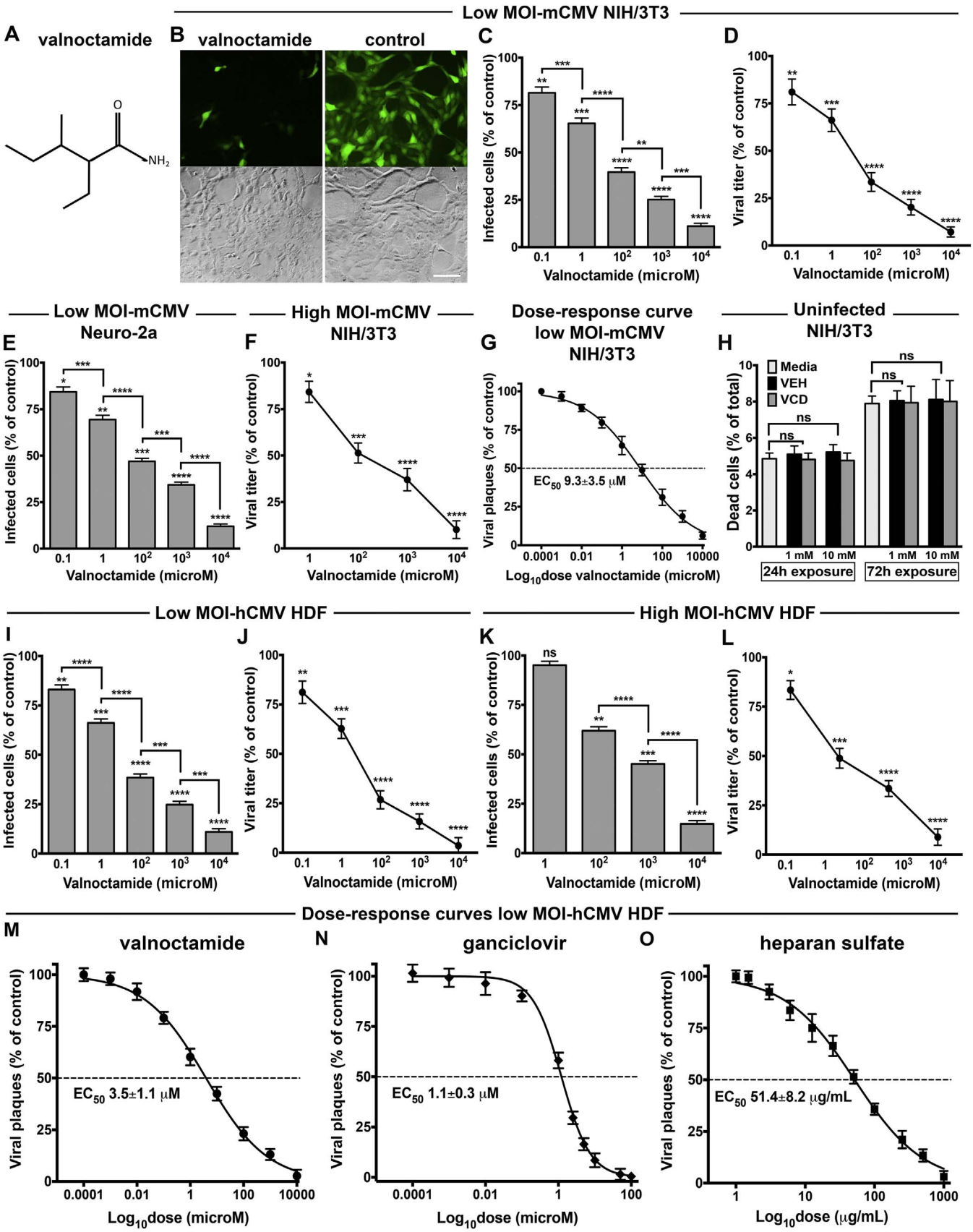

Fig. 3. Valnoctamide blocks mouse and human CMV. (A) Chemical structure of valnoctamide. (B) Microscopic fields show GFP fluorescence (top) and phase contrast (bottom) of NIH/3T3 cells pre-treated (24 h) with VCD (1 mM) or vehicle (control) prior to inoculation with mCMV (MOI 0.03). Photos captured 48 hpi; scale 50 μm. (C–F) VCD-mediated dose-dependent decrease in mCMV infection at low MOI (0.03, C–E) and high MOI (4, F) in NIH/3T3 cells (C, D, and F) and Neuro-2a (E) pre-treated for 24 h, as assessed by counting infected GFP-positive cells at 48 hpi (C–E) and viral yield assay at 72 hpi (F). (G) Dose-response analysis in NIH/3T3 cells pre-treated with VCD for 24 h, infected with mCMV-GFP (MOI 0.03), and incubated for 4 days before viral fluorescent plaque counting. The EC_{50} is shown. Mean ± SEM of 2 independent experiments. (H) The potential cytotoxic effect of VCD at 1 and 10 mM on uninfected NIH/3T3 after 24 and 72 h of exposure was assessed by the red fluorescent EthD-1 assay and results compared with vehicle (VEH) at the same concentrations and plain media. (I–L) VCD-mediated decrease in hCMV infection at low MOI (0.01, I and J) and high MOI (1, K and L) in human dermal fibroblasts, evaluated by GFP-positive cell counting at 48 hpi (K) or 72 hpi (I) and viral yield assay at 96 hpi (J and L). Mean ± SEM of 8 (C–E, and H–J) and 6 (F, K, and L) cultures; ns, not significant, $^{*}p < 0.05$, $^{**}p < 0.01$, $^{***}p < 0.001$, $^{****}p < 0.0001$, one-way ANOVA (Bonferroni's post-hoc test). (M–O) Dose-response analysis by plaque reduction assay in HDF cells pre-treated with VCD (M), GCV (N), or HS (O) for 24 h and infected with hCMV-GFP (MOI 0.01). Viral fluorescent plaques counted at 7 dpi. Mean ± SEM of 2 independent experiments.

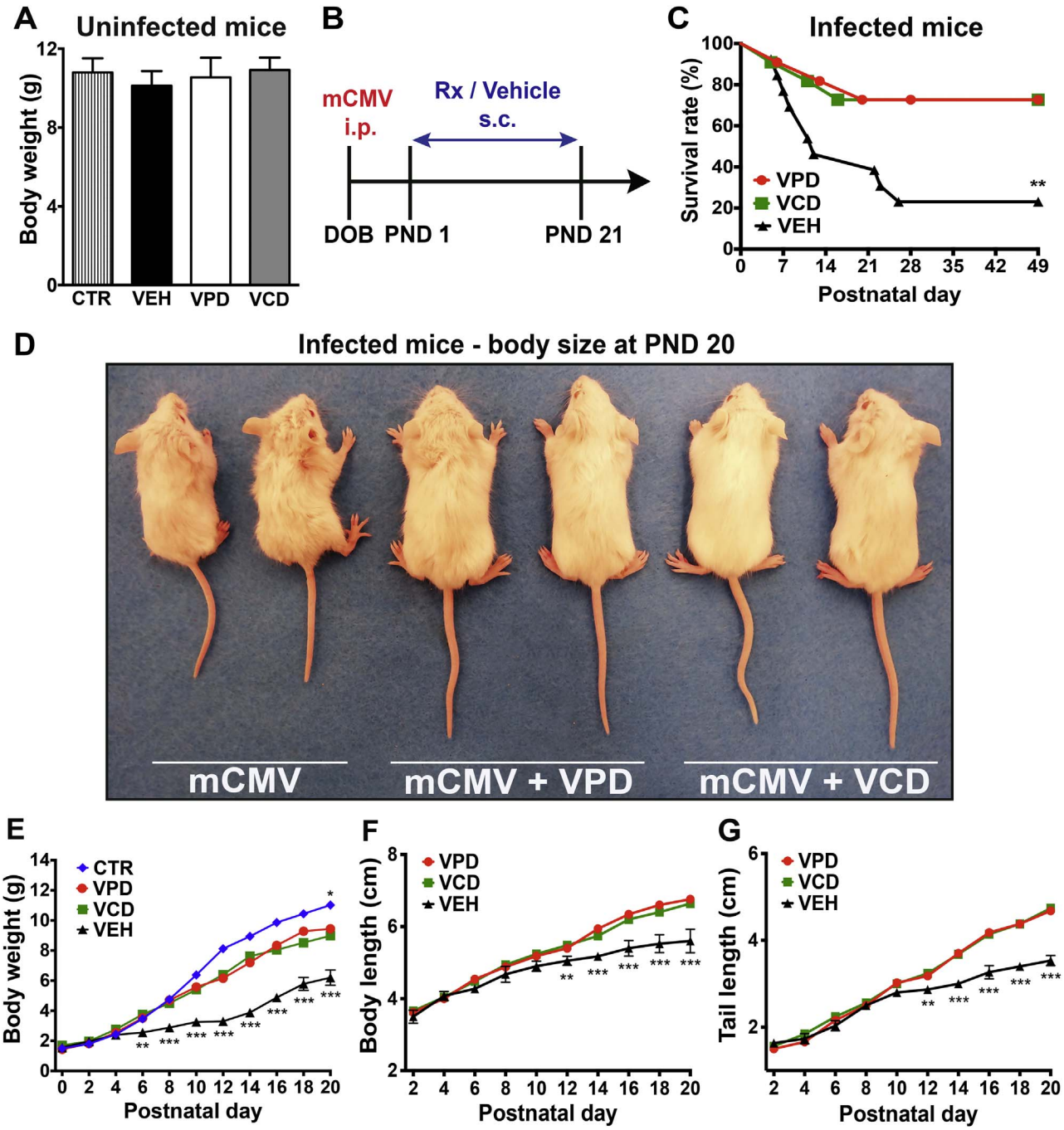

Fig. 4. Valpromide and valnoctamide safely improve survival and postnatal body growth of infected newborns. (A) Uninfected pups received 20 μL of saline (CTR), vehicle (VEH), VPD, or VCD (1.4 mg/mL), once a day, subcutaneously, from PND 1 to PND 21, when the body weight was assessed. Mean ± SEM, one-way ANOVA with Bonferroni's post-hoc test; N = 8 mice/experimental group. (B) Timeline showing mCMV infection of neonates and compound administration. (C) Survival at PND 49 assessed by Log-rank (Mantel-Cox) test; N = 11–13 mice/group. (D–G) Drug-induced improvement in postnatal body growth. Photo shows enhanced body size of VPD- and VCD-treated pups compared to vehicle (mCMV) (D). Graphs show postnatal body weight (E), body length (F), and tail length (G) increase from DOB to PND 20. CTR, control/uninfected mice treated with saline; VPD, VCD, and VEH, infected newborns treated with the indicated compounds. Mean ± SEM; error bars shown for VEH group; N = 6–9 mice/group; mixed-model ANOVA (Newman Keuls test) for VPD and VCD versus CTR (above CTR line, E) and for VPD and VCD versus VEH (below VEH line, E to G); $^{*}p < 0.05$, $^{**}p < 0.01$, $^{***}p < 0.001$.

selectively inhibits mouse and human CMV infectivity in vitro, and that this antiviral activity is independent of virus titer and cell type.

3.2. *Valnoctamide, a safer analog of VPD, blocks mouse and human CMV in cell culture*

Although VPD safety has been demonstrated in animal models of teratogenesis (Radatz et al., 1998; Okada et al., 2004), these findings may not translate to humans where VPD can be quickly metabolized (> 80%) to VPA (Bialer, 1991), which is both teratogenic and enhances CMV infection as shown earlier. Valnoctamide (VCD) is structurally similar to VPD (Fig. 3A), and lacks the free carboxylic group and HDAC inhibitory activity associated with the embryotoxic and teratogenic effects of VPA (Bialer et al., 1990, 2015; Shekh-Ahmad et al., 2014). However, unlike VPD, VCD shows negligible conversion to its corresponding free acid (valnoctic acid) in humans. VCD was originally marketed as an anxiolytic drug

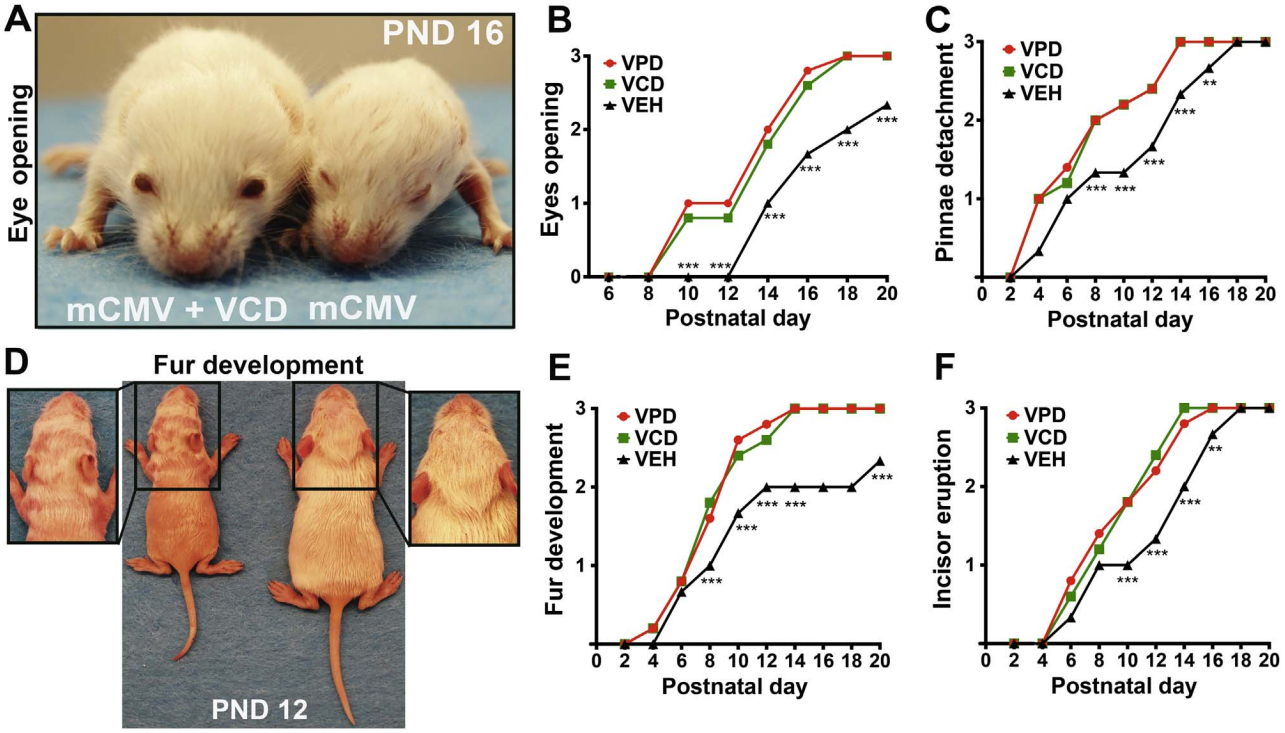

Fig. 5. Daily valpromide and valnoctamide administration ameliorates postnatal somatic development. (A–F) Graphs show progressive improvement of multiple parameters of postnatal growth. Mean ± SEM; error bars not shown for clarity. N = 6–9 mice/group; mixed-model ANOVA (Newman Keuls test) for VPD and VCD versus VEH; $^{**}p < 0.01$, $^{***}p < 0.001$. Photos show the differential status of eye opening (A) and the delayed development of fur in an infected/untreated pup (left) compared to an infected newborn treated with VCD (right) (D); marked difference in growth is also evident.

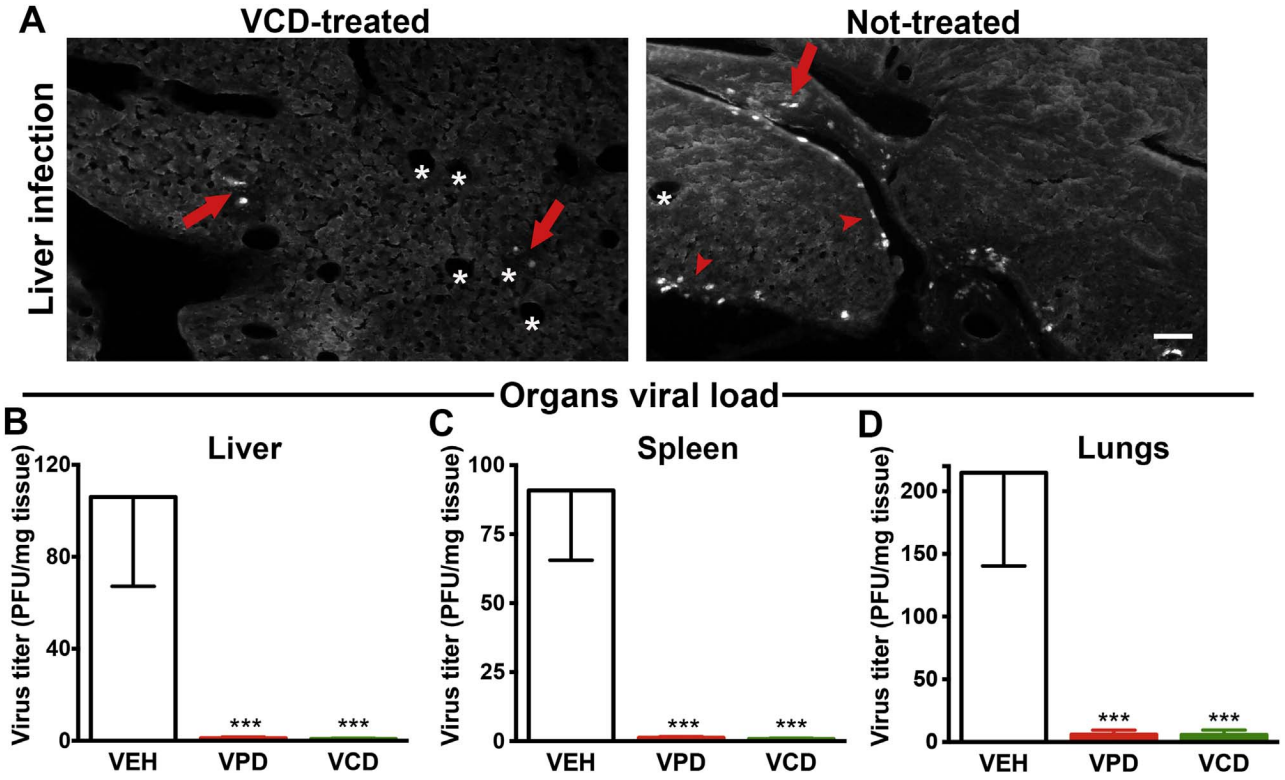

Fig. 6. Valpromide and valnoctamide substantially decrease CMV load in target organs. (A) A small number of cells show CMV infection in the liver of PND 12 mice infected on DOB and treated daily with VCD until PND 10 (left); in contrast, a higher number was commonly found in the liver of pups receiving vehicle (right). GFP-positive cells are localized both in the parenchyma (arrows) and in the sub-peritoneal area (arrowheads). Asterisks indicate lobule central veins. Scale 100 μm. (B–D) Infected newborns treated with VPD, VCD, or VEH from PND 1-10, were euthanized at PND 12, and tissue samples from liver, spleen, and lungs were collected for measurement of viral titer by plaque assay. Bar graphs show titers as PFU/mg of tissue; mean ± SEM; N = 6 mice/group; $^{***}p < 0.001$, one-way ANOVA, Bonferroni's post-hoc test.

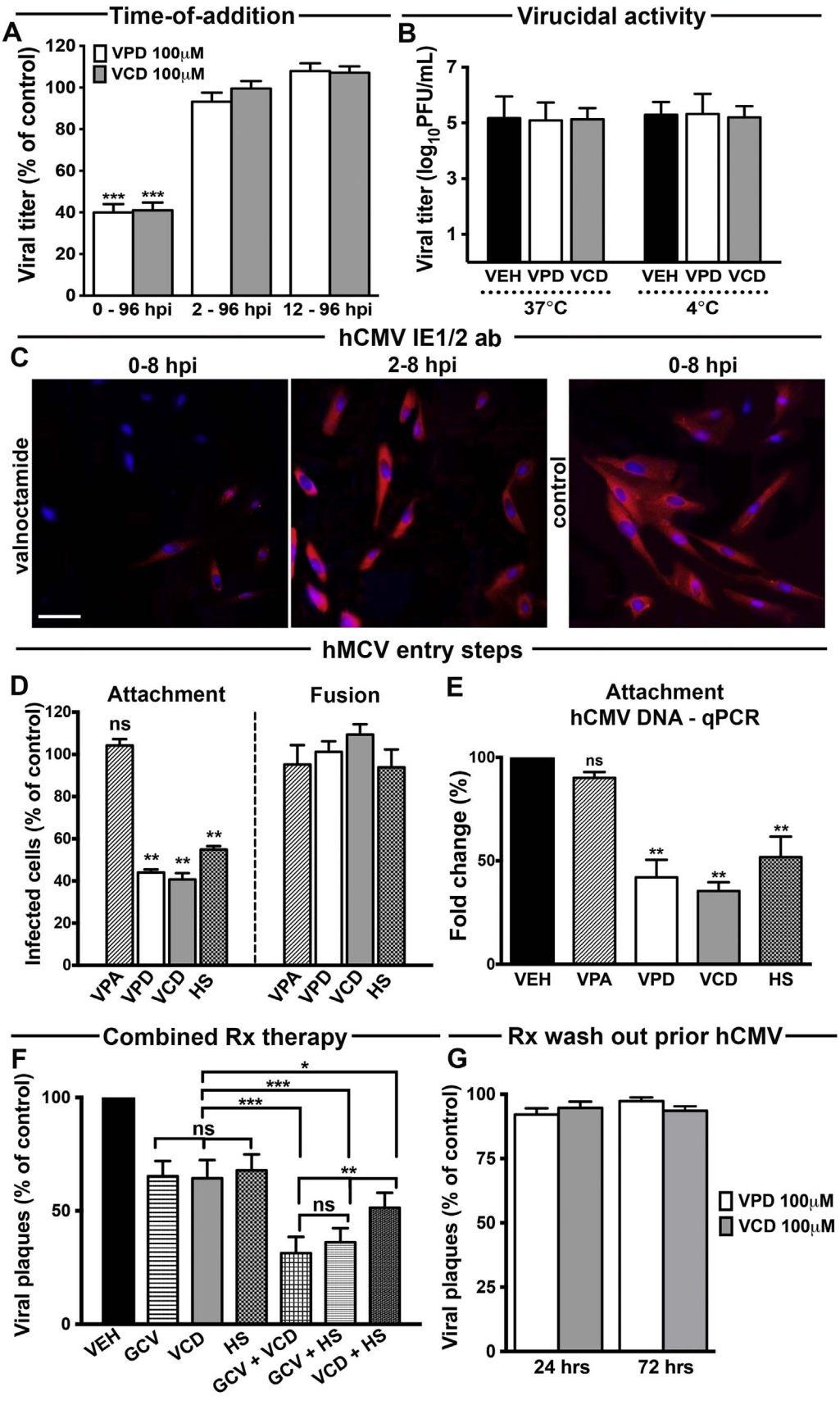
Time-of-addition
A
Viral titer (% of control)
VPD 100μM
VCD 100μM
0 - 96 hpi
2 - 96 hpi
12 - 96 hpi
Virucidal activity
B
Viral titer (log10PFU/mL)
VEH VPD VCD
VEH VPD VCD
37°C
4°C
hCMV IE1/2 ab
C
0-8 hpi
2-8 hpi
0-8 hpi
valnoctamide
control
hMCV entry steps
D
Attachment
Fusion
Infected cells (% of control)
ns
VPA VPD VCD HS
E
Attachment
hCMV DNA - qPCR
Fold change (%)
VEH VPA VPD VCD HS
Combined Rx therapy
F
Viral plaques (% of control)
VEH GCV VCD HS GCV + VCD GCV + HS VCD + HS
Rx wash out prior hCMV
G
Viral plaques (% of control)
24 hrs
72 hrs
VPD 100μM
VCD 100μM

(Nirvanil®) in several European countries in the 1960s and recently investigated as therapeutic agent for seizure disorders and acute mania in humans (Bialer et al., 1990, 2015; Stepansky, 1960; Barel et al., 1997; Bersudsky et al., 2010). In contrast to VPA, a number of animal studies have shown no embryotoxicity or teratogenic activity of VCD (Radatz et al., 1998; Shekh-Ahmad et al., 2014; Mawasi et al., 2015; Wlodarczyk et al., 2015). Further confirmation of VCD's safety profile is demonstrated from both preclinical and clinical studies examining its anti-convulsant and mood stabilizing actions (Bialer et al., 1990, 2015; Winkler et al., 2005; Shekh-Ahmad et al., 2015; Barel et al., 1997; Bersudsky et al., 2010). Therefore, we tested VCD on mCMV and hCMV in vitro.

VCD induced a substantial inhibition of mCMV infection independent of cell type or virus titer (Fig. 3B–F), as measured by counting cells expressing the GFP virus reporter or assessing virus replication. Significant anti-CMV activity was still identified in the nanomolar range. The plaque reduction assay showed a robust dose-dependent inhibition of mCMV infectivity, with an EC_{50} concentration of 9.3 ± 3.5 μM (Fig. 3G). Similar to VPD, VCD at 1 and 10 mM displayed no cytotoxic effect in uninfected NIH/3T3 cells (Fig. 3H), thus defining a SI > 1000 for mCMV.

VCD also blocked infectivity and replication of hCMV at low and high titer in human fibroblasts (Fig. 3I–L), and dose-response analysis revealed an EC_{50} of 3.5 ± 1.1 μM (Fig. 3M). Again, no cytotoxicity was evident in uninfected human fibroblasts exposed to 1 and 10 mM VCD, thus conferring the drug a SI > 2800 for hCMV.

3.3. Dose-response analysis of known antiviral compounds by plaque reduction assay

The antiviral properties of well-known inhibitors of CMV infection, GCV and heparan sulfate (HS), were assessed for comparative purposes in a dose-escalation analysis by plaque reduction assay in HDF cells infected with hCMV (MOI 0.01), as performed for VPD and VCD.

GCV targets viral DNA polymerase and is approved for CMV treatment in humans (Mercorelli et al., 2011). HS acts as a soluble mimic of heparan sulfate proteoglycans (HSPGs), cell surface anionic polysaccharides used by CMV for attachment to the cell (Compton et al., 1993). HS is not an approved anti-CMV drug due to its strong anticoagulant activity in vivo, an undesired side-effect.

Human CMV infectivity was inhibited by both GCV and HS in a dose-dependent manner with EC_{50} of 1.1 ± 0.3 μM for GCV (Fig. 3N) and 51.4 ± 8.2 μg/mL (~80 μM) for HS (Fig. 3O).

3.4. Valpromide and valnoctamide substantially attenuate CMV-related disease in vivo

Perinatal hCMV infection can cause serious and potentially fatal disease in neonates (Mocarski et al., 2007), in whom therapeutic options are severely limited by the toxicity and carcinogenicity of available antiviral drugs (Mercorelli et al., 2011).

Prior to testing anti-CMV efficacy, we evaluated drug safety with daily administration of both compounds in control, uninfected developing mice. No adverse effects on survival (data not shown) or postnatal body growth (Fig. 4A) were detected.

Inasmuch as the drugs appeared safe in developing mice, we next assessed VPD and VCD in a mouse model of severe perinatal mCMV infection (Fig. 4B) (Slavuljica et al., 2015). VPD and VCD treatment induced substantial improvement in infected newborns health, with a three-fold decrease in death rate (Fig. 4C). Survival of mCMV-infected, untreated pups was 23%, compared to 72% for VPD- or VCD-treated mice. Additional benefits of drug treatment were also identified. VPD and VCD administration ameliorated the mCMV-induced detrimental effects on body growth as assessed by body weight, body length, and tail length (Fig. 4D–G); infected mice weighed nearly 50% less than control mice at postnatal day 20 ($p < 0.001$), whereas VPD- or VCD-treated infected pups showed a body weight reduction of only 18% (Fig. 4E). Thus, both VPD and VCD attenuated the deficient body growth induced by perinatal mCMV infection. Both drugs markedly improved other parameters of somatic development, including eyelid opening, pinnae detachment, fur maturation, and incisor eruption (Fig. 5A–F). Of note, VPD and VCD generated a significant ($p < 0.01$) improvement in CMV-infected neonate health as early as 5 days after initiation of treatment.

After intraperitoneal inoculation, CMV infection spreads to several organs, including liver, spleen, and lungs. To investigate whether the beneficial effects observed in the infected pups were related to the ability of VPD and VCD to decrease CMV levels, we analyzed these organs from infected mice at 12 dpi by viral plaque assay (Fig. 6A–D). CMV titers were decreased by greater than 2 logs in all tested tissues of drug-treated infected newborns, thus suggesting that the VPD- and VCD-mediated inhibitory effects on CMV infection observed in vitro also occur in vivo and lead to a substantial improvement in CMV-infected animal outcome.

3.5. Valpromide and valnoctamide suppress CMV by inhibiting virus attachment to the cell

Despite being used for decades to treat neurological dysfunctions, the mechanism(s) of action of VPD and VCD in the brain remain unclear (Monti et al., 2009; Bialer et al., 2015; Spampanato and Dudek, 2014). VPA-mediated inhibition of HDAC enhances infection by hCMV (Kuntz-Simon and Obert, 1995; Michaelis et al., 2004, 2005). Both VPD and VCD lack this epigenetic activity (Okada et al., 2004; Fujiki et al., 2013).

To gain insight into the underlying mechanisms of VPD and VCD inhibition of CMV, we tested the drugs by addition at different time-points during the course of hCMV infection (Fig. 7A). The drug concentration employed for testing was 100 μM, which is below the therapeutic range for safely treating mood disorders and epilepsy in humans (Brodie and Dichter, 1996; Pisani et al., 1986, 1981; Matalon et al., 2011; Bialer et al., 2015; Shekh-Ahmad et al., 2014; Barel et al., 1997; Bersudsky et al., 2010; Spampanato and Dudek, 2014; Witvrouw et al., 1997). When the compounds were present from the time of viral challenge through 96 hpi, viral

Fig. 7. Valpromide and valnoctamide inhibit hCMV attachment to cell. (A). HDF cells infected with hCMV-GFP (MOI 0.01) (t=0) were exposed to VPD, VCD, or vehicle (100 μM) simultaneously, or 2 or 12 h after virus inoculation until media collection at 96 hpi. Viral replication assessed by titer determination using a plaque assay on HDF monolayers. (B) A drug (100 μM)/undiluted hCMV mixture was incubated for 2 h at 37 °C or 4 °C. Before cell inoculation, the solution was diluted to 10 nM (ineffective drug concentration). (C) Human fibroblasts infected with hCMV (MOI 0.01) and treated with the compounds (100 μM) starting from viral challenge (t=0) or 2 hpi, were fixed and permeabilized at 8 hpi for immunofluorescence with anti-IE1/2 monoclonal antibody and DAPI staining. Scale bar 100 μm. (D and E) Attachment and fusion assays were performed as described in Materials and Methods. GFP-positive cells were counted at 72 hpi (D). Results presented as the fold change ($2^{-\Delta\Delta CT}$) of hCMV DNA in each experimental condition relative to vehicle (mean ± SEM of 2 biological replicates) (E). (F) Plaque reduction assay on HDF cells exposed to vehicle, GCV (100 nM), VCD (1 μM), HS (25 μg/mL to 40 μM), or a combination of these compounds as indicated for 24 h before hCMV inoculation (MOI 0.01). Fluorescent plaques counted at 7 dpi. The mean plaque counts for each drug were expressed as a percentage of the control (vehicle) mean plaque count, defined as 100%; $p < 0.001$ for VEH vs GCV, VCD, and HS. Rx, drug. (G) After 24 h- or 72 h-VPD, VCD, or vehicle pre-treatment (100 μM), cultures were rinsed three times and given drug-free media prior to hCMV inoculation (MOI 0.01). Plaques counted at 7 dpi. Bars: mean ± SEM of 5 (F and G), 8 (A and B), and 12 cultures (D); ns, not significant, $^{*}p < 0.05$, $^{**}p < 0.01$, $^{***}p < 0.001$, one-way ANOVA with Bonferroni's post-hoc test.

yield decreased 60%. A similar inhibition of hCMV replication was also observed with 2 h drug exposure at the time of viral challenge, followed by drug wash out (data not shown). However, no reduction in viral yield was identified when the compounds were added 2–12 h after virus inoculation (Fig. 7A).

These results indicate that the block of hCMV mediated by VPD and VCD is exerted early in the infection process, within the first 2 h of the replication cycle. We therefore tested the possibility that these agents directly inactivate virions by pre-incubating the compounds with an undiluted stock of hCMV prior to cell inoculation. When the inhibitors were subsequently diluted below an effective concentration prior to culture inoculation, no direct inactivation of free virions was observed, as determined by the absence of a drug-mediated inhibitory effect (Fig. 7B). Similar results were obtained when the pre-incubation mix was run through a 100 nm pore size filter to remove the compounds but not the virus, prior to analysis of virus infectivity at physiological and cold temperatures (percentages show hCMV viral titers in drug-treated samples as compared to vehicle: 37 °C, 98.5 ± 8% for VPD, 99.3% ± 5% for VCD; 4 °C, 100.6% ± 5% for VPD, 98.3% ± 8% for VCD).

The IE1/2 CMV promoter is active in the first few hours of CMV infection, inducing IE protein expression which in turn promotes viral replication (Mocarski et al., 2007); we investigated whether the drugs interfere with the activity of this promoter by testing a plasmid with CMV IE1/2 driving tdTomato expression. No decrease in the number of red cells was identified in the presence of VPD compared to control (96% ± 4%) after plasmid transfection, suggesting VPD does not inhibit the activity of the CMV IE1/2 promoter. In addition, we assessed IE1/2 antigen expression in hCMV infected cells exposed to the compounds either simultaneously or 2 h after viral challenge (Fig. 7C). Substantial IE1/2 was detected in fibroblasts that received vehicle or drugs after 2 hpi. In contrast, cells treated with the compounds at the time of CMV inoculation showed markedly decreased IE1/2 expression, thus suggesting that CMV inhibition by VPD and VCD occurs prior to the IE stages of the viral replication cycle.

We next examined CMV entry into the cell, which precedes IE protein expression and can be separated into two phases: (1) attachment of the viral particle to the cell surface and (2) fusion of the viral envelope with cellular membranes and penetration into the cytoplasmic space (Mocarski et al., 2007). Investigation of these phases by a 2 h incubation at 4 °C (a temperature that allows attachment but not fusion) followed by a temperature shift to 37 °C (which allows fusion) (Chan and Yurochko, 2014) and subsequent infectivity assessment by GFP-positive cell counting, showed VPD- and VCD-mediated interference with hCMV attachment to the cell (Fig. 7D). These results were confirmed by qPCR with quantification of the relative amount of hCMV DNA in infected human fibroblasts exposed to the compounds at 4 °C (Fig. 7E). In these assays, heparan sulfate was employed as a positive control given its ability to block CMV attachment in vitro by mimicking HSPGs (Compton et al., 1993).

Current approved anti-CMV compounds target viral DNA synthesis (GCV, foscarnet, cidofovir) or the hCMV major IE gene locus (fomivirsen). Since our data indicate that VPD and VCD may block a different, earlier step of CMV infection, similar to HS, we postulated that a combined administration of GCV with VCD or HS might induce a stronger viral inhibition than single drug therapy or VCD/HS association (Fig. 7F). When cells were exposed to both GCV+VCD or GCV+HS, the decrease in hCMV plaques nearly doubled compared to single drug treatment. In contrast, combination of VCD+HS only slightly increased the viral inhibition obtained with one compound, supporting the hypothesis that VPD, VCD, and HS may act on the same step of CMV infection.

Finally, prolonged cell exposure to VPD and VCD followed by drug wash out immediately before CMV inoculation resulted in no attenuation of infection (Fig. 7G), consistent with the view that the drugs did not exert persistent effects on antiviral cellular targets, such as enhancement of innate immunity. These data also suggest that the anti-CMV actions of VPD and VCD are not the result of an irreversible association of the compounds with cell surface proteins.

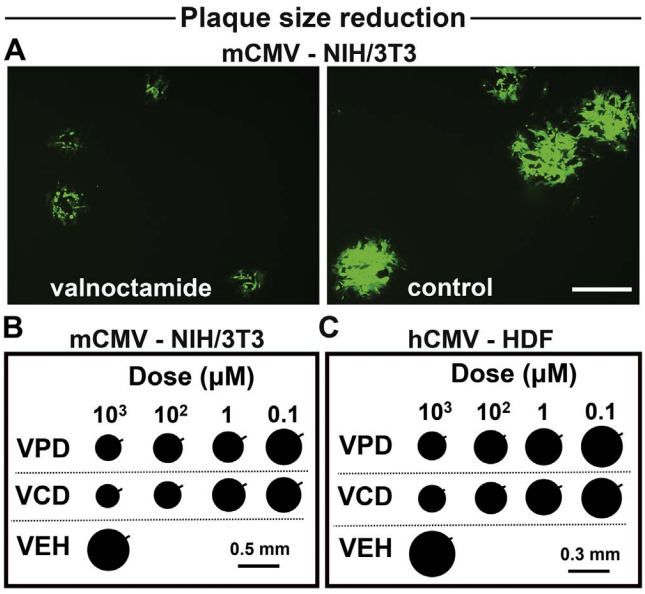

Fig. 8. Valpromide and valnoctamide effectively decrease spread of CMV infection. (A–C) Plaque size assay of NIH/3T3 cells (A and B) and human fibroblasts (C) infected with mCMV-GFP and hCMV-GFP (MOI 1) and treated with VPD, VCD, or vehicle. Viral plaque size measured 5 (mCMV) and 10 (hCMV) dpi. Representative plaques in 100 μM VCD (left) or vehicle (right); scale 300 μm (A). Mean diameter of 60 random plaques; SEM, bar on upper right side (B and C); $p < 0.05$ in 0.1 μM, $p < 0.01$ in 1 μM, $p < 0.001$ in 100 μM and 1 mM, versus vehicle.

3.6. *Valpromide and valnoctamide decrease spread of CMV infection*

Inhibition of CMV attachment to the target cell may play a role not only in the initiation of infection but also on virus spread. Murine and human fibroblast cells were exposed to the drugs after CMV inoculation and adsorption, and assessed for viral plaque size at 5 (mCMV) and 10 (hCMV) dpi. Both VPD and VCD effectively decreased spread of the CMV infection as shown by the reduced plaque size in CMV-infected drug-treated monolayers compared with the plaque size from vehicle-treated cultures (Fig. 8A–C).

4. Discussion

Human CMV is an important pathogen responsible for potentially life-threatening disease and severe complications, including pneumonitis, retinitis, encephalitis, and myocarditis in immunocompromised patients and neonatal children. Congenital CMV is the major infectious cause of birth defects and neuro-developmental disabilities, including microcephaly, hearing loss, blindness, and mental retardation (Cheeran et al., 2009; Mocarski et al., 2007; Tsutsui, 2009; Mercorelli et al., 2011).

Current anti-CMV compounds are partially effective, but are limited by poor oral bioavailability, short- and long-term toxicity, carcinogenicity, and teratogenicity (Mercorelli et al., 2011). The emergence of CMV strains resistant to the available drugs also poses significant challenges. Thus, there is a need for novel anti-CMV molecules with a safe in vivo profile utilizing alternative mechanisms of action. This is particularly relevant to CMV infections during early development.

Our work shows that VPD and VCD, two orally available drugs used for many years to treat neurological disorders, evoke an unexpected, substantial, and specific inhibition of both mouse and human CMV in vitro and in a mouse model of perinatal infection. The anti-CMV activity of these compounds has never been described.

The VPD- and VCD-mediated antiviral effect is substantiated by multiple converging lines of evidence including reduction in infected cell number, as determined with GFP reporter expression, immunocytochemistry against hCMV gB, and qPCR, reduction in cell death quantified with ethidium homodimer, reduction in virus plaque number and size, and reduction in viral replication and virion release. Importantly, both compounds showed efficacy in blocking CMV infection in vivo, leading to increased survival, improved body weight, reduced CMV-related disease, and decreased viral load in target organs of infected neonates. Furthermore, drug administration to uninfected newborn mice evoked no adverse response.

We detected relatively little cell death even at the highest concentrations of VPD and VCD as tested with the ethidium homodimer assay; we did not study the effects of the drugs on cell metabolism. VPD and VCD inhibited CMV at drug concentrations already safely employed in the clinic for anti-convulsant and mood stabilizing purposes (roughly 0.2–0.7 mM), and, more importantly, at lower drug concentrations ($\leq 100\ \mu M$) which lack neurological and psychiatric effects (Brodie and Dichter, 1996; Pisani et al., 1986, 1981; Matalon et al., 2011; Bialer et al., 2015; Shekh-Ahmad et al., 2014; Barel et al., 1997; Bersudsky et al., 2010; Spampanato and Dudek, 2014; Witvrouw et al., 1997). Thus, a safe and effective anti-CMV activity of these compounds in humans seems plausible.

Currently approved anti-CMV drugs target hCMV IE gene expression or DNA replication (Mercorelli et al., 2011). In contrast, VPD and VCD appear to act on an earlier stage of CMV infection by interfering with viral attachment to cell surface HSPGs. The initial tethering of CMV virions to HSPGs, mediated by the viral glycoproteins gB and gM/gN, functions to stabilize the virus at the cell surface until engagement of secondary receptors occurs allowing fusion and penetration (Mocarski et al., 2007; Isaacson and Compton, 2009). The VPD and VCD drug-mediated inhibition of hCMV attachment may be due to a reversible interaction with either HSPGs or free virions or may require the simultaneous presence of both the virus and the cell.

Dose-response relationship analyses revealed that GCV, currently a first-line therapy for hCMV, is a more potent compound than VPD and VCD in vitro. Thus, a less effective anti-CMV activity of VPD and VCD compared to GCV might be expected in vivo. However, given the increasing emergence of drug-resistant strains of hCMV and the potential toxicity related to long-term therapy with GCV, compounds with an alternative mechanism of action merit consideration for anti-CMV clinical trials. We show that VCD used together with GCV generates an additive effect in blocking CMV; the combination of the two drug types acting by different mechanisms of inhibition may also constitute a fertile ground for clinical consideration.

5. Conclusions

We examined two drugs, VPD and VCD, which show unexpected anti-CMV properties. In humans, VPD can be metabolized to the teratogenic and CMV-enhancing VPA (Bialer, 1991), and therefore would not be an ideal drug candidate in the clinic, particularly in the treatment of pregnant mothers and their fetuses. VCD lacks embryotoxic and teratogenic actions (Bialer et al., 1990, 2015; Shekh-Ahmad et al., 2014), and in contrast to VPD shows minimal conversion to its corresponding free acid in humans (Bialer et al., 1990). Therefore, VCD may merit consideration as a potential mode of treatment to reduce the severity of problems caused by CMV infection in conditions of reduced systemic immunity. Furthermore, there is a need for anti-CMV drugs that are safe and effective in the treatment of CMV in fetuses and neonates, and VCD merits further consideration in this regard. The fact that VCD is already approved for the treatment of neurological and psychiatric disorders in humans should greatly reduce the typically long period required to bring a new antiviral drug into use.

Conflict of interest statement

None.

Acknowledgments

We thank Yang Yang for technical help, Zhonghua Tang and Seth Guller for help with the qPCR experiment, and Justin Paglino for comments on the manuscript. This work was supported by funds from Amalia Griffini Scholarship (S.O.), rEVO Biologics (M.J. P.), and National Institutes of Health RO1 CA188359, CA175577, CA161048, and NS79274 (A.v.d. P). Funding sources had no involvement in study design; collection, analysis and interpretation of data; writing of the report; and decision to submit the article for publication.

References

Barel, S., Yagen, B., Schurig, V., Soback, S., Pisani, F., Perucca, E., et al., 1997. Stereoselective pharmacokinetic analysis of valnoctamide in healthy subjects and in patients with epilepsy. Clin. Pharmacol. Ther. 61 (4), 442–449. http://dx.doi.org/10.1016/s0009-9236(97)90194-6 (PubMed PMID: 9129561).

Bersudsky, Y., Applebaum, J., Gaiduk, Y., Sharony, L., Mishory, A., Podberezsky, A., et al., 2010. Valnoctamide as a valproate substitute with low teratogenic potential in mania: a double-blind, controlled, add-on clinical trial. Bipolar Disord. 12 (4), 376–382. http://dx.doi.org/10.1111/j.1399-5618.2010.00828.x (PubMed PMID: 20636634).

Bialer, M., 1991. Clinical pharmacology of valpromide. Clin. Pharmacokinet. 20 (2), 114–122. http://dx.doi.org/10.2165/00003088-199120020-00003 (PubMed PMID: 2029804).

Bialer, M., Haj-Yehia, A., Barzaghi, N., Pisani, F., Perucca, E., 1990. Pharmacokinetics of a valpromide isomer, valnoctamide, in healthy subjects. Eur. J. Clin. Pharmacol. 38 (3), 289–291 (Epub 1990/01/01. PubMed PMID: 2111246).

Bialer, M., Johannessen, S.I., Levy, R.H., Perucca, E., Tomson, T., White, H.S., 2015. Progress report on new antiepileptic drugs: a summary of the Twelfth Eilat Conference (EILAT XII). Epilepsy Res. 111, 85–141. http://dx.doi.org/10.1016/j.eplepsyres.2015.01.001 (PubMed PMID: 25769377).

Brodie, M.J., Dichter, M.A., 1996. Antiepileptic drugs. N. Engl. J. Med. 334 (3), 168–175. http://dx.doi.org/10.1056/nejm199601183340308 (PubMed PMID: 8531974).

Brune, W., Hengel, H., Koszinowski U.H., 2001. A mouse model for cytomegalovirus infection. In: Coligan, John E., et al. (Eds.), Current Protocols in Immunology. Chapter 19: Unit 19.7. Epub 2008/04/25. ⟨http://dx.doi.org/10.1002/0471142735.im1907s43⟩. (PubMed PMID: 18432758).

Chan, G.C., Yurochko, A.D., 2014. Analysis of cytomegalovirus binding/entry-mediated events. Methods Mol. Biol. 1119, 113–121. http://dx.doi.org/10.1007/978-1-62703-788-4_8 (PubMed PMID: 24639221).

Cheeran, M.C., Lokensgard, J.R., Schleiss, M.R., 2009. Neuropathogenesis of congenital cytomegalovirus infection: disease mechanisms and prospects for intervention. Clin. Microbiol. Rev. 22 (1), 99–126. http://dx.doi.org/10.1128/cmr.00023-08 (PubMed PMID: 19136436; PubMed Central PMCID: PMCPMC2620634).

Compton, T., Nowlin, D.M., Cooper, N.R., 1993. Initiation of human cytomegalovirus infection requires initial interaction with cell surface heparan sulfate. Virology 193 (2), 834–841. http://dx.doi.org/10.1006/viro.1993.1192 (PubMed PMID: 8384757).

Fujiki, R., Sato, A., Fujitani, M., Yamashita, T., 2013. A proapoptotic effect of valproic acid on progenitors of embryonic stem cell-derived glutamatergic neurons. Cell Death Dis. 4, e677. http://dx.doi.org/10.1038/cddis.2013.205 (PubMed PMID: 23788034; PubMed Central PMCID: PMCPMC3702299).

Fukui, Y., Shindoh, K., Yamamoto, Y., Koyano, S., Kosugi, I., Yamaguchi, T., et al., 2008. Establishment of a cell-based assay for screening of compounds inhibiting very

early events in the cytomegalovirus replication cycle and characterization of a compound identified using the assay. Antimicrob. Agents Chemother. 52 (7), 2420–2427. http://dx.doi.org/10.1128/aac.00134-08 (PubMed PMID: 18458124; PubMed Central PMCID: PMCPMC2443885).
Gandhi, M.K., Khanna, R., 2004. Human cytomegalovirus: clinical aspects, immune regulation, and emerging treatments. Lancet Infect. Dis. 4 (12), 725–738. http://dx.doi.org/10.1016/s1473-3099(04)01202-2 (PubMed PMID: 1556712).
Gault, E., Michel, Y., Dehee, A., Belabani, C., Nicolas, J.C., Garbarg-Chenon, A., 2001. Quantification of human cytomegalovirus DNA by real-time PCR. J. Clin. Microbiol. 39 (2), 772–775. http://dx.doi.org/10.1128/jcm.39.2.772-775.2001 (PubMed PMID: 11158149; PubMed Central PMCID: PMCPMC87818).
Gorres, K.L., Daigle, D., Mohanram, S., McInerney, G.E., Lyons, D.E., Miller, G., 2016. Valpromide inhibits lytic cycle reactivation of epstein-barr virus. mBio 7 (2). http://dx.doi.org/10.1128/mBio.00113-16 (PubMed PMID: 26933051; PubMed Central PMCID: PMCPMC4810481).
Guerrini, R., 2006. Valproate as a mainstay of therapy for pediatric epilepsy. Paediatr. drugs 8 (2), 113–129 (Epub 2006/04/13. PubMed PMID: 16608372).
Isaacson, M.K., Compton, T., 2009. Human cytomegalovirus glycoprotein B is required for virus entry and cell-to-cell spread but not for virion attachment, assembly, or egress. J. Virol. 83 (8), 3891–3903. http://dx.doi.org/10.1128/jvi.01251-08 (PubMed PMID: 19193805; PubMed Central PMCID: PMCPMC2663263).
Jarvis, M.A., Wang, C.E., Meyers, H.L., Smith, P.P., Corless, C.L., Henderson, G.J., et al., 1999. Human cytomegalovirus infection of caco-2 cells occurs at the basolateral membrane and is differentiation state dependent. J. Virol. 73 (6), 4552–4560 (Epub 1999/05/11. PubMed PMID: 10233913; PubMed Central PMCID: PMCPMC112495).
Jennings, H.R., Romanelli, F., 2000. Comment: potential risk of valproic acid therapy in patients who are HIV-positive. Ann. Pharmacother. 34 (11), 1348–1349 (Epub 2000/12/01. PubMed PMID: 11098354).
Kataoka, S., Takuma, K., Hara, Y., Maeda, Y., Ago, Y., Matsuda, T., 2013. Autism-like behaviours with transient histone hyperacetylation in mice treated prenatally with valproic acid. Int. J. Neuropsychopharmacol. / Off. Sci. J. Coll. Int. Neuropsychopharmacol. (CINP) 16 (1), 91–103. http://dx.doi.org/10.1017/s1461145711001714 (PubMed PMID: 22093185).
Kuntz-Simon, G., Obert, G., 1995. Sodium valproate, an anticonvulsant drug, stimulates human cytomegalovirus replication. J. Gen. Virol. 76 (Pt 6), 1409–1415. http://dx.doi.org/10.1099/0022-1317-76-6-1409 (PubMed PMID: 7782769).
Mardivirin, L., Descamps, V., Lacroix, A., Delebassee, S., Ranger-Rogez, S., 2009. Early effects of drugs responsible for DRESS on HHV-6 replication in vitro. J. Clin. Virol.: Off. Publ. Pan Am. Soc. Clin. Virol. 46 (3), 300–302. http://dx.doi.org/10.1016/j.jcv.2009.08.006 (PubMed PMID: 19758840).
Matalon, S., Rasmussen, T.A., Dinarello, C.A., 2011. Histone deacetylase inhibitors for purging HIV-1 from the latent reservoir. Mol. Med. 17 (5–6), 466–472. http://dx.doi.org/10.2119/molmed.2011.00076 (PubMed PMID: 21424110; PubMed Central PMCID: PMCPMC3105138).
Mawasi, H., Shekh-Ahmad, T., Finnell, R.H., Wlodarczyk, B.J., Bialer, M., 2015. Pharmacodynamic and pharmacokinetic analysis of CNS-active constitutional isomers of valnoctamide and *sec*-butylpropylacetamide–amide derivatives of valproic acid. Epilepsy Behav.: EB 46, 72–78. http://dx.doi.org/10.1016/j.yebeh.2015.02.040 (PubMed PMID: 25863940).
Mercorelli, B., Lembo, D., Palu, G., Loregian, A., 2011. Early inhibitors of human cytomegalovirus: state-of-art and therapeutic perspectives. Pharmacol. Ther. 131 (3), 309–329. http://dx.doi.org/10.1016/j.pharmthera.2011.04.007 (PubMed PMID: 21570424).
Michaelis, M., Kohler, N., Reinisch, A., Eikel, D., Gravemann, U., Doerr, H.W., et al., 2004. Increased human cytomegalovirus replication in fibroblasts after treatment with therapeutical plasma concentrations of valproic acid. Biochem. Pharmacol. 68 (3), 531–538. http://dx.doi.org/10.1016/j.bcp.2004.04.013 (PubMed PMID: 15242819).
Michaelis, M., Suhan, T., Reinisch, A., Reisenauer, A., Fleckenstein, C., Eikel, D., et al., 2005. Increased replication of human cytomegalovirus in retinal pigment epithelial cells by valproic acid depends on histone deacetylase inhibition. Invest. Ophthalmol. Vis. Sci. 46 (9), 3451–3457. http://dx.doi.org/10.1167/iovs.05-0369 (PubMed PMID: 16123451).
Mocarski, E.S., Shenk, T., Pass, R.F., 2007. Cytomegaloviruses. In: Fields, B.N., Knipe, D.M., Howley, P.M. (Eds.), Fields Virology. 2. Lippincott, Williams & Wilkins, Philadelphia, PA, pp. 2702–2751.
Monti, B., Polazzi, E., Contestabile, A., 2009. Biochemical, molecular and epigenetic mechanisms of valproic acid neuroprotection. Curr. Mol. Pharmacol. 2 (1), 95–109 (Epub 2009/12/22. PubMed PMID: 20021450).
Moog, C., Kuntz-Simon, G., Caussin-Schwemling, C., Obert, G., 1996. Sodium valproate, an anticonvulsant drug, stimulates human immunodeficiency virus type 1 replication independently of glutathione levels. J. Gen. Virol. 77 (Pt 9), 1993–1999. http://dx.doi.org/10.1099/0022-1317-77-9-1993 (PubMed PMID: 8810995).
Nakashima, H., Kaufmann, J.K., Wang, P.Y., Nguyen, T., Speranza, M.C., Kasai, K., et al., 2015. Histone deacetylase 6 inhibition enhances oncolytic viral replication in glioma. J. Clin. Investig. 125 (11), 4269–4280. http://dx.doi.org/10.1172/jci80713 (PubMed PMID: 26524593; PubMed Central PMCID: PMCPMC4639993).
Nau, H., Hauck, R.S., Ehlers, K., 1991. Valproic acid-induced neural tube defects in mouse and human: aspects of chirality, alternative drug development, pharmacokinetics and possible mechanisms. Pharmacol. Toxicol. 69 (5), 310–321 (Epub 1991/11/01. PubMed PMID: 1803343).
Okada, A., Kurihara, H., Aoki, Y., Bialer, M., Fujiwara, M., 2004. Amidic modification of valproic acid reduces skeletal teratogenicity in mice. Birth Defects Res. Part B: Dev. Reprod. Toxicol. 71 (1), 47–53. http://dx.doi.org/10.1002/bdrb.10057 (PubMed PMID: 14991910).
Otsuki, A., Patel, A., Kasai, K., Suzuki, M., Kurozumi, K., Chiocca, E.A., et al., 2008. Histone deacetylase inhibitors augment antitumor efficacy of herpes-based oncolytic viruses. Mol. Ther.: J. Am. Soc. Gene Ther. 16 (9), 1546–1555. http://dx.doi.org/10.1038/mt.2008.155 (PubMed PMID: 18648350).
Paglino, J.C., van den Pol, A.N., 2011. Vesicular stomatitis virus has extensive oncolytic activity against human sarcomas: rare resistance is overcome by blocking interferon pathways. J. Virol. 85 (18), 9346–9358. http://dx.doi.org/10.1128/jvi.00723-11 (PubMed PMID: 21734048; PubMed Central PMCID: PMCPMC3165768).
Paradis, F.H., Hales, B.F., 2013. Exposure to valproic acid inhibits chondrogenesis and osteogenesis in mid-organogenesis mouse limbs. Toxicol. Sci.: Off. J. Soc. Toxicol. 131 (1), 234–241. http://dx.doi.org/10.1093/toxsci/kfs292 (PubMed PMID: 23042728; PubMed Central PMCID: PMCPMC3537135).
Perucca, E., 2002. Pharmacological and therapeutic properties of valproate: a summary after 35 years of clinical experience. CNS Drugs 16 (10), 695–714 (Epub 2002/09/25. PubMed PMID: 12269862).
Phiel, C.J., Zhang, F., Huang, E.Y., Guenther, M.G., Lazar, M.A., Klein, P.S., 2001. Histone deacetylase is a direct target of valproic acid, a potent anticonvulsant, mood stabilizer, and teratogen. J. Biol. Chem. 276 (39), 36734–36741. http://dx.doi.org/10.1074/jbc.M101287200 (PubMed PMID: 11473107).
Pisani, F., Fazio, A., Oteri, G., Di Perri, R., 1981. Dipropylacetic acid plasma levels; diurnal fluctuations during chronic treatment with dipropylacetamide. Ther. Drug Monit. 3 (3), 297–301 (Epub 1981/01/01. PubMed PMID: 6798719).
Pisani, F., Fazio, A., Oteri, G., Ruello, C., Gitto, C., Russo, F., et al., 1986. Sodium valproate and valpromide: differential interactions with carbamazepine in epileptic patients. Epilepsia 27 (5), 548–552 (PubMed PMID: 3093212).
Radatz, M., Ehlers, K., Yagen, B., Bialer, M., Nau, H., 1998. Valnoctamide, valpromide and valnoctic acid are much less teratogenic in mice than valproic acid. Epilepsy Res. 30 (1), 41–48 (Epub 1998/04/29. PubMed PMID: 9551843).
Ramsburg, E., Publicover, J., Buonocore, L., Poholek, A., Robek, M., Palin, A., et al., 2005. A vesicular stomatitis virus recombinant expressing granulocyte-macrophage colony-stimulating factor induces enhanced T-cell responses and is highly attenuated for replication in animals. J. Virol. 79 (24), 15043–15053. http://dx.doi.org/10.1128/jvi.79.24.15043-15053.2005 (PubMed PMID: 16306575; PubMed Central PMCID: PMCPMC1316007).
Scattoni, M.L., Gandhy, S.U., Ricceri, L., Crawley, J.N., 2008. Unusual repertoire of vocalizations in the BTBR T+tf/J mouse model of autism. PloS One 3 (8), e3067. http://dx.doi.org/10.1371/journal.pone.0003067 (PubMed PMID: 18728777; PubMed Central PMCID: PMCPMC2516927).
Shaw, R.N., Arbiser, J.L., Offermann, M.K., 2000. Valproic acid induces human herpesvirus 8 lytic gene expression in BCBL-1 cells. AIDS 14 (7), 899–902 (Epub 2000/06/06. PubMed PMID: 10839602).
Shekh-Ahmad, T., Mawasi, H., McDonough, J.H., Yagen, B., Bialer, M., 2015. The potential of *sec*-butylpropylacetamide (SPD) and valnoctamide and their individual stereoisomers in status epilepticus. Epilepsy Behav.: EB 49, 298–302. http://dx.doi.org/10.1016/j.yebeh.2015.04.012 (PubMed PMID: 25979572).
Shekh-Ahmad, T., Hen, N., Yagen, B., McDonough, J.H., Finnell, R.H., Wlodarczyk, B.J., et al., 2014. Stereoselective anticonvulsant and pharmacokinetic analysis of valnoctamide, a CNS-active derivative of valproic acid with low teratogenic potential. Epilepsia 55 (2), 353–361. http://dx.doi.org/10.1111/epi.12480 (PubMed PMID: 24313671).
Slavuljica, I., Kvestak, D., Huszthy, P.C., Kosmac, K., Britt, W.J., Jonjic, S., 2015. Immunobiology of congenital cytomegalovirus infection of the central nervous system-the murine cytomegalovirus model. Cell. Mol. Immunol. 12 (2), 180–191. http://dx.doi.org/10.1038/cmi.2014.51 (PubMed PMID: 25042632; PubMed Central PMCID: PMCPMC4654296).
Spampanato, J., Dudek, F.E., 2014. Valnoctamide enhances phasic inhibition: a potential target mechanism for the treatment of benzodiazepine-refractory status epilepticus. Epilepsia 55 (9), e94–e98. http://dx.doi.org/10.1111/epi.12702 (PubMed PMID: 24995528; PubMed Central PMCID: PMCPMC4167227).
Stepansky, W., 1960. A clinical study in the use of valmethamide, an anxiety-reducing drug. Curr. Ther. Res., Clin. Exp. 2, 144–147 (PubMed PMID: 13834349).
Tsutsui, Y., 2009. Effects of cytomegalovirus infection on embryogenesis and brain development. Congenit. Anom. 49 (2), 47–55. http://dx.doi.org/10.1111/j.1741-4520.2009.00222.x (PubMed PMID: 19489954).
Tung, E.W., Winn, L.M., 2010. Epigenetic modifications in valproic acid-induced teratogenesis. Toxicol. Appl. Pharmacol. 248 (3), 201–209. http://dx.doi.org/10.1016/j.taap.2010.08.001 (PubMed PMID: 20705080).
van den Pol, A.N., Dalton, K.P., Rose, J.K., 2002. Relative neurotropism of a recombinant rhabdovirus expressing a green fluorescent envelope glycoprotein. J. Virol. 76 (3), 1309–1327 (Epub 2002/01/05. PubMed PMID: 11773406; PubMed Central PMCID: PMCPMC135838).
van den Pol, A.N., Mocarski, E., Saederup, N., Vieira, J., Meier, T.J., 1999. Cytomegalovirus cell tropism, replication, and gene transfer in brain. J. Neurosci.: Off. J. Soc. Neurosci. 19 (24), 10948–10965 (Epub 1999/12/14. PubMed PMID: 10594076).
Varghese, F.S., Kaukinen, P., Glasker, S., Bespalov, M., Hanski, L., Wennerberg, K., et al., 2016. Discovery of berberine, abamectin and ivermectin as antivirals against chikungunya and other alphaviruses. Antivir. Res. 126, 117–124. http://dx.doi.org/10.1016/j.antiviral.2015.12.012 (PubMed PMID: 26752081).
Vieira, J., Schall, T.J., Corey, L., Geballe, A.P., 1998. Functional analysis of the human cytomegalovirus US28 gene by insertion mutagenesis with the green fluorescent protein gene. J. Virol. 72 (10), 8158–8165 (Epub 1998/09/12. PubMed

PMID: 9733857; PubMed Central PMCID: PMCPMC110158).
Winkler, I., Blotnik, S., Shimshoni, J., Yagen, B., Devor, M., Bialer, M., 2005. Efficacy of antiepileptic isomers of valproic acid and valpromide in a rat model of neuropathic pain. Br. J. Pharmacol. 146 (2), 198–208. http://dx.doi.org/10.1038/sj.bjp.0706310 (PubMed PMID: 15997234; PubMed Central PMCID: PMCPMC1576263).
Witvrouw, M., Schmit, J.C., Van Remoortel, B., Daelemans, D., Este, J.A., Vandamme, A.M., et al., 1997. Cell type-dependent effect of sodium valproate on human immunodeficiency virus type 1 replication in vitro. AIDS Res. Hum. Retrovir. 13 (2), 187–192. http://dx.doi.org/10.1089/aid.1997.13.187 (PubMed PMID: 9007204).
Wlodarczyk, B.J., Ogle, K., Lin, L.Y., Bialer, M., Finnell, R.H., 2015. Comparative teratogenicity analysis of valnoctamide, risperidone, and olanzapine in mice. Bipolar Disord. 17 (6), 615–625. http://dx.doi.org/10.1111/bdi.12325 (PubMed PMID: 26292082; PubMed Central PMCID: PMCPMC4631615).
Wollmann, G., Drokhlyansky, E., Davis, J.N., Cepko, C., van den Pol, A.N., 2015. Lassa-vesicular stomatitis chimeric virus safely destroys brain tumors. J. Virol. 89 (13), 6711–6724. http://dx.doi.org/10.1128/jvi.00709-15 (PubMed PMID: 25878115; PubMed Central PMCID: PMCPMC4468483).
Zurbach, K.A., Moghbeli, T., Snyder, C.M., 2014. Resolving the titer of murine cytomegalovirus by plaque assay using the M2-10B4 cell line and a low viscosity overlay. Virol. J. 11, 71. http://dx.doi.org/10.1186/1743-422x-11-71 (PubMed PMID: 24742045; PubMed Central PMCID: PMCPMC4006460).

Neurobiology of Disease

Valnoctamide Inhibits Cytomegalovirus Infection in Developing Brain and Attenuates Neurobehavioral Dysfunctions and Brain Abnormalities

Sara Ornaghi,[1,2,3] Lawrence S. Hsieh,[1] Angélique Bordey,[1,4] Patrizia Vergani,[5] Michael J. Paidas,[2] and Anthony N. van den Pol[1]

[1]Department of Neurosurgery, and [2]Yale Women and Children's Center for Blood Disorders and Preeclampsia Advancement, Department of Obstetrics, Gynecology, and Reproductive Sciences, Yale University School of Medicine, New Haven, Connecticut, 06520, [3]Ph.D. Program in Neuroscience, School of Medicine and Surgery, University of Milan-Bicocca, Monza 20900, Italy, [4]Department of Neurosurgery, Xiangya Hospital, Central South University, Changsha 410008, People's Republic of China, and [5]Department of Obstetrics and Gynecology, Foundation MBBM, San Gerardo Hospital, Monza 20900, Italy

Cytomegalovirus (CMV) is the most common infectious cause of brain defects and neurological dysfunction in developing human babies. Due to the teratogenicity and toxicity of available CMV antiviral agents, treatment options during early development are markedly limited. Valnoctamide (VCD), a neuroactive mood stabilizer with no known teratogenic activity, was recently demonstrated to have anti-CMV potential. However, it is not known whether this can be translated into an efficacious therapeutic effect to improve CMV-induced adverse neurological outcomes. Using multiple models of CMV infection in the developing mouse brain, we show that subcutaneous low-dose VCD suppresses CMV by reducing the level of virus available for entry into the brain and by acting directly within the brain to block virus replication and dispersal. VCD during the first 3 weeks of life restored timely acquisition of neurological milestones in neonatal male and female mice and rescued long-term motor and behavioral outcomes in juvenile male mice. CMV-mediated brain defects, including decreased brain size, cerebellar hypoplasia, and neuronal loss, were substantially attenuated by VCD. No adverse side effects on neurodevelopment of uninfected control mice receiving VCD were detected. Treatment of CMV-infected human fetal astrocytes with VCD reduced both viral infectivity and replication by blocking viral particle attachment to the cell, a mechanism that differs from available anti-CMV drugs. These data suggest that VCD during critical periods of neurodevelopment can effectively suppress CMV replication in the brain and safely improve both immediate and long-term neurological outcomes.

Key words: brain; cytomegalovirus; development; dysfunction; infection

Significance Statement

Cytomegalovirus (CMV) can irreversibly damage the developing brain. No anti-CMV drugs are available for use during fetal development, and treatment during the neonatal period has substantial limitations. We studied the anti-CMV actions of valnoctamide (VCD), a psychiatric sedative that appears to lack teratogenicity and toxicity, in the newborn mouse brain, a developmental period that parallels that of an early second-trimester human fetus. In infected mice, subcutaneous VCD reaches the brain and suppresses viral replication within the CNS, rescuing the animals from CMV-induced brain defects and neurological problems. Treatment of uninfected control animals exerts no detectable adverse effects. VCD also blocks CMV replication in human fetal brain cells.

Introduction

Cytomegalovirus (CMV) infection of the developing brain can cause a number of brain defects, including microcephaly, cortical thinning, and cerebellar hypoplasia (Gandhi and Khanna, 2004; Mocarski et al., 2007; Cheeran et al., 2009; Tsutsui, 2009). In the United States, ~30,000 children receive diagnoses of CMV infection every year, and lifelong neurological problems, including cerebral palsy, seizures, motor impairment, intellectual disabil-

Received April 11, 2017; revised May 25, 2017; accepted May 31, 2017.

Author contributions: S.O. and A.N.v.d.P. designed research; S.O. and L.S.H. performed research; A.B., P.V., M.J.P., and A.N.v.d.P. contributed unpublished reagents/analytic tools; S.O. analyzed data; S.O. and A.N.v.d.P. wrote the paper.

This work was supported by funds from rEVO Biologics (M.J.P.) and National Institutes of Health Grants RO1-CA188359, CA-175577, CA-161048, and DK-103176 (A.N.v.d.P.). We thank John N. Davis for technical help and insightful discussions on motor and behavioral assays in adolescent mice, and Yang Yang for technical help in fluorescent staining.

The authors declare no competing financial interests.

Correspondence should be addressed to Anthony N. van den Pol, Department of Neurosurgery, Yale University School of Medicine, 333 Cedar Street, New Haven, CT 06520. E-mail: anthony.vandenpol@yale.edu.

DOI:10.1523/JNEUROSCI.0970-17.2017

 0270-6474/17/376877-17$15.00/0

ity, visual deficits, and deafness, will develop in one-fifth of these children. This makes CMV the most common severely disabling perinatal infectious agent (Kenneson and Cannon, 2007; James and Kimberlin, 2016). A link between perinatal CMV infection and autism spectrum disorder (ASD) in children and adolescents has also been proposed (Stubbs et al., 1984; Yamashita et al., 2003; Sakamoto et al., 2015; Garofoli et al., 2017). Another virus that has recently raised considerable concern, and that can evoke parallel dysfunction in the developing brain, is Zika virus; importantly, in the United States neurological dysfunction due to CMV infections is >100-fold more prevalent than that from Zika virus (Butler, 2016). CMV evokes more brain dysfunction than more widely known diseases, including spina bifida, fetal alcohol syndrome, or Down's syndrome (Cannon and Davis, 2005).

CMV can also generate problems in the CNS of adults with a compromised immune system, including transplant recipients and AIDS patients, who are at high risk for the development of potentially life-threatening CNS complications (Mocarski et al., 2007; Mercorelli et al., 2011). A key reason that CMV is particularly damaging to the developing brain relates to the reduced efficacy of the immature innate and systemic immune response to CMV in the immature CNS (van den Pol et al., 2002, 2007; Reuter et al., 2004).

Although drugs approved to treat CMV show some efficacy, their use is not recommended during pregnancy or in the neonatal period due to potential teratogenicity, short-term and long-term toxicity, and carcinogenicity. These serious side effects relate to the mechanism of anti-CMV action, the inhibition of DNA polymerase (Gandhi and Khanna, 2004; Mercorelli et al., 2011; Rawlinson et al., 2016). The emergence of drug-resistant CMV strains also poses a challenge (Mercorelli et al., 2011). No effective CMV vaccine is currently available (James and Kimberlin, 2016; Rawlinson et al., 2016). Therefore, novel anti-CMV strategies with alternative mechanisms of action and safer *in vivo* profiles are urgently needed. Valnoctamide (VCD) has been marketed since the early 1960s as an anxiolytic drug (Stepansky, 1960; Goldberg, 1961) and subsequently was tested as a mood stabilizer in patients with acute mania (Bersudsky et al., 2010). In animal models, VCD shows efficacy in both attenuating epilepsy (Lindekens et al., 2000; Isoherranen et al., 2003; Mareš et al., 2013; Pouliot et al., 2013; Shekh-Ahmad et al., 2014) and reducing neuropathic pain (Winkler et al., 2005; Kaufmann et al., 2010), in part by a mechanism that prolongs miniature IPSCs (Spampanato and Dudek, 2014). VCD shows no teratogenic effects in developing rodents (Radatz et al., 1998; Bersudsky et al., 2010; Shekh-Ahmad et al., 2014; Mawasi et al., 2015; Wlodarczyk et al., 2015; Bialer et al., 2017). Surprisingly, we recently found that VCD also inhibits CMV outside the CNS (Ornaghi et al., 2016).

Here we asked whether low-dose VCD given subcutaneously to CMV-infected neonatal mice can safely suppress CMV inside the developing brain and exert beneficial effects on neurodevelopment and behavior. We infected newborn mice on the day of birth (DOB) as a model where brain development in the newborn mouse parallels human brain development during the early second trimester of pregnancy (Clancy et al., 2001, 2007a,b; Branchi et al., 2003; Workman et al., 2013). This is a critical period of brain development where CMV can cause substantive dysfunction (Manicklal et al., 2013).

We show for the first time that VCD can protect the developing brain from CMV by both reducing the amount of virus entering the brain and by blocking viral replication and dispersal within the brain. VCD completely rescued the delayed acquisition of neurological milestones observed in infected neonatal mice. VCD treatment exerted long-lasting beneficial effects, restoring normal motor and behavioral outcomes in adolescent animals, and attenuating CMV-induced brain damage. VCD administration during critical periods of mouse brain development appeared safe and did not generate detectable adverse side effects on the neurodevelopment of uninfected control mice.

Materials and Methods

Cell lines, viruses, and chemicals

Normal human dermal fibroblasts (HDFs) were obtained from Cambrex, and primary human fetal brain astrocytes were obtained from ScienCell Research Laboratories. HDF cells were cultured in DMEM supplemented with 10% FBS and 1% penicillin streptomycin (Pen Strep; Invitrogen). Human fetal astrocytes were grown in poly-L-lysine-coated culture vessels and maintained in Astrocyte Medium (from ScienCell Research Laboratories) supplemented with 2% FBS and 1% Pen Strep. All cultures were kept in a humidified atmosphere containing 5% CO_2 at 37°C.

For *in vitro* experiments, a recombinant human CMV (hCMV, Toledo strain) expressing enhanced green fluorescent protein (EGFP) under the control of the EF1-α promoter (EGFP-hCMV) was used (Jarvis et al., 1999). Normal human fibroblasts were used to test viral EGFP expression, replication capability, and propagation, and to determine viral titers by plaque assay (Vieira et al., 1998; Jarvis et al., 1999).

CMV replication is species specific, and to study CMV *in vivo* we used a recombinant mouse CMV (mCMV; MC.55, K181 strain) that expresses EGFP (van den Pol et al., 1999), as previously reported (Ornaghi et al., 2016). NIH/3T3 cells (murine fibroblasts) were used for viral propagation and titering by plaque assay (van den Pol et al., 1999).

Recombinant CMVs were provided by Dr. E. Mocarski (Emory University, Atlanta, GA) and Dr. J. Vieira (University of Washington, Seattle, WA).

Green fluorescence was used to visualize infected cells and viral plaques. Viral titers were determined by standard plaque assay using 25% carboxymethyl-cellulose (CMC) overlay (Zurbach et al., 2014). Viral stocks were stored in aliquots at −80°C. For each experiment, a new aliquot of virus was thawed and used.

Valnoctamide (catalog #V4765) was purchased from Sigma-Aldrich as powder and was dissolved in dimethylsulfoxide (DMSO) to yield a 1 M stock solution.

Quantification of infection

Effects of VCD on hCMV infection were assessed by viral infectivity assay and viral yield reduction assay. For the infectivity assay, human fetal astrocytes were seeded at a density of 40,000 cells/well in 48-well plates and were incubated overnight before medium (0.2 ml/well) was replaced for pretreatment with VCD or vehicle at 100 μM. After 1 h of drug exposure, cells were inoculated with hCMV [multiplicity of infection (MOI), 0.1] and incubated at 37°C for 2 h to allow viral adsorption. Following incubation, cultures were washed twice with PBS and overlaid with a viscous solution containing VCD/vehicle at 100 μM in supplemented astrocyte medium (75%) and CMC (25%). GFP-positive cells were counted at 48 h postinfection (hpi).

In the virus yield reduction assay, after viral adsorption, cells were washed twice with PBS and replenished with fresh medium containing the compounds to be tested. At 72 hpi, medium was collected and titered by plaque assay using HDF monolayers to assess the drug-mediated inhibition of virus replication in human fetal brain astrocytes.

The total number of fluorescent cells/plaques per well in each condition were counted using an Olympus IX71 fluorescence microscope (Olympus Optical) connected to a SPOT RT digital camera (Diagnostic Instruments) interfaced with an Apple Macintosh computer. Each condition was tested in triplicate, and the whole experiment was repeated twice. Camera settings (exposure time and gain) were held constant between images. The contrast and color of collected images were optimized using Adobe Photoshop.

Viral entry analysis and quantitative real-time PCR assay

To evaluate the effects of VCD on hCMV attachment to human fetal astrocytes, prechilled cultures at 90% confluency in a six-well plate were treated with VCD or vehicle (100 μM) for 1 h at 4°C, followed by infection

with precooled hCMV-GFP (MOI, 0.1). After 2 h of incubation at 4°C, fetal astrocytes were rinsed three times with cold PBS to remove unattached virions then were harvested by trypsinization for viral DNA quantification using a quantitative real-time PCR (qRT-PCR) assay (Chan and Yurochko, 2014). To assess hCMV internalization into fetal astrocytes, cultures plated in plain media were inoculated with hCMV-GFP (MOI, 0.1) and incubated at 4°C for 2 h. Cells were then washed three times to remove unbound viral particles and were exposed to VCD or vehicle at 100 μM for 2 h at 37°C (to allow virus internalization) before being harvested by trypsinization for DNA quantification by qRT-PCR.

DNA was extracted from cells using the QIAamp DNA mini kit (Qiagen), and qRT-PCR was performed using TaqMan assays (Life Technologies; Gault et al., 2001; Fukui et al., 2008) for hCMV UL132 (Pa03453400_s1) and human albumin (Hs99999922_s1) genes, as previously described (Ornaghi et al., 2016). Samples from uninfected cells and without a template served as negative controls. Samples were run in duplicate using a Bio-Rad iCycler-IQ instrument, and results were analyzed with iCycler software. The amount of viral DNA in each sample relative to albumin was calculated using the comparative threshold cycle (C_T) method, and hCMV DNA was expressed as the percentage of virus bound (the "attachment" step) or internalized (the "internalization" step) using DMSO-treated samples as 100%.

Animal procedures

All animal breeding and experiments were performed in accordance with the guidelines of the Yale School of Medicine Institutional Animal Care and Use Committee (IACUC). Research was approved by the IACUC. Male and female BALB/c strain mice (6–8 weeks of age) from Taconic Biosciences were maintained on a 12 h light/dark cycle under constant temperature (22 ± 2°C) and humidity (55 ± 5%), with access to food and water *ad libitum*. One to two females were cohabited with a male of the same strain for at least 1 week to ensure fertilization. When advanced pregnancy was seen, each pregnant female was caged singularly and checked for delivery twice daily, at 8:30 A.M. and 6:30 P.M. Here we focus on inoculation of the newborn mouse, similar to the strategy we recently described for studying the actions of Zika virus in the developing mouse brain (van den Pol et al., 2017).

Paradigms of mCMV infection. Newborns were inoculated intraperitoneally with 750 pfu of mCMV-GFP in 50 μl of media on the DOB within 14 h of delivery. The DOB was considered to be postnatal day 0 (P0). Control animals received 50 μl of media intraperitoneally. To avoid any litter-size effect, large litters were culled to a maximum of eight to nine pups (Tanaka, 1998). Infected and control pups were randomly assigned to receive VCD or vehicle (DMSO) via subcutaneous injections, once a day, at a dose of 1.4 mg/ml in 20 μl of saline (28 μg/mouse), starting after virus inoculation and running from P1 to P21. Mice were monitored daily for signs of mCMV-induced disease and to determine survival; weaning occurred on P21 and mice of either sex were housed separately until testing was completed, then killed.

In addition to the intraperitoneal route, intracranial injection was performed in a group of newborn mice. Three days after birth, 2×10^4 pfu of mCMV-GFP in 1 μl of media was injected into the left cerebral hemisphere of neonatal mice under cryoanesthesia using a 10 μl Hamilton syringe with a 32-gauge needle from a midpoint between the ear and eye. Infected pups were randomly assigned to receive daily doses of VCD or vehicle (DMSO), starting 3 h after virus inoculation until P8. No deaths occurred, and at P9 mice were killed and blood, liver, spleen, and brain were collected, snap frozen, and stored at −80°C until viral titer analysis via qRT-PCR ($n = 8$/experimental group) was performed.

Early neurobehavioral assessment. Intraperitoneally infected pups and controls were assessed for neurobehavioral development according to a slightly modified Fox battery, as previously described (Fox, 1965; St Omer et al., 1991; Calamandrei et al., 1999). Evaluation was performed without knowledge of the experimental group on every other day from P2 to P14, in the light phase of the circadian cycle between 9:00 A.M. and 3:00 P.M. Each subject was tested at approximately the same time of the day. Reflexes and responses were scored in the following order: righting reflex, the time used by the pup to turn upright with all four feet when placed on its back; cliff aversion, when placed on the edge of a cliff or table top with the forepaws and face over the edge, the mouse will turn and crawl away from the edge; Forelimb grasping reflex, when the forefoot is stroked with a blunt instrument the foot will flex to grasp the instrument; forelimb placing reflex, contact of the dorsum of the foot against the edge of an object will cause the foot to raise and place itself on the surface of the object when the animal is suspended and no other foot is in contact with a solid surface; negative geotaxis, the time used by the pup to turn ~180° to either side when placed head down on a wire mesh screen (4 × 4 mm) held at a 45° angle; level screen test, pup holds onto a wire-mesh (10 × 10 cm) and is propelled across the mesh horizontally by the tail; screen climbing test, pup climbs up a vertical screen (10 × 10 cm, 90° angle) using both forepaws and hindpaws; maximal response, scored when the subject reaches the top of the vertical screen; and vibrissa placing reflex, when the mouse is suspended by the tail and lowered so that the vibrissae make contact with a solid object, the head is raised and the forelimbs are extended to grasp the object.

Latencies were measured in seconds using a stopwatch for righting reflex and negative geotaxis. The remaining behavioral variables were rated semiquantitatively in the following way: 0 = no response or occurrence of the event (R/O); 1 = slight/uncertain R/O; 2 = incomplete R/O; and 3 = a complete adult-like R/O. All timed responses were limited to a maximum of 60 s; therefore, the absence of a milestone was scored as 0/60 s (semiquantitative rating/latencies) if the mouse did not exhibit the behavior within 60 s.

This battery of tests provides a detailed assessment of functional and neurobehavioral development throughout the neonatal period since the behaviors measured are each expressed at different stages of development during the first weeks of life. Specific information about vestibular function, motor development and activity, coordination, and muscle strength can be obtained by execution of these tests (St Omer et al., 1991; Schneider and Przewlocki, 2005).

Evaluation of motor coordination and balance in adolescent mice. Motor performance of infected and control mice, with or without VCD treatment, was assessed at P28–P30 by the hindlimb-clasping, vertical pole, and challenging beam traversal tests.

In the hindlimb-clasping test, the mouse is gently lifted by the tail, grasped near its base, and the hindlimb position is observed for 10 s and scored as follows: if the hindlimbs are consistently splayed outward, away from the abdomen, it is assigned a score of 0; if one hindlimb is retracted toward the abdomen for >50% of the time suspended, it receives a score of 1; if both hindlimbs are partially retracted toward the abdomen for >50% of the time suspended, it receives a score of 2; and if its hindlimbs are entirely retracted and touching the abdomen for >50% of the time suspended, it receives a score of 3 (Tanaka et al., 2004; Guyenet et al., 2010).

The vertical pole test was conducted according to previously established protocols (Ogawa et al., 1985; Soerensen et al., 2008). Briefly, mice were individually placed head downward at the top of a vertical rough-surfaced pole (diameter, 8 mm; height, 55 cm) and allowed to descend in a round of habituation. Then, mice were placed head upward at the top of the pole. The time required for the animal to descend to the floor was recorded as the locomotor activity time (T_{LA}), with a maximum duration of 120 s. If a mouse fell, was unable to turn downward, or was unable to climb down, a default locomotor activity time value was recorded as 120 s. Each mouse was given three trials with a 30 s recovery period between trials.

The challenging beam traversal test was performed as previously described (Fleming et al., 2004, 2013). The beam consisted of four sections (25 cm each, 1 m total length), each section having a different width. The beam started at a width of 3.5 cm and gradually narrowed to 0.5 cm in the last section. Underhanging ledges (1 cm width) were placed 1.0 cm below the top surface of the beam to increase the sensitivity of the test and allow detection of subtle motor deficits (Brooks and Dunnett, 2009). Animals were trained to traverse the length of the beam starting at the widest section and ending at the narrow most difficult section. The narrow end of the beam led directly into the home cage of the animal. A bright light illuminated the start of the beam to further encourage the mouse to walk across the beam toward the home cage. Animals received 2 d of training before testing, with five trials for each day. On the day of the test, a mesh grid (1 cm squares) of corresponding width was placed over the beam

surface leaving a 1 cm space between the grid and the beam surface. Animals were then videotaped while traversing the grid-surfaced beam for a total of five trials. Videos were viewed and rated in slow motion for hindlimb slips and time to traverse across five trials by an investigator blind to the mouse experimental group. A slip was counted when the mouse was facing and moving forward and a hindlimb slipped through or outside of the grid beyond 0.5 cm below the grid surface (halfway down).

Exploratory activity and social behavior analysis. The exploratory activity was assessed in adolescent mice at P30–P40 in an adapted small open field, as previously described (Shi et al., 2003; Schneider and Przewlocki, 2005). The apparatus consisted of a plastic rectangular box measuring 20.5 × 17 × 13 cm^3 (l × width × height) with regularly spaced holes in the short (2) and long (3) walls, and illuminated by ambient fluorescent ceiling lights. The animal was placed in the center of the apparatus and its movements were video recorded over a 3 min period. Exploratory behavior was scored for the number of rearing and nose-poking (nose of an animal put inside the hole) episodes.

Sociability and preference for social novelty were investigated at 5 weeks of age in a three-compartment apparatus (Crawley, 2007; Yang et al., 2011). Initially, test and control animals were allowed to explore the apparatus freely for a 10 min period (habituation). For the social approach paradigm, an unfamiliar conspecific (same sex, similar age and weight) animal was placed into one of the side compartments and restrained by a small wire object ("social cage"). The compartment on the other side contained an empty wire object ("empty cage"). The test subject was then released into the center compartment and allowed to explore the three-compartment apparatus freely for 10 min. Behavior was videotaped and assessed for the times that the test subject spent in the three compartments and in close proximity to the social and empty cages. For the social-novelty paradigm, another unfamiliar conspecific animal was placed in the previously empty wire object ("novel cage"). The behavior of the test mouse was recorded for 10 min and assessed for the time spent exploring the known and novel conspecifics.

Assessment of mCMV distribution in the brain and viral-mediated brain abnormalities. At specific time points after infection, mice were killed by an overdose of anesthetic and transcardially perfused with sterile, cold PBS followed by 4% paraformaldehyde, and brains were harvested and weighed. Brains were then immersed overnight in 4% paraformaldehyde, and cryoprotected in 15% and then 30% sucrose for 24 h before inclusion in Tissue Freezing Medium (General Data). Some intraperitoneally infected mice became dehydrated and moribund and showed no sign of recovery; these mice were killed before the predefined killing time points and were recorded as having had a lethal response to the virus.

Fifteen-micrometer-thick sections cut with a Leica cryostat were used for GFP reporter expression assessment and immunofluorescence analysis in the brain. Sections were dried for 4 h at room temperature, rehydrated in 1× PBS, and then used for immunofluorescence assays. Briefly, tissue sections were incubated overnight at 4°C with monoclonal mouse anti-NeuN antibody (1:500; catalog #MAB377, EMD Millipore; RRID: AB_2298772) for neuronal cells and polyclonal rabbit anti-calbindin D-28K (1:500; catalog #AB1778, EMD Millipore; RRID: AB_2068336) for cerebellar Purkinje cells (PCs). Tissues were washed three times in phosphate buffer plus 0.4% Triton X-100. Secondary antibodies, including goat anti-mouse IgG and donkey anti-rabbit IgG conjugated to Alexa Fluor-594 (1:250; Invitrogen), were applied for 1 h at room temperature and then washed off. Some sections were labeled with DAPI. Vectashield Fluorescent mounting medium (Vector Laboratories) was then used for mounting.

Images were collected by using a fluorescence microscope (model IX 71, Olympus Optical).

Frozen sections were used for morphometric measurements, and cell numbers were quantified after imaging using ImageJ software (https://imagej.nih.gov/ij/; RRID: SCR_003070). The molecular layer (ML) and

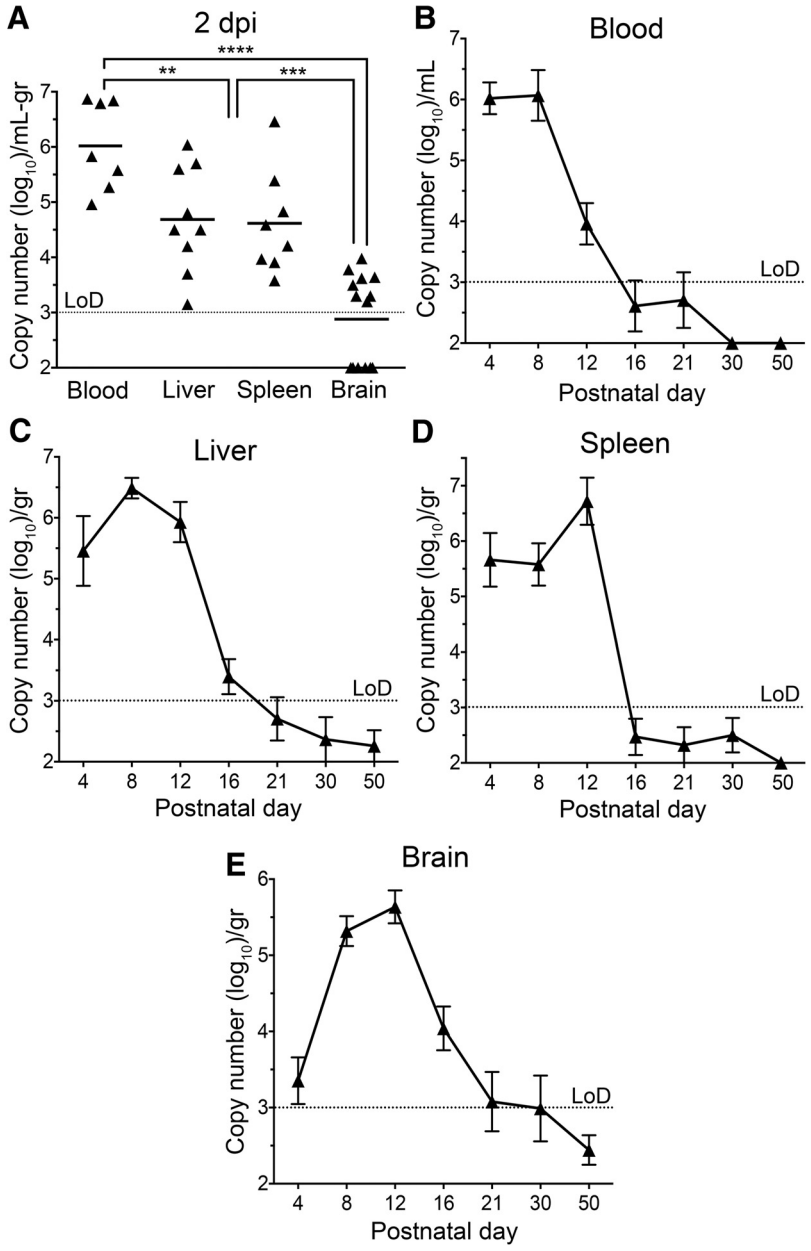

Figure 1. Kinetics of mCMV replication after intraperitoneal inoculation on day of birth. Newborn mice were infected on the DOB (day 0) with 750 pfu of mCMV. Viral load in whole blood, liver, spleen, and brain was evaluated by qRT-PCR at the indicated time points and expressed as $\log_{10}$ genome copies per gram/ml of harvested tissue/blood. In ***A***, each symbol represents an individual mouse, and horizontal bars show mean values of the groups; in ***B–E***, data are presented as the mean ± SEM with 7–10 mice/time point. Viral titers below the limit of detection (LoD, dotted line) were plotted as 2 $\log_{10}$ genome copies. In ***A***, $^{**}p < 0.01$, $^{***}p < 0.001$, $^{****}p < 0.0001$; one-way ANOVA with Bonferroni's *post hoc* test.

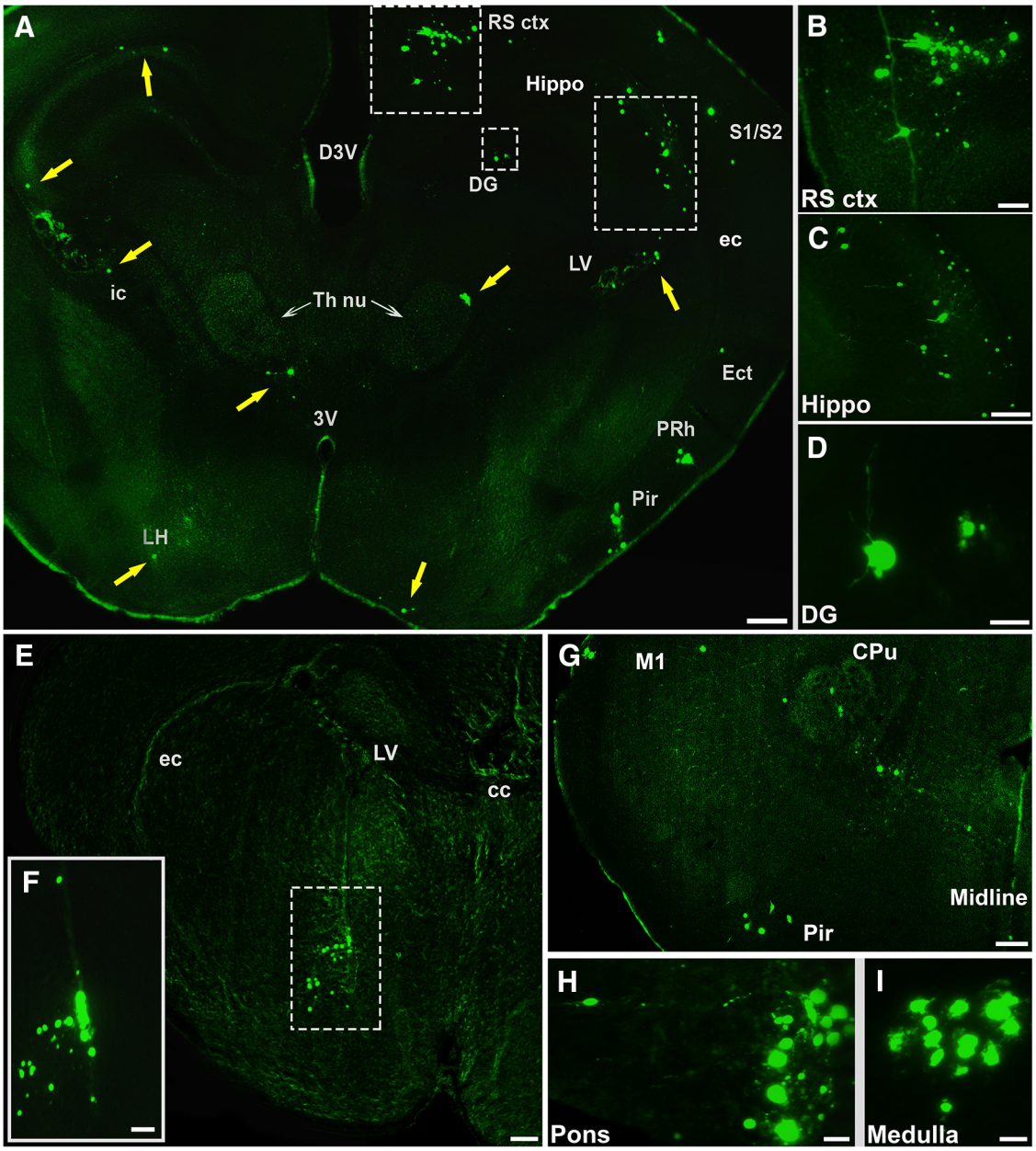

Figure 2. Scattered widespread distribution of mCMV-GFP in brains after infection of newborn mice. Detection of virus-infected cells by means of mCMV GFP reporter expression in representative coronal sections of P8 and P12 mouse brains ($n = 5$). ***A***, Single infected cells or small foci of infection (yellow arrows) can be identified in the retrosplenial cortex (RS ctx), primary and secondary somatosensory cortex (S1/S2), ectorhinal cortex (Ect), perirhinal cortex (Prh), piriform cortex (Pir), hippocampus (hippo) and dentate gyrus (DG), lateral ventricle (LV), external and internal capsule of the corpus callosum (ec and ic, respectively), lateral hypothalamic area (LH), and thalamic nuclei (Th Nu) of a P12 mouse brain. D3V, dorsal third ventricle. ***B–D*** are magnifications of the boxed areas in ***A***. ***E***, Infection of the lateral ventricle and diffusion to the adjacent brain parenchyma in a P8 brain. ***F***, Magnification of the boxed area in ***E***. cc, corpus callosum. ***G***, Photomicrograph of a P12 brain showing infection in the motor (M1) and piriform cortex, and in the striatum [caudate–putamen (CPu)]. ***H***, ***I***, Large foci of mCMV-infected cells in the pons and the medulla of a P8 animal. Scale bars: ***H***, 50 μm; ***A***, ***D***, ***E***, ***G***, ***I***, 100 μm; ***C***, ***F***, 200 μm; ***B***, 400 μm.

internal granular layer (IGL) were assessed using images of serial midsagittal cerebellar sections stained with calbindin D-28K and DAPI. Three measurements were taken at each side of the primary fissure in each section, and four sections per animal were evaluated. For the cerebellar area, midsagittal brain sections (three sections/mouse) were stained with blue fluorescent Nissl stain (NeuroTrace, catalog #N21479, Thermo Fisher Scientific), and images were collected using a 2× objective. Cell counts were performed on sections (four sections/mouse) stained with calbindin D-28K, and the number of Purkinje cells was evaluated along 500 μm of the primary fissure (both sides). All measurements and quantifications were performed on at least five animals from three different litters.

Kinetics of virus spread and replication in vivo. For measurement of mCMV replication in blood, liver, spleen, and brain, mCMV-infected mice receiving either VCD or vehicle intraperitoneally or intracranially were killed at multiple time points postinoculation, and samples were collected under sterile conditions, snap frozen, and stored at −80°C until viral titer analysis via quantitative real-time PCR ($n = 7$–10/experimental group) was performed. Mice used for viral load analysis in liver, spleen, and brain were perfused with sterile cold PBS to remove any virus contained within the blood. Total DNA was isolated using the QIAamp DNA Mini Kit (Qiagen) as per manufacturer instructions. Quantitative PCR was performed using TaqMan assays (Life Technologies) by amplification of a fragment of mCMV IE1 gene exon 4 using the following primers: forward, 5′-GGC TTC ATG ATC CAC CCT GTT A-3′; and reverse, 5′-GCC TTC ATC TGC TGC CAT ACT-3′. The probe (5′-AGC CTT TCC TGG ATG CCA GGT CTC A-3′) was labeled with the reporter

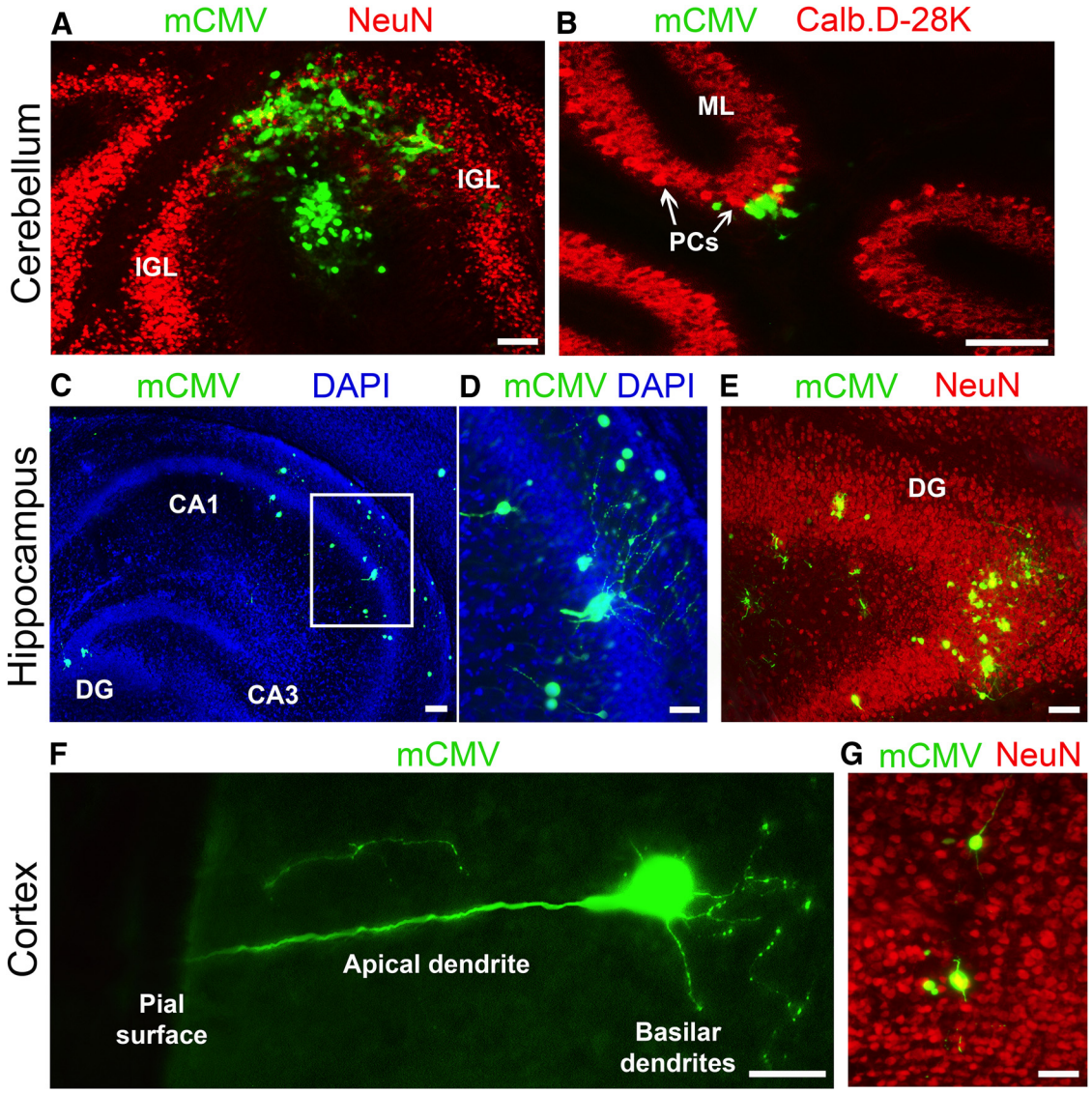

Figure 3. CMV infection of neuronal cells in the cerebellum, hippocampus, and cortex of the developing brain. ***A***, ***B***, Photomicrographs show GFP labeling of different cerebellar cell types, including neurons in the internal granular layer (***A***) and Purkinje cells (***B***), as assessed by NeuN and calbindin D-28K staining at 8 dpi ($n = 2$ brains). ***C–E***, Photographs display infection of different areas of the hippocampus (***C***), a magnification of the viral involvement of pyramidal cells in CA1 field (boxed area; ***D***), and infected neurons in the dentate gyrus (DG; $n = 2$ brains; ***E***). ***F***, Robust GFP expression in a pyramidal neuron of the motor cortex ($n = 1$ brain); note the beaded aspect of the basilar dendrites, sign of neuronal pathology. Photomicrograph of neuronal infection in the visual cortex ($n = 1$ brain; ***G***). Scale bars: ***A–E***, ***G***, 100 μm; ***F***, 50 μm.

dye FAM (Kosmac et al., 2013). qRT-PCR was performed using 20 μl reaction mixtures using the iTaq Universal SYBR Probes Supermix (Bio-Rad) and 100 ng of DNA. Samples were run in duplicate using a two-step amplification protocol. Tissue samples from uninfected mice and samples without a template served as negative controls. Viral burden was expressed as the copy number per ml per gram blood/tissue after comparison with a standard curve generated using serial 10-fold dilutions of mCMV DNA.

Experimental design and statistical analysis

Statistical significance, unless otherwise specified, was determined by one-way ANOVA or Kruskal–Wallis test followed by Bonferroni's and Dunn's *post hoc* test, respectively, for evaluation of motor performance, exploratory behavior, and brain morphometry. Early neurobehavioral development, social behavior, and viral load over time were assessed by a mixed-model ANOVA with repeated measures followed by Newman–Keuls test if there was a significant F value. Since no gender-related differences were detected in early neurodevelopment, data from male and female mice were combined. Only male mice were used for examination of motor performance and exploratory and social behavior. All analyses were conducted with GraphPad Prism version 6.0 (RRID: SCR_002798), with significance set at $p < 0.05$. Neurobehavioral assessment was performed blindly with respect to the experimental group.

Results

Peripheral inoculation of CMV causes widespread infection of the developing brain

First, we characterized the kinetics of CMV replication and dissemination after intraperitoneal inoculation of the virus in newborn mice on the DOB (P0). Forty-eight hours after intraperitoneal injection, CMV was found in the blood and at lower levels in the spleen and liver of infected mice, with only a small amount detected in the brain (Fig. 1*A*). Analysis of viral kinetics in these four organs over the course of 50 d revealed that CMV, after entering the bloodstream, quickly gained access to peripheral target organs (i.e., the liver and spleen) and began replicating to yield high viral titers by 4 d post-injection (dpi; Fig. 1*B–D*). In

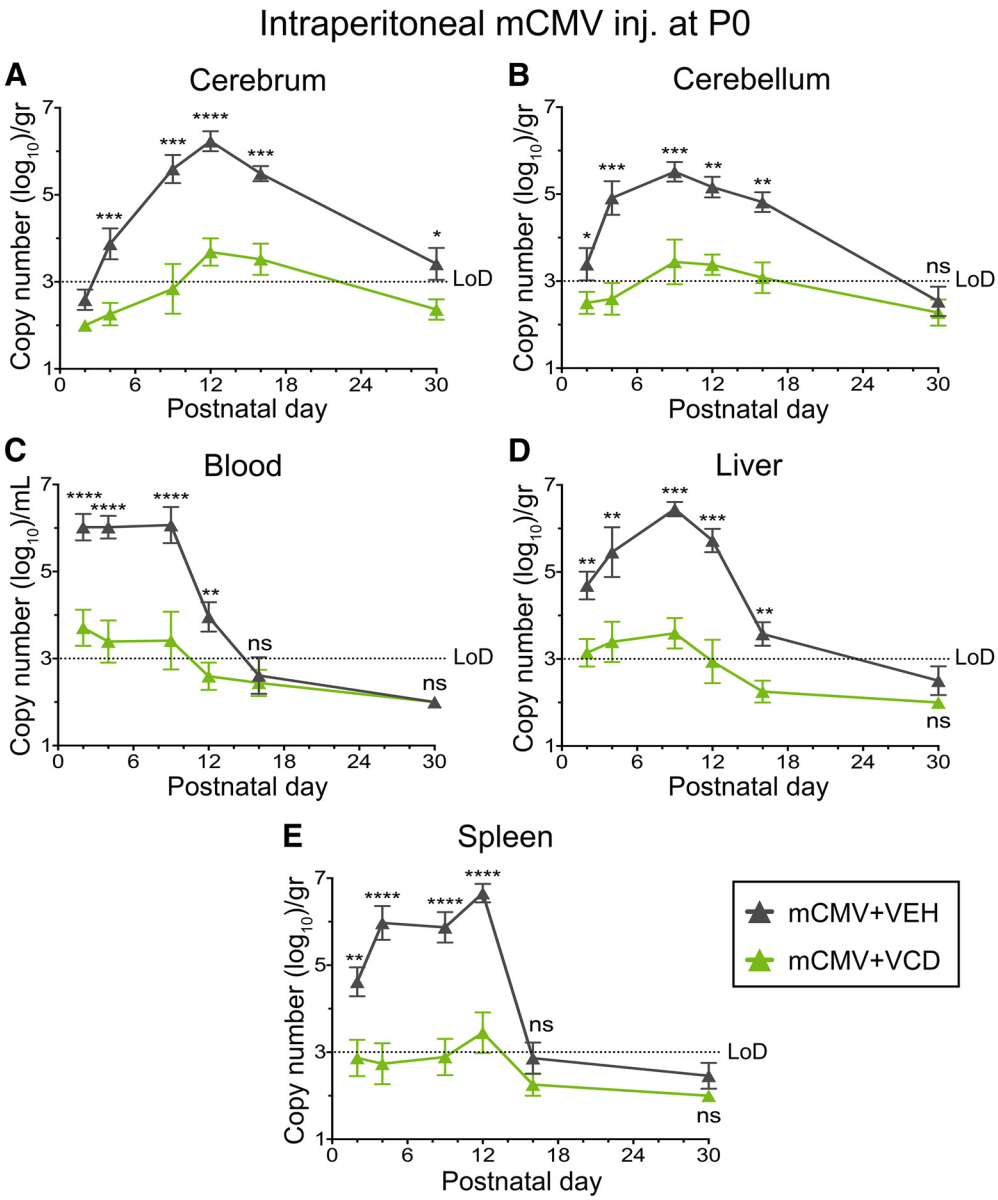

Figure 4. Valnoctamide suppresses mCMV load in the brain of mice infected intraperitoneally on the day of birth. Newborn mice were infected at P0 with 750 pfu of mCMV intraperitoneally and were randomized to receive either vehicle (mCMV + VEH) or VCD (mCMV + VCD) subcutaneously from P1 until P21. ***A–E***, Viral load was quantified in the cerebrum (***A***), cerebellum (***B***), whole blood (***C***), liver (***D***), and spleen (***E***) by qRT-PCR at the specified time points and were expressed as $\log_{10}$ genome copies per gram/ml harvested tissue/blood. Data are presented as the mean ± SEM; n = 7–10 mice/time point. Viral titers below the limit of detection (LoD, dotted line) were plotted as 2 $\log_{10}$ genome copies. ns, Not significant. *$p < 0.05$, **$p < 0.01$, ***$p < 0.001$, ****$p < 0.0001$; two-way ANOVA with postnatal day as repeated measures.

turn, similar viral titers were measured in the brain only after 8 dpi (Fig. 1*E*). After entering the brain, the virus could effectively replicate *in situ*, as suggested by the measurement of CMV loads similar to those found in the liver and spleen at the viral peak between P8 and P12 (Fig. 1*C–E*).

Upon histological examination, CMV-GFP infection of the developing mouse brain appeared widespread and scattered in nature. Isolated infected cells and infectious foci containing up to 20–25 cells could be found in multiple distant areas within the same brain. The pattern of infection also appeared heterogeneous, with different brains displaying infection in different regions. These observations are consistent with a hematogenous spread of CMV from the periphery into the developing brain of neonatal mice. Infected cells were identified in the olfactory bulb and nuclei, the cortex, corpus callosum, hippocampus, basal nuclei, choroid plexus, midbrain, superior and inferior colliculi, sylvian aqueduct, pons, medulla, cerebellum, and meninges (Fig. 2*A–I*). No CMV was detected in the spinal cord. Infection of the choroid plexus in the lateral ventricles was frequently associated with evidence of infected cells in the brain parenchyma in close proximity to the ventricle (Fig. 2*E*,*F*), a site of neural progenitor stem cell localization (Semple et al., 2013). Infection of certain brain areas, such as the thalamus and the hypothalamus, was observed less frequently compared with other regions, including the cerebellum, hippocampus, and cortex. The cerebellum was the only site consistently displaying viral infection in all the brains examined (n = 20), with robust GFP labeling in both Purkinje cells and granule neurons (Fig. 3*A*,*B*). Viral GFP was also identified in neurons of the hippocampus and in the cerebral cortex (Fig. 3*C–G*). In cortical pyramidal cells, GFP was seen in both the

apical dendrite extending toward the cortical surface and in basal dendrites ramifying closer to the cell body. Some infected neurons in the cortex displayed signs of degeneration, characterized by abnormal swelling along the dendrites (Fig. 3*F*).

Together, these results indicate that intraperitoneally administered CMV, after replicating in peripheral target organs, enters the developing brain of neonatal mice via the bloodstream or immune cells in the blood, producing a scattered and widespread infection with a highly heterogeneous pattern of propagation. Nonetheless, CMV appears to display a particular preference for the cerebellum as an infectious site.

Subcutaneous valnoctamide blocks CMV replication within the brain

Mice were infected intraperitoneally on the day of birth, and we compared the brains of infected mice treated subcutaneously with VCD with nontreated CMV-infected mice. CMV load in the brain was quantified at multiple time points after virus inoculation. Cerebrum (cortex, hippocampus, thalamus, hypothalamus, and striatum) and cerebellum were assessed separately to determine whether the viral preference for the cerebellar region, as observed in the brain section analysis, was also accompanied by higher levels of virus replication. VCD decreased the amount of virus detected in both the cerebrum and cerebellum by a very substantial amount, with an ~100- to 1000-fold decrease at all time points tested (Fig. 4*A*,*B*). The anti-CMV effect displayed a rapid onset, suppressing the viral load after only 1 and 3 d of treatment in the cerebellum and the cerebrum, respectively. In untreated infected mice, higher viral titers were identified in cerebellar samples compared with cerebrum at the beginning of infection (P4: $t = 3.704$, $p = 0.004$, paired Student's t test), suggesting that the cerebellum may represent a preferential site for initial CMV targeting in the brain. These data indicate that VCD can attenuate CMV infection detected in the brain. The observed antiviral effect of VCD in the CNS could be the consequence of a drug-mediated decrease in viral replication in the periphery. Along this line, we corroborated (Ornaghi et al., 2016) that VCD also attenuated CMV in the blood, liver, and spleen, starting quickly after therapy initiation and continuing to the end of the experiment (Fig. 4*C*–*E*). This reduction of CMV outside the brain would benefit the brain by reducing the amount of virus that ultimately can enter the CNS.

To investigate whether VCD can act directly in the brain to decrease CMV, we infected pups on P3 by direct intracranial virus inoculation. Analysis of CMV load in the blood, liver, and spleen of untreated infected mice at P9 showed no viral spread outside the CNS (data not shown). Viral titers in the cerebrum and the cerebellum were substantially lower by >100-fold in CMV-infected animals receiving VCD treatment compared with untreated CMV-infected mice ($2.99 \times 10^5 \pm 9.06 \times 10^4$ vs $2.47 \times 10^8 \pm 1.22 \times 10^8$ copy number/g tissue, $p = 0.004$ in cerebrum; $2.88 \times 10^6 \pm 1.83 \times 10^6$ vs $3.41 \times 10^8 \pm 1.52 \times 10^8$ copy number/g tissue, $p = 0.0003$ in cerebellum; Mann–Whitney U test; Fig. 5). These results indicate that subcutaneously administered low-dose VCD can enter the brain at sufficient concentrations to effectively suppress CMV replication *in situ*.

Reversal of early neurological dysfunction in CMV-infected neonatal mice

Human infants with CMV infection during early development can display substantial delays in the acquisition of neurological milestones during the first months of life (Dollard et al., 2007; Kimberlin et al., 2015). Since VCD showed a robust antiviral activity in the CNS of infected mice with a rapid attenuation of viral replication, we investigated whether this would translate into a positive therapeutic effect on the early neurological outcomes of neonatal mice.

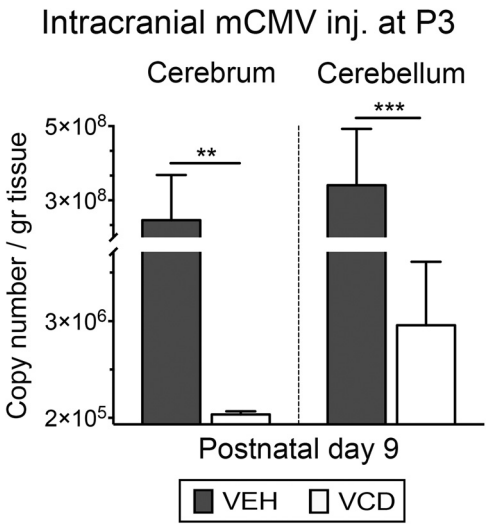

Figure 5. Subcutaneously injected valnoctamide enters the brain and suppresses mCMV replication within the brain. Quantification of mCMV load in the brain of mice intracranially infected with 2×10^4 pfu of mCMV on day 3 after birth. The amount of virus in the cerebrum (left) and the cerebellum (right) was calculated by qRT-PCR in P9 mice receiving either vehicle (VEH) or VCD subcutaneously from P3 through P8 and expressed as genome copies per gram of harvested tissue. Values are reported as the mean ± SEM; $n = 8$ mice/time-point. $^{**}p < 0.01$, $^{***}p < 0.001$, Mann–Whitney U test.

Neurobehavioral assessments were performed using a battery of tests to examine body righting and tactile reflexes, motor coordination, and muscular strength. These tests provide a detailed examination of neurontogeny throughout the neonatal period since the behaviors measured are each expressed at different periods during the first 3 weeks of postnatal life (Fox, 1965; Scattoni et al., 2008).

Here and in a number of experiments below, we compared neurological function in the following four groups of mice: noninfected controls; VCD-treated non-infected controls; CMV-infected mice; and CMV-infected mice treated with VCD. VCD was administered in a single daily subcutaneous dose (for additional details, see Materials and Methods).

CMV infection on the day of birth induced abnormal acquisition of all the neurological milestones assessed, with infected mice showing a delay of 6–10 d in the demonstration of responses similar to the uninfected controls (Fig. 6*A*–*H*). In turn, infected VCD-treated neonatal pups displayed a timely acquisition of neurological milestones in all the behaviors measured. No differences were identified in the early neurontogeny of uninfected mice receiving VCD or vehicle. Together, these data indicate that VCD treatment during early development can safely improve the short-term neurodevelopmental outcomes observed in infected neonatal mice.

Amelioration of long-term neurobehavioral outcomes in infected juvenile mice

CMV infected infants with evidence of neurological delays during the neonatal period are at increased risk of the development of long-term permanent neurological and behavioral sequelae, which manifest with a delayed onset after the first years of life (James and Kimberlin, 2016). Abnormal motor function is a

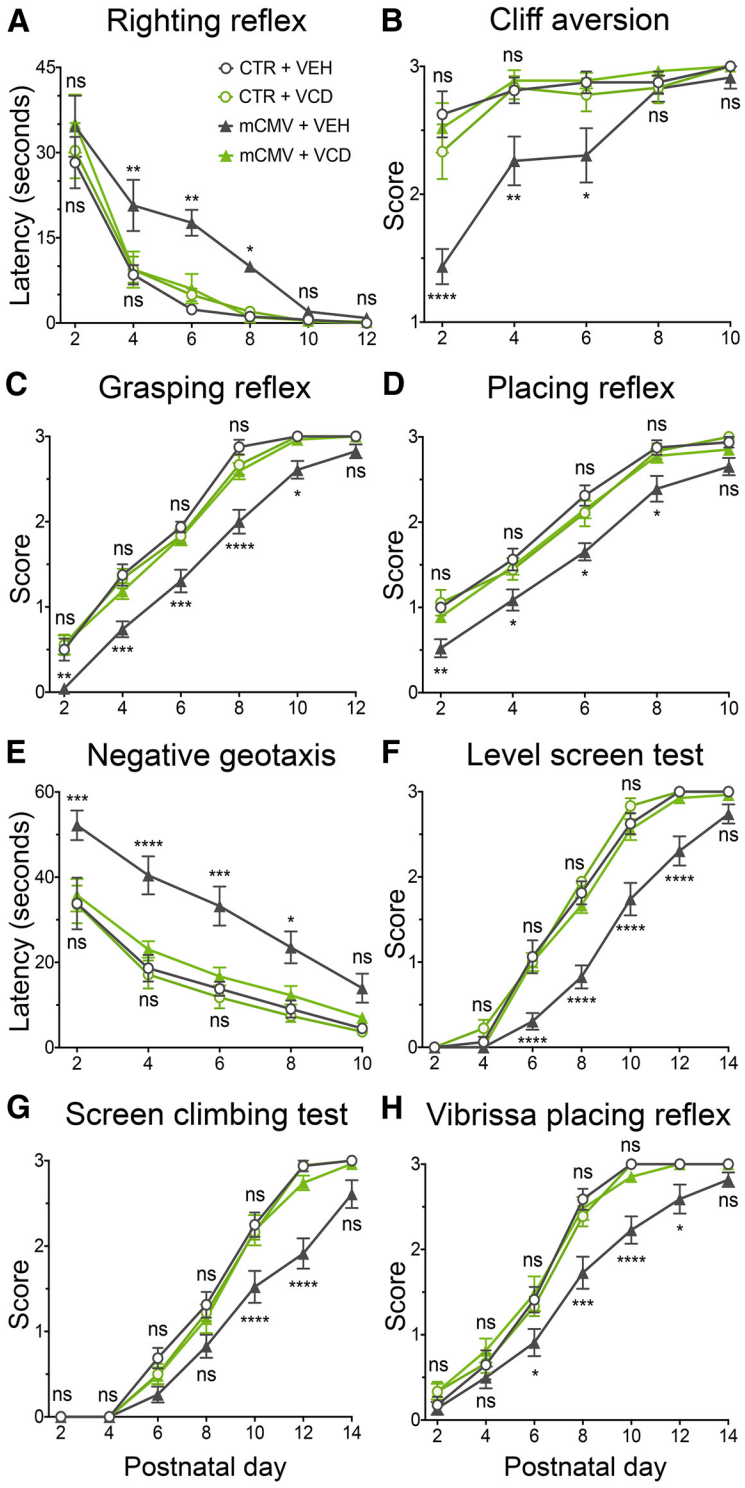

Figure 6. Delayed acquisition of neurological milestones induced by mCMV infection is completely rescued by valnoctamide therapy. ***A–H***, Graphs show neurodevelopmental delays in mCMV-infected pups (solid gray triangles) as assessed by the righting reflex (***A***), the cliff aversion (***B***), the forelimb grasping and placing reflex (***C***, ***D***), the negative geotaxis (***E***), the level screen test (***F***), the screen climbing test (***G***), and the vibrissa placing reflex (***H***; for a detailed description, see Materials and Methods). VCD-treated animals (solid green triangles) showed neurological responses similar to uninfected controls receiving either vehicle (VEH; empty gray circles) or VCD (empty green circles). Values are reported as the mean ± SEM, $n = 20–24$ mice (9–12 males)/experimental group. ns, Not significant. $^{*}p < 0.05$, $^{**}p < 0.01$, $^{***}p < 0.001$, $^{****}p < 0.0001$; two-way ANOVA with postnatal day as repeated measures. Significance is shown next to the infected, untreated mice (mCMV + VEH) line for comparison with uninfected controls (CTR + VEH and CTR + VCD) and next to control lines for comparison with VCD-treated infected pups (mCMV + VCD).

commonly observed long-term neurological complication (Turner et al., 2014). More recently, a link between ASD-like behavioral disturbances in children and adolescents and CMV infection during early development has been proposed (Sakamoto et al., 2015; Garofoli et al., 2017). Given the substantial improvement induced by VCD in the early neurontogeny of CMV-infected neonatal mice, we examined whether these beneficial effects could also ameliorate late-onset neurobehavioral abnormalities, including motor performance and social and exploratory behavior.

Motor performance

As indicated above, the cerebellum appears to be a preferential site for CMV targeting in the mouse brain. We investigated cerebellar-mediated motor functions in infected and control juvenile mice using a hindlimb-clasping test, a vertical pole test, and a challenging beam traversal test (Brooks and Dunnett, 2009; Guyenet et al., 2010; Fleming et al., 2013).

The hindlimb clasping test is a marker of cerebellar pathology commonly used for severity scoring in mouse models of cerebellar degeneration (Guyenet et al., 2010). The majority of the CMV-infected mice (9 of 13 mice) displayed an abnormal response to the clasping test, with both hindlimbs partially or entirely retracted to the abdomen when the mice were suspended by their tail for 10 s (Fig. 7*A*,*B*). VCD administration completely reversed this altered behavior, restoring a response similar to the uninfected counterparts.

By placing a mouse head upward on a vertical wooden pole, the vertical pole test allows for the examination of the ability of the animal to turn through 180° and successfully climb down the pole (Brooks and Dunnett, 2009). CMV-infected, untreated juvenile mice required a longer period to complete the task compared with both uninfected controls and CMV-infected VCD-treated animals (Fig. 7*C*). Three of 20 infected mice (15%) without treatment failed the test (e.g., showed an inability to turn the head downward or falling) in all of the three trials given, whereas no VCD-treated infected mice or uninfected controls failed in performing the task ($p = 0.03$, χ^2 test).

In addition, we evaluated fine motor coordination and balance by the challenging beam traversal test, which assesses the ability of a mouse to maintain balance while traversing a narrow, 1-m-long beam

to reach a safe platform (Carter et al., 2001; Brooks and Dunnett, 2009; Luong et al., 2011; Fleming et al., 2013). CMV infection during early development increased the time needed by the mice to cross the beam and also the frequency of slipping (Fig. 7*D*,*E*). VCD treatment significantly improved the coordination and balance of CMV-infected mice, reducing both the beam traversal time and the number of slips recorded.

Social and exploratory behavior

ASD is characterized by pervasive impairments in social interactions coupled with restricted and repetitive behaviors and decreased exploratory activity (American Psychiatric Association, 2013). To investigate whether adolescent mice with perinatal CMV infection would display social and exploratory behavioral disturbances, we assessed social interaction and novel environment exploration by means of the three-chamber test and an adapted small open field test.

Infected untreated mice showed normal sociability when exposed to a first stranger mouse, preferring the conspecific over the empty cage (novel object; Fig. 8*A*). However, a lack of preference for social novelty was found when a second stranger mouse was introduced, with infected untreated mice spending an equal amount of time in investigating the known and the novel animal (Fig. 8*B*). VCD therapy restored social novelty responses similar to levels shown in uninfected controls, with increased time devoted to examining the second stranger mouse.

Exploratory activity was assessed by quantifying the number of rearings and nose pokings of mice exposed to a novel environment over a 3 min test session (Fig. 8*C*,*D*). A substantial reduction in both rearing and hole-poking events was identified in CMV-infected untreated mice compared with control animals. Normal levels of exploratory activity were restored in infected mice receiving VCD treatment.

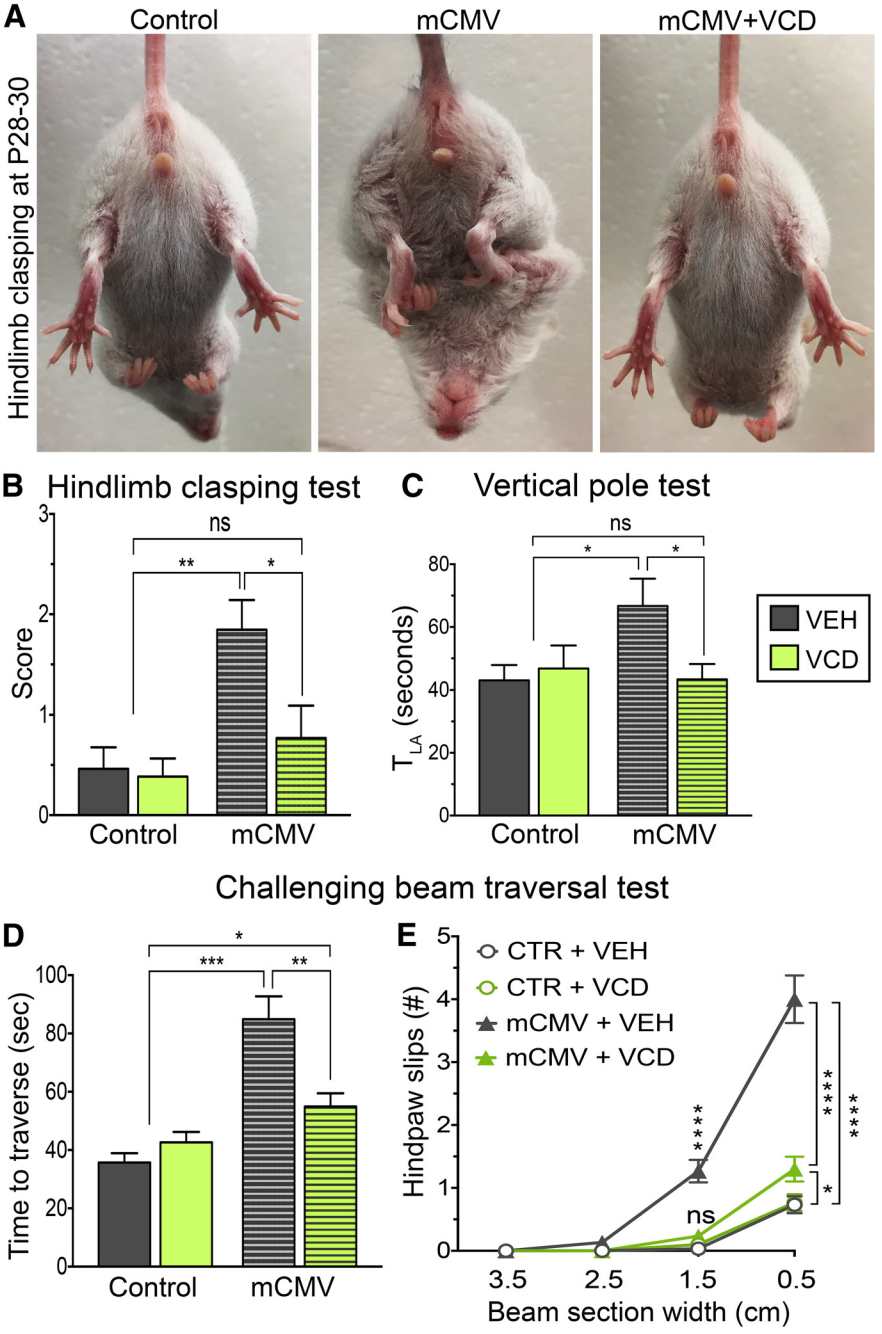

Figure 7. Impaired cerebellar-mediated motor functions in mCMV-infected mice are ameliorated by valnoctamide treatment. ***A***, Photographs display stereotypical clasping response with hindlimbs retracted to the abdomen in an mCMV-infected mouse (middle), and a normal response with splayed out hindlimbs in an uninfected control (left) and in an mCMV-infected, VCD-treated animal (right). ***B***, Scoring of clasping response according to hindlimb position. ***C***, Increased T_{LA} in infected, untreated mice in the vertical pole test, compared with VCD-treated infected animals and uninfected controls. ***D***, ***E***, Investigation of fine motor coordination and balance by challenging beam traversal test. Infected mice need more time to traverse the beam (***D***) and slip more (***E***) than the control mice. Both aspects are improved by VCD administration. Values are reported as the mean ± SEM; $n = 10–13$ mice/group. $^{*}p < 0.05$, $^{**}p < 0.01$, $^{***}p < 0.001$, $^{****}p < 0.0001$; Kruskal–Wallis test with Dunn's *post hoc* test in ***B–D***, and two-way ANOVA with repeated measures and Bonferroni's *post hoc* comparison in ***E***.

Valnoctamide attenuates CMV-induced brain defects in early development

Early-onset neurodevelopmental delays and long-term permanent neurobehavioral disabilities are commonly observed in CMV-infected babies with evidence of virally induced brain abnormalities, including decreased brain size and cerebellar hypoplasia (Gandhi and Khanna, 2004; de Vries et al., 2004; Cheeran et al., 2009; Oosterom et al., 2015; James and Kimberlin, 2016). Since VCD showed a potent and fast-acting anti-CMV activity in the brains of infected mice and appeared beneficial to both short- and long-term neurobehavioral outcomes, we investigated whether drug treatment during early development could also exert therapeutic actions on CMV-induced brain defects.

Brain size was analyzed in 1-month-old-mice by assessing the brain-to-body weight ratio (Fig. 9*A*,*B*). This measurement allows a more objective evaluation of the postnatal brain growth,

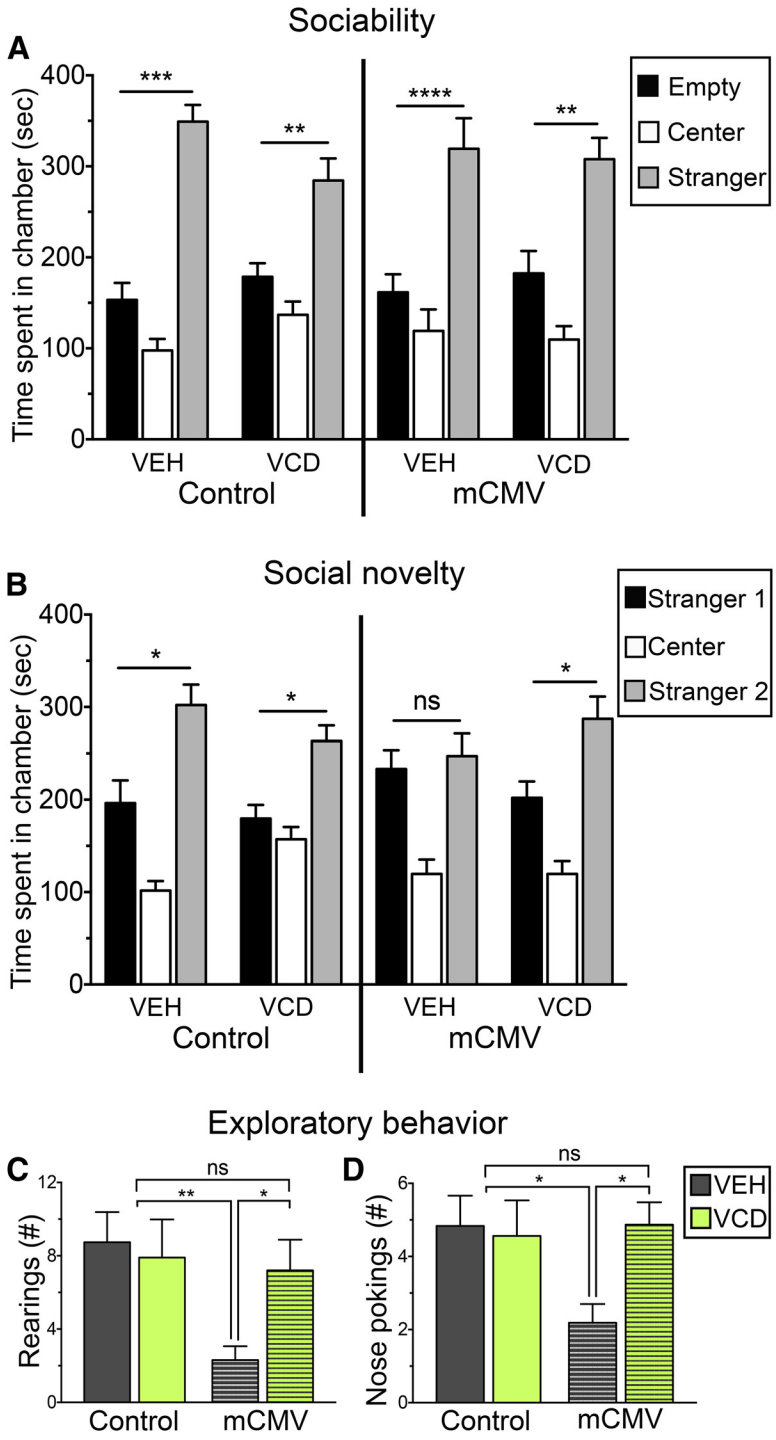

Figure 8. CMV infection during early development causes disturbances in social behavior and exploratory activity in adolescent mice. ***A***, ***B***, Sociability (***A***) and preference for social novelty (***B***) assessment in infected and control mice, with or without VCD treatment, by means of the three-chamber test. CMV-infected mice display regular sociability compared with control mice but lack a preference for a novel mouse over a known mouse. This lack of preference for social novelty is restored by VCD administration. ***C***, ***D***, Exploratory activity was assessed by quantification of rearing (***C***) and nose-poking (***D***) events in a novel environment. The altered exploratory behavior with decreased number of events identified in mCMV-infected animals is rescued by VCD. Values are reported as the mean ± SEM; $n = 10–13$ mice/group for social behavior, $n = 18–22$ mice/group for exploratory activity. ns, Not significant. $^{*}p < 0.05$, $^{**}p < 0.01$, $^{***}p < 0.001$, $^{****}p < 0.0001$; two-way ANOVA with repeated measures and Bonferroni's *post hoc* comparison in ***A*** and ***B***, Kruskal–Wallis with Dunn's *post hoc* test in ***C*** and ***D***.

compared with absolute brain weight, when somatic growth restriction is present. Subcutaneous VCD rescued the deficient brain growth induced by CMV, restoring brain-to-body weight ratio values similar to those in uninfected control mice.

Hypoplasia of the cerebellum is a common radiological finding in CMV-infected human babies (de Vries et al., 2004; Oosterom et al., 2015). A temporary delay in early postnatal cerebellar development was reported in newborn mice injected intraperitoneally with low titers of CMV (Koontz et al., 2008). In our infected mice, we identified the cerebellum as a preferential site for viral localization in the brain. We examined cerebellar anatomy and histology in control and infected mice with or without VCD therapy. CMV infection of the developing brain resulted in the disruption of cerebellar development, with a 60% decrease in the total area of this region compared with uninfected controls ($F = 8.56$, $p < 0.001$ ANOVA; Fig. 10*A*,*B*). CMV-infected mice displayed a substantial loss of PCs and a thinner ML, which contains PC dendritic trees, parallel fibers of the granule cells, Bergmann glia radial processes, and basket and stellate cells (Fig. 10*C–E*). Reduced thickness of the cerebellar IGL was also found (Fig. 10*F*). PCs were not only decreased in number but also misplaced (Fig. 10*G*). In addition, the external granular layer (EGL), normally undetectable after P21 in rodent brains (Ferguson, 1996), could still be identified in CMV-infected untreated mice at P30, whereas no EGL was visible in controls (Fig. 10*H*). Alignment of PCs and maturation of their dendritic trees, as well as granule cell precursor proliferation and inward migration from the EGL to the IGL, occur during the first 3 postnatal weeks of life in rodents (Inouye and Murakami, 1980; Ferguson, 1996). VCD treatment rescued the altered cerebellar development of infected animals, restoring normal cortical layer thickness and representation and markedly increasing PC number (Fig. 10*C–H*). These drug-mediated positive effects ultimately resulted in normalization of cerebellar size (Fig. 10*A*,*B*). No adverse side effects on either brain growth or morphometric parameters were detected in uninfected controls receiving VCD compared with their vehicle-treated counterparts.

Block of CMV infection in human fetal brain cells

Mouse and human forms of CMV share a close similarity in their viral genomes, but each retains species specificity (Rawlinson et al., 1996; Mocarski et al., 2007). In the experiments above, we used mCMV in mice. Here, to corroborate that the results we found above in our *in vivo* model with mCMV generalize to hCMV, we examined the actions of VCD on hCMV-infected human fetal astrocytes, a common cellular

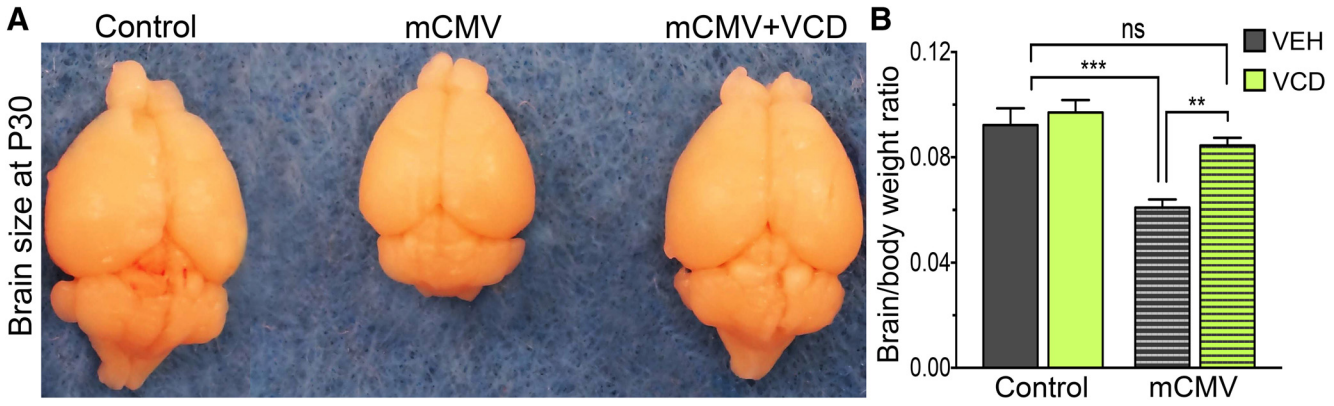

Figure 9. Valnoctamide reverses deficient brain growth induced by mCMV infection. ***A***, Photograph shows decreased brain size in an infected, untreated mouse (i.e., mCMV; middle) compared with an uninfected control (left). VCD treatment restores normal brain growth (mCMV+VCD, right). Quantification of VCD-mediated benefits on postnatal brain growth by calculation of brain-to-body weight ratio. Values are reported as the mean ± SEM; $n = 10$ mice/group (3 litters). ns, Not significant. $^{**}p < 0.01$, $^{***}p < 0.001$; one-way ANOVA with Bonferroni's *post hoc* test (***B***).

target that can play an important role in virus dispersal in the brain (Lokensgard et al., 1999; van den Pol et al., 1999). VCD substantially decreased hCMV infectivity of human fetal astrocytes as assessed by quantification of cells expressing the CMV-GFP-reporter (Fig. 11*A*). Viral replication was also diminished in the presence of the drug, with a reduction in viral titer by ~100-fold ($4.92 \times 10^5 \pm 5.84 \times 10^4$ pfu/ml in vehicle-treated cultures vs $6.31 \times 10^3 \pm 3.06 \times 10^3$ pfu/ml in VCD-treated cultures; $p < 0.0001$, Mann–Whitney *U* test; Fig. 11*B*).

VCD appears to act at an early stage of hCMV infection in fibroblasts and has no antiviral effect on the unrelated vesicular stomatitis virus (Ornaghi et al., 2016). To determine which step of the hCMV replication cycle was inhibited by VCD in human fetal astrocytes, we used a series of experiments to assess virus attachment to the cellular surface and penetration into the cytoplasmic space. This was accomplished by shifting the incubation temperature from 4°C (which allows virus attachment but not fusion and internalization) to 37°C (which allows virus fusion and internalization; Mocarski et al., 2007; Chan and Yurochko, 2014). Viral genome quantification by qRT-PCR showed that VCD appeared to block hCMV attachment to fetal astrocytes (Fig. 11*C*). In the presence of VCD, the amount of virus bound to the cell surface was decreased by 60% compared with control cultures not treated with VCD ($p = 0.0007$, unpaired Student's *t* test). VCD did not appear to block hCMV fusion/internalization in the astrocytes. This also corroborates that the mechanism of VCD block of CMV occurs at an early stage of infection and appears unrelated to the genomic mechanisms of other approved anti-CMV compounds.

Discussion

Our data show that low-dose VCD administered outside the brain during early development effectively suppresses CMV inside the brain of infected mice via two different sites of action. One is that VCD reduces peripheral levels of CMV, thereby decreasing the amount of virus available for entry into the brain. A second is that VCD acts directly within the brain to block existing brain CMV infection. These results are consistent with anti-CMV activity of VCD outside the brain (Ornaghi et al., 2016). Importantly, the antiviral action of VCD begins shortly after administration and effectively attenuates CMV levels throughout the brain during the critical period of postnatal brain development. This decrease in viral load is accompanied by a concomitant restoration of normal early neurological outcomes in infected neonatal mice treated with VCD. Late-onset neurobehavioral dysfunction, including motor impairment and social and exploratory behavior disturbances, as well as virally induced deficient brain growth and disrupted cerebellar development, are substantially attenuated in CMV-infected adolescent mice, which received VCD during the neonatal period, suggesting long-lasting beneficial effects. We detected no adverse collateral effects on the neurodevelopment of uninfected control mice treated with VCD.

An important underlying rationale of our study is that the newborn mouse brain is substantially less developed than the newborn human brain. Based on the timing of the brain growth spurt, initial neurogenesis, establishment and refinement of connections, myelination, and gliogenesis, the mouse CNS at birth is proposed to parallel the early second-trimester human fetal CNS (Clancy et al., 2001, 2007a,b; Branchi et al., 2003; Workman et al., 2013). This is a critical period for human brain development and for hCMV infection (Manicklal et al., 2013). By infecting mouse pups on the day of birth, this animal model provides an informative means to study the effects of CMV on the developing brain. Infected newborn mice display similar brain pathology and neurological symptoms to that reported in congenitally infected human infants, including microcephaly, cerebellar hypoplasia, neuronal loss, neurodevelopmental delays, motor impairments, and behavioral disturbances (Perlman and Argyle, 1992; de Vries et al., 2004; Pass et al., 2006; Lipitz et al., 2013; Kimberlin et al., 2015; De Kegel et al., 2016; James and Kimberlin, 2016). These data support the validity of this *in vivo* model for investigating CMV infection and novel anti-CMV treatments during early brain development.

Despite being partially effective, currently available CMV antiviral agents, including ganciclovir and its prodrug valganciclovir, foscarnet, cidofovir, and fomivirsen, display both toxic and teratogenic actions (Mercorelli et al., 2011; James and Kimberlin, 2016). For this reason, they are not approved or recommended for the treatment of pregnant women or infected fetuses or neonates, thus depriving those who may need it the most, or at best delaying treatment and hindering potential prevention or amelioration of CMV-induced brain defects during early development (Kimberlin et al., 2015). Because less severely infected human infants are also at risk for late-onset neurological compli-

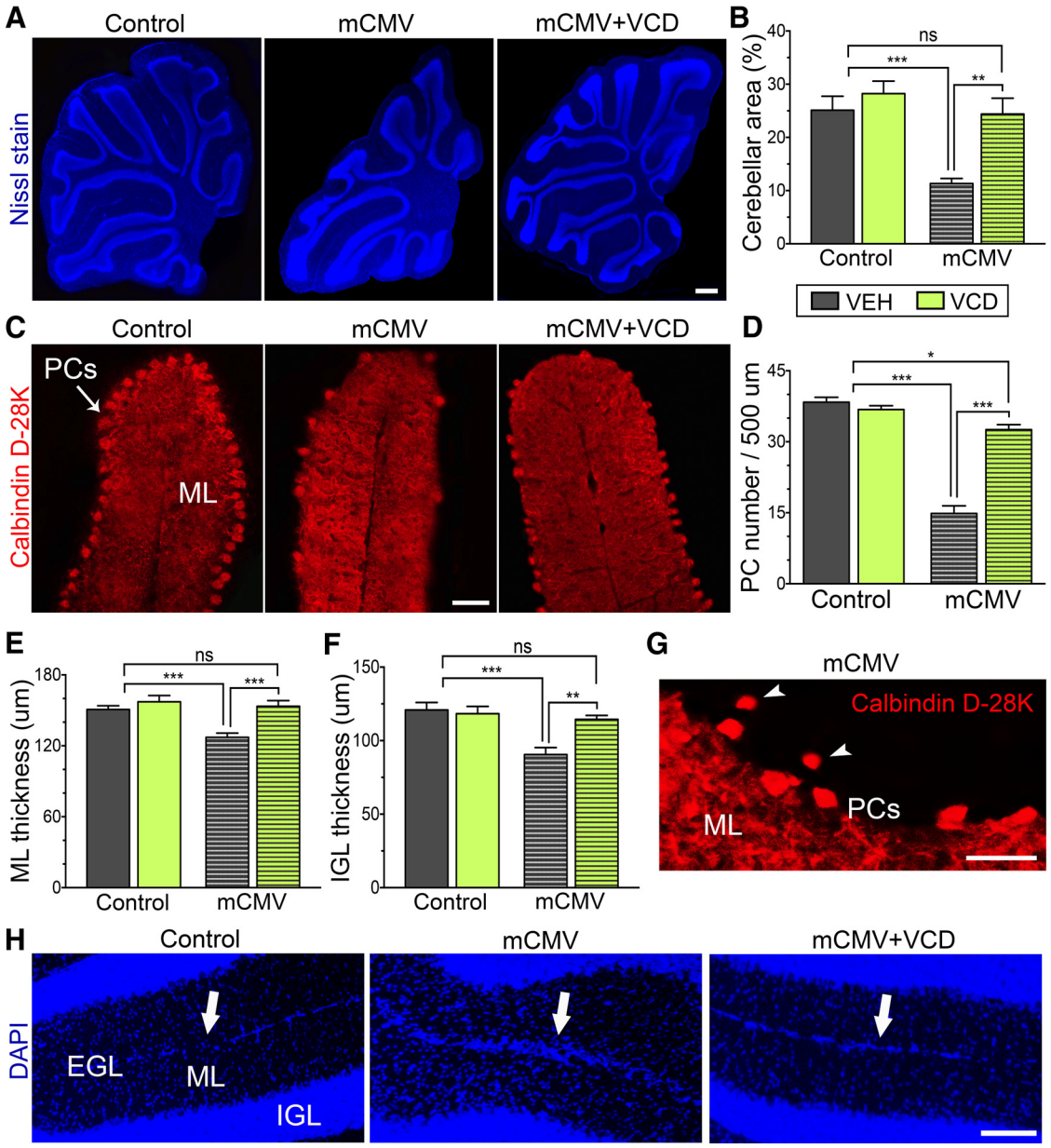

Figure 10. Valnoctamide substantially ameliorates cerebellar development in mCMV-infected mice. ***A***, Photomicrograph of representative fluorescent Nissl-stained cerebellar areas in control (left) and infected mice with (right, mCMV + VCD) or without (middle, mCMV) VCD. Note the delayed foliation in infected, untreated cerebellum, rescued by VCD. Scale bar, 200 μm. ***B***, Graph depicts cerebellar area, expressed as a percentage of total brain area (three sagittal sections/animal, five animals/group). ***C***, Photomicrograph showing cerebellar PCs and ML by means of calbindin D-28K staining. Infected, untreated cerebellum (middle) displays loss of PCs and thinner ML compared with uninfected control (left); VCD improves both parameters (right). Scale bar, 200 μm. ***D–F***, Quantification of PC number (***D***), and ML (***E***) and IGL thickness (***F***) along 500 μm of the primary fissure (prf; both sides; three sagittal sections/mouse, five mice/group). ***G***, Fluorescent micrograph of heterotopic PCs (arrowheads) identified in an infected untreated cerebellum. Scale bar, 100 μm. ***H***, Photomicrograph displays pathological persistence of EGL in mCMV-infected, untreated cerebellum at P30 (middle); no EGL could be identified at the same time point in uninfected control (left) and infected, VCD-treated cerebellum (right). Scale bar, 200 μm. Values are reported as the mean ± SEM. ns, Not significant. $^{*}p < 0.05$, $^{**}p < 0.01$, $^{***}p < 0.001$; one-way ANOVA with Bonferroni's *post hoc* test.

cations including cognitive and motor disabilities, behavioral disturbances, visual deficits, and hearing impairment (James and Kimberlin, 2016), the development of anti-CMV compounds with safer *in vivo* profiles that can be used in all infected neonates would be of substantive benefit.

VCD has shown no teratogenic or toxic activity in several studies using different animal models of early development (Radatz et al., 1998; Shekh-Ahmad et al., 2014; Mawasi et al., 2015; Wlodarczyk et al., 2015) and has been safely used for many years to treat neuropsychiatric disorders in adults (Stepansky, 1960; Goldberg, 1961; Harl, 1964). Further confirmation of its safety profile has derived from preclinical and clinical investigations of drug-mediated anti-convulsant and mood-stabilizing actions (Barel et al., 1997; Lindekens et al., 2000; Isoherranen et al., 2003; Winkler et al., 2005; Bersudsky et al., 2010; Kaufmann et al., 2010; Mareš et al., 2013; Shekh-Ahmad et al., 2015; Bialer et al., 2017; Modi et al., 2017). VCD is effective at a low-micromolar dose level, a slightly reduced level of efficacy compared with ganciclovir (Ornaghi et al., 2016); nonetheless, we found substantial CMV inhibition *in vivo* with subcutaneous delivery. We

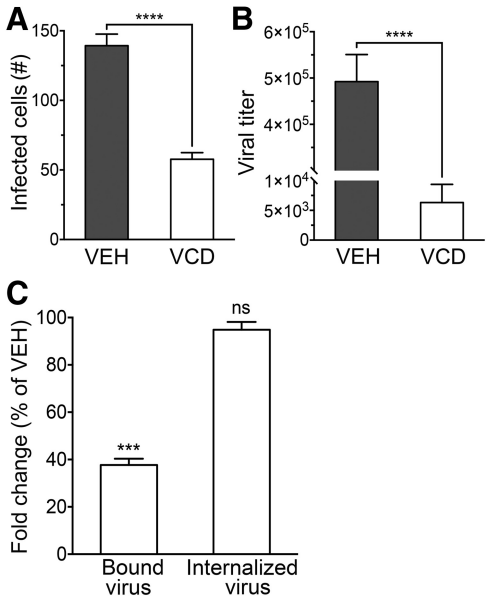

Figure 11. Valnoctamide suppresses hCMV infectivity and replication in human fetal astrocytes by blocking virus attachment to the cell. ***A***, ***B***, Human fetal astrocyte cells were pretreated (for 1 h) with VCD (100 μM) or vehicle (VEH) before inoculation with hCMV using an MOI of 0.1. VCD treatment decreased hCMV infectivity and replication as assessed by GFP-positive cell counting (***A***) and viral yield assay (***B***) at 48 hpi. ***C***, Virus-inoculated human fetal astrocytes were exposed to VCD or vehicle (100 μM) for 1 h at either 4°C or 37°C to assess hCMV attachment to ("bound virus") and internalization into ("internalized virus") the cell. Viral DNA was quantified by qRT-PCR and results expressed as the percentage of control (vehicle-treated cultures considered as 100%). Graphs represent the average of three separate experiments each performed in triplicate; error bars correspond to SE. ns, Not significant. ***$p < 0.001$, ****$p < 0.0001$, unpaired Student's t test in ***A*** and ***C***, Mann–Whitney U test in ***B***; in ***C***, significance refers to the comparison between VCD- and vehicle-treated cultures in each assay.

focused on newborn mice and identified potent anti-CMV actions of VCD; further studies focusing on VCD anti-CMV efficacy in fetal development and on the inhibition of transplacental transmission leading to brain infection will be beneficial.

The species specificity of CMV replication prevents testing the activity of novel antiviral agents on hCMV in animal models (Mocarski et al., 2007). Murine and human CMV share similar genomes, and anti-CMV drugs effective against mCMV are likely to also be active against hCMV (Rawlinson et al., 1996). The attenuation of hCMV infection of human fetal astrocytes by VCD corroborates the utility of our *in vivo* mouse model and suggests that VCD should also be effective against hCMV in the developing and adult human brain. In addition, VCD appears to act by blocking hCMV attachment to the cell membrane as described here in fetal astrocytes and previously in non-brain cells (Ornaghi et al., 2016), a mechanism of action that is different from that of currently available hCMV antiviral agents (Mercorelli et al., 2011). This also suggests the potential of VCD as a therapeutic option in immunocompromised adults, for whom the emergence of drug-resistant CMV strains has become a substantial challenge. Combination therapies, which can include two or more antiviral compounds, may help in controlling this problem, but are limited by drug-related toxicity and CMV cross-resistance to currently approved antiviral agents (Drew, 2000; James and Prichard, 2011). By displaying a good safety profile and a novel mechanism of anti-CMV activity, VCD may represent a valid therapeutic choice for effective and safe combination treatments potentially meriting testing in immunocompromised individuals. Other closely related molecules, for instance, valpromide, may also attenuate CMV (Ornaghi et al., 2016), but because valpromide can be metabolized to valproate, which can enhance virus infections, VCD is a better alternative due to the absence of conversion to valproate (Bialer et al., 1990; Bialer, 1991). That both related compounds show anti-CMV properties suggests that other structurally related compounds may also possess antiviral potential. These compounds have not previously been recognized as possessing anti-CMV actions; because both valpromide and VCD not only have similar antiepileptic actions and sedative properties in psychiatric patients, but also block CMV infections, this raises the possibility that the neurotropic and antiviral mechanisms of action may not be unrelated.

The dose of VCD we use here, with a 6 g developing mouse body weight, is 5 mg/kg. This amount is similar to or less than the dose of existing compounds used to treat CMV in clinical settings; for instance, assuming a 60 kg body weight, ganciclovir can be used from 5 up to 20 mg/kg/d in patients with serious infections (Kotton et al., 2013; Choopong et al., 2016; Genentech USA, 2016). Furthermore, the 5 mg/kg dose of VCD for treating CMV infection is lower than the dose used to attenuate seizures and neuropathic pain in neonatal and adult rodent experiments (Winkler et al., 2005; Kaufmann et al., 2010; Mareš et al., 2013; Shekh-Ahmad et al., 2014) and is less than the 20 mg/kg dose that can be used in humans to treat psychiatric dysfunction (Stepansky, 1960; Goldberg, 1961; Harl, 1964; Bersudsky et al., 2010). Together, these findings suggest that VCD may be able to attenuate CMV in the human brain at doses that should be both effective and tolerable.

CMV has been detected in a substantial number of brain tumors and has been postulated to play a role in the initiation or progression of malignant gliomas (Cobbs et al., 2007; Odeberg et al., 2007; Mitchell et al., 2008; Knight et al., 2013), although the possibility remains that CMV has a greater affinity for existing glial-type cells than for normal brain cells (van den Pol et al., 1999) rather than a causative role in oncogenesis. Although further substantiation is merited (Lau et al., 2005), if CMV does play a role in the enhancement of brain tumor growth, the use of VCD to attenuate CNS CMV may prove beneficial in attenuating tumor progression.

In conclusion, our study shows that subcutaneous low-dose VCD effectively and safely attenuates mCMV replication in the developing mouse brain and rescues these animals from virally induced brain defects and adverse neurological outcomes. We also show that VCD suppresses hCMV replication in human fetal brain cells by blocking viral attachment to the cell surface. Considering that VCD is already clinically available, has proven to be safe in multiple models of early development, and displays a novel mechanism of anti-CMV action, it merits further clinical testing for possible therapeutic utility in the treatment of CMV in the mature and developing human brain.

References

American Psychiatric Association (2013) Diagnostic and statistical manual of mental disorders (5th ed.). Arlington, VA: American Psychiatric Publishing.

Barel S, Yagen B, Schurig V, Soback S, Pisani F, Perucca E, Bialer M (1997) Stereoselective pharmacokinetic analysis of valnoctamide in healthy subjects and in patients with epilepsy. Clin Pharmacol Ther 61:442–449. CrossRef Medline

Bersudsky Y, Applebaum J, Gaiduk Y, Sharony L, Mishory A, Podberezsky A, Agam G, Belmaker RH (2010) Valnoctamide as a valproate substitute

with low teratogenic potential in mania: a double-blind, controlled, add-on clinical trial. Bipolar Disord 12:376–382. CrossRef Medline

Bialer M (1991) Clinical pharmacology of valpromide. Clin Pharmacokinet 20:114–122. CrossRef Medline

Bialer M, Haj-Yehia A, Barzaghi N, Pisani F, Perucca E (1990) Pharmacokinetics of a valpromide isomer, valnoctamide, in healthy subjects. Eur J Clin Pharmacol 38:289–291. CrossRef Medline

Bialer M, Johannessen SI, Levy RH, Perucca E, Tomson T, White HS (2017) Progress report on new antiepileptic drugs: a summary of the Thirteenth Eilat Conference on New Antiepileptic Drugs and Devices (EILAT XIII). Epilepsia 58:181–221. CrossRef Medline

Branchi I, Bichler Z, Berger-Sweeney J, Ricceri L (2003) Animal models of mental retardation: from gene to cognitive function. Neurosci Biobehav Rev 27:141–153. CrossRef Medline

Brooks SP, Dunnett SB (2009) Tests to assess motor phenotype in mice: a user's guide. Nat Rev Neurosci 10:519–529. CrossRef Medline

Butler D (2016) Zika raises profile of more common birth-defect virus. Nature 535:17. CrossRef Medline

Calamandrei G, Venerosi A, Branchi I, Chiarotti F, Verdina A, Bucci F, Alleva E (1999) Effects of prenatal AZT on mouse neurobehavioral development and passive avoidance learning. Neurotoxicol Teratol 21:29–40. CrossRef Medline

Cannon MJ, Davis KF (2005) Washing our hands of the congenital cytomegalovirus disease epidemic. BMC Public Health 5:70. CrossRef Medline

Carter RJ, Morton J, Dunnett SB (2001) Motor coordination and balance in rodents. Curr Protoc Neurosci Chapter 8:Unit 8.12. CrossRef Medline

Chan GC, Yurochko AD (2014) Analysis of cytomegalovirus binding/entry-mediated events. Methods Mol Biol 1119:113–121. CrossRef Medline

Cheeran MC, Lokensgard JR, Schleiss MR (2009) Neuropathogenesis of congenital cytomegalovirus infection: disease mechanisms and prospects for intervention. Clin Microbiol Rev 22:99–126, Table of Contents. CrossRef Medline

Choopong P, Vivittaworn K, Konlakij D, Thoongsuwan S, Pituksung A, Tesavibul N (2016) Treatment outcomes of reduced-dose intravitreal ganciclovir for cytomegalovirus retinitis. BMC Infect Dis 16:164. CrossRef Medline

Clancy B, Darlington RB, Finlay BL (2001) Translating developmental time across mammalian species. Neuroscience 105:7–17. CrossRef Medline

Clancy B, Finlay BL, Darlington RB, Anand KJ (2007a) Extrapolating brain development from experimental species to humans. Neurotoxicology 28:931–937. CrossRef Medline

Clancy B, Kersh B, Hyde J, Darlington RB, Anand KJ, Finlay BL (2007b) Web-based method for translating neurodevelopment from laboratory species to humans. Neuroinformatics 5:79–94. CrossRef Medline

Cobbs CS, Soroceanu L, Denham S, Zhang W, Britt WJ, Pieper R, Kraus MH (2007) Human cytomegalovirus induces cellular tyrosine kinase signaling and promotes glioma cell invasiveness. J Neurooncol 85:271–280. CrossRef Medline

Crawley JN (2007) Mouse behavioral assays relevant to the symptoms of autism. Brain Pathol 17:448–459. CrossRef Medline

De Kegel A, Maes L, Dhooge I, van Hoecke H, De Leenheer E, Van Waelvelde H (2016) Early motor development of children with a congenital cytomegalovirus infection. Res Dev Disabil 48:253–261. CrossRef Medline

de Vries LS, Gunardi H, Barth PG, Bok LA, Verboon-Maciolek MA, Groenendaal F (2004) The spectrum of cranial ultrasound and magnetic resonance imaging abnormalities in congenital cytomegalovirus infection. Neuropediatrics 35:113–119. CrossRef Medline

Dollard SC, Grosse SD, Ross DS (2007) New estimates of the prevalence of neurological and sensory sequelae and mortality associated with congenital cytomegalovirus infection. Rev Med Virol 17:355–363. CrossRef Medline

Drew WL (2000) Ganciclovir resistance: a matter of time and titre. Lancet 356:609–610. CrossRef Medline

Ferguson SA (1996) Neuroanatomical and functional alterations resulting from early postnatal cerebellar insults in rodents. Pharmacol Biochem Behav 55:663–671. CrossRef Medline

Fleming SM, Salcedo J, Fernagut PO, Rockenstein E, Masliah E, Levine MS, Chesselet MF (2004) Early and progressive sensorimotor anomalies in mice overexpressing wild-type human α-synuclein. J Neurosci 24:9434–9440. CrossRef Medline

Fleming SM, Ekhator OR, Ghisays V (2013) Assessment of sensorimotor function in mouse models of Parkinson's disease. J Vis Exp (76):e50303. CrossRef Medline

Fox WM (1965) Reflex-ontogeny and behavioural development of the mouse. Anim Behav 13:234–241. CrossRef Medline

Fukui Y, Shindoh K, Yamamoto Y, Koyano S, Kosugi I, Yamaguchi T, Kurane I, Inoue N (2008) Establishment of a cell-based assay for screening of compounds inhibiting very early events in the cytomegalovirus replication cycle and characterization of a compound identified using the assay. Antimicrob Agents Chemother 52:2420–2427. CrossRef Medline

Gandhi MK, Khanna R (2004) Human cytomegalovirus: clinical aspects, immune regulation, and emerging treatments. Lancet Infect Dis 4:725–738. CrossRef Medline

Garofoli F, Lombardi G, Orcesi S, Pisoni C, Mazzucchelli I, Angelini M, Balottin U, Stronati M (2017) An Italian prospective experience on the association between congenital cytomegalovirus infection and autistic spectrum disorder. J Autism Dev Disord 47:1490–1495. CrossRef Medline

Gault E, Michel Y, Dehée A, Belabani C, Nicolas JC, Garbarg-Chenon A (2001) Quantification of human cytomegalovirus DNA by real-time PCR. J Clin Microbiol 39:772–775. CrossRef Medline

Genentech USA (2016) Cytovene (ganciclovir sodium), prescribing information. South San Francisco, CA: Genentech USA.

Goldberg M (1961) Effects of a new tranquilizer, valmethamide, in psychiatric outpatient care. Dis Nerv Syst 22:346–348. Medline

Guyenet SJ, Furrer SA, Damian VM, Baughan TD, La Spada AR, Garden GA (2010) A simple composite phenotype scoring system for evaluating mouse models of cerebellar ataxia. J Vis Exp (39):e1787. CrossRef Medline

Harl FM (1964) Clinical study of valnoctamide on 70 neuropsychiatric clinic patients undergoing ambulatory treatment. Presse Med 72:753–754. Medline

Inouye M, Murakami U (1980) Temporal and spatial patterns of Purkinje cell formation in the mouse cerebellum. J Comp Neurol 194:499–503. CrossRef Medline

Isoherranen N, White HS, Klein BD, Roeder M, Woodhead JH, Schurig V, Yagen B, Bialer M (2003) Pharmacokinetic-pharmacodynamic relationships of (2S,3S)-valnoctamide and its stereoisomer (2R,3S)-valnoctamide in rodent models of epilepsy. Pharm Res 20:1293–1301. CrossRef Medline

James SH, Kimberlin DW (2016) Advances in the prevention and treatment of congenital cytomegalovirus infection. Curr Opin Pediatr 28:81–85. CrossRef Medline

James SH, Prichard MN (2011) The genetic basis of human cytomegalovirus resistance and current trends in antiviral resistance analysis. Infect Disord Drug Targets 11:504–513. CrossRef Medline

Jarvis MA, Wang CE, Meyers HL, Smith PP, Corless CL, Henderson GJ, Vieira J, Britt WJ, Nelson JA (1999) Human cytomegalovirus infection of caco-2 cells occurs at the basolateral membrane and is differentiation state dependent. J Virol 73:4552–4560. Medline

Kaufmann D, Yagen B, Minert A, Wlodarczyk B, Finnell RH, Schurig V, Devor M, Bialer M (2010) Evaluation of the antiallodynic, teratogenic and pharmacokinetic profile of stereoisomers of valnoctamide, an amide derivative of a chiral isomer of valproic acid. Neuropharmacology 58:1228–1236. CrossRef Medline

Kenneson A, Cannon MJ (2007) Review and meta-analysis of the epidemiology of congenital cytomegalovirus (CMV) infection. Rev Med Virol 17:253–276. CrossRef Medline

Kimberlin DW, Jester PM, Sánchez PJ, Ahmed A, Arav-Boger R, Michaels MG, Ashouri N, Englund JA, Estrada B, Jacobs RF, Romero JR, Sood SK, Whitworth MS, Abzug MJ, Caserta MT, Fowler S, Lujan-Zilbermann J, Storch GA, DeBiasi RL, Han JY, et al (2015) Valganciclovir for symptomatic congenital cytomegalovirus disease. N Engl J Med 372:933–943. CrossRef Medline

Knight A, Arnouk H, Britt W, Gillespie GY, Cloud GA, Harkins L, Su Y, Lowdell MW, Lamb LS (2013) CMV-independent lysis of glioblastoma by ex vivo expanded/activated Vdelta1+ gammadelta T cells. PLoS One 8:e68729. CrossRef Medline

Koontz T, Bralic M, Tomac J, Pernjak-Pugel E, Bantug G, Jonjic S, Britt WJ (2008) Altered development of the brain after focal herpesvirus infection of the central nervous system. J Exp Med 205:423–435. CrossRef Medline

Kosmac K, Bantug GR, Pugel EP, Cekinovic D, Jonjic S, Britt WJ (2013) Glucocorticoid treatment of MCMV infected newborn mice attenuates

CNS inflammation and limits deficits in cerebellar development. PLoS Pathog 9:e1003200. CrossRef Medline

Kotton CN, Kumar D, Caliendo AM, Asberg A, Chou S, Danziger-Isakov L, Humar A (2013) Updated international consensus guidelines on the management of cytomegalovirus in solid-organ transplantation. Transplantation 96:333–360. CrossRef Medline

Lau SK, Chen YY, Chen WG, Diamond DJ, Mamelak AN, Zaia JA, Weiss LM (2005) Lack of association of cytomegalovirus with human brain tumors. Mod Pathol 18:838–843. CrossRef Medline

Lindekens H, Smolders I, Khan GM, Bialer M, Ebinger G, Michotte Y (2000) In vivo study of the effect of valpromide and valnoctamide in the pilocarpine rat model of focal epilepsy. Pharm Res 17:1408–1413. CrossRef Medline

Lipitz S, Yinon Y, Malinger G, Yagel S, Levit L, Hoffman C, Rantzer R, Weisz B (2013) Risk of cytomegalovirus-associated sequelae in relation to time of infection and findings on prenatal imaging. Ultrasound Obstet Gynecol 41:508–514. CrossRef Medline

Lokensgard JR, Cheeran MC, Gekker G, Hu S, Chao CC, Peterson PK (1999) Human cytomegalovirus replication and modulation of apoptosis in astrocytes. J Hum Virol 2:91–101. Medline

Luong TN, Carlisle HJ, Southwell A, Patterson PH (2011) Assessment of motor balance and coordination in mice using the balance beam. J Vis Exp (49):e2376. CrossRef Medline

Manicklal S, Emery VC, Lazzarotto T, Boppana SB, Gupta RK (2013) The "silent" global burden of congenital cytomegalovirus. Clin Microbiol Rev 26:86–102. CrossRef Medline

Mareš P, Kubová H, Hen N, Yagen B, Bialer M (2013) Derivatives of valproic acid are active against pentetrazol-induced seizures in immature rats. Epilepsy Res 106:64–73. CrossRef Medline

Mawasi H, Shekh-Ahmad T, Finnell RH, Wlodarczyk BJ, Bialer M (2015) Pharmacodynamic and pharmacokinetic analysis of CNS-active constitutional isomers of valnoctamide and sec-butylpropylacetamide—amide derivatives of valproic acid. Epilepsy Behav 46:72–78. CrossRef Medline

Mercorelli B, Lembo D, Palù G, Loregian A (2011) Early inhibitors of human cytomegalovirus: state-of-art and therapeutic perspectives. Pharmacol Ther 131:309–329. CrossRef Medline

Mitchell DA, Xie W, Schmittling R, Learn C, Friedman A, McLendon RE, Sampson JH (2008) Sensitive detection of human cytomegalovirus in tumors and peripheral blood of patients diagnosed with glioblastoma. Neuro Oncol 10:10–18. CrossRef Medline

Mocarski, Shenk T, Pass RF (2007) Cytomegaloviruses. In: Fields virology (Fields BN, Knipe DM, Howley PM, eds), pp 2702–2751. Philadelphia: Lippincott, Williams & Wilkins.

Modi HR, Ma K, Chang L, Chen M, Rapoport SI (2017) Valnoctamide, which reduces rat brain arachidonic acid turnover, is a potential nonteratogenic valproate substitute to treat bipolar disorder. Psychiatry Res 254:279–283. CrossRef Medline

Odeberg J, Wolmer N, Falci S, Westgren M, Sundtröm E, Seiger A, Söderberg-Nauclér C (2007) Late human cytomegalovirus (HCMV) proteins inhibit differentiation of human neural precursor cells into astrocytes. J Neurosci Res 85:583–593. CrossRef Medline

Ogawa N, Hirose Y, Ohara S, Ono T, Watanabe Y (1985) A simple quantitative bradykinesia test in MPTP-treated mice. Res Commun Chem Pathol Pharmacol 50:435–441. Medline

Oosterom N, Nijman J, Gunkel J, Wolfs TF, Groenendaal F, Verboon-Maciolek MA, de Vries LS (2015) Neuro-imaging findings in infants with congenital cytomegalovirus infection: relation to trimester of infection. Neonatology 107:289–296. CrossRef Medline

Ornaghi S, Davis JN, Gorres KL, Miller G, Paidas MJ, van den Pol AN (2016) Mood stabilizers inhibit cytomegalovirus infection. Virology 499:121–135. CrossRef Medline

Pass RF, Fowler KB, Boppana SB, Britt WJ, Stagno S (2006) Congenital cytomegalovirus infection following first trimester maternal infection: symptoms at birth and outcome. J Clin Virol 35:216–220. CrossRef Medline

Perlman JM, Argyle C (1992) Lethal cytomegalovirus infection in preterm infants: clinical, radiological, and neuropathological findings. Ann Neurol 31:64–68. CrossRef Medline

Pouliot W, Bialer M, Hen N, Shekh-Ahmad T, Kaufmann D, Yagen B, Ricks K, Roach B, Nelson C, Dudek FE (2013) A comparative electrographic analysis of the effect of sec-butyl-propylacetamide on pharmacoresistant status epilepticus. Neuroscience 231:145–156. CrossRef Medline

Radatz M, Ehlers K, Yagen B, Bialer M, Nau H (1998) Valnoctamide, valpromide and valnoctic acid are much less teratogenic in mice than valproic acid. Epilepsy Res 30:41–48. CrossRef Medline

Rawlinson WD, Farrell HE, Barrell BG (1996) Analysis of the complete DNA sequence of murine cytomegalovirus. J Virol 70:8833–8849. Medline

Rawlinson WD, Hamilton ST, van Zuylen WJ (2016) Update on treatment of cytomegalovirus infection in pregnancy and of the newborn with congenital cytomegalovirus. Curr Opin Infect Dis 29:615–624. CrossRef Medline

Reuter JD, Gomez DL, Wilson JH, Van Den Pol AN (2004) Systemic immune deficiency necessary for cytomegalovirus invasion of the mature brain. J Virol 78:1473–1487. CrossRef Medline

Sakamoto A, Moriuchi H, Matsuzaki J, Motoyama K, Moriuchi M (2015) Retrospective diagnosis of congenital cytomegalovirus infection in children with autism spectrum disorder but no other major neurologic deficit. Brain Dev 37:200–205. CrossRef Medline

Scattoni ML, Gandhy SU, Ricceri L, Crawley JN (2008) Unusual repertoire of vocalizations in the BTBR T+tf/J mouse model of autism. PLoS One 3:e3067. CrossRef Medline

Schneider T, Przewlocki R (2005) Behavioral alterations in rats prenatally exposed to valproic acid: animal model of autism. Neuropsychopharmacology 30:80–89. CrossRef Medline

Semple BD, Blomgren K, Gimlin K, Ferriero DM, Noble-Haeusslein LJ (2013) Brain development in rodents and humans: identifying benchmarks of maturation and vulnerability to injury across species. Prog Neurobiol 106-107:1–16. CrossRef Medline

Shekh-Ahmad T, Hen N, Yagen B, McDonough JH, Finnell RH, Wlodarczyk BJ, Bialer M (2014) Stereoselective anticonvulsant and pharmacokinetic analysis of valnoctamide, a CNS-active derivative of valproic acid with low teratogenic potential. Epilepsia 55:353–361. CrossRef Medline

Shekh-Ahmad T, Mawasi H, McDonough JH, Yagen B, Bialer M (2015) The potential of sec-butylpropylacetamide (SPD) and valnoctamide and their individual stereoisomers in status epilepticus. Epilepsy Behav 49:298–302. CrossRef Medline

Shi L, Fatemi SH, Sidwell RW, Patterson PH (2003) Maternal influenza infection causes marked behavioral and pharmacological changes in the offspring. J Neurosci 23:297–302. Medline

Soerensen J, Jakupoglu C, Beck H, Förster H, Schmidt J, Schmahl W, Schweizer U, Conrad M, Brielmeier M (2008) The role of thioredoxin reductases in brain development. PLoS One 3:e1813. CrossRef Medline

Spampanato J, Dudek FE (2014) Valnoctamide enhances phasic inhibition: a potential target mechanism for the treatment of benzodiazepine-refractory status epilepticus. Epilepsia 55:e94–e98. CrossRef Medline

Stepansky W (1960) A clinical study in the use of valmethamide, an anxiety-reducing drug. Curr Ther Res Clin Exp 2:144–147. Medline

St Omer VE, Ali SF, Holson RR, Duhart HM, Scalzo FM, Slikker W Jr (1991) Behavioral and neurochemical effects of prenatal methylenedioxymethamphetamine (MDMA) exposure in rats. Neurotoxicol Teratol 13:13–20. CrossRef Medline

Stubbs EG, Ash E, Williams CP (1984) Autism and congenital cytomegalovirus. J Autism Dev Disord 14:183–189. CrossRef Medline

Tanaka M, Machida Y, Niu S, Ikeda T, Jana NR, Doi H, Kurosawa M, Nekooki M, Nukina N (2004) Trehalose alleviates polyglutamine-mediated pathology in a mouse model of Huntington disease. Nat Med 10:148–154. CrossRef Medline

Tanaka T (1998) Effects of litter size on behavioral development in mice. Reprod Toxicol 12:613–617. CrossRef Medline

Tsutsui Y (2009) Effects of cytomegalovirus infection on embryogenesis and brain development. Congenit Anom (Kyoto) 49:47–55. CrossRef Medline

Turner KM, Lee HC, Boppana SB, Carlo WA, Randolph DA (2014) Incidence and impact of CMV infection in very low birth weight infants. Pediatrics 133:e609–e615. CrossRef Medline

van den Pol AN, Mocarski E, Saederup N, Vieira J, Meier TJ (1999) Cytomegalovirus cell tropism, replication, and gene transfer in brain. J Neurosci 19:10948–10965. Medline

van den Pol AN, Reuter JD, Santarelli JG (2002) Enhanced cytomegalovirus infection of developing brain independent of the adaptive immune system. J Virol 76:8842–8854. CrossRef Medline

van den Pol AN, Robek MD, Ghosh PK, Ozduman K, Bandi P, Whim MD, Wollmann G (2007) Cytomegalovirus induces interferon-stimulated

gene expression and is attenuated by interferon in the developing brain. J Virol 81:332–348. CrossRef Medline

van den Pol AN, Mao G, Yang Y, Ornaghi S, Davis JN (2017) Zika virus targeting in the developing brain. J Neurosci 37:2161–2175. CrossRef Medline

Vieira J, Schall TJ, Corey L, Geballe AP (1998) Functional analysis of the human cytomegalovirus US28 gene by insertion mutagenesis with the green fluorescent protein gene. J Virol 72:8158–8165. Medline

Winkler I, Blotnik S, Shimshoni J, Yagen B, Devor M, Bialer M (2005) Efficacy of antiepileptic isomers of valproic acid and valpromide in a rat model of neuropathic pain. Br J Pharmacol 146:198–208. CrossRef Medline

Wlodarczyk BJ, Ogle K, Lin LY, Bialer M, Finnell RH (2015) Comparative teratogenicity analysis of valnoctamide, risperidone, and olanzapine in mice. Bipolar Disord 17:615–625. CrossRef Medline

Workman AD, Charvet CJ, Clancy B, Darlington RB, Finlay BL (2013) Modeling transformations of neurodevelopmental sequences across mammalian species. J Neurosci 33:7368–7383. CrossRef Medline

Yamashita Y, Fujimoto C, Nakajima E, Isagai T, Matsuishi T (2003) Possible association between congenital cytomegalovirus infection and autistic disorder. J Autism Dev Disord 33:455–459. CrossRef Medline

Yang M, Silverman JL, Crawley JN (2011) Automated three-chambered social approach task for mice. Curr Protoc Neurosci Chapter 8:Unit 8.26.

Zurbach KA, Moghbeli T, Snyder CM (2014) Resolving the titer of murine cytomegalovirus by plaque assay using the M2-10B4 cell line and a low viscosity overlay. Virol J 11:71. CrossRef Medline

Neurobiology of Disease

Zika Virus Targeting in the Developing Brain

Anthony N. van den Pol, Guochao Mao, Yang Yang, Sara Ornaghi, and John N. Davis
Department of Neurosurgery, Yale University School of Medicine, New Haven, Connecticut 06520

Zika virus (ZIKV), a positive-sense RNA flavivirus, has attracted considerable attention recently for its potential to cause serious neurological problems, including microcephaly, cortical thinning, and blindness during early development. Recent findings suggest that ZIKV infection of the brain can occur not only during very early stages of development, but also in later fetal/early neonatal stages of maturation. Surprisingly, after peripheral inoculation of immunocompetent mice on the day of birth, the first cells targeted throughout the brain were isolated astrocytes. At later stages, more neurons showed ZIKV immunoreactivity, in part potentially due to ZIKV release from infected astrocytes. In all developing mice studied, we detected infection of retinal neurons; in many mice, this was also associated with infection of the lateral geniculate, suprachiasmatic nuclei, and superior colliculus, suggesting a commonality for the virus to infect cells of the visual system. Interestingly, in mature mice lacking a Type 1 interferon response (IFNR $^{-/-}$), after inoculation of the eye, the initial majority of infected cells in the visual system were glial cells along the optic tract. ZIKV microinjection into the somatosensory cortex on one side of the normal mouse brain resulted in mirror infection restricted to the contralateral somatosensory cortex without any infection of midline brain regions, indicating the virus can move by axonal transport to synaptically coupled brain loci. These data support the view that ZIKV shows considerable complexity in targeting the CNS and may target different cells at different stages of brain development.

Key words: astrocyte; behavior dysfunction; development; infection; neurotropic; virus

Significance Statement

Zika virus (ZIKV) can cause substantial damage to the developing human brain. Here we examine a developmental mouse model of ZIKV infection in the newborn mouse in which the brain is developmentally similar to a second-trimester human fetus. After peripheral inoculation, the virus entered the CNS in all mice tested and initially targeted astrocytes throughout the brain. Infections of the retina were detected in all mice, and infection of CNS visual system nuclei in the brain was common. We find that ZIKV can be transported axonally, thereby enhancing virus spread within the brain. These data suggest that ZIKV infects multiple cell types within the brain and that astrocyte infection may play a more important role in initial infection than previously appreciated.

Introduction

Within the last 2 years, a virus of African origin, Zika virus (ZIKV), has become established in the Americas. The emergence of this virus has generated considerable alarm, particularly related to the potential for ZIKV to cause neurological complications in fetal humans, as first noted in Brazil (Kleber de Oliveira et al., 2016; Lessler et al., 2016). More recently ZIKV infection has expanded to a number of other countries within the Americas. In the United States, ZIKV has become a substantial concern as a growing number of infections are beginning to be reported in late summer 2016 (McCarthy, 2016) (http://www.cdc.gov/zika/geo/united-states.html). The most profound problem associated with ZIKV is the generation of permanent neurological dysfunction in infected fetuses. ZIKV-related brain dysfunction is found not only in obvious cases of microcephaly, which may be most commonly associated with ZIKV infection during the first trimester of human pregnancy (Brasil et al., 2016; Kleber de Oliveira et al., 2016), but also in neonates with a normal head size born from mothers infected during later stages of pregnancy (França et al., 2016; Hazin et al., 2016). The probability of fetal microcephaly in ZIKV-infected pregnant women ranges from 1% to 13%; there is a concern that other nervous system complications, although not as obvious as microcephaly, may be more prevalent (Cauchemez et al., 2016; Johansson et al., 2016; Trevathan, 2016). For instance, in addition to microcephaly, cortical thinning, abnormal limb postures, blindness and visual impairment, and auditory dysfunction have also been reported in neonates born from ZIKV-infected mothers (Calvet et al., 2016; de Carvalho Leal et al., 2016; de Fatima Vasco Aragoa et al., 2016; Driggers et al., 2016; França et al., 2016; Martines et al., 2016; van der Linden et al., 2016).

Received Oct. 6, 2016; revised Dec. 6, 2016; accepted Jan. 3, 2017.

Author contributions: A.N.v.d.P. and S.O. designed research; A.N.v.d.P., G.M., Y.Y., S.O., and J.N.D. performed research; G.M., S.O., and J.N.D. analyzed data; A.N.v.d.P. and J.N.D. wrote the paper.

This work was supported by National Institutes of Health RO1 CA175577 and CA188359. We thank Dr. Brett Lindenbach for the initial supply of ZIKV.

The authors declare no competing financial interests.

Correspondence should be addressed to Dr. Anthony N. van den Pol, Department of Neurosurgery, Yale University School Medicine, 333 Cedar Street, New Haven, CT 06520. E-mail: anthony.vandenpol@yale.edu.

DOI:10.1523/JNEUROSCI.3124-16.2017

 0270-6474/17/372161-15$15.00/0

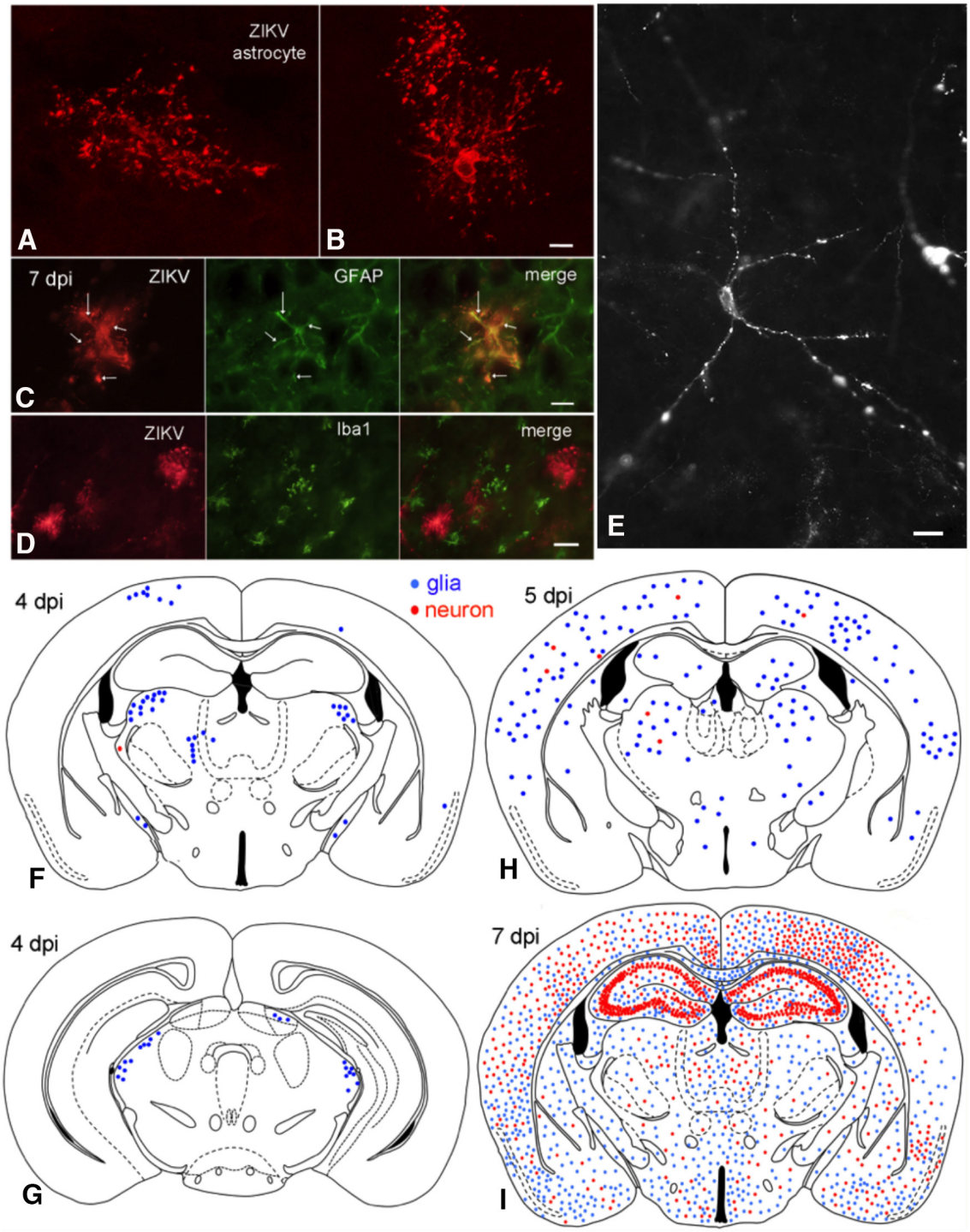

Figure 1. ZIKV enters brain after intraperitoneal inoculation. ***A***, ***B***, Confocal scanning microscope images of ZIKV-infected astrocytes. Scale bar, 8 μm. ***C***, ZIKV-infected glial cell (red) contains GFAP immunoreactivity (green). The ZIKV immunoreactivity is found out to the tips of the glial processes, whereas the GFAP is confined more to the shaft of primary and secondary processes. Scale bar, 10 μm. ***D***, No colocalization of ZIKV and Iba1 (a microglia marker) was detected. Scale bar, 12 μm. ***E***, ZIKV-infected neuron with punctate immunoreactivity at 7 dpi after P0 inoculation. Scale bar, 15 μm. ***F***, ***G***, At 4 dpi after intraperitoneal inoculation, most infected cells are glia (blue dots); only rare neurons (red dots) are infected. ***G***, More caudal midbrain region of the same mouse as in ***F***. ***H***, More cells, particularly astrocytes, are infected at 5 dpi. ***I***, At 7 dpi after intraperitoneal inoculation, ZIKV has spread throughout the brain. At this stage of development, ZIKV infects glia (blue) and neurons (red) with little preference for brain regions, with the exception in this case of strong hippocampal neuron infection, including the dentate gyrus, CA3, and CA1.

ZIKV infections are also associated with an increase in Guillain-Barré syndrome (Dos Santos et al., 2016; Paixão et al., 2016; Niemeyer et al., 2017), an immune system-mediated motor dysfunction that can lead to paralysis that often dissipates over time (Hughes and Rees, 1997).

Models for studying ZIKV have been developed focusing in part on mice immunodeficient for Type 1 IFN responses (Lazear et al., 2016; Rossi et al., 2016) or on organoid brain-like cultures (Cugola et al., 2016; Dang et al., 2016; Garcez et al., 2016; Li et al., 2016) or E15 embryonic brain slices (Brault et al., 2016). However, within the developing brain, the types of cells infected and the progression of infection has not yet received much attention despite the importance of understanding ZIKV targeting in the brain. A number of papers have examined *in utero* infections of the mouse fetus (Aliota et al.,

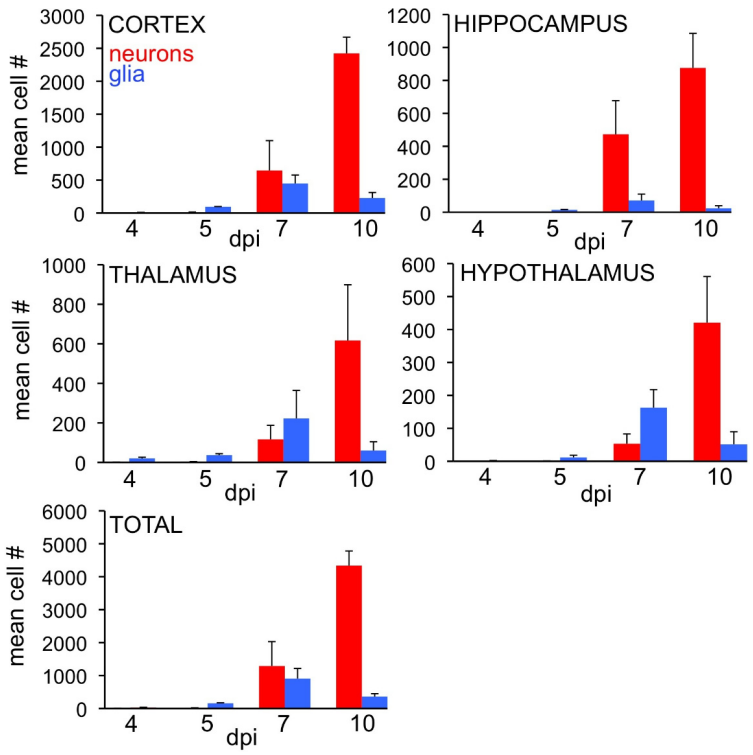

Figure 2. Relative number of infected astrocytes and neurons/section during development. The number of immunoreactive astrocytes (blue) and neurons (red) was counted at 4, 5, 7, and 10 dpi ($n = 3$/time point). Bar indicates SD. Initially at 4 and 5 dpi, most of the cells had the morphology of astrocytes in all 4 areas studied. By 7 dpi, astrocytes were still more numerous than neurons in thalamus and hypothalamus, whereas neurons were more numerous in cortex and hippocampus. By 10 dpi, infected neurons were more prevalent in all areas studied.

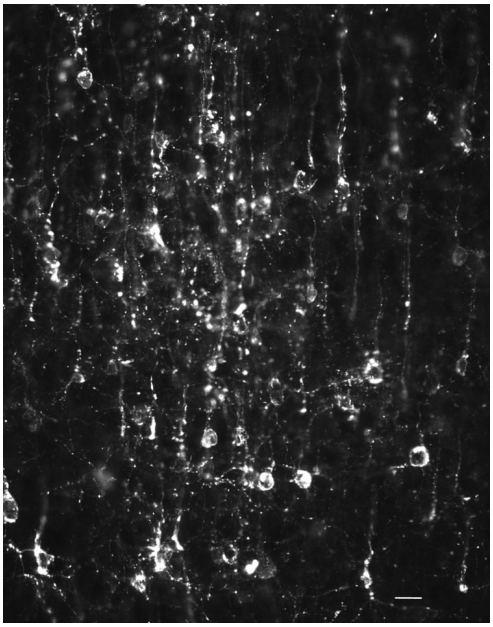

Figure 3. Cortical neurons infected with ZIKV 7 dpi after intraperitoneal inoculation at P0. Substantive infection is seen in the primary dendrites extending toward the right to the cortical surface. The beaded dendrites are typical of the neuronal deterioration in late stages of ZIKV infection. Scale bar, 30 μm.

2016; Miner et al., 2016a, b; Yockey et al., 2016); in normal mice, ZIKV generally does not infect the fetus; in immunodeficient mice lacking a Type 1 IFN response, the pregnant mother usually shows a lethal response to the virus, but the fetal mice do get infected. Our focus here is to study the ontogeny of ZIKV movement into the brain in an animal model consisting of normal newborn neonatal mice to examine the progression of ZIKV infection within the developing CNS after peripheral inoculation. An important underlying rationale of our study is that the newborn mouse brain is substantially less developed than the newborn human fetal brain. Based on initial neurogenesis, axon extension, establishment and refinement of connections, myelin formation, increase in brain volume, and early behavioral milestones, the neonatal mouse CNS at birth approximately parallels a second-trimester human fetus (Clancy et al., 2001, 2007a, b; Workman et al., 2013), and therefore represents a viable animal model for studying potential nervous system complications associated with ZIKV infection in later phases of human gestation.

Materials and Methods

Zika virus. ZIKV of the Asian lineage, from Cambodia (ZIKV FSS13025) (Heang et al., 2012), similar to the ZIKV that has entered the Americas was used. ZIKV was a gift from Dr. Brett Lindenbach (Yale University). ZIKV was harvested from infected cultures of Vero-E6 cells at 4 dpi, filtered, divided into aliquots and stored at −80°C. Harvested viral stocks were titered by plaque assay on Vero cells and typically had a concentration of 2×10^7 plaque forming units (pfu)/ml. We also used pseudorabies virus (PRV) expressing a GFP reporter (gift from Dr.Lynn Enquist, Princeton University) for one set of experiments using coinjection of both PRV+ZIKV into the left cortex: 150 nl of PRV (1.5×10^2 pfu) + 150 nl ZIKV (3×10^2 pfu), mixed together and injected simultaneously in the same volume.

Immunocytochemistry. Antiserum against ZIKV was generated in adult male rats. Seven weeks after an initial subcutaneous and intraperitoneal inoculation with ZIKV, rats were inoculated a second time. Eight days later, serum was harvested. A goat anti-rat secondary antiserum was used for immunostaining (Invitrogen A11007).

Immunostaining was done on both cell cultures and histological sections from control and inoculated mice. Frozen or vibratome sections were cut from fixed mouse brain and after incubation in normal goat serum containing 0.3% Triton X-100, were incubated in primary rat anti-ZIKV serum. After multiple washes of the primary antiserum, goat-anti-rat conjugated to Alexa-594 was used at dilutions of 1:300 to 1:1000 for 1–2 h, and was then washed off. After immunostaining, some sections were labeled with DAPI or counterlabeled with immunostaining against GFAP (ThermoFisher, PA5–16291) or IBA1/microglia (Biocare Medical, CP290A) (Ito et al., 1998) using a different fluorophore.

The ZIKV antiserum only labeled cells that had been inoculated with ZIKV and not uninfected control cells. Absence of the primary antibody resulted in no staining. The primary anti-ZIKV serum was used for immunofluorescent labeling at a dilution between 1:1000 and 1:20,000. The antiserum labeled ZIKV-infected cells well; it worked poorly in immunolabeling a different flavivirus, Yellow Fever virus-17D.

In vitro *neutralization of ZIKV infection.* To determine whether the antiserum would block ZIKV infection, a plaque reduction neutralization assay was performed, similar to that used for Dengue virus (Russell et al., 1967; Roehrig et al., 2008). Antiserum was heat-inactivated at 56°C for 30 min, then serial twofold dilutions were mixed with ZIKV and incubated for 1 h at room temperature. The dilutions were then plaque assayed in quadruplicate on Vero cells. A 50% reduction of ZIKV plaques was found at an antiserum dilution of 1:640.

Mice. Several primary strains of mice were used: immunocompetent C57BL/6 and Swiss Webster mice and immunocompromised mice that lacked the Type 1 IFNR (IFNR$^{-/-}$) and therefore showed no Type 1 IFN response. Immunocompetent neonatal mice ($n = 51$) were inoculated intraperitoneally on the day of birth (P0) with 3 μl (6×10^4 pfu) or 7 μl (4×10^5 pfu) ZIKV for survival and histological analyses, or with 10^3 or 2×10^3 pfu intraperitoneally for one survival study. Sample size was based on previous publications. Other virus concentrations are described in some of the figures. Some mice expressed GFP in the pro-opiomelanocortin (POMC) cells (gift from Dr. M.Low), and were used to identify amacrine cells in the infected retina. Mice intended for CNS immunocytochemistry were killed by anesthetic overdose at daily intervals after inoculation and perfused transcardially with saline followed by 4% paraformaldehyde.

Anesthetized mice lacking the Type 1 IFNR (IFNR$^{-/-}$) 4 weeks old were given an intraocular injection of ZIKV (1 μl containing 2×10^4 pfu ZIKV). Work with ZIKV in mice and rats was approved by the university committee on animal use. With the exception of the use of pregnant female mice to investigate the possibility of ZIKV transfer to the fetus, all other experiments used both male and female mice randomly. In survival experiments, if a mouse showed substantial deterioration with difficulty in movement and trouble feeding, it was killed, as per recommendation of the university committee on animal use.

Cell culture. A number of cell types were used *in vitro* including Vero-E6 African green monkey kidney epithelial cells obtained from C. Cepko (Harvard University), human brain primary astrocytes were described previously (Ozduman et al., 2008), and primary mouse brain cells harvested from C57BL/6 mice shortly after birth. Vero cells were grown in MEM supplemented with 10% FBS. Primary mouse and human brain cells were grown in DMEM with 10% FBS. All cultures were maintained in a Napco incubator with humidified atmosphere at 37°C with 5% CO_2.

Virus release and plaque assay. A virus release assay for ZIKV progeny was performed using human brain astrocytes. Briefly, cells were plated in 35 mm dishes and inoculated the following day with ZIKV (multiplicity of infection = 20) and allowed to adsorb for 1 h at 37°C. After adsorption, the cells were washed with PBS and 3 ml of fresh media was added to the well. At the indicated time points, 60 μl samples of media were withdrawn and replaced with the same volume of fresh media. Samples were stored at −80°C for later viral titer determination by plaque assay. The plaque assay consisted of inoculation of Vero cells grown in 12 well plates using serial dilutions of ZIKV samples for 1 h at 37°C. Cells were then washed with PBS and an overlay of 1% carboxymethyl cellulose in MEM with FBS was applied. ZIKV-infected cultures were incubated 4 d to allow time for plaque development. Plaques were visualized with crystal violet after removal of the carboxymethyl cellulose overlay.

IFN experiments in human and mouse brain cells. Nearly confluent primary cultures of human and mouse brain cells were grown in 24 well plates and pretreated for 12 h with IFN-αA/D (Sigma I4401) at the indicated concentrations. After IFN pretreatment, cultures were inoculated with ZIKV (6×10^5 pfu/well) or media (control) and incubated for 2 d. Cells were then fixed and ZIKV immunocytochemical labeling was done. ZIKV-infected cells were counted from triplicate wells for each condition.

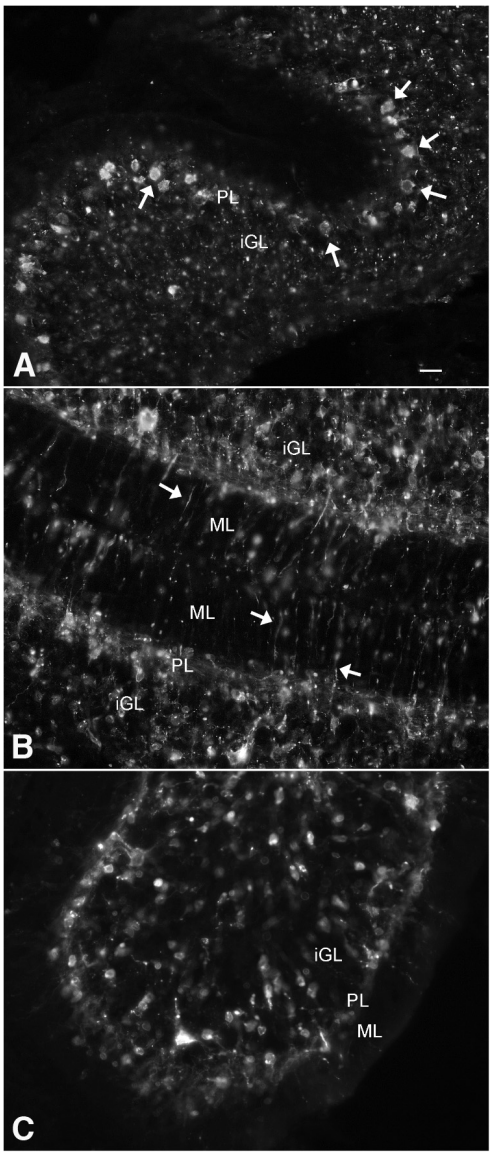

Figure 4. ZIKV heterogeneity of infection in cerebellum. At 7 dpi after intraperitoneal inoculation at P0, the cerebellum from the same mouse shows different stages and cell types of infection in different lobes of the cerebellar cortex in ***A–C***. ***A***, Arrows indicate Purkinje cells in Purkinje cell layer and punctate labeling suggestive of late-stage infection in the granule layer. ***B***, Thin processes in the molecular layer are seen, and a large number of cells in the granule layer. ***C***, Unlike in ***B***, few processes or infected cells are detected in the molecular layer. Scale bar, 30 μm. iGL, Internal granule cell layer; PL, Purkinje cell layer containing cell bodies of Purkinje cells and Bergmann glia; ML, molecular layer.

Results

ZIKV invasion of developing brain

To study the natural progression of ZIKV infection in the developing brain, normal immune competent C57BL/6 mice were inoculated intraperitoneally on the day of birth with the Asian lineage of ZIKV (ZIKV FSS13025); this is the lineage of ZIKV that has spread to the Americas and has raised serious concerns about ZIKV-induced brain dysfunctions. Intraperitoneal inoculations in part model the potential movement of the virus transplacentally along the umbilical cord into the fetus better than subcutaneous application. Mice ($n = 27$) were killed by anesthetic overdose and fixative perfusion at daily intervals from 1 d post inoculation (1 dpi) to 10 dpi and at longer intervals after 10 dpi. We used a high-titer anti-ZIKV antiserum we raised in rats; the antiserum blocked ZIKV infection *in vitro* and was selective with immunocytochemistry for ZIKV-infected cells and did not label noninfected cells (see Fig. 4). We found no detectable ZIKV immunoreactivity in the brain at 1 and 2 dpi. At 3 dpi, we began to find ZIKV infection in muscles of the head, in the neural retina, and in a small number of cells within the brain. At 4 dpi ($n = 6$ of 6), infection in the brain was common, and consistently found in all mice ($n = 18$) after 4 dpi indicating a strong propensity for CNS infections after inoculation of the virus outside the brain (Fig. 1*F–I*).

Although most previous studies, in particular those based on brain organoids, have focused on potential infections of neuronal progenitor cells, surprisingly, initial infections targeted glial cells of the normal developing brain, particularly cells with an astrocyte morphology and a large number of short processes; both cell body and glial processes to their terminal endfeet showed robust

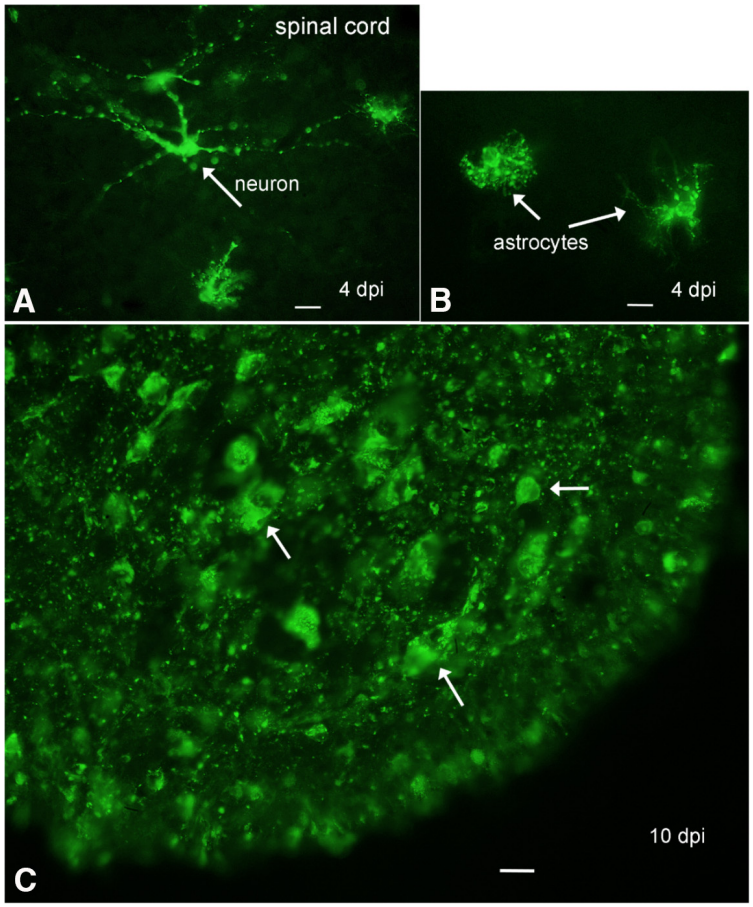

Figure 5. ZIKV in spinal cord. ***A***, In the lumbar spinal cord gray matter, an immunoreactive degenerating neuron is seen (arrow) along with some immunoreactive glia, 4 dpi. Scale bar, 20 μm. ***B***, Two immunoreactive astrocytes are shown (arrows), 4 dpi. Scale bar, 20 μm. ***C***, By 10 dpi, the ventral horn of the spinal cord is filled with ZIKV-immunoreactive cells and processes. Scale bar, 15 μm.

ZIKV immunoreactivity as detected with fluorescence and confocal laser microscopy (Fig. 1*A*,*B*). ZIKV-infected glial cells with an astrocyte morphology expressed the astrocyte antigen GFAP immunoreactivity in many of the glial processes (Fig. 1*C*) but did not express microglia antigen Iba1 (Fig. 1*D*). One possible explanation for the initial astrocyte targeting may be the glial endfeet that wrap around the vasculature and present one of the first cellular targets for a virus leaving a blood vessel.

Neurons were infected soon after the glia, either from ZIKV released by infected glia or as primary infections via the vascular system. In initial stages of infection at 4 and 5 dpi, isolated infected glia far outnumbered neurons, as shown by the high number of cells with astrocyte morphology (Fig. 1*F*,*G*, blue) compared with those with a neuronal morphology (Fig. 1*F–H*, red). Over the next 2–3 d (6–8 dpi), the number of infected neurons increased (Fig. 1*I*) to the point that neurons began to outnumber infected glia in some brain areas. High densities of infected neurons were detected in different brain regions, sometimes initially on one side of the brain, suggestive of local release and infection. In some mice at 7 dpi, robust neuronal infection was seen in CA1 and CA3 regions of the hippocampus (Fig. 1*I*), raising concerns about long-term memory problems in ZIKV-infected human fetuses. We quantified the number of astrocytes and neurons in 4 brain regions from 4 to 10 dpi. All regions showed a predominant initial infection of astrocytes at 4 and 5 dpi. The hippocampus showed the greatest neuronal density at 7 dpi; and all regions studied, including cortex, hippocampus, thalamus, and hypothalamus, showed greater infection of neurons than of astrocytes by 10 dpi (Fig. 2).

We found no propensity for infections to develop around the ventricular system in developing mice (Fig. 1*F–I*), arguing against a hypothesis that ZIKV initially enters the brain via the CSF at this stage of development. ZIKV infection was characterized by granular immunoreactivity, typical of the ZIKV "factories" that have been described (Bell et al., 1971). ZIKV was found not only in the cell body, but immunoreactive granules could be found far out in distal dendrites (Fig. 1*E*). In cortical pyramidal cells, ZIKV granular immunoreactivity was seen in both the primary large apical dendrite extending toward the cortical surface (Fig. 3) and also in smaller secondary basal dendrites ramifying closer to the cell body. In cortical interneurons, ZIKV granules were found in the cell body and multiple dendrites. Thin immunoreactive axons were detected at later stages of neuronal infection.

One striking finding was the initial widespread but sparse infection throughout multiple brain regions seen in all 4 dpi mice ($n = 6$) after intraperitoneal inoculation (Fig. 1*F*,*G*). In many cases, only a few cells were infected in any given region. Although not a common initial target of the virus, the cerebellum showed very strong infection by 7–10 dpi. The cerebellum is of particular interest during this period because it is one of the few areas of the brain in which (granule) neurons are still being generated from neural precursor cells during the postnatal day 6–10 period of development. Considerable heterogeneity of infection was noted, particularly in the early phase of infection. Even in a single cerebellum, different cells, including granule cells, Purkinje cells, and Bergmann glia, at different stages of infection appeared in different lobes of the developing cerebellar cortex (Fig. 4). ZIKV immunoreactivity was seen in cells and processes in different layers, including the molecular, Purkinje, and inner granule cell layer with different levels of infection and cell deterioration in different regions of the same cerebellum (Fig. 4).

To examine the spinal cord of developing mice, P0 mice ($n = 6$) received intraperitoneal inoculations of ZIKV. As we found motor dysfunction involving the hind limbs (see below), we focused on the lumbar spinal cord, a region of the cord that innervates the hind legs. Similar to the brain, small numbers of infected cells were seen at 4 dpi in the gray matter of the spinal cord. Astrocytes were often infected (Fig. 5*B*), and neurons were also found (Fig. 5*A*). By 10 dpi, the entire gray matter was heavily infected with cells in all spinal cord lamina. An image of the high infection rate in the ventral horn of lumbar cord is shown in Fig. 5*C*. All 6 mice examined from 4 to 10 dpi showed ZIKV infection in the lumbar spinal cord after intraperitoneal inoculation.

To determine the time course of ZIKV infection and detection in brain cells, we inoculated human brain cultures consisting

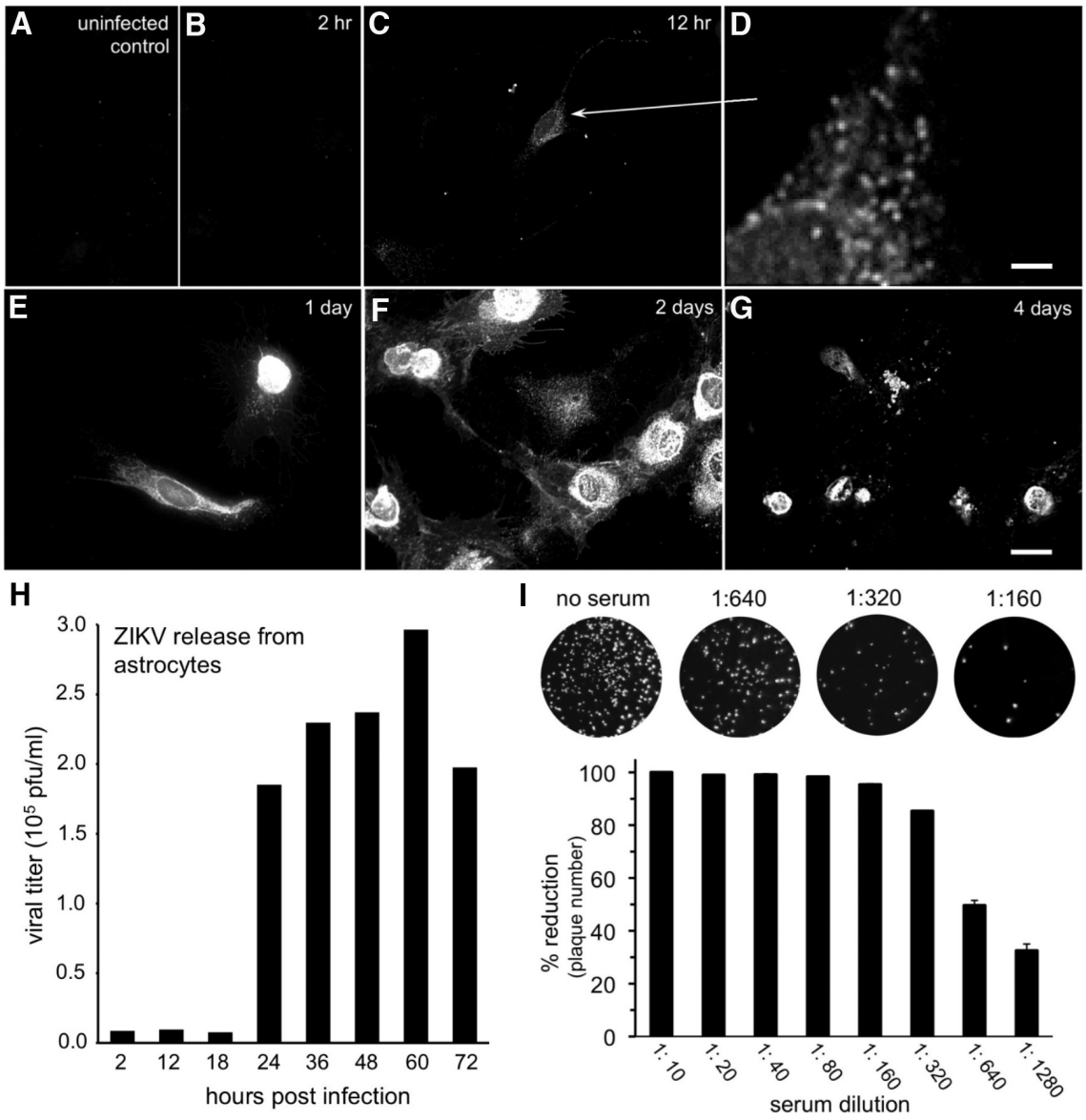

Figure 6. Time course of ZIKV infection of brain cells. Primary human brain cells, mostly astrocytes, were inoculated at time 0, then fixed and immunostained at the indicated intervals. Immunoreactivity was not seen in uninfected control cultures (***A***) or at 2 h (***B***) post inoculation (hpi). ***C***, ***D***, At 12 hpi, faint immunoreactivity was detected in granules (***D***, enlarged region shown by arrow). Scale bar, 2.5 μm. Immunoreactivity became stronger up to 2 d (***E***, ***F***) post inoculation (dpi). ***G***, By 4 dpi, many of the immunoreactive cells were dead or dying. Scale bars: ***A–C***, ***E–G***, 25 μm. ***H***, Viral release was measured using additional cultures infected after ZIKV (multiplicity of infection 20) inoculation for 1 h, then washed and supplied with fresh media. Media samples were harvested at the indicated time points, and viral concentration was measured by plaque assay. ***I***, ZIKV antiserum harvested from inoculated rats and used for immunolabeling was tested for the ability to neutralize ZIKV infection *in vitro*. Top, Counterstained cultures show the decline in viral plaque number after exposure to increasing concentrations of antiserum, corroborating antibody selectivity. Bottom, Bar graph indicates that a 50% reduction in ZIKV plaque number was obtained at 1:640 antiserum dilution. Error bars indicate SEM ($n = 4$).

mostly of astrocytes, and examined these at multiple intervals after inoculation (Fig. 6*A–G*). ZIKV immunoreactivity was first detected at 12 hpi, and stronger staining at 1–3 dpi; by 4 dpi, infected cells showed substantial degeneration and cell death as determined with phase contrast microscopy and dead-cell ethidium homodimer labeling. Based on an *in vitro* progeny virus release assay, glia showed a productive infection and began to release new progeny ZIKV by 24 h after inoculation as determined by plaque assay of the culture medium (Fig. 6*H*). These data suggest that ZIKV may begin infecting cells in the brain 24 h earlier than we detect infection, and that astrocyte release of new ZIKV progeny may account for at least part of the increase in subsequent neuronal infection. Flaviviruses in general are often cytolytic but in some cells can establish a chronic infection (Lindenbach and Rice, 2001). In the current study, we found multiple indications that ZIKV infection led to cell death, including a reduced cell number *in vitro* as infection continued, labeling of infected cultured cells with the dead cell stain ethidium homodimer, the appearance of cells in the brain at late stages of infection with beaded processes and degenerating cell body, and the loss of neurons from some brain regions, such as the hippocampus in later stages of infection.

Previous reports based in part on *in vitro* brain organoid cultures have shown that ZIKV infects neural precursors (Cugola et al., 2016; Dang et al., 2016; Li et al., 2016) consistent with our detection of strong cerebellar infection during the period of granule cell generation during P7–P10 cerebellar development (Fig. 4). In neonatal mice, neither the subventricular zone nor the

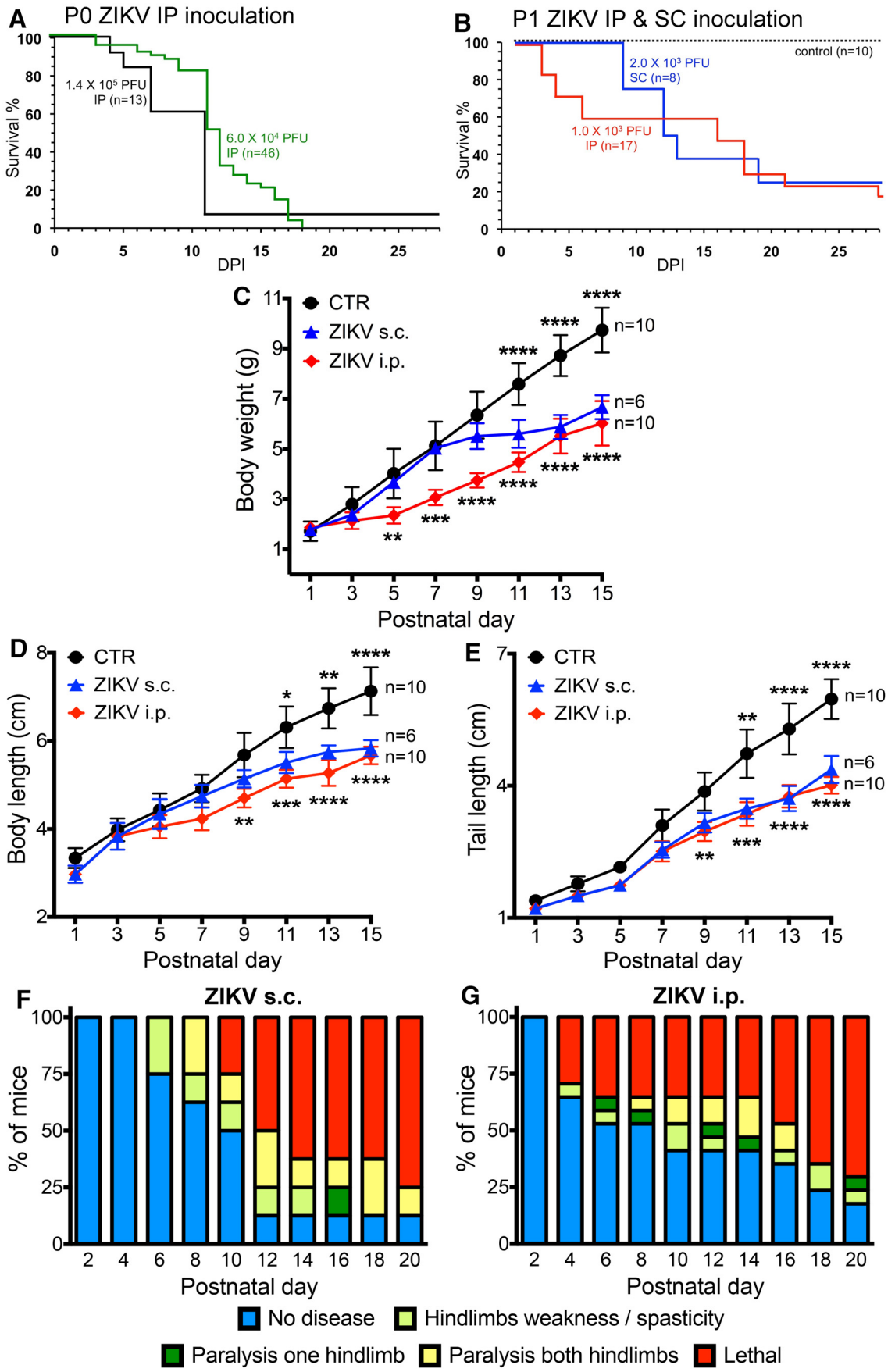

Figure 7. Zika virus in newborn mice induces neurological disease and death. ***A***, Survival for P0 mice inoculated with 1.4×10^5 (black line, $n = 13$) or 6×10^4 pfu intraperitoneally (green line, $n = 46$). Total, $n = 59$. C57BLand Swiss Webster mice were used; because we found no statistical difference between the two strains, data were combined. ***B***, Survival for slightly older P1 mice with 10^3 pfu intraperitoneally ($n = 17$) or 2×10^3 subcutaneously ($n = 8$). Noninfected controls, $n = 10$; total, $n = 35$. ***$p < 0.001$, survival at P28 (Log-rank, (*Figure legend continues.*)

rostral migratory stream between the subventricular zone and the olfactory bulb, both sites containing neural progenitor cells, showed any preferential early infection (Fig. 1*F–I*). In older P18 brains of mice surviving P0 ZIKV inoculation, areas were identified containing sporadic infected cells in addition to groups of dead cells that lacked detectable active ZIKV infection, suggesting local elimination of the virus in the maturing brain.

Neurological/behavioral dysfunction

Neonatal infection, either by intraperitoneal or subcutaneous inoculation ($n = 84$ for i.p. and s.c.), was often lethal within 2–3 weeks (Fig. 7*B*) for higher doses (6×10^4 to 1.4×10^5 pfu). With lower doses ($1–2 \times 10^3$ pfu), approximately one-fourth of the animals survived past 3 weeks (Fig. 7*B*). Subsequent to ZIKV inoculation, behavioral and developmental disturbances were noted indicating neurological deterioration, including reduced body weight gain (Fig. 7*C*) and reduced growth with reduced body length and attenuated tail length (Fig. 7*D*,*E*). We also studied neurological dysfunction from the time of infection. Infected mice showed a progressive increase in motor dysfunction particularly involving the hind legs (Fig. 7*F*,*G*). ZIKV-mediated neurological disturbances were first seen at 3 and 4 dpi with intraperitoneal inoculation (Fig. 7*G*), and slightly later with subcutaneous inoculation (Fig. 7*F*), consistent with the first detection of ZIKV in the brain. The ongoing behavioral and neurological deterioration of infected mice suggests that the ZIKV lethality may in large part be due to the spread of ZIKV within the brain over time.

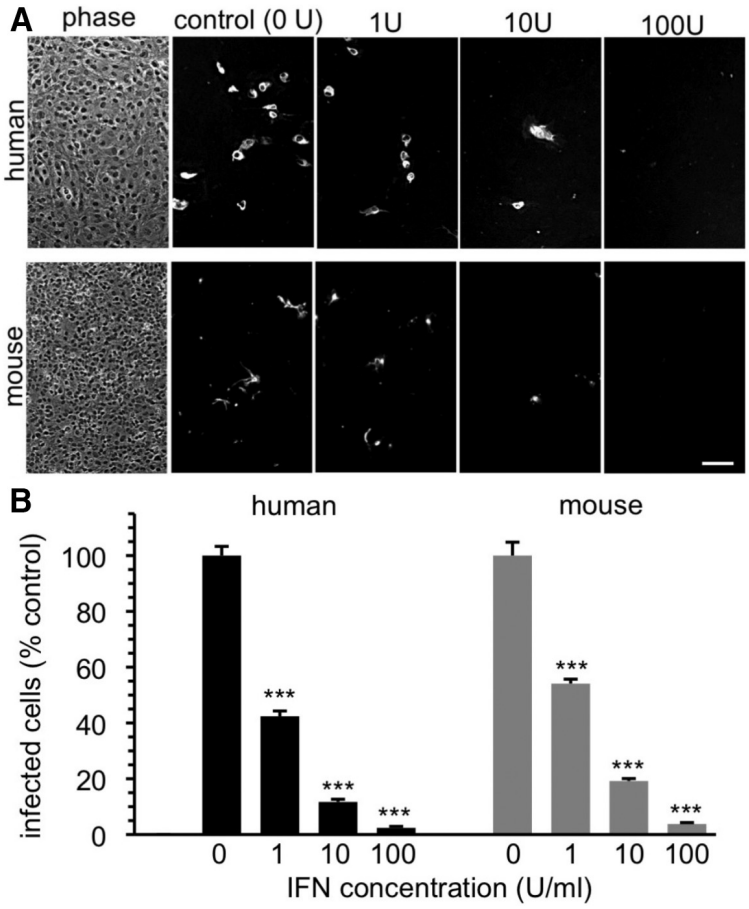

Figure 8. Type 1 IFN blocks ZIKV infection of human and mouse brain cells. ***A***, Human (top) and mouse (bottom) brain cells were inoculated with ZIKV in the absence (0 U) or presence of 1, 10, and 100 U/ml IFN (Sigma I4401). Left, Phase shows typical cell density. Cells were fixed and immunostained at 2 dpi. Scale bar, 100 μm. ***B***, Bar graph represents percentage infected cells, with controls set to 100%. IFN reduces infection in a dose-dependent manner. Error bars indicate SEM ($n = 3$). ***$p < 0.01$ (ANOVA with Bonferroni post-test).

ZIKV in normal and IFNR deficient adult mice

In contrast to developing mice, normal adult mice receiving ZIKV intraperitoneally ($n = 10$) showed no lethal response to the virus and no long-term symptoms, as previously noted (Dang et al., 2016; Rossi et al., 2016). We examined the brains of adult mice inoculated intraperitoneally with ZIKV and found no infection within the CNS at 7–10 dpi ($n = 7$), suggesting that the normal immune system is sufficient to keep the virus out of the brain after early development. However, direct intracranial microinjection of ZIKV (0.5 μl/10^4 pfu) was lethal in 3 of 6 normal mice. Similar to adult mice, adult rats ($n = 3$) inoculated with ZIKV peripherally showed no obvious adverse symptoms over a period of 2 months.

Because one critical factor in the developing brain is a reduced IFN response (Lazear et al., 2016; Rossi et al., 2016), we tested adult IFNR$^{-/-}$ mice lacking the Type I IFNR. ZIKV was lethal in 6 of 6 adult IFNR$^{-/-}$ mice after intracerebral injection (0.5 μl/10^4 pfu). Immunocytochemical analysis of adult IFNR$^{-/-}$ mice at 6 d after intraperitoneal inoculation revealed widespread ZIKV infection throughout the brain with both astrocytes and neurons showing strong virus immunoreactivity, indicating that IFN plays an important role in attenuating ZIKV infection in the CNS. During development, Type 1 IFN responses increase with age to provide a first line of defense against viral infections of the brain, and in the adult can upregulate antiviral gene expression even at some distance from the initial site of virus infection (van den Pol, 2006; van den Pol et al., 2007, 2014). However, during early development, IFN responses to virus presence may be weaker than in the adult (van den Pol et al., 2007), potentially allowing virus spread in the immature brain.

In vitro experiments showed that both mouse and human brain cells are protected against ZIKV by Type 1 IFN (Fig. 8), similar to the ability of IFN to attenuate ZIKV infection in skin cells (Hamel et al.,

←

(*Figure legend continued.*) Mantel-Cox) test. The 25% survival in ZIKV subcutaneously, 22.2% survival in ZIKV intraperitoneal controls (CTR). ***C–E***, Somatic parameters of postnatal development. Data are mean ± SEM. Two-way ANOVA with postnatal day as repeated measures, Holm-Sidak's multiple-comparison test: *$p < 0.05$; **$p < 0.01$; ***$p < 0.001$; ****$p < 0.0001$. ZIKV subcutaneously versus CTR shown above CTR line; ZIKV intraperitoneally versus CTR shown below ZIKV intraperitoneal line. ***F***, Neurological symptoms were assessed for 20 d for P1 mice inoculated subcutaneously with 2×10^3 pfu ZIKV similar to the observations of Lazear et al. (2016) in older mice. Chart shows that neurological symptoms occur in greater numbers of mice over time. ***G***, P1 mice were infected intraperitoneally with 10^3 pfu with ZIKV and signs of neurological dysfunction assessed for 20 d. The percentage of each group of mice displaying the indicated motor dysfunction is shown. These are from the same mice evaluated for lethality and somatic development.

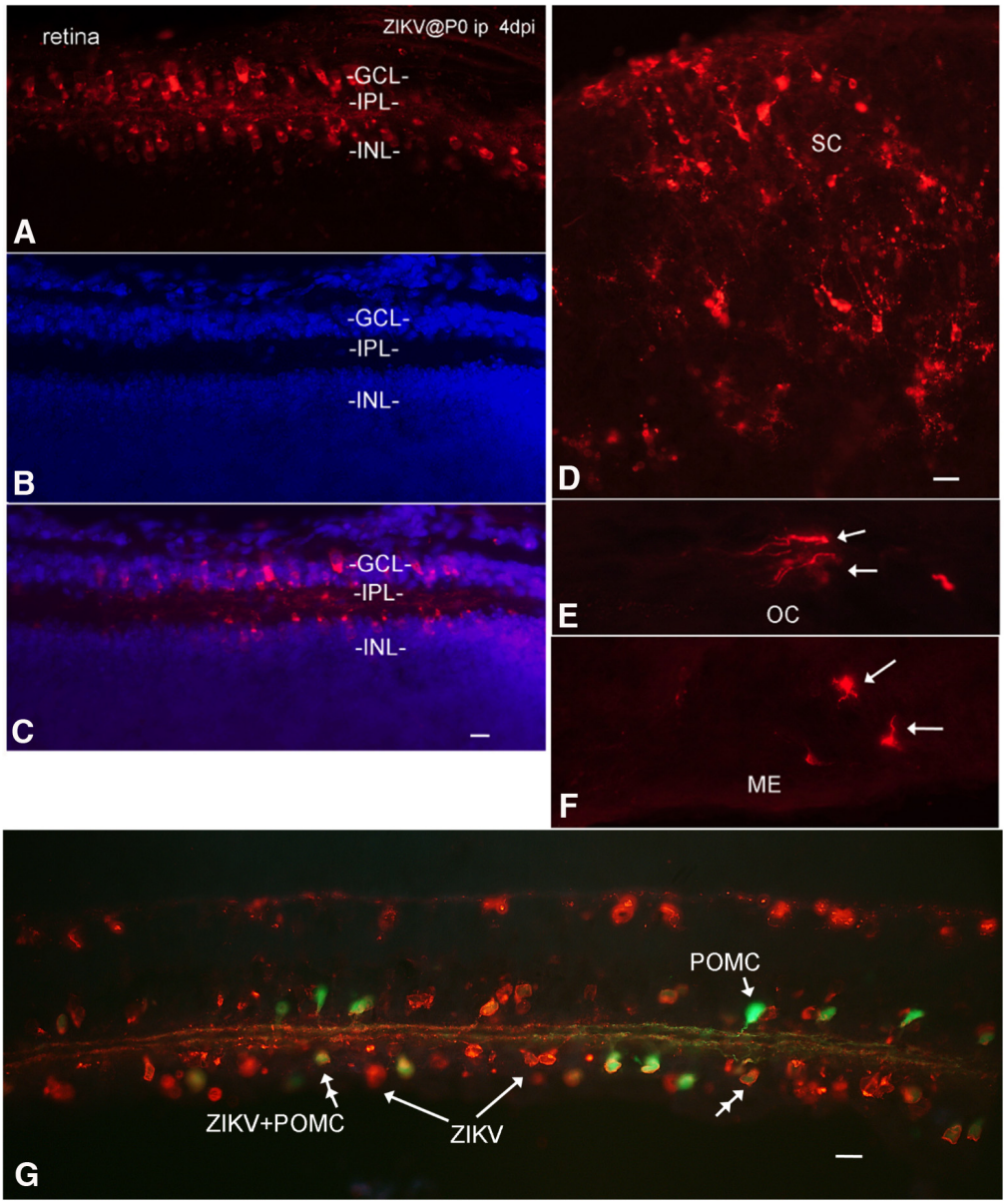

Figure 9. Infection of visual system and other brain loci after intraperitoneal inoculation. ***A–C***, Retina at 4 dpi after P0 inoculation; intraperitoneal ZIKV infects the ganglion cell layer (GCL) and the inner nuclear layer (INL). Immunoreactive processes are found in the internal plexiform layer (IPL). Red represents ZIKV immunoreactivity. Blue represents DAPI counterstain. Scale bar, 8 μm. ***D***, ZIKV in superior colliculus. ***E***, ZIKV in optic chiasm (OC). ***F***, Directly caudal to the optic chiasm is the median eminence (ME), which also showed infection. Scale bar, 15 μm. ***G***, Transgenic mouse expressing GFP in retinal POMC cells was inoculated at P0. By 7 dpi, both GFP-expressing amacrine cells (double arrowhead) and GFP-negative cells showed ZIKV infection. Green represents POMC amacrine cells. Orange represents ZIKV. Scale bar, 15 μm.

2015). Maturation of the IFN responses within the brain may be one important factor that reduces the likelihood of problematic ZIKV infection in later development and in adults.

Similar to previous reports (Cugola et al., 2016), intraperitoneal inoculation of pregnant normal mice ($n = 7$) with ZIKV from gestational day 6–14 showed no evidence of transplacental virus transfer to the fetus ($n = 14$ from 7 pregnancies), as determined with immunocytochemistry. Newborn mice ($n = 22$ mice from 5 litters) of ZIKV-infected mothers tended to be slightly smaller than controls ($n = 10$ mice from 2 litters) ($p < 0.05$ ANOVA) for the first 2–3 weeks of development, but over time returned to normal size, further arguing against ZIKV infection in these neonates. We attribute the slower initial neonatal growth to transient ZIKV-mediated debilitation in the mothers, all of whom recovered with no long-term symptoms.

ZIKV infection of the visual system

A substantial number of human cases of microcephaly associated with ZIKV infections also show ocular dysfunction and pathological disturbances to the retina as well as optic nerve abnormalities. In addition, some cases of retinal dysfunction have been associated with ZIKV infection in the absence of microcephaly (Miranda et al., 2016; Ventura et al., 2016a, b; de Paula Freitas et al., 2016). With intraperitoneal inoculations at P0, all 14 mice studied showed some retinal infection by 4 dpi and later; similarly, 2 of 2 mice inoculated at P0 subcutaneously showed retinal infection. Cells in both the retinal ganglion cell layer and in the inner nuclear layer were commonly infected (Fig. 9*A–C*). Optic nerves leaving the retina contained ZIKV-immunoreactive axons. The brains of mice studied with retinal infection also showed infection (5 of 5) of at least some part of the CNS visual system,

including retina, optic chiasm (Fig. 9*E*), suprachiasmatic nucleus, lateral geniculate nucleus, and/or superior colliculus (Fig. 9*D*). Infection of glia in the median eminence and hypothalamic arcuate nucleus, a region of the brain with a weak blood–brain barrier outside and just caudal to the optic chiasm, commonly showed infection (Fig. 9*F*). In transgenic mice expressing GFP in retinal GABAergic amacrine cells under control of the POMC promoter (Gallagher et al., 2010), ZIKV-infected a number of these amacrine cells, indicated by coexpression of GFP and ZIKV immunoreactivity; ZIKV also infected many cells that were negative for POMC-GFP by 7 dpi (Fig. 9*G*).

To examine infection of the visual system further, ZIKV was applied by intraocular inoculation to mice ($n = 4$, 4–6 weeks old) lacking a Type 1 IFN response due to the absence of the IFNR ($IFNR^{-/-}$); the lack of Type 1 IFN response in these mice parallels the weak IFN response found during early development (van den Pol et al., 2002, 2007). At 3 and 4 dpi, infection was found in the optic nerve and visual system loci within the brain, including the lateral geniculate, superior colliculus, and suprachiasmatic nuclei (Fig. 10*A–E*). Surprisingly, the infections seen in the optic nerve often included glial cells within the optic chiasm and optic tract (Fig. 10*C*). Groups of infected optic nerve glia were found along the optic tract from the optic chiasm to the lateral geniculate nucleus, an unusual mechanism of virus spread. In addition, both astrocytes and neurons were infected in the visual system nuclei. A number of infected cells within the optic tract and optic chiasm expressed the astrocyte antigen GFAP (Fig. 11). Associated with the glial labeling was infection of the meninges at the surface of the brain, particularly adjacent to the infected cells. To corroborate the finding of glial cells along infected nerves within the brain, we also examined the sciatic nerve after intramuscular injection in the hind leg of $IFNR^{-/-}$ mice (4–6 weeks old). Again, we found infected glial cells associated with the sciatic nerve (Fig. 10*F*). It is notable that both the normal neonates and near-adult and adult $IFNR^{-/-}$ mice showed strong initial infection of astrocytes.

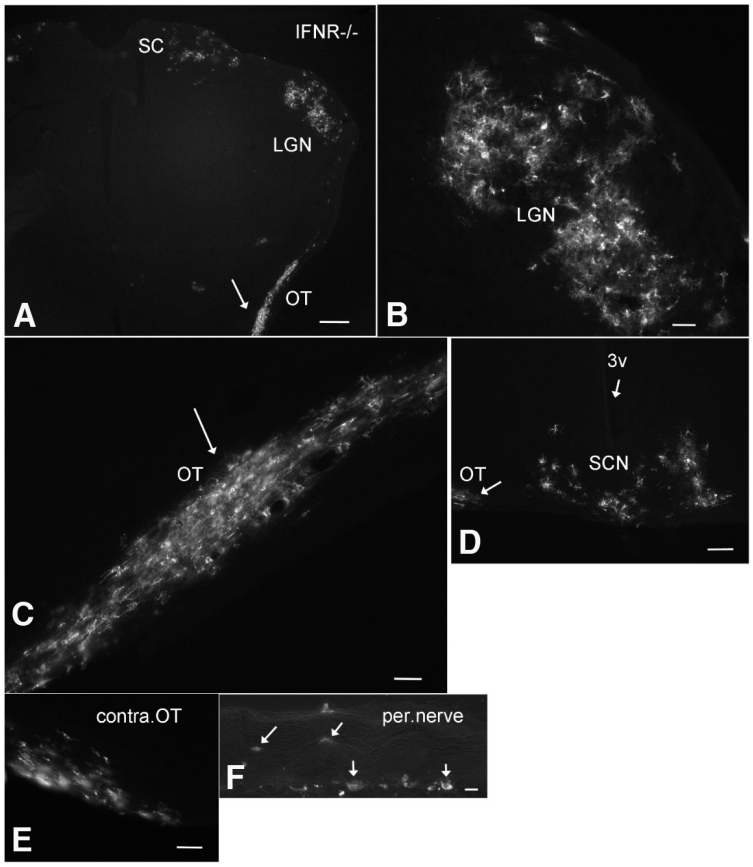

Figure 10. ZIKV infects the visual system in $IFNR^{-/-}$ mouse. ***A–E***, After intraocular inoculation of 4-week-old $IFNR^{-/-}$ mice, ZIKV was identified at 4 dpi in visual system regions (***A***), including the optic tract (OT), lateral geniculate nucleus (LGN), superior colliculus (SC), and the suprachiasmatic nucleus (SCN). Contralateral to ***C***, the other optic tract also showed ZIKV infection. ***F***, In another $IFNR^{-/-}$ mouse, intramuscular injection into the hind leg led to ZIKV infection of cells in and around the peripheral (per.) nerve innervating the leg. Scale bars: ***A***, 200 μm; ***B***, 60 μm; ***C***, 40 μm; ***D***, 60 μm; ***E***, 40 μm; ***F***, 30 μm.

Axonal transport of ZIKV

In the course of examining brains of mice inoculated intraperitoneally on the day of birth, in later stages of infection, in some mice we found infection in mirror image on opposite sides of the brain. One possible explanation for this is axonal transport from a common area of innervation, or axonal projections between corresponding regions on opposite sides of the brain. To determine whether ZIKV is transported intra-axonally to distant brain regions, we made microinjections of ZIKV into the left cortex of normal mice (4 weeks old, $n = 4$), and killed mice at 3 and 4 dpi. Here we used 300 or 500 nl, a volume 100 times smaller than that used in classical work showing that ZIKV does infect the brain (Bell et al., 1971); further, unlike the early work, we did not use virus harvested from developing brain inoculations. At 3 dpi, we found infected neurons not only in different cortical layers at the injection site, but also in the contralateral cortex. By 4 dpi, we detected robust infection at the injection site (Fig. 12*A*,*F*), and a growing number of infected neurons in the contralateral cortex (Fig. 12*B*,*F*) and ipsilateral and contralateral striatum (Fig. 12*D*,*E*); both regions receive axonal innervation from the cortex (Molyneaux et al., 2007). Importantly, in the middle region of the brain between the two sets of infected cortical neurons, there were no detectable infected cells of any sort, arguing against virus diffusion from one side of the brain to the distant contralateral side (Fig. 12*C*,*F*).

To corroborate the results above, we used coinjections of ZIKV with the Bartha strain of PRV that serves as a viral axonal tracer (Card et al., 1993, 1995). Both the PRV GFP reporter and red ZIKV immunofluorescence was found in the same region of the injected side of the cortex, and in the contralateral cortex showing a mirror image of the injected side (Fig. 13). In the cortex contralateral to the injected side, some neurons expressed the PRV reporter only (Fig. 13*B*), others expressed ZIKV immunoreactivity only (Fig. 13*A*), and a third group expressed both PRV GFP reporter together with ZIKV immunoreactivity. The coinjections corroborated our initial interpretation because cells on the side of the brain contralateral to the injection showed both green GFP reporter (from PRV) and red immunofluorescence indicating ZIKV. Together, these data suggest that at least some

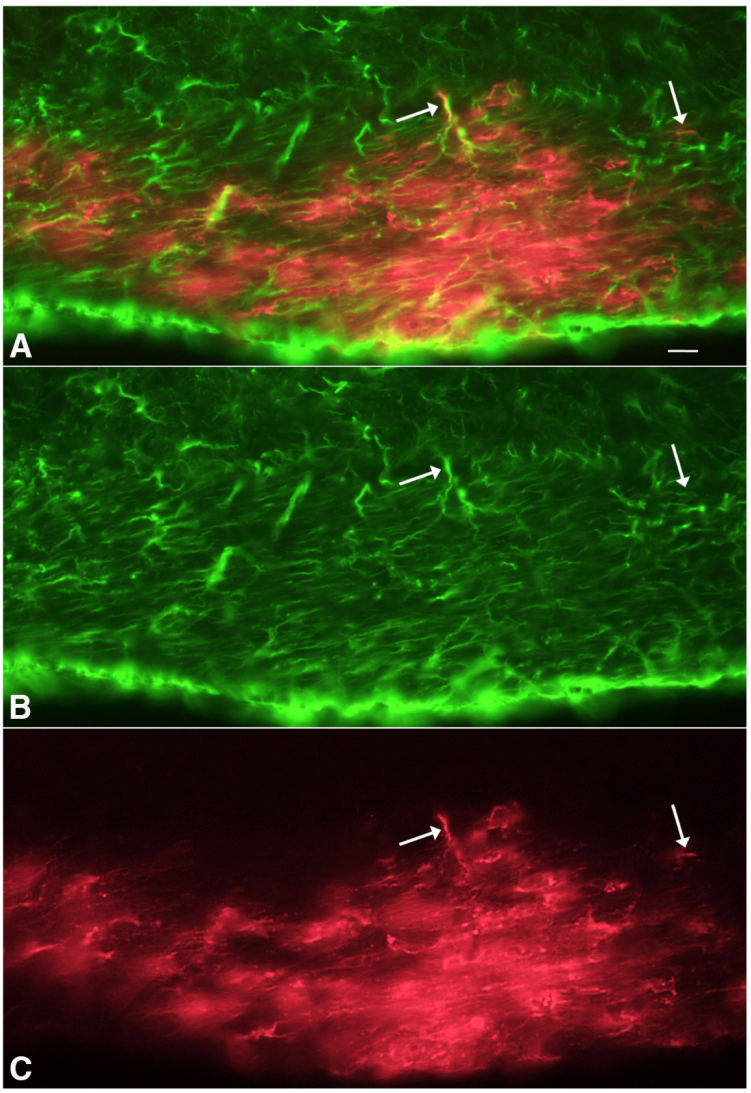

Figure 11. ZIKV-infected cells (red) in optic chiasm colabeled with GFAP. ***A***, Merged image from red ZIKV infections (***C***) and green immunostaining for GFAP (***B***) after intraocular inoculation in IFNR $^{-/-}$ mouse, 4 dpi. ***A–C***, Same microscope field. Scale bar, 5 μm.

axonal pathways within the brain can transport ZIKV to infect neurons in a distant brain site.

Discussion

A number of recent papers have examined ZIKV infections in different mouse models, particularly in immunodeficient mice (Lazear et al., 2016; Rossi et al., 2016). In addition, 3D organoid *in vitro* brain cultures have been elegantly used to describe a propensity of ZIKV to infect neuronal progenitor cells in early brain development (Cugola et al., 2016; Dang et al., 2016; Garcez et al., 2016; Li et al., 2016); a potential limitation of organoid cultures is the lack of a vascular system and the absence of the normal types of immune cells.

Our animal model of early ZIKV infection emulates the early second trimester of human brain development; during the second trimester of human brain development and P0 mouse CNS development, there are a number of parallels, including cortical layer II/III and IV neurogenesis, onset of retinal waves of action potential propagation, peak of optic nerve axon number, and peak of subventricular zone expansion in the developing cortex (Clancy et al., 2007a, b; Workman et al., 2013). A key difference between our neonatal model and an *in utero* model is the absence of placental virus inhibition in the neonate. Both the structure and the immune components of the placenta constitute a biological barrier that blocks microorganisms in the pregnant mother from easily accessing the fetus (Mor and Cardenas, 2010; Robbins and Bakardjiev, 2012).

Another virus that can generate many of the same neurological symptoms as ZIKV if infections occur in the fetal period is the unrelated cytomegalovirus, which uses a double-stranded DNA genome; CMV is often considered the most common infectious agent causing permanent neurological dysfunction in the developing human, and these problems can include sensory, motor, memory, and other complications. Importantly, CMV can continue to induce neurological dysfunction even during early neonatal development (Bray et al., 1981; Perez-Jimenez et al., 1998; Gaytant et al., 2002; Dollard et al., 2007; Mocarski et al., 2007; Tsutsui, 2009), raising the question of whether ZIKV can similarly evoke neurological problems during the same neonatal developmental period in humans; these later neurological problems would be more subtle and difficult to diagnose than microcephaly, a current focus of ZIKV concern.

Here we studied developing newborn normal mice. Our data show, for the first time, that after peripheral inoculation, there is a substantial initial infection of glial cells within the brain, particularly cells with a morphology and GFAP antigen expression consistent with astrocytes. Infected isolated astrocytes were found throughout the brain, indicating that this was a widespread occurrence and suggesting a large number of ZIKV penetrations into the developing brain. Over the next few days of development, the number of infected neurons showed a substantial increase such that the relative number of infected neurons exceeded the number of infected astrocytes by P10. Consistent with our *in vitro* demonstration of ZIKV progeny release from infected glia, astrocytes may not only show the first signs of infection but may also serve to further amplify and distribute infectious virus to nearby neurons and glia. Similar to ZIKV, CMV also tends to target astrocytes (van den Pol et al., 2007). That glia are not necessarily a common cell target of other viruses in the developing brain is shown by vesicular stomatitis virus, which targets neurons rather than glia (van den Pol et al., 2002, 2014).

Interestingly, in the early stages of brain infection, microglia showed little ZIKV immunoreactivity, whereas astrocytes in the same brain were commonly infected. Our finding of the initial selective infection of astrocytes does not argue against a perspective that in earlier stages of brain development, macrophages that can be infected by ZIKV (Quicke et al., 2016) may migrate into the brain carrying the virus in a Trojan-horse mechanism of spreading infection. Although infected astrocytes were previously found after large-

volume brain-derived ZIKV injections directly into the brain (Bell et al., 1971), we show, for the first time, that the native virus initially selects and targets astrocytes after peripheral inoculation during the period of mouse development immediately after birth.

We found behavioral problems in ZIKV-inoculated neonatal mice, often involving hind limbs. Motor deficits may relate to the common infection of the cerebellum, motor cortex, or spinal cord.

Another striking finding here was the consistent infection of the retina in all mice inoculated intraperitoneally or subcutaneously at birth. This differs from previous work in both younger and older periods of development. Eye infections were very rare in fetal infections, occurring in only 5% of those infected (Miner et al., 2016b). ZIKV subcutaneous inoculations at older postnatal day 8 showed only a subset (50%) of mice with eye infections; P8 is approximately equivalent to the third trimester near-term fetus in humans, whereas our P0 inoculation parallels the second trimester (Clancy et al., 2001, 2007a, b; Workman et al., 2013). The retinal infections from P0 inoculation were not restricted to a single-cell type but rather were found in a number of different cells in the ganglion cell layer and inner nuclear layer. In addition to retinal infection, in many mice the CNS visual system showed signs of infection. Consistent with our finding of early astrocyte infection throughout the brain, astrocytes were commonly infected in visual system pathways.

An increase in caspase-3 immunoreactivity was reported in the brain after P8 inoculations (Miner et al., 2016b), suggesting a response to virus or to degeneration of the optic nerve following ZIKV retinal infection. Our data show that the virus itself displays an early preference for infecting regions of the brain subserving vision in the developing mouse brain at a developmental stage equivalent to mid-gestation in human CNS development. ZIKV infection of the regions of the brain involved in sight suggests that visual problems arising from ZIKV fetal infection in humans (Ventura et al., 2016b; de Paula Freitas et al., 2016) may not only arise from retinal infections, which were very prevalent in our studies in developing mice, but also from infection of the optic nerve or regions of the brain involved in vision.

After ZIKV microinjections into one side of the brain, 3–4 d later, the opposite mirror image region of the cortex showed infection, whereas the middle of the brain between the two cortices showed no infection of any cells. These data suggest axonal transport of the virus from one side of the brain to the synaptically connected contralateral cortex. We also used a coinjection of ZIKV with the retrogradely transported herpes Type 1 porcine PRV expressing a GFP reporter. In the cortex, contralateral to the site of coinjection, we found both ZIKV immunoreactivity and PRV reporter gene expression, consistent with the view that both viruses were axonally transported. Our data on ZIKV transport in the cortex are consistent with previous reports showing that axonally transported tracers label parallel groups of cells on opposite sides of the cortex after unilateral injection (Wise and Jones, 1976), and support the hypothesis that ZIKV can be transported within axons to infect distant sites within the brain. Contralateral axonal transport of ZIKV in the cortex is also consistent with our data from ocular injections of the virus that resulted in infection of the CNS visual system. Axonal transport of another flavivirus, West Nile Virus, has previously been described (Samuel et al., 2007).

In conclusion, the robust and consistent early infection of astrocytes before neurons was unexpected and suggests the infection of astrocytes merits more attention in brain infections in humans, particularly given the important roles of astrocytes in maintenance of the blood–brain barrier, en-

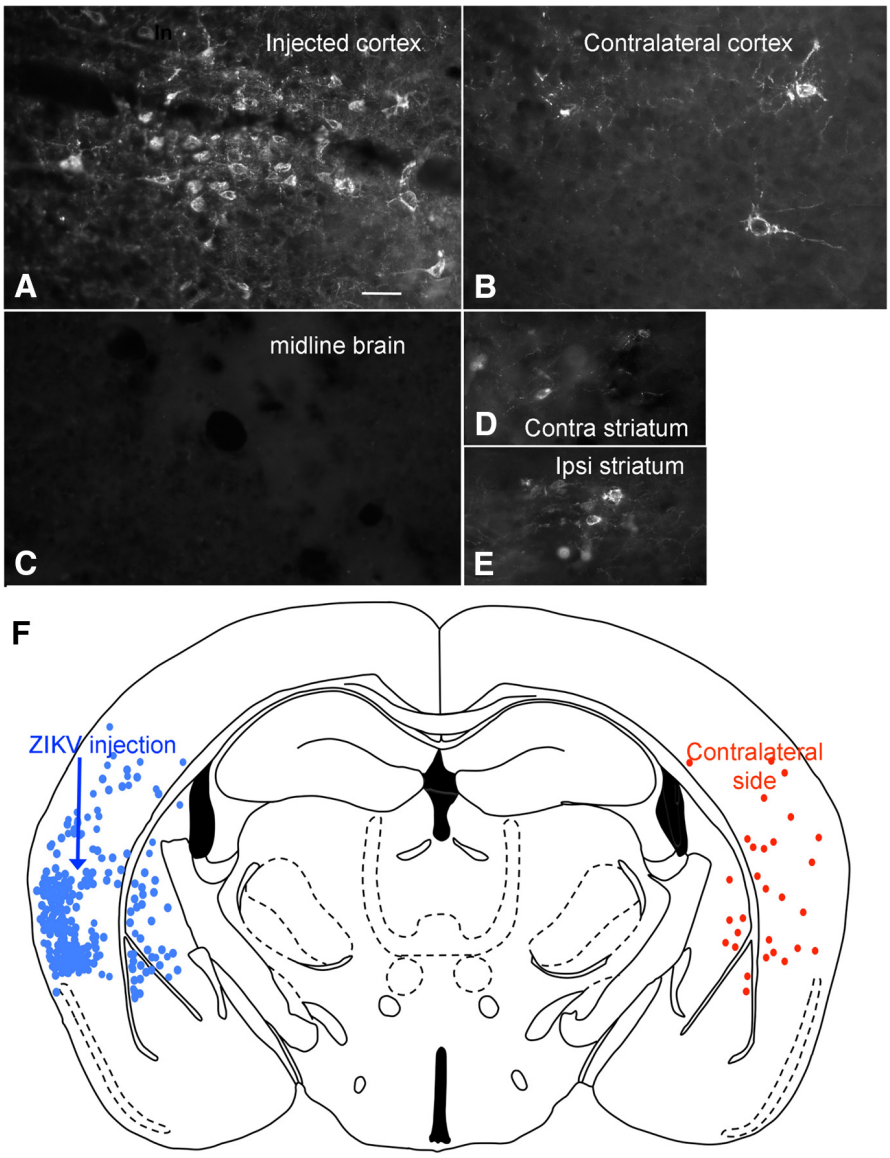

Figure 12. Axonal transport of ZIKV from one brain region to another. After intracortical microinjection (300 nl) into the left cortex (***A***, ***F***), 4 d later strong infection was found in the contralateral right cortex (***B***, ***F***) and in the contralateral (contra) (***D***) and ipsilateral (ipsi) (***E***) striatum. A few cells were also detected in the amygdala. All these regions are synaptically connected with the cortex. No detectable infection was found in the middle region of the brain (***C***). ***F***, Composite image with all infected cells drawn from two sections of the same brain. Scale bar, 30 μm.

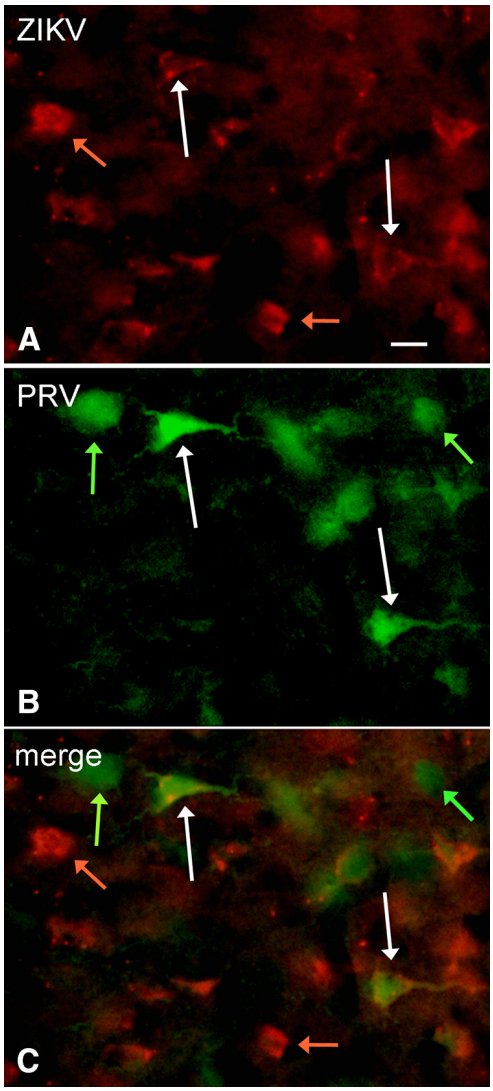

Figure 13. Axonal transport of PRV and ZIKV to contralateral cortex. After comicroinjection (300 nl) of PRV and ZIKV to the left cortex, both viruses are carried by axonal transport to the contralateral right cortex by 3 dpi. ***A***, ZIKV immunoreactivity. Scale bar, 18 μm. ***B***, PRV GFP green reporter expression. ***C***, Merged image showing that some cells are infected only with ZIKV (orange arrows), only with PRV (green arrows), or with both PRV and ZIKV (white arrows).

hancement of myelination, CNS repair and inflammation, development and migration of neurons, guidance of growing axons, and neurotransmitter modulation (Khakh and Sofroniew, 2015). Attenuating ZIKV infection of astrocytes may reduce subsequent infection of nearby neurons. The common infection of retina and central visual nuclei in our studies suggests that visual problems found in newborns from ZIKV-infected mothers could arise from both peripheral (retina) and CNS complications. That ZIKV can be transported axonally appears to constitute one mechanism underlying the spread of the virus within the brain.

References

Aliota MT, Caine EA, Walker EC, Larkin KE, Camacho E, Osorio JE (2016) Characterization of lethal zika virus infection in AG129 Mice. PLoS Negl Trop Dis 10:e0004682. CrossRef Medline

Bell TM, Field EJ, Narang HK (1971) Zika virus infection of the central nervous system of mice. Arch Gesamte Virusforsch 35:183–193. CrossRef Medline

Brasil P, Pereira JP Jr, Moreira ME, Ribeiro Nogueira RM, Damasceno L, Wakimoto M, Rabello RS, Valderramos SG, Halai UA, Salles TS, Zin AA, Horovitz D, Daltro P, Boechat M, Raja Gabaglia C, Carvalho de Sequeira P, Pilotto JH, Medialdea-Carrera R, Cotrim da Cunha D, Abreu de Carvalho LM, et al. (2016) Zika virus infection in pregnant women in Rio de Janeiro-preliminary report. N Engl J Med 375:2321–2334. CrossRef Medline

Brault JB, Khou C, Basset J, Coquand L, Fraisier V, Frenkiel MP, Goud B, Manuguerra JC, Pardigon N, Baffet AD (2016) Comparative analysis between flaviviruses reveals specific neural stem cell tropism for Zika virus in the mouse developing neocortex. EBioMedicine 10:71–76. CrossRef Medline

Bray PF, Bale JF, Anderson RE, Kern ER (1981) Progressive neurological disease associated with chronic cytomegalovirus infection. Ann Neurol 9:499–502. CrossRef Medline

Calvet G, Aguiar RS, Melo AS, Sampaio SA, de Filippis I, Fabri A, Araujo ES, de Sequeira PC, de Mendonça MC, de Oliveira L, Tschoeke DA, Schrago CG, Thompson FL, Brasil P, Dos Santos FB, Nogueira RM, Tanuri A, de Filippis AM (2016) Detection and sequencing of Zika virus from amniotic fluid of fetuses with microcephaly in Brazil: a case study. Lancet Infect Dis 16:653–660. CrossRef Medline

Card JP, Rinaman L, Lynn RB, Lee BH, Meade RP, Miselis RR, Enquist LW (1993) Pseudorabies virus infection of the rat central nervous system: ultrastructural characterization of viral replication, transport, and pathogenesis. J Neurosci 13:2515–2539. Medline

Card JP, Dubin JR, Whealy ME, Enquist LW (1995) Influence of infectious dose upon productive replication and transynaptic passage of pseudorabies virus in rat central nervous system. J Neurovirol 1:349–358. CrossRef Medline

Cauchemez S, Besnard M, Bompard P, Dub T, Guillemette-Artur P, Eyrolle-Guignot D, Salje H, Van Kerkhove MD, Abadie V, Garel C, Fontanet A, Mallet HP (2016) Association between Zika virus and microcephaly in French Polynesia, 2013–15: a retrospective study. Lancet 387:2125–2132. CrossRef Medline

Clancy B, Darlington RB, Finlay BL (2001) Translating developmental time across mammalian species. Neuroscience 105:7–17. CrossRef Medline

Clancy B, Finlay BL, Darlington RB, Anand KJ (2007a) Extrapolating brain development from experimental species to humans. Neurotoxicology 28:931–937. CrossRef Medline

Clancy B, Kersh B, Hyde J, Darlington RB, Anand KJ, Finlay BL (2007b) Web-based method for translating neurodevelopmental from laboratory species to humans. Neuroinformatics 5:79–94. CrossRef Medline

Cugola FR, Fernandes IR, Russo FB, Freitas BC, Dias JL, Guimarães KP, Benazzato C, Almeida N, Pignatari GC, Romero S, Polonio CM, Cunha I, Freitas CL, Brandão WN, Rossato C, Andrade DG, Faria Dde P, Garcez AT, Buchpigel CA, Braconi CT, et al. (2016) The Brazilian Zika virus strain causes birth defects in experimental models. Nature 534:267–271. CrossRef Medline

Dang J, Tiwari SK, Lichinchi G, Qin Y, Patil VS, Eroshkin AM, Rana TM (2016) Zika virus depletes neural progenitors in human cerebral organoids through activation of the innate immune receptor TLR3. Cell Stem Cell 19:258–265. CrossRef Medline

de Carvalho Leal M, Ferreira Muniz L, da Silva Caldas Neto S, van der Linden V, Ferreira Ramos RC (2016) Sensorineural hearing loss in a case of congenital Zika virus. Braz J Otorhinolaryngol 30:piiS1808–8694(16)30127–6. CrossRef Medline

de Fatima Vasco Aragoa M, van der Linden V, Brainer-Lima AM, Coeli RR, Rocha MA, Sobral da Silva P, Durce Costa Gomes de Carvalho M, van der Linden A, Cesario de Holanda A, Valenca MM (2016) Clinical features and neuroimaging (CT and MRI) findings in presumed Zika virus related congenital infection and microcephaly: retrospective case series study. Br Med J 353:i1901. CrossRef Medline

de Paula Freitas B, de Oliveira Dias JR, Prazeres J, Sacramento GA, Ko AI, Maia M, Belfort R Jr (2016) Ocular findings in infants with microcephaly associated with presumed Zika virus congenital infection in Salvador, Brazil. JAMA Ophthalmol 134:529–535. CrossRef Medline

Dollard SC, Grosse SD, Ross DS (2007) New estimates of the prevalence of neurological and sensory sequelae and mortality associated with congenital cytomegalovirus infection. Rev Med Virol 17:355–363. CrossRef Medline

Dos Santos T, Rodriguez A, Almiron M, Sanhueza A, Ramon P, de Oliveira WK, Coelho GE, Badaró R, Cortez J, Ospina M, Pimentel R, Masis R, Hernandez F, Lara B, Montoya R, Jubithana B, Melchor A, Alvarez A, Aldighieri S, Dye C, et al. (2016) Zika virus and the Guillain-Barré syn-

drome: case series from seven countries. N Engl J Med 375:1598–1601. CrossRef Medline

Driggers RW, Ho CY, Korhonen EM, Kuivanen S, Jääskeläinen AJ, Smura T, Rosenberg A, Hill DA, DeBiasi RL, Vezina G, Timofeev J, Rodriguez FJ, Levanov L, Razak J, Iyengar P, Hennenfent A, Kennedy R, Lanciotti R, du Plessis A, Vapalahti O (2016) Zika virus infection with prolonged maternal viremia and fetal brain abnormalities. N Engl J Med 374:2142–2151. CrossRef Medline

França GV, Schuler-Faccini L, Oliveira WK, Henriques CM, Carmo EH, Pedi VD, Nunes ML, Castro MC, Serruya S, Silveira MF, Barros FC, Victora CG (2016) Congenital Zika virus syndrome in Brazil: a case series of the first 1501 livebirths with complete investigation. Lancet 388:891–897. CrossRef Medline

Gallagher SK, Witkovsky P, Roux MJ, Low MJ, Otero-Corchon V, Hentges ST, Vigh J (2010) β-Endorphin expression in the mouse retina. J Comp Neurol 518:3130–3148. CrossRef Medline

Garcez PP, Loiola EC, Madeiro da Costa R, Higa LM, Trindade P, Delvecchio R, Nascimento JM, Brindeiro R, Tanuri A, Rehen SK (2016) Zika virus impairs growth in human neurospheres and brain organoids. Science 352:816–818. CrossRef Medline

Gaytant MA, Steegers EA, Semmekrot BA, Merkus HM, Galama JM (2002) Congenital cytomegalovirus infection: review of the epidemiology and outcome. Obstet Gynecol Surv 57:245–256. CrossRef Medline

Hamel R, Dejarnac O, Wichit S, Ekchariyawat P, Neyret A, Luplertlop N, Perera-Lecoin M, Surasombatpattana P, Talignani L, Thomas F, Cao-Lormeau VM, Choumet V, Briant L, Desprès P, Amara A, Yssel H, Missé D (2015) Biology of Zika virus infection in human skin cells. J Virol 89:8880–8896. CrossRef Medline

Hazin AN, Poretti A, Turchi Martelli CM, Huisman TA, Huisman TA, Di Cavalcanti Souza Cruz D, Tenorio M, van der Linden A, Pena LJ, Brito C, Gil LH, de Barros Miranda-Filho D, Marques ET, Alves JG (2016) Computed tomographic findings in microcephaly associated with Zika virus. N Engl J Med 374:2193–2195. CrossRef Medline

Heang V, Yasuda CY, Sovann L, Haddow AD, Travassos da Rosa AP, Tesh RB, Kasper MR (2012) Zika virus infection, Cambodia, 2010. Emerg Infect Dis 18:349–351. CrossRef Medline

Hughes RAC, Rees JH (1997) Clinical and epidemiologic features of Guillain-Barré Syndrome. J Infect Dis 176 [Suppl 2]:S92–S98.

Ito D, Imai Y, Ohsawa K, Nakajima K, Fukuuchi Y, Kohsaka S (1998) Microglia-specific localization of a novel calcium binding protein, Iba1. Brain Res Mol Brain Res 57:1–9. CrossRef Medline

Johansson MA, Mier-y-Teran-Romero L, Reefhuis J, Gilboa SM, Hills SL (2016) Zika and the risk of microcephaly. N Engl J Med 375:1–4. CrossRef Medline

Khakh BS, Sofroniew MV (2015) Diversity of astrocyte functions and phenotypes in neural circuits. Nat Neurosci 18:942–952. CrossRef Medline

Kleber de Oliveira W, Cortez-Escalante J, De Oliveira WT, do Carmo GM, Henriques CM, Coelho GE, Araújo de França GV (2016) Increase in reported prevalence of microcephaly in infants born to women living in areas with confirmed Zika virus transmission during the first trimester of pregnancy-Brazil, 2015. MMWR Morb Mortal Wkly Rep 65:242–247. CrossRef Medline

Lazear HM, Govero J, Smith AM, Platt DJ, Fernandez E, Miner JJ, Diamond MS (2016) A mouse model of Zika virus pathogenesis. Cell Host Microbe 19:720–730. CrossRef Medline

Lessler J, Chaisson LH, Kucirka LM, Bi Q, Grantz K, Salje H, Carcelen AC, Ott CT, Sheffield JS, Ferguson NM, Cummings DA, Metcalf CJ, Rodriguez-Barraquer I (2016) Assessing the global threat from Zika virus. Science 353:aaf8160. CrossRef Medline

Li C, Xu D, Ye Q, Hong S, Jiang Y, Liu X, Zhang N, Shi L, Qin CF, Xu Z (2016) Zika virus disrupts neural progenitor development and leads to microcephaly in mice. Cell Stem Cell 19:120–126. CrossRef Medline

Lindenbach BD, Rice CM (2001) Flaviviridae: the viruses and their replication. In: Fields virology (Knipe DM, Howley PM, eds), pp 991–1041. Philadelphia: Lippincott Williams Wilkins.

Martines RB, Bhatnagar J, Keating MK, Silva-Flannery L, Muehlenbachs A, Gary J, Goldsmith C, Hale G, Ritter J, Rollin D, Shieh WJ, Luz KG, Ramos AM, Davi HP, Kleber de Oliveria W, Lanciotti R, Lambert A, Zaki S (2016) Notes from the field: evidence of Zika virus infection in brain and placental tissues from two congenitally infected newborns and two fetal losses—Brazil, 2015. MMWR Morb Mortal Wkly Rep 65:159–160. CrossRef Medline

McCarthy M (2016) US officials issue travel alert for Miami area as Zika cases rise to 15. Br Med J 354:i4298.

Miner JJ, Cao B, Govero J, Smith AM, Fernandez E, Cabrera OH, Garber C, Noll M, Klein RS, Noguchi KK, Mysorekar IU, Diamond MS (2016a) Zika virus infection during pregnancy in mice causes placental damage and fetal demise. Cell 165:1081–1091. CrossRef Medline

Miner JJ, Sene A, Richner JM, Smith AM, Santeford A, Ban N, Weger-Lucarelli J, Manzella F, Rückert C, Govero J, Noguchi KK, Ebel GD, Diamond MS, Apte RS (2016b) Zika virus infection in mice causes panuveitis with shedding of virus in tears. Cell Rep 16:3208–3218. CrossRef Medline

Miranda HA 2nd, Costa MC, Frazão MA, Simão N, Franchischini S, Moshfeghi DM (2016) Expanded spectrum of congenital ocular findings in microcephaly with presumed Zika infection. Ophthalmology 123:1788–1794. CrossRef Medline

Mocarski E, Shenk T, Pass R (2007) Cytomegaloviruses. In: Fields virology (Knipe DM, Howley PM, eds), pp 2701–2772. Philadelphia: Lippincott Williams Wilkins.

Molyneaux BJ, Arlotta P, Menezes JR, Macklis JD (2007) Neuronal subtype specification in the cerebral cortex. Nat Rev Neurosci 8:427–437. CrossRef Medline

Mor G, Cardenas I (2010) The immune system in pregnancy: a unique complexity. Am J Reprod Immunol 63:425–433. CrossRef Medline

Niemeyer B, Niemeyer R, Borges R Marchiori E (2017) Acute disseminated encephalomyelitis following Zika virus infection. Eur Neurol 77:45–46. CrossRef Medline

Ozduman K, Wollmann G, Piepmeier JM, van den Pol AN (2008) Systemic vesicular stomatitis virus selectively destroys multifocal glioma and metastatic carcinoma in brain. J Neurosci 28:1882–1893. CrossRef Medline

Paixão ES, Barréto F, Teixeira Mda G, Costa Mda C, Rodrigues LC (2016) History, epidemiology, and clinical manifestations of Zika: a systematic review. Am. J Public Health 106:606–612. CrossRef Medline

Pérez-Jiménez A, Colamaria V, Franco A, Grimau-Merino R, Darra F, Fontana E, Zullini E, Beltramello A, Dalla-Bernardina B (1998) Epilepsy and disorders of cortical development in children with congenital cytomegalovirus infection. Rev Neurol 26:42–49. Medline

Quicke KM, Bowen JR, Johnson EL, McDonald CE, Ma H, O'Neal JT, Rajakumar A, Wrammert J, Rimawi BH, Pulendran B, Schinazi RF, Chakraborty R, Suthar MS (2016) Zika virus infects human placental macrophages. Cell Host Microbe 20:83–90. CrossRef Medline

Robbins JR, Bakardjiev AI (2012) Pathogens and the placental fortress. Curr Opin Microbiol 15:36–43. CrossRef Medline

Roehrig JT, Hombach J, Barrétt AD (2008) Guidelines for plaque-reduction neutralization testing of human antibodies to Dengue viruses. Viral Immunol 21:123–132. CrossRef Medline

Rossi SL, Tesh RB, Azar SR, Muruato AE, Hanley KA, Auguste AJ, Langsjoen RM, Paessler S, Vasilakis N, Weaver SC (2016) Characterization of a novel murine model to study Zika virus. Am J Trop Med Hyg 94:1362–1369. CrossRef Medline

Russell PK, Nisalak A, Sukhavachana P, Vivona S (1967) A plaque reduction test for Dengue virus neutralizing antibodies. J Immunol 99:285–290. Medline

Samuel MA, Wang H, Siddharthan V, Morrey JD, Diamond MS (2007) Axonal transport mediates West Nile virus entry into the central nervous system and induces acute flaccid paralysis. Proc Natl Acad Sci U S A 104:17140–17145. CrossRef Medline

Trevathan E (2016) Editorial brain malformation surveillance in the Zika era. Birth Defects Res A Clin Mol Teratol 106:869–874. CrossRef Medline

Tsutsui Y (2009) Effects of cytomegalovirus infection on embryogenesis and brain development. Congenit Anom (Kyoto) 49:47–55. CrossRef Medline

van den Pol AN (2006) Viral infections in the developing and mature brain. Trends Neurosci 29:398–406. CrossRef Medline

van den Pol AN, Dalton KP, Rose JK (2002) Relative neurotropism of a recombinant rhabdovirus expressing a green fluorescent envelope glycoprotein. J Virol 76:1309–1327. CrossRef Medline

van den Pol AN, Robek MD, Ghosh PK, Ozduman K, Bandi P, Whim MD, Wollmann G (2007) Cytomegalovirus induces interferon-stimulated gene expression and is attenuated by interferon in the developing brain. J Virol 81:332–348. CrossRef Medline

van den Pol AN, Ding S, Robek MD (2014) Long-distance interferon signaling within the brain blocks virus spread. J Virol 88:3695–3704. CrossRef Medline

van der Linden V, Filho EL, Lins OG, van der Linden A, Aragão Mde F, Brainer-Lima AM, Cruz DD, Rocha MA, Sobral da Silva PF, Carvalho MD, do Amaral FJ, Gomes JA, Ribeiro de Medeiros IC, Ventura CV, Ramos RC (2016) Congenital Zika syndrome with arthrogryposis: retrospective case series study. Br Med J 354:i3899. CrossRef Medline

Ventura CV, Maia M, Dias N, Ventura LO, Belfort R Jr (2016a) Zika: neurological and ocular findings in infant without microcephaly. Lancet 387: 2502. CrossRef Medline

Ventura CV, Maia M, Travassos SB, Martins TT, Patriota F, Nunes ME, Agra C, Torres VL, van der Linden V, Ramos RC, Rocha MÂ, Silva PS, Ventura LO, Belfort R Jr (2016b) Risk factors associated with the ophthalmoscopic findings identified in infants with presumed Zika virus congenital infection. JAMA Ophthalmol 134:912–918. CrossRef Medline

Wise SP, Jones EG (1976) The organization and postnatal development of the commissural projection of the rat somatic sensory cortex. J Comp Neurol 168:313–343. CrossRef Medline

Workman AD, Charvet CJ, Clancy B, Darlington RB, Finlay BL (2013) Modeling transformations of neurodevelopment sequences across mammalian species. J Neurosci 33:7368–7383. CrossRef Medline

Yockey LJ, Varela L, Rakib T, Khoury-Hanold W, Fink SL, Stutz B, Szigeti-Buck K, van den Pol A, Lindenbach BD, Horvath TL, Iwasaki A (2016) Vaginal exposure to Zika virus during pregnancy leads to fetal brain infection. Cell 166:1247–1256. CrossRef Medline